

**UC Irvine**

**UC Irvine Electronic Theses and Dissertations**

**Title**

The Dynamics of Quantum Coherences in Phase Space: Theory and Application to Molecular Spectroscopy

**Permalink**

<https://escholarship.org/uc/item/22r6d6zf>

**Author**

Green, Austin Tyler

**Publication Date**

2024

Peer reviewed|Thesis/dissertation

UNIVERSITY OF CALIFORNIA,  
IRVINE

The Dynamics of Quantum Coherences in Phase Space: Theory and Application to  
Molecular Spectroscopy

DISSERTATION

submitted in partial satisfaction of the requirements  
for the degree of

DOCTOR OF PHILOSOPHY

in Chemistry

by

Austin Tyler Green

Dissertation Committee:  
Professor Craig C. Martens, Chair  
Professor Vladimir A. Mandelshtam  
Professor Shaul Mukamel

2024



# DEDICATION

You asked, ‘Who is this that darkens my counsel with words without knowledge?’  
Surely I spoke of things I did not understand, things too wonderful for me to know.  
You said, ‘Listen now, and I will speak; I will question you, and you shall answer me.’  
My ears had heard of you but now my eyes have seen you.

Job 42:3-5

For Mom, Dad, Ashley, Abbey, Soyeon, and Ari. For your love, support, and patience,  
while I’ve been “digging away.”

# TABLE OF CONTENTS

	Page
<b>LIST OF FIGURES</b>	<b>vi</b>
<b>LIST OF TABLES</b>	<b>xiii</b>
<b>LIST OF SYMBOLS</b>	<b>xiv</b>
<b>ACKNOWLEDGMENTS</b>	<b>xv</b>
<b>VITA</b>	<b>xvii</b>
<b>ABSTRACT OF THE DISSERTATION</b>	<b>xx</b>
<b>1 Introduction</b>	<b>1</b>
1.1 Preliminary Concepts . . . . .	3
1.1.1 Quantum Mechanics . . . . .	3
1.1.2 Molecular Spectroscopy . . . . .	5
1.1.3 Quantum Coherence . . . . .	7
1.2 Motivation . . . . .	12
1.2.1 Quantum Technology . . . . .	12
1.2.2 Frontiers in Ultrafast Spectroscopy and Chemistry . . . . .	14
1.3 Challenges in Quantum Molecular Dynamic Simulations . . . . .	15
1.3.1 Intractability of Exact Quantum Solutions . . . . .	16
1.3.2 Complexity of Molecular Systems . . . . .	19
1.3.3 Nonadiabaticity and the Born-Oppenheimer Approximation . . . . .	23
1.3.4 Approximate Theories in Quantum Dynamics . . . . .	26
1.4 Methods . . . . .	34
1.4.1 The Wigner-Moyal Representation . . . . .	34
1.4.2 The Time-Domain: The Interplay of Dynamics and Spectroscopy . . . . .	35
1.5 Scope of Work . . . . .	37
1.5.1 Organization of Thesis . . . . .	38
1.5.2 Typography and Conventions . . . . .	39
<b>2 Theoretical Background: Classical Dynamics in Phase Space</b>	<b>41</b>
2.1 Elements of the Hamiltonian Formulation . . . . .	42
2.1.1 Definition of a Hamiltonian System . . . . .	42

2.1.2	Hamiltonian Dynamics as an Initial Value Problem . . . . .	43
2.1.3	Poisson Brackets and the Liouvillian . . . . .	47
2.1.4	Integration . . . . .	49
2.2	The Phase Space Picture . . . . .	53
2.3	Statistical Ensembles . . . . .	54
2.3.1	The Gibbs Ensemble . . . . .	54
2.3.2	Liouville's Theorem . . . . .	55
2.3.3	Ensemble Solutions to Liouville's Equation . . . . .	57
2.3.4	Expectations and Correlation Functions . . . . .	58
<b>3</b>	<b>Theoretical Background: Quantum Dynamics in Phase Space</b>	<b>60</b>
3.1	Overview of Formulation . . . . .	63
3.2	Weyl Symbols and Wigner Transforms . . . . .	64
3.2.1	Weyl Symbols . . . . .	64
3.2.2	Wigner Transforms . . . . .	66
3.2.3	Algebraic Properties of the Cross Wigner Transform . . . . .	67
3.3	Wigner Functions . . . . .	69
3.3.1	Statistics of Pure State Wigner Functions . . . . .	69
3.3.2	Inversion: Recovering the Wavefunction from the Wigner Function . .	72
3.3.3	Symmetries of Pure State Wigner Functions . . . . .	73
3.4	The Star Product . . . . .	74
3.4.1	Janus Operator Definition . . . . .	75
3.4.2	Bivector Definition . . . . .	76
3.4.3	Bopp Shifts . . . . .	80
3.4.4	Integral Definitions . . . . .	80
3.5	The Moyal Bracket . . . . .	85
3.5.1	The Moyal Bracket as a Lie Bracket . . . . .	88
3.5.2	The Wigner Moyal Equation . . . . .	89
3.6	Star Algebra and Identities . . . . .	90
3.6.1	Moyal Algebra . . . . .	91
3.6.2	Trace Properties . . . . .	91
3.7	Gaussian Weyl Symbols and Hudson States . . . . .	93
3.7.1	Hudson's Theorem . . . . .	94
3.7.2	Hudson States . . . . .	96
3.7.3	Connection with Squeezed Coherent States . . . . .	99
<b>4</b>	<b>Wigner-Moyal Solution to Displaced Oscillator Model</b>	<b>101</b>
4.1	Background . . . . .	103
4.1.1	Displaced Oscillator Model . . . . .	103
4.1.2	Thawed Gaussian Wavepackets . . . . .	105
4.2	Thawed Moyal Dynamics: Derivation and Approximations . . . . .	107
4.2.1	The Coherence Wigner Function Equation of Motion . . . . .	108
4.2.2	Thawed Gaussian Wigner Function Approach . . . . .	110
4.2.3	Thawed Gaussian Wavepacket Approach . . . . .	112
4.2.4	Approximations to Thawed Moyal Dynamics . . . . .	114

4.3	Results . . . . .	118
4.3.1	Thawed Moyal Solution to 1-D Displaced Oscillator . . . . .	118
4.3.2	Comparison with Trajectory Ensemble Solution . . . . .	127
4.3.3	Equal Frequency Case and Hot Bands . . . . .	132
4.3.4	Thawed Moyal Solution to 2-D Displaced Oscillator . . . . .	141
4.4	Discussion . . . . .	155
4.4.1	Kinematics of the Quantum and Semiclassical Coherence . . . . .	155
4.4.2	Correlation Functions and Spectra . . . . .	159
4.4.3	Trajectory Ensemble Solutions and 2-D Oscillators . . . . .	161
4.5	Applications and Future Work . . . . .	162
<b>5</b>	<b>The Star Coherence Representation</b>	<b>164</b>
5.1	Star Coherence Identity . . . . .	165
5.2	Derivation of Star Coherence Equations of Motion . . . . .	167
5.2.1	Population Equation of Motion . . . . .	168
5.2.2	Phase Equation of Motion . . . . .	170
5.3	Special Cases and Approximations . . . . .	185
5.3.1	Noncyclic Nearest Neighbor: 2LS - Factorization . . . . .	185
5.3.2	The 2 Level System and Semiclassical Truncation . . . . .	187
5.4	Discussion . . . . .	189
5.5	Applications and Future Work . . . . .	191
<b>6</b>	<b>Moyal Assisted Dynamics and Hudson Density Estimation</b>	<b>194</b>
6.1	Single Hudson Density Estimation: Harmonic . . . . .	195
6.2	Single Hudson Density Estimation: Morse . . . . .	201
6.3	$K$ -Hudson Density Estimation Algorithm . . . . .	205
6.4	Discussion . . . . .	211
6.5	Applications and Future Work . . . . .	214
<b>7</b>	<b>Conclusion</b>	<b>215</b>
	<b>Bibliography</b>	<b>218</b>
	<b>Appendix A Star Product Identities and Truncations</b>	<b>229</b>
	<b>Appendix B Star Product of Two Gaussian Weyl Symbols</b>	<b>234</b>

# LIST OF FIGURES

	Page
1.1 Quantum versus classical orbits. (a) Bohr model of the atom with discrete orbits. (b) Classical orbits of planetary motion. . . . .	4
1.2 Quantum state transitions. (a) The Bohr frequency for absorption and emission of a photon $h\nu$ of radiation. (b) A quantum system with two state manifold containing several internal states. The latter is typical of two electronic states $G$ and $E$ containing a set of vibrational states $g_n$ and $e_n$ . . . . .	6
1.3 Sum of two waves (red and blue) and their resulting superposition (purple). (a) A constructive coherent superposition. (b) A destructive coherent superposition. (c) A partially coherent superposition. . . . .	7
1.4 The double slit experiment for a quantum particle. Probability distribution for slit 1 opened (blue). Probability distribution for slit 2 opened (red). Quantum probability distribution for both slits opened (purple). Classical probability distribution for both slits opened (dashed purple). . . . .	9
1.5 A classical bit and a qubit. . . . .	13
1.6 Growth of various complexity classes with respect to dimension $N$ . . . . .	18
1.7 Internal coordinates of a molecule with 2 nuclei and 2 electrons. . . . .	21
1.8 Position vector complexity graphs for various molecules. . . . .	22
1.9 Nonadiabatic mixed quantum-classical methods. (a) Ehrenfest. (b) Surface Hopping. (c) Spawning/Cloning. . . . .	29
1.10 Path integral interpretation of semiclassical theories. . . . .	32
2.1 Evolution of a harmonic oscillator in phase space (left to right, top to bottom). Hamiltonian vector field $X_H$ (black arrows). State of the system $(q(t'), p(t'))$ (green dot). Trajectory $(q(t), p(t))$ (light green curve). . . . .	54
2.2 Example of incompressible Hamiltonian flow. Trajectories emanating from different initial conditions maintain their distance apart in phase space. . . .	56
2.3 Evolution of a trajectory ensemble for the harmonic oscillator in phase space (left to right, top to bottom). Hamiltonian vector field $X_H$ (black arrows). State of the ensemble $(q(t'), p(t'))$ (green swarm). Mean trajectory $(q(t), p(t))$ (light green curve). . . . .	58
3.1 A Wigner function contains the marginals $ \psi(q) ^2$ and $ \phi(p) ^2$ as projections in phase space along the $q$ and $p$ axes. . . . .	70



3.2	Example of two orthogonal Wigner functions for the harmonic oscillator. Ground state (blue). First excited state (red). Wavefunctions (top). Wigner functions (bottom). The ground state Wigner function is positive-definite. The first excited state is not positive definite. . . . .	72
3.3	The symplectic phase space volume element of the integral representation of the star product. . . . .	82
3.4	(a) Statistical parametrization of a Hudson state Wigner function. (b) Examples of Hudson states generated by squeeze $\hat{S}$ and displacement $\hat{D}$ of the harmonic oscillator ground state. . . . .	98
4.1	(a) Displaced oscillator model for electronic states $j = 1, 2$ and a nuclear coordinate $q$ . (b) Franck-Condon excitation of the displaced oscillator by an ultrafast laser pulse. . . . .	104
4.2	Coherence correlation function for Telluride I (Initialization I) calculated by Thawed Moyal Dynamics (Moyal). . . . .	120
4.3	Linear absorption spectrum for Telluride I (Initialization I) calculated by Thawed Moyal Dynamics (Moyal). . . . .	120
4.4	Phase space portraits for $\text{Re}(\rho_{12}(q, p, t))$ for Telluride I (Initialization I) calculated by Thawed Moyal Dynamics (Moyal). Time increasing left-to-right, top-to-bottom ( $t = 0, t = \tau_M/4, t = \tau_M/2, t = 3\tau_M/4, t = \tau_M, t = 4\tau_M$ ) for vibrational period $\tau_M$ . Ground state orbit: $(Q_1(t), P_1(t))$ (blue). Excited state orbit: $(Q_2(t), P_2(t))$ (red). Coherence orbit: $(Q(t), P(t))$ (purple). Coherence mean (black). . . . .	121
4.5	Coherence correlation function for Telluride I (Initialization I) calculated by Thawed Moyal Dynamics (Linearized Moyal). . . . .	122
4.6	Linear absorption spectrum for Telluride I (Initialization I) calculated by Thawed Moyal Dynamics (Linearized Moyal). . . . .	122
4.7	Phase space portraits for $\text{Re}(\rho_{12}(q, p, t))$ for Telluride I (Initialization I) calculated by Thawed Moyal Dynamics (Linearized Moyal). Time increasing left-to-right, top-to-bottom ( $t = 0, t = \tau_M/4, t = \tau_M/2, t = 3\tau_M/4, t = \tau_M, t = 4\tau_M$ ) for vibrational period $\tau_M$ . Ground state orbit: $(Q_1(t), P_1(t))$ (blue). Excited state orbit: $(Q_2(t), P_2(t))$ (red). Coherence orbit: $(Q(t), P(t))$ (purple). Coherence mean (black). . . . .	123
4.8	Coherence correlation function for Telluride I (Initialization I) calculated by Thawed Moyal Dynamics (Semiclassical). . . . .	124
4.9	Linear absorption spectrum for Telluride I (Initialization I) calculated by Thawed Moyal Dynamics (Semiclassical). . . . .	124
4.10	Phase space portraits for $\text{Re}(\rho_{12}(q, p, t))$ for Telluride I (Initialization I) calculated by Thawed Moyal Dynamics (Semiclassical). Time increasing left-to-right, top-to-bottom ( $t = 0, t = \tau_{SC}/4, t = \tau_{SC}/2, t = 3\tau_M/4, t = \tau_{SC}, t = 4\tau_{SC}$ ) for vibrational period $\tau_{SC}$ . Ground state orbit: $(Q_1(t), P_1(t))$ (blue). Excited state orbit: $(Q_2(t), P_2(t))$ (red). Coherence orbit: $(Q(t), P(t))$ (green). Coherence mean (black). . . . .	125
4.11	Coherence correlation function for Telluride I (Initialization I) calculated by Thawed Moyal Dynamics (Linearized Semiclassical). . . . .	126

4.12	Linear absorption spectrum for Telluride I (Initialization I) calculated by Thawed Moyal Dynamics (Linearized Semiclassical). . . . .	126
4.13	Phase space portraits for $\text{Re}(\rho_{12}(q, p, t))$ for Telluride I (Initialization I) calculated by Thawed Moyal Dynamics (Linearized Semiclassical). Time increasing left-to-right, top-to-bottom ( $t = 0, t = \tau_{SC}/4, t = \tau_{SC}/2, t = 3\tau_M/4, t = \tau_{SC}, t = 4\tau_{SC}$ ) for vibrational period $\tau_{SC}$ . Ground state orbit: $(Q_1(t), P_1(t))$ (blue). Excited state orbit: $(Q_2(t), P_2(t))$ (red). Coherence orbit: $(Q(t), P(t))$ (green). Coherence mean (black). . . . .	127
4.14	Coherence correlation function for Telluride I (Initialization I) calculated by Semiclassical Thawed Moyal Dynamics (black) compared with Semiclassical trajectory ensemble (green) for $\mathcal{N} = 1000$ . . . . .	129
4.15	Linear absorption spectrum for Telluride I (Initialization I) calculated by Semiclassical Thawed Moyal Dynamics (black) compared with Semiclassical trajectory ensemble (green) for $\mathcal{N} = 1000$ . . . . .	129
4.16	Phase space portraits for $\text{Re}(\rho_{12}(q, p, t))$ for Telluride I (Initialization I) calculated by Semiclassical Thawed Moyal Dynamics (black) compared with Semiclassical trajectory ensemble (green) for $\mathcal{N} = 2500$ . Time increasing left-to-right, top-to-bottom ( $t = 0, t = \tau_{SC}/4, t = \tau_{SC}/2, t = 3\tau_M/4, t = \tau_{SC}, t = 4\tau_{SC}$ ) for vibrational period $\tau_{SC}$ . Ground state orbit: $(Q_1(t), P_1(t))$ (blue). Excited state orbit: $(Q_2(t), P_2(t))$ (red). Coherence orbit: $(Q(t), P(t))$ (green). Coherence mean (black). . . . .	130
4.17	Coherence correlation function for Telluride I (Initialization I) calculated by Linearized Semiclassical Thawed Moyal Dynamics (black) compared with Linearized Semiclassical trajectory ensemble (light green) for $\mathcal{N} = 1000$ . . . . .	131
4.18	Linear absorption spectrum for Telluride I (Initialization I) calculated by Linearized Semiclassical Thawed Moyal Dynamics (black) compared with Linearized Semiclassical trajectory ensemble (light green) for $\mathcal{N} = 1000$ . . . . .	131
4.19	Phase space portraits for $\text{Re}(\rho_{12}(q, p, t))$ for Telluride I (Initialization I) calculated by Linearized Semiclassical Thawed Moyal Dynamics (black) compared with Linearized Semiclassical trajectory ensemble (green) for $\mathcal{N} = 2500$ . Time increasing left-to-right, top-to-bottom ( $t = 0, t = \tau_{SC}/4, t = \tau_{SC}/2, t = 3\tau_M/4, t = \tau_{SC}, t = 4\tau_{SC}$ ) for vibrational period $\tau_{SC}$ . Ground state orbit: $(Q_1(t), P_1(t))$ (blue). Excited state orbit: $(Q_2(t), P_2(t))$ (red). Coherence orbit: $(Q(t), P(t))$ (light green). Coherence mean (black). . . . .	132
4.20	Coherence correlation function for Telluride I-S (Initialization I) calculated by Thawed Moyal Dynamics (Moyal). . . . .	133
4.21	Linear absorption spectrum for Telluride I-S (Initialization I) calculated by Thawed Moyal Dynamics (Moyal). . . . .	134
4.22	Phase space portraits for $\text{Re}(\rho_{12}(q, p, t))$ for Telluride I-S (Initialization I) calculated by Thawed Moyal Dynamics (Moyal). Time increasing left-to-right, top-to-bottom ( $t = 0, t = \tau_M/4, t = \tau_M/2, t = 3\tau_M/4, t = \tau_M, t = 4\tau_M$ ) for vibrational period $\tau_M$ . Ground state orbit: $(Q_1(t), P_1(t))$ (blue). Excited state orbit: $(Q_2(t), P_2(t))$ (red). Coherence orbit: $(Q(t), P(t))$ (purple). Coherence mean (black). . . . .	134

4.23	Coherence correlation function for Telluride I-S (Initialization I) calculated by Thawed Moyal Dynamics (Linearized Semiclassical). . . . .	135
4.24	Linear absorption spectrum for Telluride I-S (Initialization I) calculated by Thawed Moyal Dynamics (Linearized Semiclassical). . . . .	135
4.25	Phase space portraits for $\text{Re}(\rho_{12}(q, p, t))$ for Telluride I-S (Initialization I) calculated calculated by Thawed Moyal Dynamics (Linearized Semiclassical). Time increasing left-to-right, top-to-bottom ( $t = 0, t = \tau_{SC}/4, t = \tau_{SC}/2, t = 3\tau_M/4, t = \tau_{SC}, t = 4\tau_{SC}$ ) for vibrational period $\tau_{SC}$ . Ground state orbit: $(Q_1(t), P_1(t))$ (blue). Excited state orbit: $(Q_2(t), P_2(t))$ (red). Coherence orbit: $(Q(t), P(t))$ (green). Coherence mean (black). . . . .	136
4.26	Coherence correlation function for Telluride I (Initialization II) calculated by Thawed Moyal Dynamics (Moyal). . . . .	138
4.27	Linear absorption spectrum for Telluride I (Initialization II) calculated by Thawed Moyal Dynamics (Moyal). . . . .	138
4.28	Phase space portraits for $\text{Re}(\rho_{12}(q, p, t))$ for Telluride I (Initialization II) calculated calculated by Thawed Moyal Dynamics (Moyal). Time increasing left-to-right, top-to-bottom ( $t = 0, t = \tau_M/4, t = \tau_M/2, t = 3\tau_M/4, t = \tau_M, t = 4\tau_M$ ) for vibrational period $\tau_M$ . Ground state orbit: $(Q_1(t), P_1(t))$ (blue). Excited state orbit: $(Q_2(t), P_2(t))$ (red). Coherence orbit: $(Q(t), P(t))$ (purple). Coherence mean (black). . . . .	139
4.29	Coherence correlation function for Telluride I (Initialization II) calculated by Thawed Moyal Dynamics (Linearized Semiclassical). . . . .	139
4.30	Linear absorption spectrum for Telluride I (Initialization II) calculated by Thawed Moyal Dynamics (Linearized Semiclassical). . . . .	140
4.31	Phase space portraits for $\text{Re}(\rho_{12}(q, p, t))$ for Telluride I (Initialization II) calculated calculated by Thawed Moyal Dynamics (Linearized Semiclassical). Time increasing left-to-right, top-to-bottom ( $t = 0, t = \tau_{SC}/4, t = \tau_{SC}/2, t = 3\tau_M/4, t = \tau_{SC}, t = 4\tau_{SC}$ ) for vibrational period $\tau_{SC}$ . Ground state orbit: $(Q_1(t), P_1(t))$ (blue). Excited state orbit: $(Q_2(t), P_2(t))$ (red). Coherence orbit: $(Q(t), P(t))$ (green). Coherence mean (black). . . . .	140
4.32	Coherence correlation function for Telluride II (Initialization III) with 1 : 1 resonance calculated by Thawed Moyal Dynamics (Moyal). . . . .	143
4.33	Linear absorption spectrum for Telluride II (Initialization III) with 1 : 1 calculated by Thawed Moyal Dynamics (Moyal). . . . .	143
4.34	Phase space portraits for $\text{Re}(\rho_{12}(q, p, t))$ for Telluride II (Initialization III) with 1 : 1 resonance calculated by Thawed Moyal Dynamics (Moyal). Time increasing left-to-right, top-to-bottom ( $t = 0, t = \tau_M/4, t = \tau_M/2, t = 3\tau_M/4, t = \tau_M, t = 4\tau_M$ ) for vibrational period $\tau_M$ . Ground state orbit: $(Q_1(t), P_1(t))$ (blue). Excited state orbit: $(Q_2(t), P_2(t))$ (red). Coherence orbit: $(Q(t), P(t))$ (purple). Coherence mean (black). . . . .	144
4.35	Coherence correlation function for Telluride II (Initialization III) with 1 : 1 resonance calculated by Thawed Moyal Dynamics (Linearized Semiclassical). . . . .	145
4.36	Linear absorption spectrum for Telluride II (Initialization III) with 1 : 1 resonance calculated by Thawed Moyal Dynamics (Linearized Semiclassical). . . . .	145

4.37	Phase space portraits for $\text{Re}(\rho_{12}(q, p, t))$ for Telluride II (Initialization III) with 1 : 1 resonance calculated by Thawed Moyal Dynamics (Linearized Semiclassical). Time increasing left-to-right, top-to-bottom ( $t = 0, t = \tau_{SC}/4, t = \tau_{SC}/2, t = 3\tau_M/4, t = \tau_{SC}, t = 4\tau_{SC}$ ) for vibrational period $\tau_{SC}$ . Ground state orbit: $(Q_1(t), P_1(t))$ (blue). Excited state orbit: $(Q_2(t), P_2(t))$ (red). Coherence orbit: $(Q(t), P(t))$ (green). Coherence mean (black). . . . .	146
4.38	Coherence correlation function for Telluride II (Initialization III) with 2 : 1 resonance calculated by Thawed Moyal Dynamics (Moyal). . . . .	147
4.39	Linear absorption spectrum for Telluride II (Initialization III) with 2 : 1 calculated by Thawed Moyal Dynamics (Moyal). . . . .	147
4.40	Phase space portraits for $\text{Re}(\rho_{12}(q, p, t))$ for Telluride II (Initialization III) with 2 : 1 resonance calculated by Thawed Moyal Dynamics (Moyal). Time increasing left-to-right, top-to-bottom ( $t = 0, t = \tau_M/4, t = \tau_M/2, t = 3\tau_M/4, t = \tau_M, t = 4\tau_M$ ) for vibrational period $\tau_M$ . Ground state orbit: $(Q_1(t), P_1(t))$ (blue). Excited state orbit: $(Q_2(t), P_2(t))$ (red). Coherence orbit: $(Q(t), P(t))$ (purple). Coherence mean (black). . . . .	148
4.41	Coherence correlation function for Telluride II (Initialization III) with 2 : 1 resonance calculated by Thawed Moyal Dynamics (Linearized Semiclassical). . . . .	149
4.42	Linear absorption spectrum for Telluride II (Initialization III) with 2 : 1 resonance calculated by Thawed Moyal Dynamics (Linearized Semiclassical). . . . .	149
4.43	Phase space portraits for $\text{Re}(\rho_{12}(q, p, t))$ for Telluride II (Initialization III) with 2 : 1 resonance calculated by Thawed Moyal Dynamics (Linearized Semiclassical). Time increasing left-to-right, top-to-bottom ( $t = 0, t = \tau_{SC}/4, t = \tau_{SC}/2, t = 3\tau_M/4, t = \tau_{SC}, t = 4\tau_{SC}$ ) for vibrational period $\tau_{SC}$ . Ground state orbit: $(Q_1(t), P_1(t))$ (blue). Excited state orbit: $(Q_2(t), P_2(t))$ (red). Coherence orbit: $(Q(t), P(t))$ (green). Coherence mean (black). . . . .	150
4.44	Coherence correlation function for Telluride II (Initialization III) with 1 : $\sqrt{2}$ resonance calculated by Thawed Moyal Dynamics (Moyal). . . . .	151
4.45	Linear absorption spectrum for Telluride II (Initialization III) with 1 : $\sqrt{2}$ calculated by Thawed Moyal Dynamics (Moyal). . . . .	151
4.46	Phase space portraits for $\text{Re}(\rho_{12}(q, p, t))$ for Telluride II (Initialization III) with 1 : $\sqrt{2}$ resonance calculated by Thawed Moyal Dynamics (Moyal). Time increasing left-to-right, top-to-bottom ( $t = 0, t = \tau_M/4, t = \tau_M/2, t = 3\tau_M/4, t = \tau_M, t = 4\tau_M$ ) for vibrational period $\tau_M$ . Ground state orbit: $(Q_1(t), P_1(t))$ (blue). Excited state orbit: $(Q_2(t), P_2(t))$ (red). Coherence orbit: $(Q(t), P(t))$ (purple). Coherence mean (black). . . . .	152
4.47	Coherence correlation function for Telluride II (Initialization III) with 1 : $\sqrt{2}$ resonance calculated by Thawed Moyal Dynamics (Linearized Semiclassical). . . . .	153
4.48	Linear absorption spectrum for Telluride II (Initialization III) with 1 : $\sqrt{2}$ resonance calculated by Thawed Moyal Dynamics (Linearized Semiclassical). . . . .	153

4.49	Phase space portraits for $\text{Re}(\rho_{12}(q, p, t))$ for Telluride II (Initialization III) with $1 : \sqrt{2}$ resonance calculated by Thawed Moyal Dynamics (Linearized Semiclassical). Time increasing left-to-right, top-to-bottom ( $t = 0, t = \tau_{SC}/4, t = \tau_{SC}/2, t = 3\tau_M/4, t = \tau_{SC}, t = 4\tau_{SC}$ ) for vibrational period $\tau_{SC}$ . Ground state orbit: $(Q_1(t), P_1(t))$ (blue). Excited state orbit: $(Q_2(t), P_2(t))$ (red). Coherence orbit: $(Q(t), P(t))$ (green). Coherence mean (black). . . . .	154
4.50	Cat-jjectory and zombie cat. The average orbits of the quantum coherence follow a cat-jjectory modulated by each state's frequency whereas semiclassically approximated coherence follows an average frequency orbit or zombie cat. . .	156
4.51	Examples of cat-jjectory trochoid orbits of the quantum coherence. . . . .	157
4.52	Example of preservation of the minimum uncertainty volume in real and imaginary phase spaces for Telluride I (Initialization I) calculated by the Thawed Moyal Dynamics quantum solution. . . . .	159
5.1	Example of a noncyclic nearest neighbor Hamiltonian. . . . .	186
5.2	(a) Liouville space picture for third order response function. (b) One of eight paths and propagation scheme in the Star Coherence Representation. . . . .	193
6.1	Comparison of coherence correlation function for Telluride I (Initialization I) calculated by Moyal Assisted Dynamics - Single Hudson Density Estimation for $\mathcal{N} = 1000$ (orange) with and exact quantum Thawed Moyal Dynamics (purple). . . . .	199
6.2	Comparison of linear absorption spectrum for Telluride I (Initialization I) calculated by Moyal Assisted Dynamics - Single Hudson Density Estimation for $\mathcal{N} = 1000$ (orange) with and exact quantum Thawed Moyal Dynamics (black). . . . .	199
6.3	Phase space portraits for $\text{Re}(\rho_{12}(q, p, t))$ for Telluride I (Initialization I) calculated by Moyal Assisted Dynamics - Single Hudson Density Estimation for $\mathcal{N} = 1000$ . Time increasing left-to-right, top-to-bottom ( $t = 0, t = \tau_M/4, t = \tau_M/2, t = 3\tau_M/4, t = \tau_M, t = 4\tau_M$ ) for vibrational period $\tau_M$ . Ground state orbit: $(Q_1(t), P_1(t))$ (blue). Excited state orbit: $(Q_2(t), P_2(t))$ (red). Coherence orbit: $(Q(t), P(t))$ (purple). Coherence mean (black). . . . .	200
6.4	Comparison of coherence correlation function for Telluride I-M ( $D_2 = 1$ , Initialization I) calculated by Moyal Assisted Dynamics - Single Hudson Density Estimation (orange) for $\mathcal{N} = 1000$ with Thawed Moyal Dynamics for the harmonic fit (purple). . . . .	201
6.5	Comparison of linear absorption spectrum for Telluride I-M ( $D_2 = 1$ , Initialization I) calculated by Moyal Assisted Dynamics - Single Hudson Density Estimation (orange) for $\mathcal{N} = 1000$ with Thawed Moyal Dynamics for the harmonic fit (black). . . . .	202

6.6	Phase space portraits for $\text{Re}(\rho_{12}(q, p, t))$ for Telluride I-M ( $D_2 = 1$ , Initialization I) calculated by Moyal Assisted Dynamics - Single Hudson Density Estimation for $\mathcal{N} = 1000$ . Time increasing left-to-right, top-to-bottom ( $t = 0, t = \tau_M/4, t = \tau_M/2, t = 3\tau_M/4, t = \tau_M, t = 4\tau_M$ ) for vibrational period $\tau_M$ . Ground state orbit: $(Q_1(t), P_1(t))$ (blue). Excited state orbit: $(Q_2(t), P_2(t))$ (red). Coherence orbit: $(Q(t), P(t))$ (purple). Coherence mean (black). . . .	202
6.7	Comparison of coherence correlation function for Telluride I-M ( $D_2 = 0.1$ , Initialization I) calculated by Moyal Assisted Dynamics - Single Hudson Density Estimation (orange) for $\mathcal{N} = 1000$ with Thawed Moyal Dynamics for the harmonic fit (purple). . . . .	203
6.8	Comparison of linear absorption spectrum for Telluride I-M ( $D_2 = 0.1$ , Initialization I) calculated by Moyal Assisted Dynamics - Single Hudson Density Estimation (orange) for $\mathcal{N} = 1000$ with Thawed Moyal Dynamics for the harmonic fit (black). . . . .	203
6.9	Phase space portraits for $\text{Re}(\rho_{12}(q, p, t))$ for Telluride I-M ( $D_2 = 0.1$ , Initialization I) calculated by Moyal Assisted Dynamics - Single Hudson Density Estimation for $\mathcal{N} = 1000$ . Time increasing left-to-right, top-to-bottom ( $t = 0, t = \tau_M/4, t = \tau_M/2, t = 3\tau_M/4, t = \tau_M, t = 4\tau_M$ ) for vibrational period $\tau_M$ . Ground state orbit: $(Q_1(t), P_1(t))$ (blue). Excited state orbit: $(Q_2(t), P_2(t))$ (red). Coherence orbit: $(Q(t), P(t))$ (purple). Coherence mean (black). . . .	204
6.10	Comparison of clustering algorithms for sample trajectory swarms of Morse oscillator. . . . .	208
6.11	Phase space portraits for $\text{Re}(\rho_{12}(q, p, t))$ for Telluride I-M ( $D_2 = 0.1$ , Initialization I) calculated by Moyal Assisted Dynamics - K-Means Hudson Density Estimation for $\mathcal{N} = 1000$ . Time increasing left-to-right, top-to-bottom ( $t = 0, t = \tau_M/4, t = \tau_M/2, t = 3\tau_M/4, t = \tau_M, t = 4\tau_M$ ) for vibrational period $\tau_M$ . Ground state orbit: $(Q_1(t), P_1(t))$ (blue). Excited state orbit: $(Q_2(t), P_2(t))$ (red). Coherence orbit: $(Q(t), P(t))$ (purple). Coherence mean (black). . . .	210
6.12	von Neumann Lattice of coherent states in phase space. . . . .	212

# LIST OF TABLES

	Page
1.1 Quantum transitions and regimes of classical radiation corresponding to their transition frequency by frequency, wavelength, and energy per photon. . . . .	6
3.1 Comparison of Quantum mechanics in Hilbert space and the Wigner-Moyal Representation. . . . .	63
4.1 System Parameters (Telluride I) for displaced oscillator model in atomic units.	119
4.2 Initialization parameters for displaced oscillator model in atomic units. . . . .	119
4.3 System Parameters (Telluride I-S) for displaced oscillator model in atomic units.	133
4.4 Initialization parameters for “hot band” displaced oscillator model in atomic units. . . . .	137
4.5 System Parameters (Telluride II) for 2-D displaced oscillator model in atomic units. . . . .	141
4.6 Initialization parameters for 2-D displaced oscillator model in atomic units. . . . .	142
6.1 K-Hudson Cluster Density Estimation benchmark for various cluster algorithms. Run time (seconds), memory (megabytes), number of clusters, and conditional entropy of one fit averaged over training set. . . . .	209

# LIST OF SYMBOLS

$\{ \}$	Set
$x \in \{ \}$	Element $x$ of the set $\{ \}$
$x \in [a, b]$	Element $x$ of the interval $a \leq x \leq b$
$\mathbb{Z}$	Set of integer numbers
$\mathbb{R}$	Set of real numbers
$\mathbb{C}$	Set of complex numbers
$\mathbb{R}_{\geq 0}$	Set of positive real numbers including zero
$\mathbb{R}_{> 0}$	Set of positive real numbers
$\mathcal{O}(\cdot)$	To order of or complexity class
$\text{Re}(z)$	Real part of complex quantity $z$
$\text{Im}(z)$	Imaginary part of complex quantity $z$
$\text{Abs}(z)$ or $ z $	Absolute magnitude of complex quantity $z$
$\bar{z}$ or $z^*$	Complex conjugate complex quantity $z$
$\mathbf{x}$	Vector $\mathbf{x}$
$\mathbf{X}$	Matrix $\mathbf{X}$
$\mathbf{X}^T$	Transpose of matrix $\mathbf{X}$
$\mathbf{X}^{-1}$	Inverse of matrix $\mathbf{X}$
$\det(\mathbf{X})$	Determinant of matrix $\mathbf{X}$
$\mathbf{1}_N$	$N \times N$ Identity matrix
$\mathbf{0}_N$	$N \times N$ Zero matrix
$\mathbf{J}$	$2N \times 2N$ Symplectic structure matrix
$\text{Tr}(A)$	Trace of quantity $A$
$\hat{A}$	Operator $\hat{A}$
$\hat{A}^\dagger$	Hermitian adjoint of operator $\hat{A}$
$[\hat{A}, \hat{B}]$	Commutator of operators $\hat{A}$ and $\hat{B}$
$\{\hat{A}, \hat{B}\}$	Anticommutator of matrices $\hat{A}$ and $\hat{B}$
$a \star b$	Star (Moyal) product of functions $a$ and $b$
$[a, b]$	Poisson bracket of functions $a$ and $b$
$[a, b]_\star$	Moyal (Sine) bracket of functions $a$ and $b$
$[a, b]_n$	Poisson bivector of functions $a$ and $b$ truncated to $\mathcal{O}(\hbar^n)$
$\{a, b\}_\star$	Baker (Cosine) bracket of functions $a$ and $b$



# ACKNOWLEDGMENTS

Dissertations are the capstone of graduate work. Given my length of time in graduate school, it follows that I have many people to thank and without whom, this thesis could hardly have been started, let alone completed.

In chronological order, I would like to thank the faculty of Penn State’s Geoscience department. In particular, Peter Heaney and Maureen Feineman, who gave me many research opportunities and nurtured my scientific curiosity during those formative undergrad years. Even after I switched fields of study from geology to chemistry, Profs. Heaney and Feineman continued to advise me and advocate for my academic success. I would like to thank Thomas Cundari of the University of North Texas. He was my mentor for a National Science Foundation Research Experience for Undergraduates internship. The REU experience solidified my desire to go to graduate school. I owe so much to James B. Anderson, — or as I called him, “The Count of Monte Carlo”. As my research advisor in chemistry, Jim taught me a wealth about kinetics and quantum mechanics, their history, and science as a profession. Whether hosting dinners at his home with his lovely wife or coming into lab on Saturdays to run some calculations together, his spirit and generosity had a profound impact on me. Jim passed in 2021, but his kindness, contributions to science, and character, no one will forget.

Cornell was a wonderful place to learn theory and begin grad school. I grateful for the opportunities provided by my research chair, Nandini Ananth and my committee members, Roger Loring and Greg Ezra. Professor Ezra, I would like to thank especially. He continued to encourage me long after my time at Cornell. He was instrumental in the decision to come to UC Irvine to finish my graduate studies. This thesis is inspired by his scholarship and expertise in phase space dynamics.

At UCI, I’ve had many wonderful mentors. Foremost, I would like to thank my advisor, Craig Martens. Craig’s creativity and scientific prowess, is only exceeded by his friendliness. His humor is contagious and often takes a turn for the self-deprecating. On more than one occasion Craig has likened himself to Don Quixote, “chasing after windmills,” in chemical physics. If that’s the case, its been a fun “misadventure” serving as his Sancho. Craig, in short, has been a wellspring of knowledge and encouragement. Not a moment was wasted in our diversions. He and his wife, Becky, have shown my wife and me, far more hospitable than the traditional PI-grad student relationship solicits.

Shaul Mukamel has also had indelible role in my research at UCI. Shaul is known by many as pioneer in nonlinear spectroscopy, —a sort of modern day Sommerfeld, motivated by physics as a measurable science. He has also has been a wonderful mentor. His focus has helped me tremendously, often curbing the excesses of my research habits. It is easy to get lost in formalism, but Shaul was able to steer me in productive direction with his questions. In the same vein, I would like to thank my mentor Sergei Tretiak of Los Alamos National Laboratory. He was a welcoming host during my time at LANL and the Center for Integrated Nanotechnologies. His guidance helped not lose sight of research objectives and concrete problems.

In my personal life, I owe everything to my family and friends. I would like to thank my parents, sisters, and remarkable wife, Soyeon (and our cat, Ariel). They've supported me through the ups and downs of this journey. Likewise, I'd like to remember my friends back home in Pittsburgh and my church brothers in Orange County: Nick, Max, Evan, Kyle, Josh, Scott, Kelly, and Yef. Your friendship carried me and has been a blessing.

Lastly, I would like to thank all the sources of financial contribution that made research possible: the UCI-School of Physical Sciences Los Alamos National Lab Fellowship sponsored by LANL and the UC SoCal HUB, the Division of Teaching Initiative Fellowship from UCI's DTEI, the UCI Chemistry Department's Dissertation Fellowship, and the Brython Davis Fellowship provided by Brython Parry Davis Trust. Without these, I wouldn't have had the time and resources to complete this work.

# VITA

Austin Tyler Green

## EDUCATION

<b>Doctor of Philosophy in Chemistry</b>	<b>2024</b>
University of California, Irvine	<i>Irvine, CA</i>
<b>Master of Science in Chemistry</b>	<b>2016</b>
Cornell University	<i>Ithaca, NY</i>
<b>Bachelor of Science in Chemistry</b>	<b>2014</b>
The Pennsylvania State University	<i>University Park, PA</i>

## AWARDS

<b>Wolfsberg Award in Theoretical Chemistry</b>	<b>2024</b>
University of California, Irvine	
<b>Brython Davis Fellowship</b>	<b>2024</b>
University of California	
<b>UCI-LANL Graduate Fellowship</b>	<b>2023</b>
University of California, Irvine / Los Alamos National Lab	
<b>Graduate Dissertation Fellowship</b>	<b>2023</b>
Department of Chemistry, University of California, Irvine	
<b>Contributions to Teaching Award</b>	<b>2021</b>
Department of Chemistry, University of California, Irvine	
<b>Division of Teaching Excellence Initiative Fellowship</b>	<b>2020</b>
University of California, Irvine	
<b>UC Cuba Research and Travel Fellowship</b>	<b>2019</b>
University of California	
<b>NSF Research Experience for Undergraduate Fellowship</b>	<b>2013</b>
University of North Texas	
<b>Ellis George Scholarship</b>	<b>2012</b>
College of Earth and Mineral Sciences, The Pennsylvania State University	
<b>Hedberg Scholarship</b>	<b>2012</b>
Department of Geosciences, The Pennsylvania State University	
<b>Teas Scholarship</b>	<b>2011</b>
College of Earth and Mineral Sciences, The Pennsylvania State University	

## RESEARCH EXPERIENCE

<b>Graduate Research Assistant</b> Department of Chemistry, University of California, Irvine	<b>2019–2024</b> <i>Irvine, CA</i>
<b>Production Chemist</b> RokaBio, Institute for Environmental Health Inc.	<b>2018–2019</b> <i>Kent, WA</i>
<b>Graduate Research Assistant</b> Department of Chemistry & Chemical Biology, Cornell University	<b>2014–2018</b> <i>Ithaca, NY</i>
<b>REU Intern</b> University of North Texas	<b>2013</b> <i>Denton, TX</i>

## TEACHING EXPERIENCE

<b>University of California, Irvine</b>	
CHEM 132B : Quantum Principles	<i>W '24, W '20</i>
CHEM 231A : Fundamentals of Quantum Mechanics	<i>F '23, F '22, F '21</i>
CHEM 5 : Mathematical and Scientific Computing	<i>Su '22, W '22, F '20, F '19</i>
CHEM 1A : General Chemistry	<i>Su '22</i>
CHEM 232A : Thermodynamics and Intro. to Stat. Mech.	<i>W '21, W '23</i>
CHEM 132C: Molecular Structure	<i>Sp '20</i>
<b>Cornell University</b>	
CHEM 3900 : Honors Physical Chemistry II	<i>F '16, F '15</i>
CHEM 3890 : Honors Physical Chemistry I	<i>F '15, F '14</i>
CHEM 2870 : Introductory Physical Chemistry	<i>F '14</i>

## PUBLICATIONS

A First Principles Derivation of Energy Conserving Momentum Jumps in Surface Hopping Simulations. D. Huang, A.T. Green, and C.C. Martens. *J. Chem. Phys.* 159, 214108 (2023). Editors Pick.

Zombie Cats on the Quantum-Classical Frontier. A.T. Green and C.C. Martens. *J. Chem. Phys.* 159, 204102 (2023).

## CONFERENCES

Moyal-Assisted Dynamics: Estimating Molecular Quantum Coherences from Classical Ensembles. A.T. Green. Challenge Institute for Quantum Computation and Institute of Pure and Applied Mathematics' Winter School on Quantum Information Science for Chemistry, Los Angeles, CA. 02/20/24. Poster Presentation.

Moyal-Assisted Dynamics: Quantum Coherences from Classical Trajectories. A.T. Green. Non-equilibrium Phenomena, Nonadiabatic Dynamics and Spectroscopy Workshop, Telluride, CO. 10/2/23. Invited Talk.

Quantum Coherence from Classical Ingredients: High-Fidelity Dynamics for Chemistry and Spectroscopy. A.T. Green. UC Chemistry Symposium, Lake Arrowhead, CA. 04/23/23. Platform Talk. Best in Physical Division.

Wavepackets Calculations for Coherence Dynamics. A.T. Green. Excited State and Nonadiabatic Dynamics Cybertraining. State University of New York, Buffalo, Remote. 06/26/21. Oral Presentation. 3rd Prize.

Zombie Cats: Quantum Phase Space Corrections for Time-dependent Spectroscopy. A.T. Green. UC Chemistry Symposium, Remote. 03/3/21. Platform Talk.

The Short-time Limit of Mapping Variable Ring Polymer Molecular Dynamics. A.T. Green and N. Ananth. Faraday Discussion: Reaction Rate Theory, Cambridge, UK. 09/19/16. Poster Presentation.

A Modern View of IH+HI Kinetics. A.T. Green and J.B. Anderson. 247th ACS National Meeting & Exposition, Dallas, TX. 03/16/14. Oral Presentation.

H<sub>2</sub> Activation by PdO: The Oxo Ligand Utility. A.T. Green, G. Schoendorff, and T.R. Cundari. 247th ACS National Meeting & Exposition, Dallas, TX. 03/16/14. Poster Presentation.

PdO + H<sub>2</sub>: An Ab Initio Study. A.T. Green, ACS Central Pennsylvania Chapter Undergraduate Research Symposium, University Park, PA. 09/19/13. Poster Presentation.

# ABSTRACT OF THE DISSERTATION

The Dynamics of Quantum Coherences in Phase Space: Theory and Application to  
Molecular Spectroscopy

By

Austin Tyler Green

Doctor of Philosophy in Chemistry

University of California, Irvine, 2024

Professor Craig C. Martens, Chair

Quantum coherences are phase relations between distinct quantum states responsible for quantum interference. Many emerging technologies in computing, metrology, and energy generation, share the goal of exploiting macroscopic control of quantum coherence to design high-efficiency devices. A central issue in quantum technology is sustaining coherence at scale. While accurate quantum dynamics methods are essential to the design of these materials and the nonlinear spectroscopic techniques used to characterize them, exact quantum solutions for these systems are intractable. What is needed is a quantum dynamics method which approximates coherences accurately, scales sensibly, and has control over the extent of quantumness assumed in the equations of motion. To address this problem, a new phase space quantum dynamics method is developed. Working in the Wigner-Moyal representation, exact solutions to the coherence dynamics of a two-state displaced oscillator and model conical intersection are derived using a Thawed Gaussian ansatz. This Thawed Moyal solution corrects the lower order semiclassical approach traditionally used in time-domain spectroscopy. Using the kinematic insights of the Thawed Moyal theory, a new formalism called the Star Coherence Representation is derived. The Star Coherence Representation solves the unitary evolution of a pure state quantum density entirely in terms of its populations and relative phases, with explicit dependence on the off-diagonal coherences eliminated.

This representation instead constructs quantum coherences on-the-fly in terms of the instantaneous values of the populations and phases. By recasting evolution in terms of population distribution functions, quantum equations of motion to be solved by linearly scaling classical trajectory ensembles which are parallelizable and amenable to statistical estimation through standard techniques of machine learning.

# Chapter 1

## Introduction

Coherence is an intrinsically quantum mechanical phenomenon that has direct macroscopic implications. Recent advances have greatly enhanced our ability to observe coherence in both light and matter ... To realize full control of largescale quantum-coherent systems ... has the potential to revolutionize fields as diverse as information processing, sensor technology, and energy generation through the control of the outcome of chemical reactions or the instantaneous state of a material [1].

---

Hemminger et al., 2015

A field of research is defined by the questions it aims to answer. This thesis belongs to the field of quantum dynamics which asks: —“Given the state of a quantum system, how do the probabilities of particular experimental outcomes or observables change in time?” While this question may seem to be of only narrow academic interest, it’s one of general importance with profound implications for human society and technology.

Specifically this work tries to address, “To what extent can the dynamics of quantum coherences be described using statistics generated by classical trajectory ensembles?” The motivations behind this question are practical and philosophical. While it’s true most quan-



tum technologies share the goal of manipulating quantum coherence for some technological end: computing, communication, transferring information or energy, to describe something “intrinsically quantum mechanical” in terms of classical quantities may appear backwards. It is an attempt to explain something by what it is known not to be.

Though such a research strategy may seem ill-fated, it is in good company. Quantum mechanics, since its inception has been understood and developed by what it stands in contrast to; namely, the direct phenomenological experience of humans through classical physics [2–5]. Strange quantum effects such as zero-point energy, tunneling, exchange, entanglement, and so on, would hardly be interesting exceptions to the rules of classical physics were there not an appreciation of what’s classical in the first place. The concepts and formalism codified into modern quantum theory are a testament to this and coherence is no different.

But a classically inspired framework isn’t just illuminating, it’s useful. Classical trajectories are a preferred device for simulating the dynamics and spectra of complex many-bodied quantum systems like molecules because they are computationally cheap. The decades following the development of quantum theory and scientific computing have been marked by a proliferation of approximate quantum dynamical theories that employ classical(like) trajectory ensembles to emulate quantum dynamics. Methods belonging to this tradition: semiclassical [6–8], mixed quantum-classical [9, 10], and path-integral theories [11, 12] have been demonstrated to capture many quantum effects essential to predicting chemical reaction dynamics and resolving molecular spectra. Despite this, unlike zero-point energy and tunneling, recovering quantum coherence remains a challenge.

While sharing many of the same objectives and philosophy of these schools of approximate theories, this thesis differs in methodology. The Wigner-Moyal [13, 14] or phase space formulation of quantum mechanics is employed. This formulation has many advantages unique to it and is well-suited for constructing quantum dynamics out of classical statistics. Framing the problem of quantum evolution in terms of classical statistics also frees one to employ all

the tools of machine learning and parallelized computing. This makes quantum phase space approach amenable to studying the effect of quantum coherences at scale.

This chapter begins by introducing of some preliminary concepts. After defining quantum mechanics, molecular spectroscopy, and quantum coherence, their applications to quantum technology which broadly motivate research are considered. The following section reviews challenges in quantum molecular dynamics simulations and common approximate theories. The fourth section introduces the two primary methods employed throughout the dissertation: the Wigner-Moyal Representation and time-domain spectroscopy. The chapter concludes with an outline of the work and a brief discussion of typographical conventions assumed throughout the thesis.

## 1.1 Preliminary Concepts

### 1.1.1 Quantum Mechanics

Quantum mechanics is a science of a handful of postulates manipulated by linear algebra [15]. Postulates, by definition, are axioms which cannot be proven. Instead their validation lies in their internal consistency and corroboration with experiment. One of the most important postulates of quantum mechanics and arguably the “most tested” is the Schrödinger equation,

$$i\hbar \frac{d}{dt} |\Psi(t)\rangle = \hat{H} |\Psi(t)\rangle \quad (1.1)$$

where the vector  $|\Psi(t)\rangle$  represents the state of a quantum system and the Hamiltonian operator  $\hat{H}$  relates to energy and the time evolution of  $|\Psi(t)\rangle$ . The Schrödinger equation exactly describes the motion and forces of non-relativistic quantum systems just as Newton’s 2<sup>nd</sup> law does for classical systems. The Schrödinger equation is the “mechanics” of quantum

mechanics. Solving it allows one to determine a quantum state, predict its time-evolution, and design experiments to extract the state’s information through measurement.

The “quantum” in quantum mechanics refers to *quanta* (plural of quantum). A “quantum” is a discrete amount or of unit of something. Energy and many observable properties of physical systems at small scales, contrary to human experience, are not a continuum of values (a real number  $\mathbb{R}$ ), but rather exist in unit multiples (whole numbers or integers  $\mathbb{Z}$ ). This fact is concisely summarized by Planck’s original postulate [16],

$$S = nh. \tag{1.2}$$

Planck’s postulate states that  $S$ , the mechanical *action* of a system, exists only in integer multiples of a universal constant  $h = 6.626 \times 10^{-34}$  Joules·seconds. Action has dimensions of energy  $\times$  time and given that action is quantized actually implies many physical properties are also, like energy and space. The germ of the idea is easily appreciated in the Bohr model of the atom (Fig. 1.1).

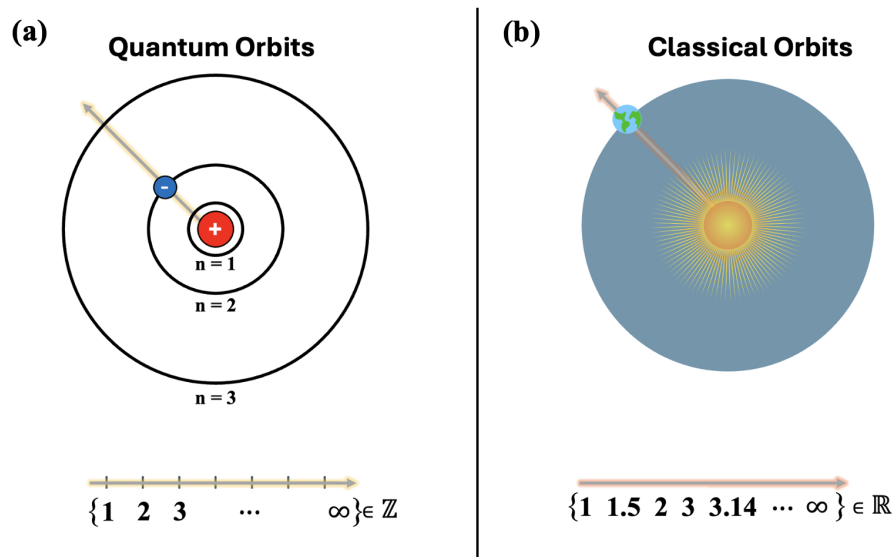


Figure 1.1: Quantum versus classical orbits. (a) Bohr model of the atom with discrete orbits. (b) Classical orbits of planetary motion.

In the Bohr model of the atom, electrons can only occupy particular quantized energy levels. This restriction implies electrons cannot occupy an arbitrary orbit around the nucleus, but rather only those fixed by the quantized energy. This is in stark contrast to the classical physics of the macroscopic world. For example, in the orbit of a planet around a star there is no restriction in Newton's (or Einstein's) law of gravitation requiring it satisfy certain integer multiples of energy or angular momentum.

### 1.1.2 Molecular Spectroscopy

The Bohr model is only a crude caricature of atoms, valid for atomic hydrogen, but it illustrates an essential feature of quantum mechanics. From the Bohr model a more general principle can be abstracted which relates the transition between two quantum states to classical electromagnetic radiation. In a quantum system with two levels, the frequency of radiation which promotes transitions between a ground  $|g\rangle$  and an excited state  $|e\rangle$  is given by

$$\nu = \frac{E_e - E_g}{h} \quad (1.3)$$

The Bohr frequency<sup>1</sup> determines the frequency of radiation needed to be absorbed or emitted to produce a transition between two quantum states (Fig. 1.2a). Because the Bohr frequency for different molecular degrees of freedom (electronic, vibrational, rotational, spin, etc.) occur at different regimes of the electromagnetic field [17, 18], classical radiation can be used to stimulate and probe specific a quantum transition within a molecular degree of freedom without perturbing others (Tab. 1.1).

Moreover, transitions that fall within the same regime and of the same degree of freedom will have frequencies of a similar magnitude, but different values. Thus a radiation source can be tuned to a particular frequency to isolate a specific quantum transition without perturbing

---

<sup>1</sup>Often the reduced form of Planck's constant  $\hbar = h/2\pi$  is convenient for calculations and the Bohr frequency is reported in angular frequency,  $\omega = E_e - E_g/\hbar$ .

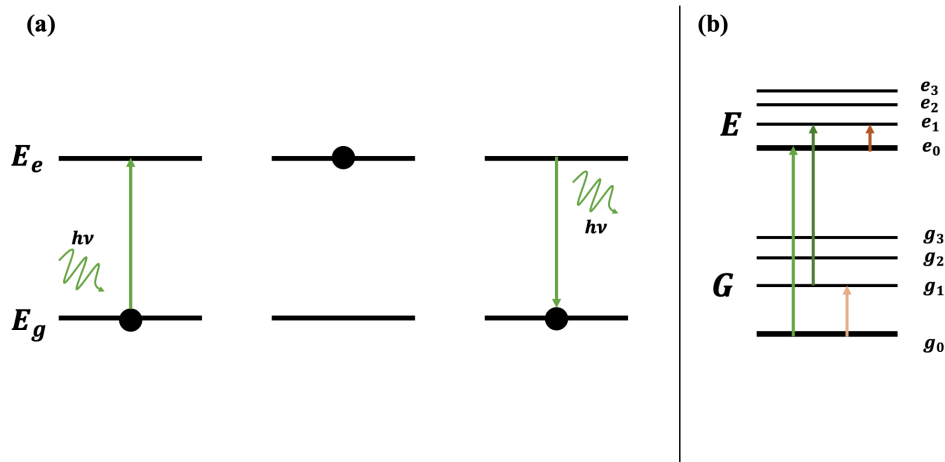


Figure 1.2: Quantum state transitions. (a) The Bohr frequency for absorption and emission of a photon  $h\nu$  of radiation. (b) A quantum system with two state manifold containing several internal states. The latter is typical of two electronic states  $G$  and  $E$  containing a set of vibrational states  $g_n$  and  $e_n$ .

Electromagnetic Radiation Regimes and Corresponding Quantum Transitions			
Radiation Regime	Frequency (Hz)	Wavelength (m)	Energy (J)
$\gamma$ ray	$\geq 10^{20}$	$\leq 10^{-12}$	$\geq 10^{-14}$
X-ray	$10^{16} - 10^{20}$	$10^{-8} - 10^{-12}$	$10^{-18} - 10^{-14}$
UV-Vis	$10^{14} - 10^{16}$	$10^{-6} - 10^{-8}$	$10^{-20} - 10^{-18}$
Infrared	$10^{13} - 10^{14}$	$10^{-5} - 10^{-6}$	$10^{-21} - 10^{-20}$
Microwave	$10^9 - 10^{13}$	$10^{-1} - 10^{-5}$	$10^{-25} - 10^{-21}$
Radiowave	$\leq 10^9$	$\geq 10^{-1}$	$\leq 10^{-25}$

Table 1.1: Quantum transitions and regimes of classical radiation corresponding to their transition frequency by frequency, wavelength, and energy per photon.

others within the same manifold (Fig. 1.2b). The significance of quantization of bound molecular systems is that one can precisely control the motion of a quantum system with a radiation field in a way for which there is no classical analog. This is what the field of molecular spectroscopy investigates and the essential idea behind quantum control [19].

At the most basic level, spectroscopic techniques are classified according to the frequency of radiation used (Tab. 1.1). Molecular spectroscopy typically concerns itself with the transitions among molecular degrees of freedom: vibrational, rotational, and electronic states. Degrees of freedom whose Bohr frequencies are comparable can couple to produce richer

spectra and more complex motion (ex. vibronic = vibrational + electronic or rovibrational = rotational + vibrational).

Modern molecular spectroscopic techniques can further be categorized by whether the incident radiation is resonant or off-resonant with the Bohr frequency, the power-law dependence of the observable on the radiation field (linear vs. nonlinear), whether the calculation or experiment is done in the frequency or the time domain, and whether molecular process being probed is coherent or incoherent [20].

### 1.1.3 Quantum Coherence

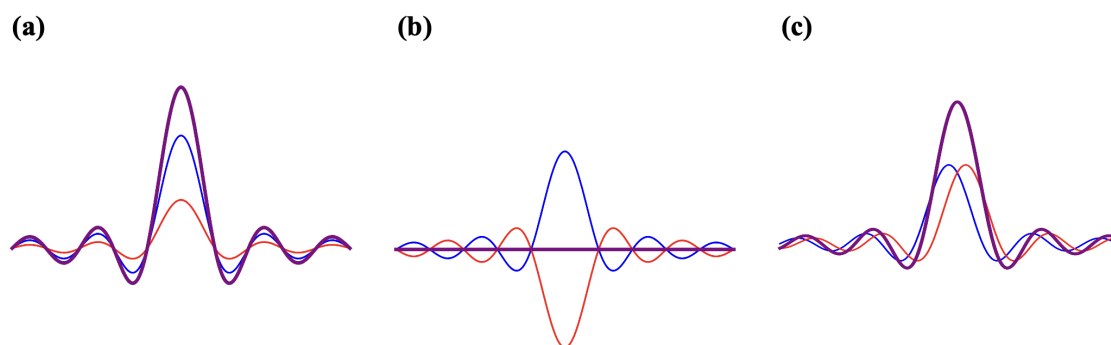


Figure 1.3: Sum of two waves (red and blue) and their resulting superposition (purple). (a) A constructive coherent superposition. (b) A destructive coherent superposition. (c) A partially coherent superposition.

Coherence is wave phenomenon with its origin in classical physics [21]. So it's important to distinguish *classical coherence* from *quantum coherence*. In classical physics, coherence refers to a tendency of waves to “stick together” in time or space or both.<sup>2</sup> A more precise term for this stickiness is *correlation* or being “in phase.” If a set of two or more waves are in phase or correlated, their amplitudes when summed will constructively interfere (Fig. 1.3a). Alternatively, if a set of waves are exactly out of phase or anti-correlated with one another,

---

<sup>2</sup>Latin: *cohaerere* = *co* + *haerere* = “together, with” + “to stick, cling.”

their superposition will destructively interfere (Fig. 1.3b). This resulting wave for either case is called a “coherent superposition.” In an “incoherent superposition,” the set of waves have random phases. The resulting wave is an average over the components in the superposition, but with the intensities adding as opposed to the amplitudes. Coherence, in the classical sense, describes the extent of inference between a set of waves ranging from fully coherent to fully incoherent with partial coherent between (Fig. 1.3c).

Quantum coherence, is conceptual similarly classical coherence, but with some important distinctions. A quantum state  $\psi$  is a complex function (or equivalently a complex vector,  $|\psi\rangle$ ), and by postulate, is interpreted as a probability amplitude. The square modulus of this amplitude indicates the probability density  $\mathcal{P}$  of measuring that state or an observable associated with it

$$\mathcal{P}(\Psi) = \Psi^* \Psi = |\Psi|^2. \quad (1.4)$$

A quantum state  $\Psi$  prepared in a two-component superposition

$$\Psi = \psi_1 + \psi_2 \quad (1.5)$$

has a probability density which is not a simple sum of its components square moduli

$$\mathcal{P}_C(\Psi) = |\psi_1|^2 + |\psi_2|^2 \quad (1.6)$$

but rather contains additional nonclassical interference terms resulting from the fact  $\Psi$  is complex

$$\begin{aligned} \mathcal{P}_Q(\Psi) &= |\psi_1 + \psi_2|^2 = (\psi_1^* + \psi_2^*)(\psi_1 + \psi_2) \\ &= \psi_1^* \psi_1 + \psi_2^* \psi_2 + \psi_1^* \psi_2 + \psi_2^* \psi_1 \\ &= |\psi_1|^2 + |\psi_2|^2 + 2\text{Re}(\psi_1^* \psi_2). \end{aligned} \quad (1.7)$$

In other words, the sum of the square moduli is generally not equal to the square modulus of the sum. The presence of the nonclassical interference terms indicates there is a phase relationship, —coherence, between the components in the superposition. The nonclassicality of the interference can be easily understood through the double-slit experiment (Fig. 1.4).

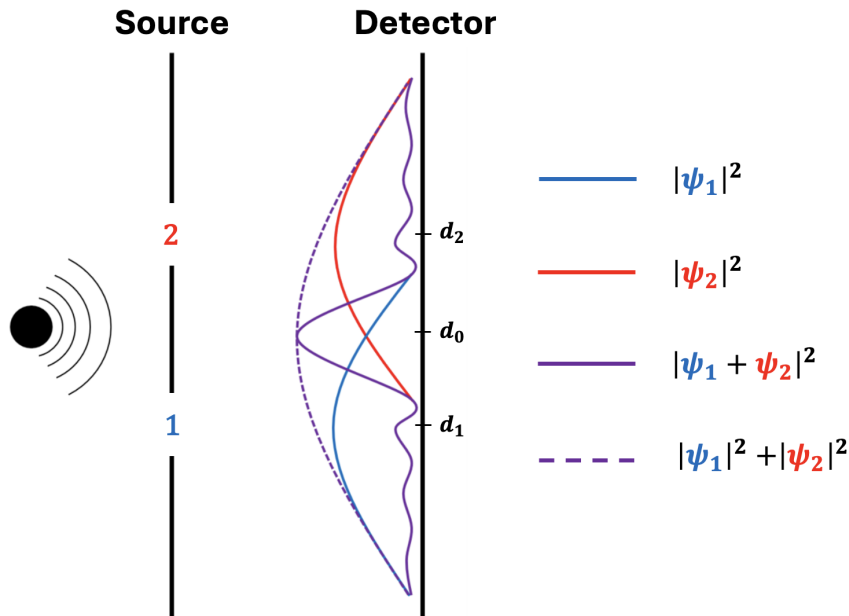


Figure 1.4: The double slit experiment for a quantum particle. Probability distribution for slit 1 opened (blue). Probability distribution for slit 2 opened (red). Quantum probability distribution for both slits opened (purple). Classical probability distribution for both slits opened (dashed purple).

In the double slit experiment [22], a quantum particle emanates from a source like a wave front. What is expected classically is: (a) if slit 1 is opened and slit 2 is closed, after a series of measurements the particle is observed with a distribution  $\mathcal{P}(\psi_1) = |\psi_1|^2$  centered about slit 1. Alternatively, if (b) slit 2 is opened and slit 1 closed, after a series of measurements the particle is observed with a distribution  $\mathcal{P}(\psi_2) = |\psi_2|^2$  about the center of the slit 2. For these two configurations, (a) and (b) classical and quantum physics predict the same distribution. If however, (c) both slit 1 and slit 2 are opened simultaneously what is predicted classically and quantum mechanically is different. Classically one expects a distribution  $\mathcal{P}_C$  (Eq. 1.6), namely the simply sum of the components as configured in (a) and (b). What is observed



quantum mechanically, however, is not the simple sum of components, but the distribution  $\mathcal{P}_Q$  (Eq. 1.7) with interference fringes arising from the phase relations between each outcome or components of the superposition.

Note that although the classical distribution  $P_C$  and the quantum distribution  $P_Q$  for the superposition state of both slits opened are different, both have their maximum amplitude centered about the arithmetic mean of the maxima of the component distributions,  $d_0 = \frac{1}{2}(d_1 + d_2)$ . That is, the quantum distribution containing the coherence is geometrically related to the means of the component distributions  $\mathcal{P}(\psi_1)$  and  $\mathcal{P}(\psi_2)$ . This picture will resurface in the phase space formalism developed in this thesis for calculating quantum.

## The Density Matrix

To make the definition of *quantum coherence* more explicit, it is helpful to introduce a matrix representation of the pure quantum state  $|\Psi\rangle$  in a basis  $\{|\psi_n\rangle\}$ . Let  $c_n$  be the relative weights of each basis component  $\{|\psi_n\rangle\}$  with  $c_n(t) = \langle\psi_n|\Psi(t)\rangle \in \mathbb{C}$ . For an  $N$  component superposition in this basis, one has

$$|\Psi(t)\rangle = \sum_{n=1}^N c_n(t)|\psi_n\rangle \quad (1.8)$$

where the  $c_n(t)$  are probability amplitudes. The pure state density  $\hat{\rho}(t)$  in  $\{|\psi_n\rangle\}$  is

$$\hat{\rho}(t) = |\Psi(t)\rangle\langle\Psi(t)| = \sum_{m,n=1}^N c_m^*(t)c_n(t)|\psi_n\rangle\langle\psi_m| \quad (1.9)$$

which can be written in the form of a matrix

$$\rho_{mn}(t) = \begin{pmatrix} \rho_{11} & \rho_{12} & \cdots & \rho_{1N} \\ \rho_{21} & \rho_{22} & \cdots & \rho_{2N} \\ \vdots & \vdots & \ddots & \vdots \\ \rho_{N1} & \rho_{N2} & \cdots & \rho_{NN} \end{pmatrix} \quad (1.10)$$

Because density matrix is Hermitian,

$$\rho_{mn} = \rho_{nm}^* \quad (1.11)$$

it follows that diagonal elements  $m = n$  are real ( $\rho_{mm} = \rho_{mm}^*$ ) while off-diagonal elements are complex with their transposes are related by the conjugation (Eq. 1.11). Recall the diagonal elements  $\rho_m$  are the square moduli of the probability amplitudes  $c_m$  in the original superposition. The diagonal elements thus indicate the probability the quantum system is in state  $|\psi_m\rangle$  and are called *populations*. The off-diagonal elements  $\rho_{mn}$  are cross terms of the probability amplitudes  $c_m^* c_n$  which is the phase interference between states  $|m\rangle$  and  $|n\rangle$ . For this reason the off-diagonal elements of the density are called *coherences*.

Populations and coherences are not independent of one another. For a pure state density  $\hat{\rho} = |\Psi\rangle\langle\Psi|$ , the coherence is related to the two populations of the states comprising it through the Schwarz equality

$$\rho_{mm}\rho_{nn} = |\rho_{mn}|^2 \quad (1.12)$$

This is a second feature of quantum coherences which will resurface in the phase space formalism developed in this thesis.

## 1.2 Motivation

Having defined quantum systems, coherence, and introduced the notion of quantum selectivity in molecular spectroscopy, the broader impacts motivating this work can be discussed. Although quantum coherence is a property of the microscale, it can be observed and controlled macroscopically. Lasers and superconductors are two well-known examples of this [23–25]. In lasers, a coherent radiation beam is produced by the phase and frequency alignment of photons generated through stimulated emission. In superconductors coherence arises from the coupling and synchronization of electron spins leading to zero electrical resistance and expulsion of the interior magnetic field. Although lasers and superconductors can be found in any present-day physics lab, they are routinely used outside science in computers, medical imaging, and power grids. These examples illustrate two key points about quantum coherence: (1) quantum coherence can be a property of radiation (light) or matter and (2) quantum coherence can be used to develop new technologies which are then again recycled into exploring new frontiers in fundamental science.

### 1.2.1 Quantum Technology

The single most anticipated use for quantum coherence is the development of practical quantum computers [26–28]. The essential difference between a classical computer and a quantum computer is their fundamental unit of information. A classical computer’s computational state is composed of classical bits (Cbits), each of which can possess two possible states, 0 or 1. A quantum computer’s computational state is composed of quantum bits (qubits), each of which exist in a superposition between the two classical states (Fig. 1.5).  $n$  Cbits can hold  $2^n$  classical states while a single qubit can contain a potentially infinite number of classical states [29].

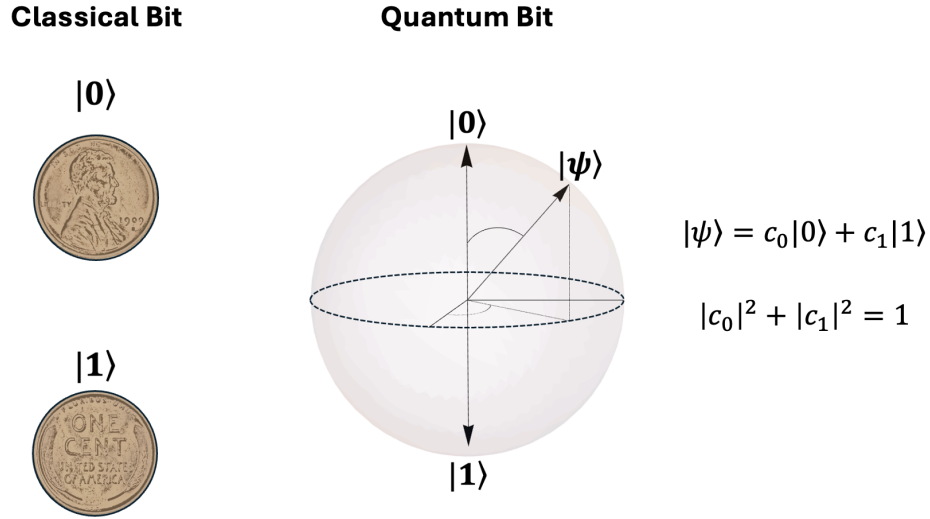


Figure 1.5: A classical bit and a qubit.

The advantage of a quantum computer over a classical is that the former can, theoretically, solve certain classes of problems exponentially faster and could store exponentially more information. Research in quantum computing today is partly theoretical and partly experimental. The theoretical side focuses often on translating classical algorithms into quantum algorithms which could be run on a quantum computer [30, 31]. The experimental side tends to focus on developing the physical hardware to realize qubits. A fundamental barrier to the practical quantum computers is sustaining the quantum coherence of qubits over time and length scales long enough to perform calculations. Many different hardware candidates for qubits have been proposed: trapped ion, photon, topological, superconducting, spin, and molecular qubits [32], —all with their relative advantages and challenges. But shared by all is the need to sustain the coherence at scale. For this reason, molecular qubits are a current topic of research in quantum computing [33, 34].

Using quantum coherence as a phenomenon to be harnessed is hardly unique to computation. Quantum sensors, like those commonly used in atomic clocks, and are being developed to detect microscopic changes in magnetic fields, temperature, and gravitation with precision, impossible to achieve by classical means [35, 36]. Likewise quantum cryptography and

communication are active areas of research addressing problems like key distribution and information transmission on channels without “eavesdropping.” What all these quantum technologies share in common is the exploitation of quantum coherence for precisions and efficiencies which can not be achieved by classical physics.

## 1.2.2 Frontiers in Ultrafast Spectroscopy and Chemistry

As mentioned above there is a symbiotic feedback between engineering and fundamental science. When the laser was developed it was heralded as a “device without a use.” Now lasers are commonplace in personal electronics and medicine. As power sources for lasers increase, so do their ability to resolve microscopic events in fundamental chemistry. Elementary processes in chemistry like electron and proton transfer occur on ultrafast timescales (less than  $10^{-15}$  seconds) [37–40]. New free-electron X-ray lasers allow unprecedented resolution and control over these events and novel spectroscopic techniques are being developed in tandem to the new laser technology.

One such method, Transient redistribution of ultrafast electronic coherences in attosecond ( $10^{-18}$  seconds) Raman signal (TRUECARS) allows one to isolate electronic coherence generated by a nuclear wavepacket passing through conical intersections [41–44]. Conical intersections refer to special degeneracies in the energy spectrum of molecules which are believed to be responsible for the efficiency of naturally occurring light-harvesting materials [45, 46]. In many cases the goal is to reverse-engineer the efficiency energy generation in Nature by understanding the role coherence plays in these processes [47, 48].

The theoretical issue underlying these applications, is “How to simulate the dynamics of quantum coherences in molecular systems?”

## 1.3 Challenges in Quantum Molecular Dynamic Simulations

The underlying physical laws necessary for the mathematical theory of a large part of physics and the whole of chemistry are thus completely known, and the difficulty is only that the exact application of these laws leads to equations much too complicated to be soluble. It therefore becomes desirable that approximate practical methods of applying quantum mechanics should be developed, which can lead to an explanation of the main features of complex atomic systems without too much computation [49].

---

P.A.M. Dirac, 1929

This well-known excerpt from Dirac’s paper, “Quantum Mechanics of Many-Electron Systems,” succinctly summarizes the position of theoretical chemistry and quantum molecular dynamics. For theoretical chemistry, unlike many other sciences, the laws to predict the phenomenon interest are known. The main issue is direct application of these laws is infeasible for all but the simplest of systems. In this sense, theoretical chemistry is a science of approximations. Desirable approximations, simplify the computational cost of solving a given problem. But to be useful, approximations must also retain essential features of the problem and provide conceptual insight. Dirac’s diagnosis of the field is still true today. Even with modern petaFLOP supercomputing facilities, the many-bodied Schrödinger equation can be solved within chemical precision for only a handful of degrees of freedom [50].

In this section, to motivate the methods developed in this thesis, some of challenges of quantum molecular dynamics simulations are revisited. It’s necessary to appreciate what computational complexity is strictly quantum and what additional complexity is introduced by molecule specifically. Approximate methods can be categorized by how they reduce quantum complexity. In the discussion which follows, the complexity of solving the Schrödinger equation for molecular systems is also true generally of for all equivalent formulations.

### 1.3.1 Intractability of Exact Quantum Solutions

But before discussing the cost of exact quantum solutions, it is important to distinguish between different kinds of solutions. *Analytic solutions* are solutions obtained by mathematical manipulations leading to a closed-form solution, —essentially a solution that could be written down by hand. *Numerical solutions*, in contrast, require a computer and typically amount to using an algorithm to numerically integrate the Schrödinger equation or diagonalize its Hamiltonian. *Exact solutions* solve the Schrödinger equation with no error or error bounded to a desired level of precision. *Approximate solutions* are those which have some error introduced by an approximation at some stage of the calculation.

A solution can be either analytic or numerical and either exact or approximate. The virtue of analytic solutions is that because they are closed-form mathematical expressions, they lend themselves more easily to interpretation and can be used as a zeroth order result in approximating more complex systems (viz. perturbation theory). Numerical solutions are the default for more complex quantum systems like molecules. Because exactly solving the many-bodied Schrödinger equation is an inordinate computational problem, as will be discussed, the bulk of theoretical research is centered around developing approximate numerical solutions for complex quantum systems.

#### The Schrödinger Equation as an Eigenvalue Problem

The Schrödinger equation,

$$i\hbar \frac{d}{dt} |\Psi(t)\rangle = \hat{H} |\Psi(t)\rangle$$

introduced as postulate above, is the time-dependent form of the Schrödinger equation for a single particle. It is a first order, linear, partial differential equation with the formal solution

[51],

$$|\Psi(t)\rangle = e^{-\frac{i}{\hbar}\hat{H}t}|\Psi(0)\rangle. \quad (1.13)$$

The operator exponential acting on the initial quantum state  $|\Psi(0)\rangle$  is called the time-evolution operator,

$$\hat{U}(t) = e^{-\frac{i}{\hbar}\hat{H}t}. \quad (1.14)$$

Because  $\hat{H}$  is Hermitian, its exponential, —the time evolution operator  $\hat{U}$  is a unitary operator (Stone's Theorem) [52]. And because  $\hat{U}$  is a function of an operator (viz.  $\hat{U} = f(\hat{H})$ ), to calculate its action on  $|\Psi(0)\rangle$  and solve the time evolution, it is necessary to calculate the eigenvalues/vectors of  $\hat{H}$ . This naturally leads to the time-independent form of the Schrödinger equation

$$\hat{H}|\Psi\rangle = E|\Psi\rangle. \quad (1.15)$$

Solving Eq. 1.15 for a bound system amounts to finding a basis set  $\{|\psi_n\rangle\}$  such that

$$\hat{H}|\psi_n\rangle = E_n|\psi_n\rangle \quad (1.16)$$

where  $E_n$  are the eigenvalues of  $|\Psi\rangle$  represented in  $\{|\psi_n\rangle\}$ . And the formal solution is given by

$$|\Psi(t)\rangle = \sum_n c_n e^{-iE_n t/\hbar} |\psi_n\rangle \quad (1.17)$$

Viewed as an eigenvalue problem, solving the time-dependent Schrödinger equation amounts to solving the time-independent Schrödinger equation. Because the Hamiltonian is Hermitian, a formal solution exists as a consequence of the Spectral Theorem [53]. Namely, for Hermitian operators like  $\hat{H}$  there exists an orthonormal basis of  $\{|\psi_n\rangle\}$  which diagonalizes the matrix representation of the operator. This procedure is referred to as the *eigendecomposition* of  $\hat{H}$ . And though the Schrödinger equation is theoretically solvable, eigendecomposition algorithms typically scale cubically as  $\mathcal{O}(N^3)$  for an  $N \times N$  matrix [54].



In itself, this would not be the death-knell for exact numerical solutions by eigendecomposition, but in generalizing to a quantum system with not one but  $M$  particles, the situation quickly becomes unmanageable. Each of the  $M$  particles will have  $N$  basis functions. The total number of basis functions needed to describe  $|\Psi\rangle$  is  $N^M$ :

$$\{|\psi_n\rangle\} = \{|\psi_n^{(1)}\rangle \otimes |\psi_n^{(2)}\rangle \otimes |\psi_n^{(M)}\rangle\}, \quad (1.18)$$

and the Hamiltonian needed to be diagonalized is  $N^M \times N^M$ . Thus the complexity of the quantum problem grows exponentially  $\mathcal{O}(N^M)$  meaning the computational resources (memory and time) needed scales exponentially with system size (Fig. 1.6). This phenomenon is often called “The Curse of Dimensionality,” in numerical analysis [55] and is implicit in all quantum dynamics problems.

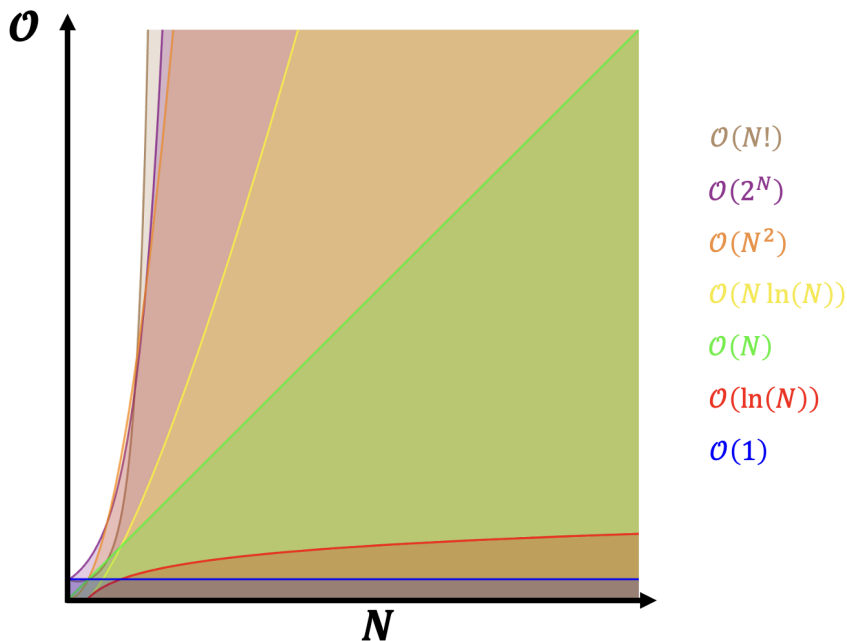


Figure 1.6: Growth of various complexity classes with respect to dimension  $N$ .

For this reason exact eigendecomposition is infeasible for systems with greater than a few particles. Other methods to solve the Schrödinger equation don't fair much better [56].

Viewed as a differential equation, the Schrödinger equation can be solved by numerical integration. For quadrature methods, “The Curse of Dimensionality” is manifested through number and dimension of grid points needed to discretize the wavefunction. For Monte Carlo methods, which are better suited for higher dimensional problems, the complexity reemerges in the number of statistical samplings required for convergence. An idiom commonly used in simulations of quantum systems is “There is no free lunch.”<sup>3</sup> In other words, the complexity of solving energy spectrum or dynamics of a quantum system goes somewhere even if a clever algorithm is used.

### 1.3.2 Complexity of Molecular Systems

Hereto the complexity of solving general quantum systems has been alluded to. Solving the Schrödinger equation is exponentially costly as the number of particles in the system grow. Molecules are quantum systems composed of many nuclei and electrons. Exact solutions are intractable for all but the simplest of molecules because of the number of basis functions needed for each particle. This complexity can also be viewed from the perspective of the molecular Hamiltonian. The time-independent molecular Schrödinger equation is:

$$\hat{H}(\hat{\mathbf{R}}, \hat{\mathbf{r}}) \Psi(\mathbf{R}, \mathbf{r}) = E\Psi(\mathbf{R}, \mathbf{r}) \quad (1.19)$$

The molecular Hamiltonian [58] for a system of  $N$  nuclei and  $n$  electrons is given by

$$\hat{H}(\hat{\mathbf{R}}, \hat{\mathbf{r}}) = \hat{T}_N + \hat{T}_e + \hat{V}_{NN}(\hat{\mathbf{R}}) + \hat{V}_{ee}(\hat{\mathbf{r}}) + \hat{V}_{Ne}(\hat{\mathbf{R}}, \hat{\mathbf{r}}) \quad (1.20)$$

---

<sup>3</sup>This phrase was popularized by the economist, Milton Friedman, to describe opportunity cost in free-market economies [57].

where the kinetic energy operators of the nuclei and electrons are given by

$$\hat{T}_N = \sum_{k=1}^N \left( -\frac{\hbar^2}{2M_k} \nabla_k^2 \right) \quad (1.21)$$

$$\hat{T}_e = \sum_{i=1}^n \left( -\frac{\hbar^2}{2m_e} \nabla_i^2 \right) \quad (1.22)$$

with  $M_k$  and  $m_e$  as the  $k^{\text{th}}$  nuclear and electronic masses, respectively. The potential energy operator for the nuclear-nuclear, electronic-electronic, and nuclear-electronic interactions are

$$\hat{V}_{NN}(\hat{\mathbf{R}}) = \frac{1}{2} \sum_{k \neq k'}^N \frac{Z_k Z_{k'}}{\mathbf{R}_{kk'}} \quad \text{with} \quad \mathbf{R}_{kk'} = |\mathbf{R}_k - \mathbf{R}_{k'}| \quad (1.23)$$

$$\hat{V}_{ee}(\hat{\mathbf{r}}) = \frac{1}{2} \sum_{i \neq i'}^n \frac{1}{\mathbf{r}_{ii'}} \quad \text{with} \quad \mathbf{r}_{ii'} = |\mathbf{r}_i - \mathbf{r}_{i'}| \quad (1.24)$$

$$\hat{V}_{ee}(\hat{\mathbf{R}}, \hat{\mathbf{r}}) = - \sum_{k=1}^N \sum_{i=1}^n \frac{Z_k}{\mathbf{R}_{ki}} \quad \text{with} \quad \mathbf{R}_{ki} = |\mathbf{R}_k - \mathbf{r}_i| \quad (1.25)$$

The position vectors which the interactions in the molecular Hamiltonian depend on are the relative distances between each unique pair of particles (Fig. 1.7). To illustrate the growth in the number of these variables with increasing molecular structure, a simple visual mnemonic can be employed. Each particle in a molecule can be represented as a vertex in a polygon with the number of relative position vectors in the Hamiltonian counted as the number of edges and unique diagonals of the polygon. By plane geometry number of edges in a  $p$ -sided polygon is  $p$  and the number of unique diagonal are

$$d = \frac{p(p-3)}{2} \quad (1.26)$$

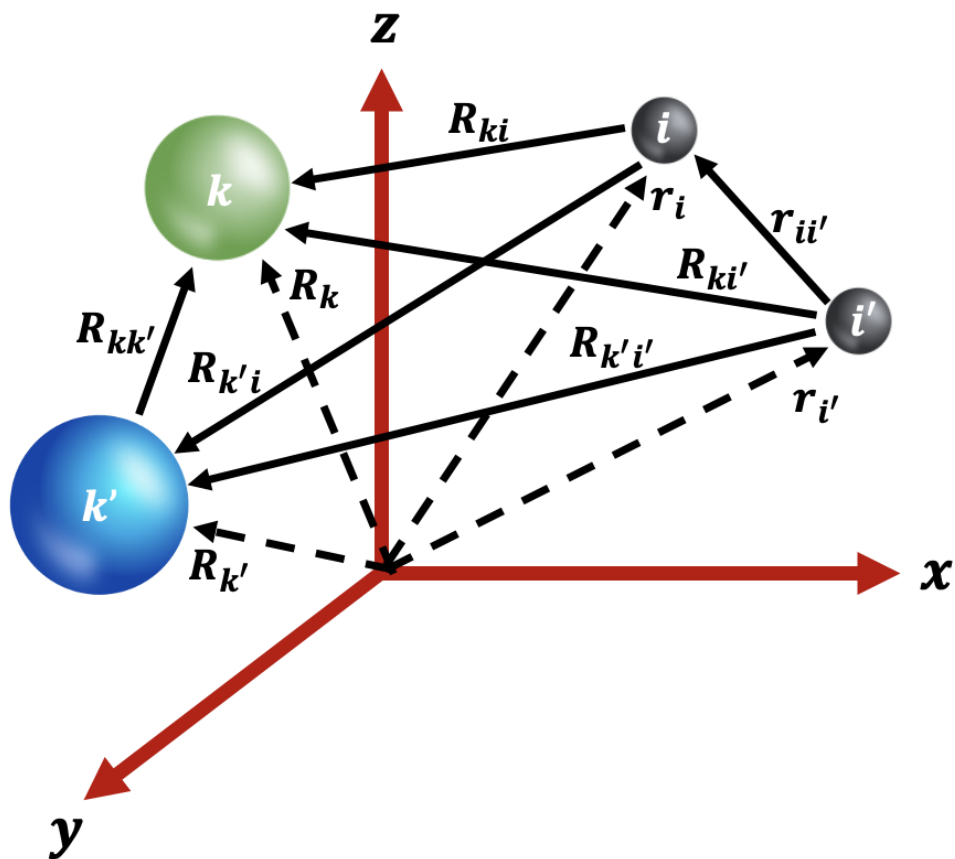


Figure 1.7: Internal coordinates of a molecule with 2 nuclei and 2 electrons.

hence the number of sides plus unique diagonals is

$$f = \frac{1}{2}(d-1) \quad (1.27)$$

For a molecule with  $n$  electrons and  $N$  nuclei, the total number of particles is  $p = N + n$  and the number of relative position vectors is  $f$ . The number of relative position vectors scale quadratically as  $\mathcal{O}(p^2)$ . For molecular hydrogen, one has two electrons and two nuclei resulting in 6 relative position vectors (Fig. 1.8). For the simplest hydrocarbon, methane, there are 105 relative position vectors. For the simplest aromatic, benzene, there are 1,431. For a simple organic chromophore, porphine, there are 19,900. And because each vector is a 3-D object, one actually has  $3f$  coordinates to keep track of in simulation.

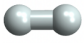
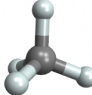
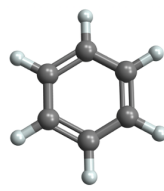
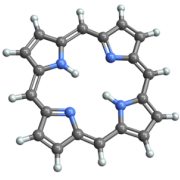

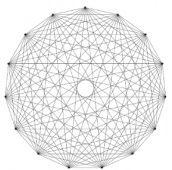

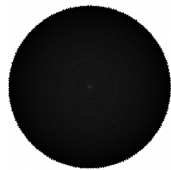
	Diatomic Hydrogen ( $H_2$ )	Methane ( $CH_4$ )	Benzene ( $C_6H_6$ )	Porphine ( $C_{20}H_{14}N_4$ )
Molecular Structure				
Position Vectors	$2 N + 2 e = 4$ particles $\# R_{kk'} = 1$ $\# r_{ii'} = 1$ $\# R_{ki} = 4$ Total vectors = 6	$5 N + 10 e = 15$ particles $\# R_{kk'} = 10$ $\# r_{ii'} = 45$ $\# R_{ki} = 50$ Total vectors = 105	$12 N + 42 e = 54$ particles $\# R_{kk'} = 66$ $\# r_{ii'} = 861$ $\# R_{ki} = 504$ Total vectors = 1,431	$38 N + 162 e = 200$ particles $\# R_{kk'} = 703$ $\# r_{ii'} = 13,041$ $\# R_{ki} = 6,156$ Total vectors = 19,900
Complexity Graph	 Edges = 6	 Edges = 105	 Edges = 1,431	 Edges = 19,900

Figure 1.8: Position vector complexity graphs for various molecules.

Given the complexity of interactions in molecular systems grows quadratically with the number of particles and the number of basis functions grow exponentially with the number of particles, it is easily to see one is at an impasse. But not all is lost, physical and chemical knowledge suggest not all degrees of freedom are as essential as others.

For example, in quantum chemistry valence electron are more reactive than their core. Pseudo-potentials can be used to approximate chemically inert interior electrons with simulation resources reserved for the valence electrons. In quantum molecular dynamics, nuclei because they are more massive than electrons, can be regarded as slow moving or fixed in some situations. This latter simplification is the rationale behind the Born-Oppenheimer approximation [59].

### 1.3.3 Nonadiabaticity and the Born-Oppenheimer Approximation

Returning to the molecular Hamiltonian, let an electronic Hamiltonian be defined by the the electronic kinetic energy operator, electronic-electronic interactions, the electronic-nuclear interactions, plus the repulsive nuclear-nuclear interactions,

$$\hat{H}_e(\hat{\mathbf{R}}, \hat{\mathbf{r}}) = \hat{T}_e + \hat{V}_{ee}(\hat{\mathbf{r}}) + \hat{V}_{Ne}(\hat{\mathbf{R}}, \hat{\mathbf{r}}) + \hat{V}_{NN}(\hat{\mathbf{R}}). \quad (1.28)$$

If the nuclei are stationary, then the time-independent molecular Schrödinger equation becomes

$$\hat{H}_e(\hat{\mathbf{R}}, \hat{\mathbf{r}}) \phi_n(\mathbf{r}, \mathbf{R}) = \varepsilon_n(\mathbf{R}) \phi_n(\mathbf{r}, \mathbf{R}) \quad (1.29)$$

$\phi_n$  are called the adiabatic molecular wavefunctions and their eigenvalues  $\varepsilon_n(\mathbf{R})$  are termed adiabatic energies. Both the adiabatic wavefunctions and their eigenenergies are parametrically dependent on the nuclear positions  $\mathbf{R}$ . Choosing the adiabatic wavefunctions as a basis  $\{\phi\}$ , the total molecular wavefunction  $\Psi(\mathbf{R}, \mathbf{r})$  can be expanded as

$$\Psi(\mathbf{R}, \mathbf{r}) = \sum_n \chi_n(\mathbf{R}) \phi_n(\mathbf{R}, \mathbf{r}) \quad (1.30)$$

where  $\chi(\mathbf{R})$  is the nuclear wavefunction in the adiabatic basis. Substituting  $\Psi(\mathbf{R}, \mathbf{r})$  into Eq. 1.29 and integrating over electronic degrees of freedom yield the nuclear Schrödinger equation in the adiabatic basis

$$\left(\hat{T}(\hat{\mathbf{R}}) + \varepsilon_m(\hat{\mathbf{R}})\right) \chi_m(\hat{\mathbf{R}}) + \sum_n \hat{D}_{mn}(\hat{\mathbf{R}}) \chi_n(\mathbf{R}) = E \chi_m(\mathbf{R}) \quad (1.31)$$

The operator  $\hat{D}$  which couples nuclear and electronic motion is referred to as *nonadiabatic coupling* operator and is given by

$$\hat{D}_{mn}(\hat{\mathbf{R}}) = - \sum_{i=1} \frac{\hbar^2}{M_i} \left( A_{mn}^i \frac{\partial}{\partial \mathbf{R}_i} + \frac{1}{2} B_{mn}^i \right) \quad (1.32)$$

with

$$A_{mn}^i = \langle \phi_m | \nabla_{\mathbf{R}_i} | \phi_n \rangle \quad (1.33)$$

$$B_{mn}^i = \langle \phi_m | \nabla_{\mathbf{R}_i}^2 | \phi_n \rangle \quad (1.34)$$

In matrix form, the nuclear Schrödinger equation in the adiabatic basis is

$$(\mathbf{T} + \mathbf{V}) \mathbf{X}(\mathbf{R}) = E \mathbf{X}(\mathbf{R}) \quad (1.35)$$

where

$$V_{mn}(\mathbf{R}) = \text{diag}(\varepsilon_m(\mathbf{R})) \quad (1.36)$$

$$T_{mn}(\mathbf{R}) = T(\mathbf{R})\delta_{mn} + D_{mn}(\mathbf{R}) \quad (1.37)$$

Note the nuclear potential operator is diagonal while the nuclear kinetic energy is nondiagonal in Eq. 1.35 and is called the *adiabatic basis*. Alternatively, one can diagonalize the nuclear kinetic energy operator at the expense of the nuclear potential energy operator and this representation is called the *diabatic basis* [60].

Solving Eq. 1.35 for the nuclear wavefunctions and eigenenergies is particularly challenging owing to the presence of the nonadiabatic coupling operator  $D_{mn}$ . This is because it requires computing many gradients numerically in simulation. Were  $D_{mn}$  diagonal ( $D_{m \neq n} = 0$ ), the total molecular wavefunction would factorize as

$$\Psi_n(\mathbf{R}, \mathbf{r}) = \chi_n(\mathbf{R}) \phi_n(\mathbf{r}) \quad (1.38)$$

and the nuclear Schrödinger equation becomes

$$\left(\hat{T}_N + \varepsilon_n(\mathbf{R}) + \hat{D}_{nn}(\mathbf{R})\right) \chi_n(\mathbf{R}) = E\chi(\mathbf{R}) \quad (1.39)$$

Eq. 1.38 is called the *adiabatic approximation*.<sup>4</sup> The justification for the adiabatic approximation is that matrix element  $A_{mn}^i$  and  $B_{mn}^i$  are relatively small in comparison to the electronic kinetic energies (roughly the mass ratio of an electron to a proton, 1 : 1836) and can approximately be neglected.

If  $D_{nn}$  is neglected altogether, one has completely separable dynamics. The nuclei satisfy

$$\left(\hat{T}_N + \varepsilon_n(\mathbf{R})\right) \chi_n(\mathbf{R}) = E\chi(\mathbf{R}) \quad (1.40)$$

where  $\varepsilon_n(\mathbf{R})$  are the adiabatic eigenenergies are now called adiabatic potential energy functions  $V_n(\mathbf{R})$ . This approximation is called the *Born-Oppenheimer approximation*. Often-times in literature the Born-Oppenheimer approximation and adiabatic approximation are used synonymously [58]. The technical distinct is the former refers to a complete neglect of the nonadiabatic coupling operator. This distinction is consistent with Born's original use of the term [61].

The Born-Oppenheimer approximation provides an intuitive picture of quantum molecular dynamics. A given potential energy function  $V_n(\mathbf{R})$  which contains both nuclear-nuclear and electron-nuclear potential energies is a function of nuclear configuration  $\mathbf{R}$ .  $V_n(\mathbf{R})$  can be viewed as surface and a representative point on the surface indicates the instantaneous nuclear geometry of the molecule. Motion on the surface corresponds to vibrations of nuclei at a given electronic energy. The potential energy surface picture although a powerful

---

<sup>4</sup>The term adiabatic comes from its use in classical mechanics which in turn is borrowed from its use in thermodynamics. In classical mechanics, an adiabatic approximation to a coupled system assumes separability between degrees of freedom owing to large differences in timescales between slow degrees of freedom and fast ones.



tool for interpreting reaction dynamics is limited by several issues. (1)  $\mathbf{R}$  is in general a large dimensional vector and it is difficult to visualize motion on a surface of greater than two dimensions. (2) Potential energy surfaces can possess conical intersections indicating an energy degeneracy between two or several  $V_n(\mathbf{R})$ . At these points, the Born-Oppenheimer separation is qualitatively incorrect. (3) The Born-Oppenheimer approximation is only applicable to regimes where electronic states are well-defined and transitions between them are infrequent or slow, namely when  $D_{mn}$  is close to zero which is generally not true.

In practice, most chemistry involves rapid transitions between electronic states coupled to nuclear motion where  $D_{mn}$  is appreciable. Recalling that  $A_{mn}$  and  $B_{mn}$  are overlaps of cross terms between different adiabatic basis functions (Eqs. 1.33-1.34), nonadiabatic transitions have significant quantum coherence. How best to retain nonadiabaticity in quantum molecular dynamics theories is an ongoing field of research [62, 63]. To describe nonadiabatic coherence in quantum molecular dynamics, the Born-Oppenheimer approximation cannot be used to give qualitatively accurate results. In many cases, for this reason the diabatic representation is preferable. For systems where there is strong coupling between nuclear and electronic motion (which is to say there is non-negligible quantum coherence between the nuclear and electronic degrees of freedom), other kinds of approximations are needed.

### 1.3.4 Approximate Theories in Quantum Dynamics

There are numerous approximations one can make to manage the complexity of the Schrödinger equation. The Born-Oppenheimer approximation is but one common approximation which provides a scaffolding for building more advanced theories for the quantum dynamics of molecules. Stepping back, two general options to lessen the computational overhead of quantum dynamics are: (1) to reduce the dimensionality of the problem  $N$  or (2) to approximate some portion of the quantum system with dynamics that scale less than exponentially

$\mathcal{O}(M^N)$ . The former amounts to integrating out or averaging over some degrees of freedom while the latter, in practice, retains the size of the original system, but treats evolution of some degrees of freedom with classical dynamics which scale linearly  $\mathcal{O}(N)$ . Both strategies, dimensionality reduction and approximation by classical dynamics, suppose a prior knowledge of which degrees of freedom ought to be integrated out or treated classically. This is not always obvious. And because quantum coherence, —by its nature, is nonlocal, coherence effects can be lost by approximating of degrees of freedom in these ways.

In practice, approximations will conform to the type of quantum dynamical system being simulated. For example, a single atom isolated in the gas phase, a molecule immersed in a solvent or adhered to a surface, a molecule with separable electronic structure ( $\pi$  vs  $\sigma$ , valence vs. core), or a molecule exposed to a radiation field, will have different degrees of freedom which are more relevant to quantum evolution and emergent coherence effects. In this thesis, attention is given to improving trajectory-based methods which approximate degrees of freedom with classical evolution in small molecules. For this class of theories there are two common schools of approximation: mixed quantum-classical and semiclassical methods.

### **Mixed Quantum-classical Methods**

Mixed quantum-classical methods take a quantum equation of motion for the full system (typically the Schrödinger equation or the quantum Liouville equation), parse degrees of freedom into those to be treated by classical dynamics and those to be solved by quantum dynamics [9, 10]. In the particular case of nonadiabatic molecular dynamics, the nuclear degrees of freedom are evolved by classical(like) equations of motion and the electronic degrees of freedom are treated quantum mechanically. For example, the exact Schrödinger

equation for such a system is

$$i\hbar \frac{\partial \Psi(\mathbf{R}, \mathbf{r}, t)}{\partial t} = \hat{H}(\hat{\mathbf{R}}, \hat{\mathbf{r}}) \Psi(\mathbf{R}, \mathbf{r}, t). \quad (1.41)$$

The total Hamiltonian is separated into a classical (nuclear) kinetic energy and a quantum (electronic) Hamiltonian

$$\hat{H}(\hat{\mathbf{R}}, \hat{\mathbf{r}}) = \hat{T}_C + \hat{H}_Q(\hat{\mathbf{R}}, \hat{\mathbf{r}}) \quad (1.42)$$

The wavefunction is taken to be parametrically dependent on the nuclear degrees of freedom  $\Psi(\mathbf{R}, \mathbf{r}, t) \rightarrow \Psi(\mathbf{r}, t; \mathbf{R})$  and evolves according to

$$i\hbar \frac{\partial \Psi(\mathbf{r}, t; \mathbf{R})}{\partial t} = \hat{H}_Q(\hat{\mathbf{R}}, \hat{\mathbf{r}}) \Psi(\mathbf{r}, t; \mathbf{R}) \quad (1.43)$$

while the classical degrees of freedom evolve as classical trajectories governed by Newton's equations of the form

$$M \frac{d^2 \mathbf{R}}{dt^2} = -\nabla_{\mathbf{R}} V(\hat{H}_Q, \psi, t) \quad (1.44)$$

The specific form of the quantum potential  $V$  in Eq. 1.44 and how it is solved algorithmically varies in mixed quantum-classical methods. The least sophisticated mixed quantum-classical method is Ehrenfest Dynamics [9], and  $V$  is the expectation of electronic Hamiltonian

$$M \frac{d^2 \mathbf{R}}{dt^2} = -\nabla_{\mathbf{R}} \langle \psi | \hat{H}_Q | \psi \rangle \quad (1.45)$$

In Ehrenfest dynamics, the forces on the nuclei are derived from an average potential energy surface (Fig. 1.9). And while simple, qualitatively it can't describe nonadiabatic transitions between states.

To obtain more qualitative accuracy, methods have been developed to allow transitions between electronic states. Surface Hopping methods [64], by contrast take the forces on the

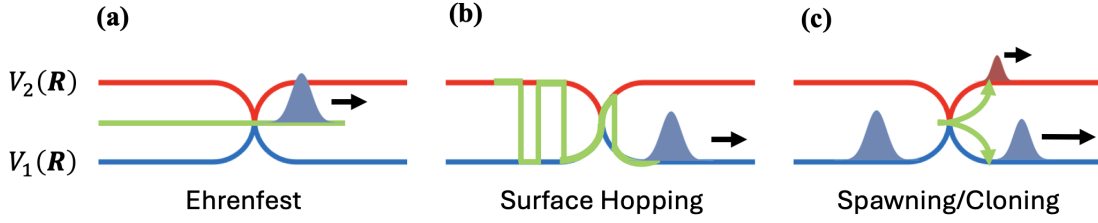


Figure 1.9: Nonadiabatic mixed quantum-classical methods. (a) Ehrenfest. (b) Surface Hopping. (c) Spawning/Cloning.

nuclei to derive from the gradient of the instantaneous potential energy surface  $V_m$  occupied

$$M \frac{d^2 \mathbf{R}}{dt^2} = -\nabla_{\mathbf{R}} V_m(\mathbf{R}) \quad (1.46)$$

and transitions between the electronic energy states occur stochastically with a probability

$$P_{n \leftarrow m} = \frac{2\Delta t}{\hbar} \text{Re} \left( \frac{\langle \psi_n | \frac{\partial}{\partial t} | \psi_m \rangle}{\langle \phi_m | \phi_m \rangle} \right) \quad (1.47)$$

where  $\Delta t$  is the time-step and the numerator in Eq. 1.47 is the nonadiabatic coupling between these states. There are various implementations of Surface Hopping including [65] those which combine path integral [66] and mapping variable [67] theories. The primary short coming of Surface Hopping methods is that they are not rigorously derivable from first principles and have well-known issue of over-coherence [68, 69]. Namely, at surface crossings the nuclear wavepacket should split into separate channels and decohere. To correct this issue, multi-spawning and cloning methods have been developed to allow bifurcations of the wavepacket at crossings and correct over-coherence [70, 71]. Nonetheless, these theories are fairly involved and the rules for spawning and cloning, although sensible, can be viewed as ad hoc.

A more fundamental issue belies all mixed quantum-classical methods, not just the nonadi-

abatic molecular dynamics theories discussed above. By treating, some degrees of freedom of the quantum system classically and others quantum mechanically, the feedback between their dynamics accrue errors [72, 73]. To this end, semiclassical methods, which treat all degrees of freedom with the same level of theory, are advantageous.

## Semiclassical Methods

The idea behind semiclassical<sup>5</sup> methods is fairly straightforward. As opposed to splitting degrees of freedom of a quantum system into those treated quantum mechanically and those treated classically, instead all degrees of freedom are treated at a level of theory between classical and quantum dynamics [6, 8, 74].

The Wentzel–Kramers–Brillouin (WKB) approximation helps illustrate this concept. Let

$$\psi(q) = e^{iS(q,E)/\hbar} \tag{1.48}$$

be an energy eigenstate of the one dimensional Hamiltonian

$$\hat{H} = -\frac{\hbar^2}{2m} \frac{d^2}{dq^2} + V(q) \tag{1.49}$$

with energy  $E$ . The exponential of the wavefunction can be expanded in powers of  $\hbar$  as

$$S(q, E) = S_0(q, E) + \frac{\hbar}{i} S_1(q, E) + \left(\frac{\hbar}{i}\right)^2 S_2(q) + \dots + \mathcal{O}(\hbar^n) \tag{1.50}$$

If one truncates the series to zeroth order  $\mathcal{O}(\hbar^0)$  [6], and substitutes the wavefunction into

---

<sup>5</sup>The term semiclassical is used in quantum mechanics in two very different ways. In one sense it is used to denote a quantum system immersed in a classical radiation field (as opposed to a quantum radiation field). In the other sense, it refers to an asymptotic expansion of a quantum equation of motion in powers of  $\hbar$  truncated to a finite order  $\mathcal{O}(\hbar^n)$  to approximate the quantum equation. Throughout this thesis, semiclassical is used only in this latter sense.

the time-independent Schrödinger equation

$$-\frac{\hbar^2}{2m} \frac{d^2\psi(q)}{dq^2} + (V(q) - E)\psi(q) = 0 \quad (1.51)$$

the classical Hamilton-Jacobi equation is recovered

$$\frac{1}{2m} \left( \frac{\partial S_0(q, E)}{\partial q} \right)^2 + V(q) - E = 0 \quad (1.52)$$

with the zeroth order action given by

$$S_0(q, E) = \pm \int_{q_0}^q p(q', E) dq' \quad (1.53)$$

The Hamilton-Jacobi equation is often called “the classical limit of the Schrödinger equation.” The Hamilton-Jacobi equation blurs the distinction between particle and wave with  $S_0(q, E)$  pictured as a surface of constant action emanating perpendicular to the trajectory of the particle akin to a wavefront. Physically, the  $\pm$  sign indicates trajectories of energy  $E$  with both positive and negative momentum (viz. trajectories traveling in either direction). The expansion in Eq. 1.50 is asymptotic and lower orders actions can be used to determine the higher order actions. To first order in  $\mathcal{O}(\hbar)$ , one can show

$$\frac{dS_1(q, E)}{dq} = \frac{1}{2} \frac{d^2 S_0}{dq^2} \left( \frac{dS_0}{dq} \right)^{-1} \quad (1.54)$$

with the solution

$$S_1(q, E) = -\frac{1}{2} \ln(p(q, E)) + \text{constant} \quad (1.55)$$

and the semiclassical wavefunction to this order is

$$\psi(q) \approx \pm \frac{1}{\sqrt{p(q, E)}} \exp \left( +\frac{i}{\hbar} \int_{q_0}^q p(q', E) dq' \right) \quad (1.56)$$

Eq. 1.56 is called the *WKB approximation* or wavefunction. The interpretation is: to  $\mathcal{O}(\hbar)$ , the quantum wavefunction can be approximated by summing over trajectories with energy  $E$  starting at  $q_0$  and arriving at  $q$ . Note the prefactor has dimensions of a probability density and the argument of the exponential is a dimensionless complex number. Semiclassical approximations, thus, represent the wavefunction as a classical density appended by a complex phase (the action integral of a classical trajectory). This is a hallmark of all semiclassical theories. In general, there are many such trajectories with beginning at  $q_0$  and terminating at  $q$  with an energy  $E$ , and semiclassical approximations often involve summing over these different possibilities,

$$\psi^{SC}(q) \approx \pm \sum_n \frac{1}{\sqrt{p_n(q, E)}} \exp\left(+\frac{i}{\hbar} \int_{q_0}^q p_n(q', E) dq'\right). \quad (1.57)$$

Thus semiclassical theories are naturally formulated in terms of path integrals. Because semiclassical theories involve an asymptotic expansion in  $\hbar$ , they can be viewed as a quantum corrections to classical mechanics or a low order approximation to quantum mechanics (Fig. 1.10). Moreover semiclassical theory can be equivalently formulated in the time-domain (as opposed to energy). Time-domain semiclassical theories are have been widely and successfully applied to modeling complex reaction dynamics and molecular spectroscopy [6].

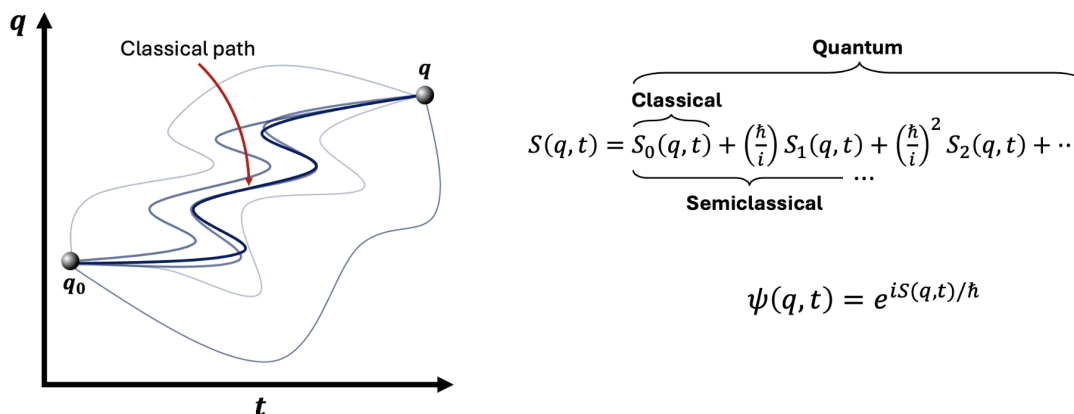


Figure 1.10: Path integral interpretation of semiclassical theories.

There are a number of advantages of semiclassical theories. Foremost, they avoid the feed-

back problem of mixed quantum-classical methods by treating all degrees of freedom at the same level of approximation. They are able to capture quantum effects like tunneling, zero-point energy, and depending on the level of sophistication of the theory, some extent of quantum coherence [75]. Their most compelling strength is because they construct quantum dynamics from classical trajectories, their solutions scale linearly  $\mathcal{O}(N)$ . Thus semiclassical methods can be used to simulate quantum effects in larger systems. Since semiclassical theories construct quantum dynamics, order-by-order in  $\hbar$ , they are tailored to understand the emergence of classical mechanics out of quantum mechanics and loss of quantum coherence (decoherence).

But semiclassical methods are not without shortcomings. The fundamental flaw in semiclassical theories is the “sign problem.” The summing over many oscillatory phase factors makes converging semiclassical results particularly challenging. And because classical trajectories are used to proxy the underlying quantum density, they, —like classical systems, can be sensitive to initial conditions. A variety of filtering and sampling methods have been developed address these issues with success, but this comes at the expense of increasing the computational overhead [76, 77].

To summarize this section, molecules are complex assemblages of electrons and nuclei. Solving the quantum dynamics of a general quantum system is exponentially costly. The added issue of quantum dynamics in molecules is the unavoidable size of the system and coupling between nuclear and electronic degrees of freedom. If the goal is to understand how quantum coherences mediate molecular processes like reaction dynamics and spectroscopy, an approximate theory which doesn’t neglect coherence between molecular degrees of freedom, but scales sensibly is necessary. For this reason, a trajectory-based approach is desirable, but one which circumvent issues implicit in mixed quantum-classical and semiclassical theories.



## 1.4 Methods

### 1.4.1 The Wigner-Moyal Representation

The primary formalism employed in this thesis is the Wigner-Moyal Representation [13, 78]. In the Wigner-Moyal Representation, the quantum density is transformed into a probability distribution function on phase space

$$\hat{\rho} \rightarrow W(\mathbf{q}, \mathbf{p}).$$

The distribution  $W(\mathbf{q}, \mathbf{p})$  is called the Wigner function and evolves under the phase space representation of the quantum Liouville equation called the Wigner-Moyal equation:

$$\frac{\partial \hat{\rho}}{\partial t} = \frac{1}{i\hbar} [\hat{H}, \hat{\rho}] \rightarrow \frac{\partial W}{\partial t} = [H, W]_{\star}$$

where  $[A, B]_{\star} = \frac{1}{i\hbar} (A \star B - B \star A)$  is the phase space analog of a commutator (called the Moyal bracket). The star product (denoted  $\star$ ) is a special non-commutative product akin to typical products of operators. Functions  $A$  and  $B$  are phase space representations of operators or observables called Weyl symbols.

This formulation, although less familiar than traditional Hilbert space approaches, has many unique merits. Historically classical mechanics, classical optics, and classical statistical mechanics were formulated in phase space. Phase space provides a unified domain for describing the statistics of optical and mechanical phenomena.

For the purpose of developing trajectory-based quantum molecular dynamics methods, the Wigner-Moyal representation is particularly well-suited. The Wigner-Moyal equation can be developed semiclassically akin to the WKB wavefunction as an expansion of its star product. It can recover classical mechanics in the classical limit  $\hbar \rightarrow 0$  or  $\mathcal{O}(\hbar^0)$  truncation. Thus

Wigner-Moyal representation gives one control of the degree of quantumness of a solution. In some cases the Wigner-Moyal equation's solution can be resummed to obtain an exact quantum result without approximation.

As a consequence of the quantum state being represented as a probability distribution in the Wigner-Moyal Representation, the Wigner function can naturally be sampled by trajectories to generate classical estimations of quantum expectation and dynamics. A well-known complication with the Wigner-Moyal Representation is that Wigner function is that is not a proper probability distribution. Namely, Wigner functions are not positive-definite on phase space and can possess regions of negative probabilities. These negative probabilities are the hallmark of quantum interference and coherence in superposition states. While this would seem to present a hurdle to sampling the Wigner function with classical trajectory ensembles, the primary contribution of this thesis is a theory to address this precise issue.

### 1.4.2 The Time-Domain: The Interplay of Dynamics and Spectroscopy

To illustrate the formalism developed in this thesis, linear absorption spectra are calculated for simple model systems. The *time-dependent* or *time-domain* formulation of spectroscopy is employed. Time-domain spectroscopy is best understood in contrast to the *energy-domain*.

Traditionally in the energy-domain [79], a general bound-state spectrum  $\sigma(\Omega)$  is computed by

$$\sigma(\Omega) = \sum_n |c_n|^2 \delta(\Omega - \Omega_n) \quad (1.58)$$

where  $\Omega_n = E_n/\hbar$  and  $c_n$  is the probability amplitude of the total wavefunction  $|\Psi\rangle$  expressed in the basis  $\{|\psi_n\rangle\}$  with  $c_n = \langle\psi_n|\Psi\rangle$ .

The eigenenergies are obtained by the time-independent Schrödinger equation

$$\hat{H}\psi_n = E_n\psi_n \quad (1.59)$$

Thus to use the energy-domain one needs first to obtain the eigenenergies  $E_n$  by solving the time-independent Schrödinger equation. The number of eigenenergies for molecules of roughly 10 atoms can be as large as  $10^{15}$  eigenenergies and intractable for reasons discussed. Moreover, supposing all eigenenergies could be calculated, they can't be easily resolved and assigned to a particular transition. The reliance of eigenvalues makes the energy-domain ill-suited for molecular spectroscopy calculations.

The time-domain approach, however, can circumvent the direct eigenvalue problem. For a bound state in a complete orthonormal basis  $\{|\psi_n\rangle\}$  satisfying Eq. 1.59, its general solution is

$$\begin{aligned} |\Psi(t)\rangle &= \sum_n c_n e^{-iE_n t/\hbar} |\psi_n\rangle \\ &= \hat{U}(t) |\Psi(0)\rangle \end{aligned} \quad (1.60)$$

In the time-domain, the spectrum  $\sigma$  is Fourier transform of the autocorrelation of the wavefunction,

$$\sigma(\Omega) = \frac{1}{2\pi} \int \langle \Psi(0) | \Psi(t) \rangle e^{i\Omega t} dt \quad (1.61)$$

Superficially the time-domain doesn't look like an improvement over the energy-domain. The formal solution Eq. 1.60 still has eigenvalues. The subtlety is  $|\Psi(t)\rangle$  doesn't need to be propagated exactly. Often an approximate time-evolution operator  $\hat{U}_{approx}(t)$  representing any of the approximate methods discussed above will suffice to resolve important transitions

in the spectrum. Thus in the time-domain, the spectrum typically calculated as

$$\begin{aligned}\sigma(\Omega) &\approx \frac{1}{2\pi} \int \langle \Psi(0) | \hat{U}_{approx}(t) | \Psi(0) \rangle e^{i\Omega t} dt \\ &\approx \frac{1}{2\pi} \int \langle \Psi(0) | \Psi_{approx}(t) \rangle e^{i\Omega t} dt\end{aligned}\tag{1.62}$$

Time and the energy-domain are just different Fourier representations of the same spectrum and mathematically equivalent. This can be shown by inserting Eq. 1.60 into Eq. 1.61 which yields

$$\begin{aligned}\sigma(\Omega) &= \frac{1}{2\pi} \int dt e^{i\Omega t} c_m^* c_n e^{-E_n t/\hbar} \langle \psi_m | \psi_n \rangle \\ &= \frac{1}{2\pi} \int dt e^{i\Omega t} c_m^* c_n \delta_{mn} e^{-E_n t/\hbar} e^{i\Omega t}\end{aligned}\tag{1.63}$$

And from the integral identity of the delta function

$$\delta(x - x_0) = \frac{1}{2\pi} \int dk e^{ik(x-x_0)}\tag{1.64}$$

the energy-domain spectrum is recovered

$$\sigma(\Omega) = \sum_n |c_n|^2 \delta\left(\Omega - \frac{E_n}{\hbar}\right) = \sum_n |c_n|^2 \delta(\Omega - \Omega_n)\tag{1.65}$$

## 1.5 Scope of Work

In this thesis, a trajectory-based quantum dynamics theory in phase space is developed for simulating quantum coherence dynamics and molecular spectra. The theory is born out of insights gained from original work solving the evolution of a vibrational coherence generated by a vertical excitation in displaced oscillator models. It is shown the traditional semiclassical solution for the 2 level quantum system fails to qualitatively describe the evolution of the quantum coherence leading to incorrect spectra. Using a Thawed Gaussian ansatz for the

Wigner function, the exact quantum solution is derived in phase space. By retaining higher orders in the Wigner-Moyal equation, the qualitative errors in the semiclassical solution can be corrected. This solution gives an intuitive picture of linear dynamics in 2 level quantum systems with the evolution of the quantum coherence in phase space being modulated by trajectories on both states simultaneously.

This insight is inspired a new formulation of the Wigner-Moyal equation called the Star Coherence Representation. The Star Coherence Representation solves the dynamics of the quantum density in terms of the evolution of the population Wigner functions and quantum phases with coherences calculated on-the-fly in terms of these quantities. This approach is the main original contribution of the thesis. Equations of motion for an  $N$  level quantum system are derived in this representation. To solve these equations, algorithms are developed, Moyal Assisted Dynamics and Hudson Density Estimation, which involves fitting classical trajectory ensembles to positive-definite Wigner functions (Hudson states) using various density estimation techniques. The approach is illustrated for harmonic and Morse potentials and captures the effects of anharmonic dynamics.

Because the contents of this thesis are largely method development, illustrations of its use are limited to small model systems. There is much room for future work. Applications to larger systems, nonlinear spectroscopies, and the generalizations to open quantum systems are alluded to, but not treated in detail.

### **1.5.1 Organization of Thesis**

Chapters 2 and 3 provide theoretical background on dynamics in phase space. Chapter 2 is a brief review of classical Hamiltonian dynamics, their phase space picture, and treatment of classical statistical ensembles. This is included to draw comparisons with Wigner-Moyal Representation. Chapter 3 is a detailed review of the Wigner-Moyal Representation. It is

an important chapter because it establishes the concepts, terminology, and notation used in original work in the succeeding chapters of the dissertation. Chapter 4 details a newly derived Thawed Gaussian solution for the displaced oscillator model and its comparison with traditional semiclassical approaches. Chapter 5 introduces the Star Coherence Representation and includes the derivation of its equations of motion for a general  $N$  level quantum system. Chapter 6 investigates solving the Star Coherence equations of motion with classical trajectory ensembles. The Moyal Assisted Dynamics and Hudson Density Estimation algorithms are introduced and their application to anharmonic systems illustrated. Chapter 7 concludes the work with a recap of the key results followed by a discussion of generalization and applications to systems of interest and nonlinear spectroscopic probes. The original contributions of this thesis are the contents of Chapters 4-7.

## 1.5.2 Typography and Conventions

A glossary of symbols has been provided to clarify some choices of notation. There are some regularly occurring conventions to note. Vector quantities are indicated with bolded lowercase letters  $\mathbf{x} = (x_1, \dots, x_n)$  and matrices with uppercase letters like  $\mathbf{X}$ . Operators are always indicated with a hat  $\hat{X}$ . Weyl symbols of operators are written as functions and without any  $W$  subscript. Wigner functions are indicated by  $W$  or  $\rho$  interchangeably. For example,  $W_\rho$ ,  $\rho$ ,  $W_\Psi$ , and  $W$  are equivalent for a pure state density. Complex conjugation is indicated by asterisks when working with Hilbert space quantities, but overlines are employed for phase space. For example  $\hat{\rho}_{mn} = (\hat{\rho}_{nm})^*$  in Hilbert space would be rendered as  $\rho_{mn} = \overline{\rho_{nm}}$  in phase space. Integral transforms are specified by rectangular bracket preceded by a script letter. For example  $\hat{\mathcal{F}}[g]$  and  $\hat{\mathcal{F}}^{-1}[g]$  read as the Fourier transform and Inverse Fourier transform of  $g$  respectively.

All integrals with unspecified limits are by default taken over all space

$$\int dx f(x) = \int_{-\infty}^{\infty} dx f(x)$$

and integrals over vector quantities are expressed by a single integrand over the bolded differential

$$\int d\mathbf{x} f(\mathbf{x}) = \int_{-\infty}^{\infty} dx_n \cdots \int_{-\infty}^{\infty} dx_1 f(x_1, \cdots, x_n).$$

## Chapter 2

# Theoretical Background: Classical Dynamics in Phase Space

The highest level of insight into quantum systems can be had only through a good grasp of classical mechanics. Even when classical and quantum mechanics are differing qualitatively and perhaps by orders of magnitude, the underlying answers are often still classical in origin, using classically determined amplitude and phase interference [6].

---

Eric Heller, 2018

Although quantum mechanics cannot be understood apart from classical physics, its beyond the scope of this thesis to provide a complete review of classical mechanics. There are plenty of great texts which the reader can reference (see [80–84] ) including Heller’s well-illustrated volume. Instead a self-contained synopsis of classical dynamics in phase space is attempted. The focus is to introduce the Hamiltonian formulation of classical mechanics and statistical ensemble enough that comparisons with the Wigner-Moyal Representation may be drawn. Given this scope, any discussion of Lagrangians, transformation theory, action-angle variables, is intentionally excluded.



## 2.1 Elements of the Hamiltonian Formulation

### 2.1.1 Definition of a Hamiltonian System

A *Hamiltonian system* of  $N$  degrees of freedom is defined by the set of  $2N$  first order differential equations (Hamilton's equations):

$$\frac{dq_i}{dt} = \frac{\partial H}{\partial p_i} \quad (2.1)$$

$$\frac{dp_i}{dt} = -\frac{\partial H}{\partial q_i} \quad (2.2)$$

for  $i \in [1, N]$  and where the scalar function  $H = H(q_1, \dots, q_N, p_1, \dots, p_N) \in \mathbb{R}$  is the Hamiltonian. The independent variables  $q_i \in \mathbb{R}$  and  $p_i \in \mathbb{R}$  are the generalized position and conjugate momentum for the  $i^{\text{th}}$  degree of freedom. The  $2N$  set of position and momentum are collectively referred to as the *canonical variables*.<sup>1</sup> Their values define the *state* of the classical system.

Vectorizing the canonical variables  $\mathbf{q} = (q_1, \dots, q_N)^T \in \mathbb{R}^N$  and  $\mathbf{p} = (p_1, \dots, p_N) \in \mathbb{R}^N$ , Hamilton's equations can be rewritten

$$\dot{\mathbf{q}} = \nabla_{\mathbf{p}} H \quad (2.3)$$

$$\dot{\mathbf{p}} = -\nabla_{\mathbf{q}} H \quad (2.4)$$

with  $H = H(\mathbf{q}, \mathbf{p})$  and where dots denote time derivatives,  $\dot{\mathbf{q}} = \frac{d\mathbf{q}}{dt}$  and  $\dot{\mathbf{p}} = \frac{d\mathbf{p}}{dt}$ .

The conjugate equations can be consolidated by letting  $\mathbf{z} = (\mathbf{q}, \mathbf{p})^T \in \mathbb{R}^{2N}$  and by introducing

---

<sup>1</sup>The term “canonical” in classical mechanics means “standard” or “by the canon” of literature of classical mechanics.

the symplectic structure matrix

$$\mathbf{J} = \begin{pmatrix} \mathbf{0}_N & \mathbf{1}_N \\ -\mathbf{1}_N & \mathbf{0}_N \end{pmatrix}. \quad (2.5)$$

Hamiltonian's equation can now be written compactly as

$$\dot{\mathbf{z}} = \mathbf{J}\nabla_{\mathbf{z}}H. \quad (2.6)$$

Eq. 2.6 defines a Hamiltonian system.<sup>2</sup> Although generally the Hamiltonian may generally be a function of time,  $H(\mathbf{z}, t)$ , only time-independent Hamiltonians  $H = H(\mathbf{z})$  will be considered. When this is the case the system is said to be *conservative* or *autonomous*.

Although not shown here, Hamilton's equations can be derived directly from The Principle of Extreme Action (Hamilton's Principle) [83]. Hamilton's equations are no less general. The dynamics of all conservative classical systems are by default Hamiltonian. Given the variety of conceivable dynamic systems described by known differential equations [85], it's remarkable that all energy-conserving mechanical processes in Nature should be take this specific form. Hamilton's equations are a set of  $2N$  ordinary differential equations subject to a symplectic structure. These features impose a specific algebra between canonical variables, restrict the behavior of solutions (trajectories) and impose a geometry on the domain of solutions (phase space) which will now be discussed.

### 2.1.2 Hamiltonian Dynamics as an Initial Value Problem

Having defined a conservative Hamiltonian system, its natural to ask, "What class of differential equations does Eq. 2.6 belong to, do solutions exist, and if so, how are they solved?"

---

<sup>2</sup>To be more precise, this equation defines a *canonical* Hamiltonian system meaning that  $J$  is even dimensional. It is possible to define more general Hamiltonian systems by a different choice of a structure matrix, but such systems are not typical in conservative motion.

Hamilton's equations are an instance of an *initial value problem* for a system of first order ordinary differential equations [86]. Such a system is described by the equations

$$\frac{d\mathbf{z}}{dt} = f(\mathbf{z}) \quad (2.7)$$

subject to the initial condition  $\mathbf{z}(t_0) = \mathbf{z}_0$ . Provided some modest conditions of continuity are met, solutions to Eq. 2.7, not only exist, but are unique. This is guaranteed by the Picard's Theorem (Existence and Uniqueness Theorem).

The conditions of continuity are formalized in the Lipschitz inequality. Namely if a function  $f(t, z_1, \dots, z_{2N})$  on a region  $D \in \mathbb{R}^{2N+1}$  is continuous in  $D$  and there exists a constant  $K \in \mathbb{R}_{>0}$  such that for any two points  $(t, z_1, \dots, z_{2N})$  and  $(t', z'_1, \dots, z'_{2N})$  in  $D$ ,

$$|f(t, z_1, \dots, z_{2N}) - f(t', z'_1, \dots, z'_{2N})| \leq K \sum_{i=1}^{2N} |z_i - z'_i|, \quad (2.8)$$

is satisfied, the system is said to be *Lipschitz continuous*.

The Picard Theorem states that for a system of first order ordinary differential equations on a region  $D \in \mathbb{R}^{2N+1}$

$$\begin{aligned} \frac{dz_1}{dt} &= f_1(t, z_1, \dots, z_{2N}) \\ &\vdots \\ \frac{dz_{2N}}{dt} &= f_{2N}(t, z_1, \dots, z_{2N}) \end{aligned} \quad (2.9)$$

if each function  $f_1, \dots, f_{2N}$  on  $D$  satisfies the Lipschitz condition, then for a real number  $t_0$  there will be an interval  $(t_0 - \epsilon, t_0 + \epsilon)$  on which there exists solutions  $z_1(t), \dots, z_{2N}(t)$  and given the constants  $z_1(t_0), \dots, z_{2n}(t_0)$  at  $t_0$ , the solutions satisfying these initial values

$$\begin{aligned} z_1(t_0) &= z_1(0) \\ &\vdots \\ z_{2N}(t_0) &= z_{2N}(0) \end{aligned} \quad (2.10)$$

and are unique [87, 88] .

These set of constants at  $t_0$  are the *initial values* or *initial conditions*. There is a physical significance to Picard’s Theorem. It implies that classical mechanical systems evolve in time deterministically. Given an initial state, integrating the system of differential equations uniquely determine the state at the next instant in time. This picture will be revisited in the following discussion of trajectories in phase space. For now note, Hamiltonian systems belong to the specific class differential equations known as first order initial value problems. The solutions to these problems exist and are unique by Picard’s Theorem. The issue then is “How to obtain these solutions?” This will depend on the form of the Hamiltonian  $H(\mathbf{z})$  in Eq. 2.6.

For a general Hamiltonian, there isn’t a prescriptive method for obtaining exact, closed form solutions. Solutions are typically obtained by numerical integration. The numerical stability of these solutions will depend on the numerical integration algorithm (integrator) employed. Symplectic integrators are known to preserve the symplectic structure of Hamiltonian dynamics and yield stable solutions. They are the default method for numerical solutions to Hamiltonian problems. But two important cases for which solutions can be readily obtained and are well understood are *linear systems* and *separable systems*.

Quadratic Hamiltonians, polynomials of degree two or less in canonical variables, are *linear systems* [86]. A quadratic Hamiltonian is defined by

$$H(\mathbf{z}) = \frac{1}{2} \mathbf{z}^T \mathbf{L} \mathbf{z} \tag{2.11}$$

where the matrix  $L \in \mathbb{R}^{2N \times 2N}$  is symmetric ( $L = L^T$ ). Hamilton’s equations for quadratic Hamiltonians are a linear system of first order ordinary differential equations

$$\dot{\mathbf{z}} = \mathbf{J} \mathbf{L} \mathbf{z}. \tag{2.12}$$

Obtaining solutions reduces to the linear algebraic problem of determining the eigenvalue/vectors of the matrix  $\mathbf{JL}$ . Because the dynamics of quadratic Hamiltonians are linear, their solutions in a limited sense resembles quantum dynamics.

A *separable system* is defined by a separable Hamiltonian. A separable Hamiltonian of  $N$  degrees of freedom factorizes into a sum of  $N$  one degree of freedom Hamiltonians

$$H(\mathbf{z}) = \sum_{i=1}^N H_i(z_i) \quad (2.13)$$

with

$$H(\mathbf{z}) = T(\mathbf{p}) + V(\mathbf{q}) \quad (2.14)$$

where  $T(\mathbf{p})$  and  $V(\mathbf{q})$  are the kinetic energy and potential energy functions. Hamilton's equations for a separable system reduce to

$$\frac{dp_i}{dt} = -\frac{V(\mathbf{q})}{dq_i} \quad (2.15)$$

$$\frac{dq_i}{dt} = \frac{T(\mathbf{p})}{dp_i}. \quad (2.16)$$

Separable differential equations can be solved straightforwardly by quadrature. In limited cases, quadrature can be done analytically through evaluating certain integrals and algebraic manipulations. Generally quadrature is done numerically on a grid to the required level of precision [89]. Because integration by quadrature is simple, it is highly practical to transform a Hamiltonian system to a canonical coordinate system in which the Hamiltonian is fully or mostly separable. When this cannot be done, systems are often approximated as separable. All separable systems are integrable by quadrature. The bulk of Hamiltonian formalism: Poisson brackets, transformation theory, the adiabatic approximation, and perturbation theory, is focused on the identification of a coordinate system that separates most (if not all) degrees of freedom (exactly or approximately) to render it integrable and

therefore solvable.

### 2.1.3 Poisson Brackets and the Liouvillian

As discussed above, Hamiltonian systems describe conservative classical motion. Their dynamics are an instance of an initial value problem. Linear and separable systems constitute important subclasses of systems which can be solved readily. Solving through integration can be facilitated by a prudent choice of coordinate system in which the Hamiltonian is separable. To identify such a coordinate system, it is helpful to introduce an important quantity called the Poisson bracket.

Consider two phase space function (dynamical variables)  $f(\mathbf{q}, \mathbf{p})$  and  $g(\mathbf{q}, \mathbf{p})$ . Their *Poisson bracket* is defined as

$$[f, g] = (\nabla_z f)^T \mathbf{J} (\nabla_z g) = \sum_{i=1}^N \frac{\partial f}{\partial q_i} \frac{\partial g}{\partial p_i} - \frac{\partial f}{\partial p_i} \frac{\partial g}{\partial q_i} \quad (2.17)$$

The Poisson bracket has the specific algebraic properties of a *Lie bracket*

$$[f, g] = -[g, f] \quad (\text{Antisymmetry}) \quad (2.18)$$

$$[af + bg, h] = a[f, h] + b[g, h] \quad (\text{Left Linearity}) \quad (2.19)$$

$$[h, af + gb] = a[h, f] + b[h, g] \quad (\text{Right Linearity}) \quad (2.20)$$

$$[f, [g, h]] + [g, [h, f]] + [h, [f, g]] = 0 \quad (\text{Jacobi Identity}) \quad (2.21)$$

plus the additional property of a product rule

$$[fg, h] = [f, h]g + f[g, h] \quad (\text{Leibniz Rule}) \quad (2.22)$$

where  $h(\mathbf{q}, \mathbf{p})$  and  $a, b \in \mathbb{R}$ . These algebraic properties are a consequence of the symplectic structure matrix  $\mathbf{J}$  which defines the Hamiltonian system.

The utility of Lie brackets is that they can be used to integrate, identify symmetries, and derive perturbative solutions to nontrivial dynamics. When two functions  $X$  and  $Y$  commute under a Lie bracket  $[X, Y] = 0$ , this implies the vector flows of  $X$  and  $Y$  define a surface embedded in some manifold  $\mathcal{M}$  where  $X$  and  $Y$  are local coordinate vectors [83]. For the Poisson bracket, the local coordinates are the canonical variables and satisfy the relations

$$[q_i, q_j] = [p_i, p_j] = 0 \quad (2.23)$$

and

$$[q_i, p_j] = \delta_{ij} \quad (2.24)$$

and Hamilton's equations can be expressed in terms of Poisson Brackets as

$$\dot{\mathbf{q}} = [\mathbf{q}, H] \quad (2.25)$$

$$\dot{\mathbf{p}} = [\mathbf{p}, H]. \quad (2.26)$$

Together these imply for an arbitrary dynamic variable  $f(\mathbf{q}, \mathbf{p}, t)$ , its total time derivative can be computed by bracketing it with the Hamiltonian

$$\frac{df}{dt} = [f, H] + \frac{\partial f}{\partial t}. \quad (2.27)$$

Note if the dynamic variable  $f$  is time-independent, the rightmost term vanishes in Eq. 2.27.

It is useful to introduce an operator  $\hat{\mathcal{L}} = -[H, \cdot]$  called the *Liouvillian*.<sup>3</sup> Using the Liouvillian

---

<sup>3</sup>Some authors define the Liouvillian using as  $\hat{\mathcal{L}} = -i[H, \cdot]$ . But provided it is defined and used consistently, the factor of  $i$  is immaterial [90].

Eq. 2.27 can be rewritten as

$$\frac{df}{dt} = \hat{\mathcal{L}}f + \frac{\partial f}{\partial t} \quad (2.28)$$

where the action of  $\hat{\mathcal{L}}$  on  $f$  is given by  $\hat{\mathcal{L}}f = -[H, f]$ . The physical significance of the Liouvillian is that it gives a criterion for identifying conserved quantities which relate to mechanical symmetries of the system. For example, the action of the Liouvillian on a time-independent Hamiltonian vanishes as a result of the antisymmetry of the Poisson Bracket,

$$\hat{\mathcal{L}}H = -[H, H] = 0 \quad (2.29)$$

This implies the conservation of energy of the system along its solutions (trajectories). In general, such if a time-independent dynamic variable  $f(\mathbf{q}, \mathbf{p})$  vanishes with the Liouvillian,

$$\hat{\mathcal{L}}f = 0 \quad (2.30)$$

it is conserved along the trajectory and is termed a *constant of motion*. Constants of motion are also called integral curves because of their invariance under motion induced by the Hamiltonian.

### 2.1.4 Integration

Identifying constants of motion not only reveals information about the symmetries of the mechanical problem, but can simplify the task of integration. For a conservative Hamiltonian system of  $N$  degrees of freedom, if there are  $N$  constants of motion  $[I_n, H] = 0$  such that

$$[I_m, I_n] = 0 \quad (2.31)$$



for all  $m, n \in [1, N]$ , the system is said to be *completely integrable*. The relationship between the constants of motion in Eq. 2.31 should look familiar. It is the Poisson bracket definition for the canonical variables (Eqs. 2.23-2.24). The constants of motion  $\mathbf{I} = (I_1, \dots, I_N)$  can be taken as new momenta, conjugate to new position coordinates  $\mathbf{Q} = (Q_1, \dots, Q_N)$  and  $(\mathbf{Q}, \mathbf{I})$  used as canonical variables in place of  $(\mathbf{q}, \mathbf{p})$ .

The advantage of the  $(\mathbf{Q}, \mathbf{I})$  coordinate system over  $(\mathbf{q}, \mathbf{p})$  is that because each  $I_n$  is constant in time, its conjugate variable  $Q_n$  vanishes from the Hamiltonian

$$-\frac{dI_n}{dt} = \frac{\partial H}{\partial Q_n} = 0. \quad (2.32)$$

Coordinates which satisfy Eq. 2.32 are called *ignorable* (or cyclic). For each ignorable coordinate  $Q_n$ , its equation of motion will be a linear function of time

$$\frac{dQ_n}{dt} = \frac{\partial H}{\partial I_n}, \quad (2.33)$$

and solving the dynamics is a trivial task by quadrature.

To summarize, for a *completely integrable* system of  $N$  degrees of freedom, there all  $N$  ignorable coordinates  $Q_n$  conjugate to the constants of motion  $I_n$ . For such a system the Hamiltonian is a function of only the momenta  $H = H(\mathbf{I})$ . As a result, solving the dynamics of a completely integrable system is trivial because each coordinate  $Q_n$  is a linear function of time and its conjugate momentum  $I_n$  is constant. While all integrable systems are solvable by this procedure (and all separable systems are integrable), not all Hamiltonian systems are integrable. However, even in this case the Liouvillian can still be used to obtain exact or approximation solutions.

Returning to Eq. 2.28, its formal solution is

$$f(\mathbf{q}, \mathbf{p}; t) = e^{\hat{\mathcal{L}}(t-t_0)} f(\mathbf{q}, \mathbf{p}; t_0) \quad (2.34)$$

where  $t_0$  is the initial time. This equation indicates the time-evolution of an arbitrary dynamical variable is obtained by action of operator  $e^{\hat{\mathcal{L}}(t-t_0)}$  on the dynamical variable. For this reason  $e^{\hat{\mathcal{L}}(t-t_0)}$  is sometimes called the *classical propagator*. Because the propagator is a function of an operator, in this case the Liouvillian, its action is given in terms of a Taylor series representation

$$\begin{aligned} f(\mathbf{q}, \mathbf{p}; t) &= \left( \sum_{k=0}^{\infty} \frac{(t-t_0)^k}{k!} \hat{\mathcal{L}}^k \right) f(\mathbf{q}, \mathbf{p}; t_0) \\ &= \left( 1 + (t-t_0)\hat{\mathcal{L}} + \frac{(t-t_0)^2}{2}\hat{\mathcal{L}}^2 + \dots \right) f(\mathbf{q}, \mathbf{p}; t_0) \\ &= \left( 1 - (t-t_0)[H, \cdot] + \frac{(t-t_0)^2}{2}[H, [H, \cdot]] - \dots \right) f(\mathbf{q}, \mathbf{p}; t_0) \end{aligned} \quad (2.35)$$

The physical interpretation of this equation is that the unfolding of the dynamics of the system is generated by repeated action of the Liouvillian on a dynamical variable. Each order of time  $\mathcal{O}(t^n)$  corresponds to  $n$ -fold actions of the Liouvillian. The series in Eq. 2.35 is infinite and for general systems is approximated to a given time order. However, there are two important cases in which it can be used to obtain exact analytic results: (1) when the series terminates through the vanishing of derivatives or (2) when it can be resumed to a closed form expression. Because this idea will reemerge in next chapter in relation to the star product, a worked example for the 1-D harmonic oscillator is provided below [91].

---

**Example:** Solving Dynamics by the Liouvillian for a Harmonic Oscillator

Consider a 1-D harmonic oscillator of  $m = \omega = 1$ . Its Hamiltonian is  $H = \frac{1}{2}(p^2 + q^2)$ .

Hamilton's equations in the Liouvillian representation give

$$\frac{dq}{dt} = \hat{\mathcal{L}}q = -[H, q] = p, \quad \frac{dp}{dt} = \hat{\mathcal{L}}p = -[H, p] = -q$$

which have the formal solution(Eq. 2.28):

$$q(t) = e^{-\hat{\mathcal{L}}t}q(0) = \sum_{n=0}^{\infty} \frac{t^n}{n!} \hat{\mathcal{L}}^n q(0), \quad p(t) = e^{-\hat{\mathcal{L}}t}p(0) = \sum_{n=0}^{\infty} \frac{t^n}{n!} \hat{\mathcal{L}}^n p(0).$$

By repeated action of the Liouvillian and using the recursive property  $\hat{\mathcal{L}}^{n+1} = \hat{\mathcal{L}}^n (\hat{\mathcal{L}})$ , one finds:

$$\begin{aligned} \hat{\mathcal{L}}^2 q &= \hat{\mathcal{L}} (\hat{\mathcal{L}}q) = \hat{\mathcal{L}}(p) = -q & \hat{\mathcal{L}}^2 p &= \hat{\mathcal{L}} (\hat{\mathcal{L}}p) = \hat{\mathcal{L}}(-q) = -p \\ \hat{\mathcal{L}}^3 q &= \hat{\mathcal{L}} (\hat{\mathcal{L}}^2 q) = \hat{\mathcal{L}}(-q) = -p & \hat{\mathcal{L}}^3 p &= \hat{\mathcal{L}} (\hat{\mathcal{L}}^2 p) = \hat{\mathcal{L}}(-p) = q \\ \hat{\mathcal{L}}^4 q &= \hat{\mathcal{L}} (\hat{\mathcal{L}}^3 q) = \hat{\mathcal{L}}(-p) = q & \hat{\mathcal{L}}^4 p &= \hat{\mathcal{L}} (\hat{\mathcal{L}}^3 p) = \hat{\mathcal{L}}(q) = p \\ \hat{\mathcal{L}}^5 q &= \hat{\mathcal{L}} (\hat{\mathcal{L}}^4 q) = \hat{\mathcal{L}}(q) = -q & \hat{\mathcal{L}}^5 p &= \hat{\mathcal{L}} (\hat{\mathcal{L}}^4 p) = \hat{\mathcal{L}}(p) = -q \end{aligned}$$

Collecting like powers for the canonical variables, the series can be resumed in terms of transcendental functions to yield the exact equations of motion,

$$\begin{aligned} q(t) &= q(0) \left( 1 - \frac{t^2}{2!} + \frac{t^4}{4!} - \dots \right) + p(0) \left( t - \frac{t^3}{3!} + \frac{t^5}{5!} - \dots \right) \\ &= q(0)\cos(t) + p(0)\sin(t) \\ p(t) &= -q(0) \left( t - \frac{t^3}{3!} + \frac{t^5}{5!} - \dots \right) + p(0) \left( 1 - \frac{t^2}{2!} + \frac{t^4}{4!} - \dots \right) \\ &= -q(0)\sin(t) + p(0)\cos(t). \end{aligned}$$


---

## 2.2 The Phase Space Picture

Hereto formal properties of the Hamiltonian systems and their solutions have been discussed. The discussion has focused on mathematical properties imposed by the symplectic structure  $\mathbf{J}$  implicit in Hamiltonian dynamics. These abstract properties can be given a visual interpretation which appeals to geometric intuition and vividly illustrates the strength of the Hamiltonian formulation of classical dynamics.

Recall a conservative Hamiltonian system is a system of first order differential equations in positions and momenta of the system. In the language of differential equations, the righthand side of Hamilton's equations (Eq. 2.6) defines the vector field of the system  $X_H$ ,

$$\frac{d\mathbf{z}}{dt} = \mathbf{J}\nabla_z H = \left( \frac{\partial H}{\partial \mathbf{p}}, -\frac{\partial H}{\partial \mathbf{q}} \right) = X_H \quad (2.36)$$

Solving the time evolution of the system amounts to solving for the parametric curve  $(\mathbf{q}(t), \mathbf{p}(t))$  passing through the vector field of  $X_H$  for a given initial condition  $(q(t_0), p(t_0))$ . This can be seen by rearranging Eq. 2.36

$$d\mathbf{z} = X_H dt \quad (2.37)$$

As a consequence of Picard's theorem each initial condition  $(\mathbf{q}(t_0), \mathbf{p}(t_0))$  has its own integral curve. In the language of mechanics, the integral curve is called a *trajectory* and each point in trajectory represents the *state* of the system at a given time. This is illustrate below for the 1-D harmonic oscillator.

In Fig. 2.1 the state of the system is represented by a point which is pulled through phase space by the Hamiltonian vector field  $X_H$ . Because the harmonic oscillator is periodic, the trajectory passes through itself as a closed orbit. Phase space orbits correspond to stable motion of a physical system.

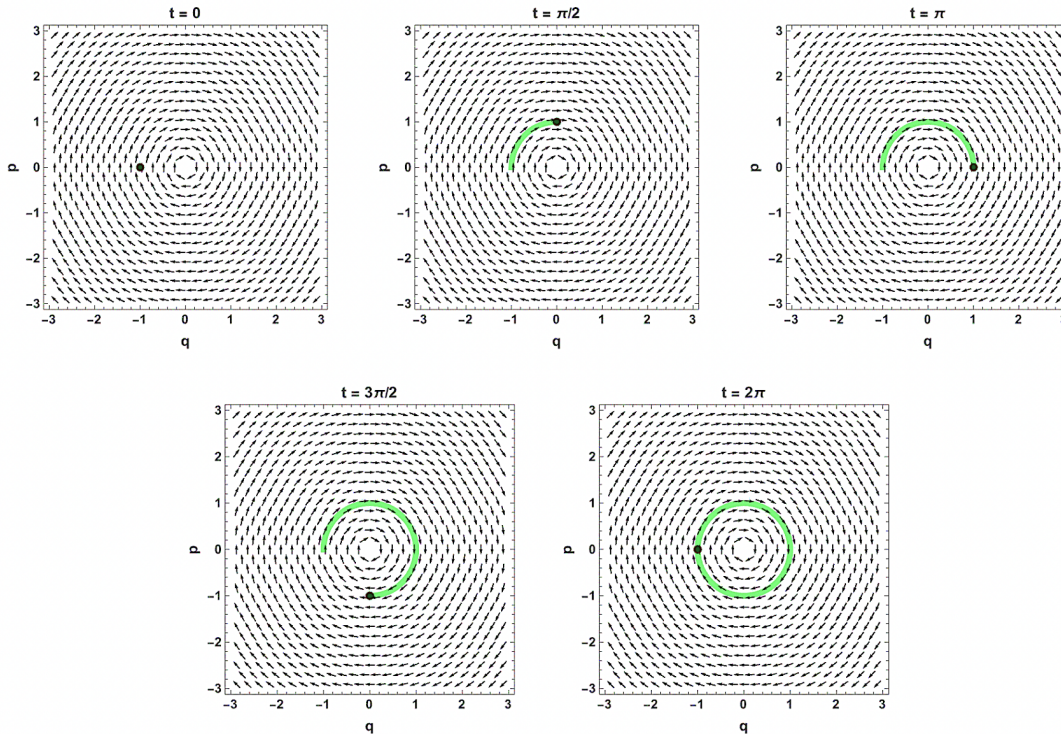


Figure 2.1: Evolution of a harmonic oscillator in phase space (left to right, top to bottom). Hamiltonian vector field  $X_H$  (black arrows). State of the system  $(q(t'), p(t'))$  (green dot). Trajectory  $(q(t), p(t))$  (light green curve).

## 2.3 Statistical Ensembles

The phase picture is more general than a device for visualizing the time-evolution of a single Hamiltonian system. It can be used to describe probabilistic mixtures of Hamiltonian systems through the use of ensemble averages. This was the original purpose of phase space as conceived by Gibbs [92]. Statistical ensembles allow us to introduce experimental uncertainty to the physical system and relate their dynamics to macroscopic properties.

### 2.3.1 The Gibbs Ensemble

Consider a set of  $\mathcal{N}$  of statistically independent replicas of the same Hamiltonian system each occupying a different state. Such a set is termed a *statistical ensemble*. Each replica

is represented by a point in phase space. One can define a density of states  $D(\mathbf{q}, \mathbf{p})$  as the fraction of replicas  $\mathcal{N}$  enclosed in a volume  $\Omega$  about an arbitrary point in phase space,

$$D(\mathbf{q}, \mathbf{p}) = \frac{\mathcal{N}}{\Omega}. \quad (2.38)$$

In the limit of large of a large number of replicas ( $\mathcal{N} \rightarrow \infty$ ) or vanishing volume ( $\Omega \rightarrow 0$ ), the phase points will become dense and coalesce into a continuous distribution

$$\rho(\mathbf{q}, \mathbf{p}) = \lim_{\substack{\mathcal{N} \rightarrow \infty \\ \Omega \rightarrow 0}} D(\mathbf{q}, \mathbf{p}) \quad (2.39)$$

which can be interpreted as a probability distribution. Given an arbitrary region in phase space,  $\rho(\mathbf{q}, \mathbf{p})$  indicates the probability of the system occupying that state. But for  $\rho$  to be a proper probability distribution it must satisfy normalization

$$1 = \int \int d\mathbf{q} d\mathbf{p} \rho(\mathbf{q}, \mathbf{p}) \quad (2.40)$$

and be positive-definite

$$\rho(\mathbf{q}, \mathbf{p}) > 0 \quad \forall \mathbf{q}, \mathbf{p}. \quad (2.41)$$

These two criteria define the probability density of a statistical ensemble.

### 2.3.2 Liouville's Theorem

The probability density obeys an important conservation law called *Liouville's Theorem* which states the density is constant along any trajectory in phase space. Thus phase space volume is conserved under time evolution. To see this, one substitutes  $\rho$  into Eq. 2.27 gives

$$\frac{d\rho}{dt} = [\rho, H] + \frac{\partial \rho}{\partial t}. \quad (2.42)$$

Because the classical phase space density is constructed out of states obeying Hamilton's equations whose trajectories can not cross, the flow of the density is incompressible (Fig. 2.2) and the density around any phase point must be constant

$$\frac{\partial \rho}{\partial t} = 0 \tag{2.43}$$

and thus

$$\frac{\partial \rho}{\partial t} = [H, \rho] = \hat{\mathcal{L}}\rho. \tag{2.44}$$

Eq. 2.44 is called Liouville's Equation or *Liouville's Theorem*. Although Liouville's Theorem can be derived for more general flows, for Hamiltonian systems it is ultimately a consequence of Picard's theorem for the uniqueness of solutions. The physical significance of Liouville's theorem is that the total probability of the ensemble is conserved under time evolution.

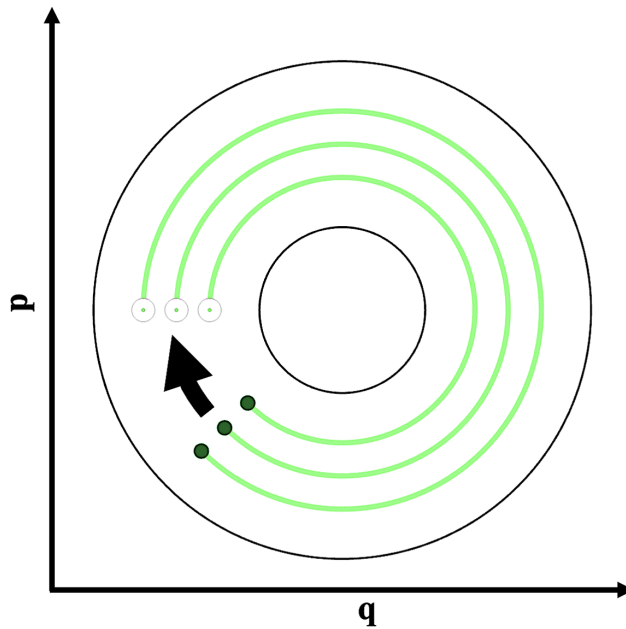


Figure 2.2: Example of incompressible Hamiltonian flow. Trajectories emanating from different initial conditions maintain their distance apart in phase space.

### 2.3.3 Ensemble Solutions to Liouville's Equation

Like a single Hamiltonian systems, for statistical ensemble there are only a few limited cases by which one can obtain analytical solutions to the equation of motion for the density. The techniques for solving these situations involve employing methods of characteristics [93], computing the eigenvalues of the Liouvillian to determine an integrating factor [94], or a Taylor expansion through the formal solution like in Eq. 2.35. In practice, for general systems the Liouville equation is solved by trajectory ensembles.

The trajectory ensemble approach is simple. First one samples the initial density  $\mathcal{N}$  times to generate an ensemble of initial conditions

$$(\mathbf{q}^{(n)}(t_0), \mathbf{p}^{(n)}(t_0)) \sim \rho(\mathbf{q}, \mathbf{p}, 0). \quad (2.45)$$

Each initial state is evolved by solving Hamilton's equation to form an ensemble of trajectories

$$\Gamma(\mathbf{q}, \mathbf{p}, t) = \frac{1}{\mathcal{N}} \sum_{n=1}^{\mathcal{N}} \delta(\gamma - \gamma^{(n)}(\mathbf{q}, \mathbf{p}, t)) \quad (2.46)$$

where

$$\delta(\gamma - \gamma^{(n)}(\mathbf{q}, \mathbf{p}, t)) = \delta(q - q^{(n)}(t), p - p^{(n)}(t)) = \delta(q - q^{(n)}(t)) \delta(p - p^{(n)}(t)) \quad (2.47)$$

Note the ensemble  $\Gamma$  is a sum of sharply localized delta functions. In practice, to obtain an estimate of  $\rho$  from  $\Gamma$ ,  $\Gamma$  is convolved with a smoothing function or fit to a positive-definite distribution (typically, a normal distribution). A Gaussian statistical ensemble for the harmonic oscillator is illustrated in Fig. 2.3.



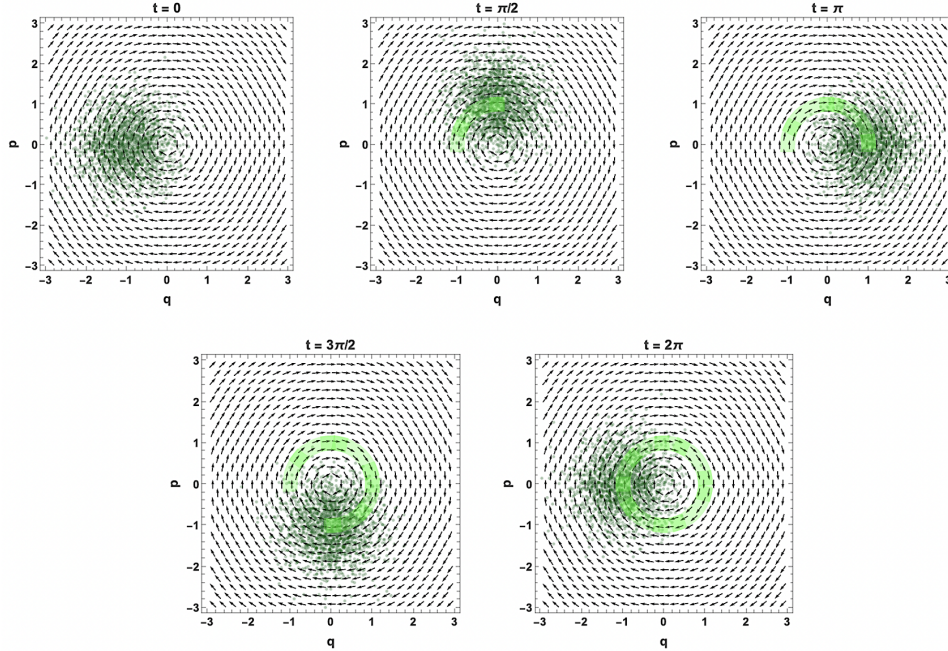


Figure 2.3: Evolution of a trajectory ensemble for the harmonic oscillator in phase space (left to right, top to bottom). Hamiltonian vector field  $X_H$  (black arrows). State of the ensemble  $(q(t'), p(t'))$  (green swarm). Mean trajectory  $(q(t), p(t))$  (light green curve).

### 2.3.4 Expectations and Correlation Functions

In both quantum mechanics and classical statistical mechanics, the goal is not so much to determine the time evolution of the state, but rather predict experimentally measurable quantities (observables) from it. Because in classical statistical mechanics, the state of the physical system is represented by a probability distribution  $\rho(\mathbf{q}, \mathbf{p}, t)$  of the ensemble, experimentally observable quantities like expectations or correlation functions are calculated as phase space averages over this distribution.

Suppose a dynamical variables  $f(\mathbf{q}, \mathbf{p}, t)$  corresponds to some observable. It's expectation is computed by

$$\langle f(t) \rangle = \frac{\int \int d\mathbf{q} d\mathbf{p} \rho(\mathbf{q}, \mathbf{p}, t) f(\mathbf{q}, \mathbf{p}, 0)}{\int \int d\mathbf{q} d\mathbf{p} \rho(\mathbf{q}, \mathbf{p}, t)} \quad (2.48)$$

where the denominator ensures normalization. Note oftentimes, a trace is used to denote

integration over all phase space

$$\text{Tr} ( ) = \int \int d\mathbf{q} d\mathbf{p}$$

It follows from Liouville's theorem that for a conservative system probability is conserved under time evolution,

$$\text{Tr} (\rho (\mathbf{q}, \mathbf{p}, 0)) = \text{Tr} (\rho (\mathbf{q}, \mathbf{p}, t)) = 1 \quad (2.49)$$

and its sufficient to use initial distribution for the normalization. Eq. 2.48 becomes

$$\langle f (t) \rangle = \frac{\text{Tr} (\rho (\mathbf{q}, \mathbf{p}, t) f (\mathbf{q}, \mathbf{p}, t))}{\text{Tr} (\rho (\mathbf{q}, \mathbf{p}, 0))} \quad (2.50)$$

Likewise because  $f$  depends on time only parametrically through the states of the ensemble [90],

$$f (\mathbf{q}, \mathbf{p}, t) = f (\mathbf{q}(t), \mathbf{p}(t)) = f (\mathbf{q}, \mathbf{p}; t)$$

Eq. 2.50 can be calculated by evolving  $f$  instead of  $\rho$

$$\langle f (t) \rangle = \frac{\text{Tr} (\rho (\mathbf{q}, \mathbf{p}, 0) f (\mathbf{q}, \mathbf{p}, t))}{\text{Tr} (\rho (\mathbf{q}, \mathbf{p}, 0))} \quad (2.51)$$

Similarly, time correlation functions between dynamical variables  $f (\mathbf{q}, \mathbf{p}, t)$  and  $g (\mathbf{q}, \mathbf{p}, t)$  are calculated as

$$\langle f (0) g (t) \rangle = \frac{\text{Tr} (\rho (\mathbf{q}, \mathbf{p}, 0) f (\mathbf{q}, \mathbf{p}, 0) g (\mathbf{q}, \mathbf{p}, t))}{\text{Tr} (\rho (\mathbf{q}, \mathbf{p}, 0))} \quad (2.52)$$

# Chapter 3

## Theoretical Background: Quantum Dynamics in Phase Space

There are at least three logically autonomous alternative paths to quantization. The first is the standard one utilizing operators in Hilbert space, developed by Heisenberg, Schrödinger, Dirac, and others in the 1920s. The second one relies on path integrals, and was conceived by Dirac and constructed by Feynman. The third one is the phase-space formulation based on Weyl's correspondence between functions in phase space and quantum mechanical operators in Hilbert space [13].

---

Curtright, Fairlie, and Zachos, 2014

The dynamics of classical systems admit several equivalent formulations (Newtonian, Lagrangian, Hamiltonian). These formulations differ in mathematical representations of the dynamic system, but are derived from the same underlying physical law (Principle of Extreme Action) [95]. In a similar way, quantum mechanics admits numerous formulations equivalent to standard Hilbert space representations like the Schrödinger equation and the quantum Liouville equation [96]. Different formulations of quantum mechanics have different

merits, challenges, and domains of application. In this regard, the phase space formulation of quantum mechanics is no different.

Formulations of quantum mechanics can be distinguished by their representation of quantum state and its equation of motion, but all formulations fall into three different categories organized by how quantization is achieved. Quantization is the process by which the  $i$ 's and  $\hbar$ 's, responsible for discreteness and interference, are imposed physical quantities and observables. Hilbert space formulations achieve quantization through the canonical commutation relations  $[\hat{q}, \hat{p}] = i\hbar$  [97]. Path integral formulations quantize through discretization of the quantum action integral [22]. Phase space formulations of quantum mechanics, in contrast, achieve quantization through a special non-commutative product. In the Wigner-Moyal Representation of quantum phase space, this is the Moyal or star product. Familiarity with the star product is essential to calculations in the quantum phase space.

By the beginning of 20<sup>th</sup> century, the phase space or Hamiltonian formulation of classical mechanics reviewed in the previous chapter was the default framework for solving classical dynamical problems. This raises an obvious question: “If phase space was the preferred formulation for solving classical dynamical problems, why wasn’t it —and to a large degree, still isn’t it, the standard method for solving quantum dynamical problems?”

The answer to this question is partly essential and partly incidental, but underlines some of virtues and challenges of quantum phase space. The original quantum theory (Old quantum theory) actually began in phase space as an attempt to quantize classical oscillator motion (Bohr-Sommerfeld quantization) [98]. By the 1920s the limits of this approach were apparent and were immediately succeeded by the wave and matrix mechanics of Schrödinger and Heisenberg, respectively. At that time phase space seemed like an outmoded device to describe “the new physics.” The uncertainty principle seems to prohibit defining a state in phase space or at least in the classical sense of a localized point, possessing a definite position and momentum. Moreover, the issue of indeterminacy in quantum measurement seemed to

preclude the classical picture of a state undergoing continuous trajectory motion. At this time, it was unclear how to describe quantum mechanical motion in phase space.

In addition conceptual hurdles, the development, dissemination, and use of quantum phase space methods was hindered by the mathematics it assumes. Unlike standard Hilbert space or path integral approaches where quantization is fairly intuitive, requiring little more than a knowledge of linear algebra or differential equations, the mathematics to describe phase space quantization is novel. The formal process of quantizing phase space (called *deformation quantization*) amounts to using a small parameter (in this case  $\hbar$ ) to transform a commuting algebra (classical mechanics) into a non-commuting one (quantum mechanics) [99–101]. This math wasn't codified until the 1960s [102], relies heavily on harmonic analysis [103]. Moreover, its generalization to non-Cartesian phase spaces was challenging enough to solicit a Fields Medal in mathematics [104, 105].

Following conceptual and mathematical hurdles, the phase space formulation of quantum mechanics has suffered for a merely incidental reasons. Unlike wave mechanics, matrix mechanics, and path integral formulations, which were developed in the span of a few short years by a few select individuals who focused on atomic and nuclear physics, the phase space formulation of quantum mechanics developed over the better part the 20<sup>th</sup> century by dozens of scientists working in fields as disparate as thermodynamics, optics, signal-processing, pure statistics, pure mathematics, string theory, chemical physics, particle physics, in addition to plain quantum theory [78, 106–110]. Consequently, its taken time for results to be communicated across disciplines and a coherent formalism to emerge.

In this chapter, the key ingredients of the Wigner-Moyal Representation are surveyed. This chapter is important because it integrates the formal results of the few seminal texts [13, 14, 78] and review articles [111–113] on the Wigner-Moyal Representation. It also establishes the terminology and typographical conventions for the original research in the following chapters.

### 3.1 Overview of Formulation

Quantum Mechanics in Hilbert Space and Phase Space		
State	$\hat{\rho} =  \Psi\rangle\langle\Psi $	$W(\mathbf{q}, \mathbf{p})$
Observables	$\hat{A}$	$A(\mathbf{q}, \mathbf{p})$
Products	$\hat{A}\hat{B}$	$A(\mathbf{q}, \mathbf{p}) \star B(\mathbf{q}, \mathbf{p})$
Expectations	$\text{Tr}(\hat{\rho}\hat{A})$	$\int \int d\mathbf{q} d\mathbf{p} W(\mathbf{q}, \mathbf{p})A(\mathbf{q}, \mathbf{p})$
Dynamics	$\frac{\partial \hat{\rho}}{\partial t} = \frac{1}{i\hbar} [\hat{H}, \hat{\rho}]$	$\frac{\partial W}{\partial t} = [H, W]_{\star}$

Table 3.1: Comparison of Quantum mechanics in Hilbert space and the Wigner-Moyal Representation.

A formulation of quantum mechanics requires a representation of the quantum state, a representation for observables, a multiplicative rule for computing products of observables, an equation of motion, and a method for calculating expectations. These ingredients for the Wigner-Moyal Representation and standard Hilbert space formulation of the quantum density are tabulated above (Tab. 3.1).

In the Wigner-Moyal Representation, the quantum state is represented by a quasi-probability distribution on phase space called the Wigner function,  $W(\mathbf{q}, \mathbf{p})$ . Unlike a classical probability distribution, the Wigner function is generally not positive-definite and possesses regions of negative probabilities. These negative probabilities can be viewed as a measure of quantum interference or coherence and lack any classical analog.

Observables in the Wigner-Moyal representation are functions on phase space called Weyl symbols,  $A(\mathbf{q}, \mathbf{p})$ . To impose the non-commutativity, Weyl symbols are multiplied through

the non-commutative star product,

$$A \star B \neq B \star A$$

The star product quantizes Weyl symbols through deformation of classical phase space, taking  $\hbar$  as the deformation parameter. The star product can be evaluated through differentiation or integration. Differential evaluations of the product can be truncated to an arbitrary order in  $\hbar$  and historically have been used to develop semiclassical approximations to quantum equations of motion.

Expectations are calculated through traces over phase space in a way closely analogous to classical statistical mechanics, but with dynamic variables replaced by Weyl symbols, commutative multiplication replaced by star multiplication, and the probability density distribution replaced by the Wigner function. The Wigner function's equation of motion (Wigner-Moyal equation) is the phase space representation of the quantum Liouville equation. The Wigner-Moyal equation resembles the classical Liouville equation only for quadratic potentials (linear dynamics). For general potentials, the Wigner-Moyal equation admits compressible probability flows relating sink and source terms in the dynamic vector field and stagnation points [114–117]. This feature complicates a traditional interpretation of the distribution represented in terms of ensembles of deterministically evolving trajectories, but not irrevocably.

## 3.2 Weyl Symbols and Wigner Transforms

### 3.2.1 Weyl Symbols

The most direct route to the phase space formulation of quantum mechanics is to understand how to translate familiar results in Hilbert space to phase space. The instrument for doing

this in the Wigner-Moyal Representation is known the *Weyl Correspondence*. For an operator in Hilbert space  $\hat{A} \in \mathcal{H}$ , the Weyl-Correspondence specifies the integral transform

$$A(\mathbf{q}, \mathbf{p}) = O_{\mathcal{W}} [\hat{A}] = \int d\mathbf{y} e^{-\frac{i}{\hbar} \mathbf{p} \cdot \mathbf{y}} \langle \mathbf{q} + \frac{\mathbf{y}}{2} | \hat{A} | \mathbf{q} - \frac{\mathbf{y}}{2} \rangle. \quad (3.1)$$

to obtain a phase space representation of the quantum operator. This phase space function is called the *Weyl symbol* of the operator. The Fourier Transform in Eq. 3.1 is called the *Weyl Transform*. It can be equivalently calculated in the momentum representation as

$$A(\mathbf{q}, \mathbf{p}) = O_{\mathcal{W}} [\hat{A}] = \int d\mathbf{y} e^{-\frac{i}{\hbar} \mathbf{q} \cdot \mathbf{y}} \langle \mathbf{p} + \frac{\mathbf{y}}{2} | \hat{A} | \mathbf{p} - \frac{\mathbf{y}}{2} \rangle. \quad (3.2)$$

Weyl symbols like  $A(\mathbf{q}, \mathbf{p})$  are like classical dynamical variables, but generally contain  $i$ 's and  $\hbar$ 's and are generally complex. The Weyl Transform takes any Hilbert space operator to its phase space Weyl symbol. One can show for an operator which is a separable function of canonical operators  $\hat{A}(\hat{q}, \hat{p}) = f_q(\hat{q}) + f_p(\hat{p})$ , its Weyl symbol is simply that same function, but of canonical variables. For example, polynomials of canonical operators

$$O_{\mathcal{W}} [\hat{q}^n] = q^n$$

$$O_{\mathcal{W}} [\hat{p}^m] = p^m$$

$$O_{\mathcal{W}} [\hat{q}^n + \hat{p}^m] = q^n + p^m$$

If, however, the operator is not separable into unmixed functions of canonical operators this rule does not hold. For example

$$O_{\mathcal{W}} [\hat{q}^n \hat{p}^m] \neq q^n p^m$$

and Weyl Transform must be calculated explicitly by Eq. 3.1. If the operator in a Weyl Transform happens to be the density operator  $\hat{\rho} = |\psi\rangle\langle\psi|$ , one obtains a phase space repre-



sentation of the quantum density

$$\begin{aligned}
O_{\mathcal{W}}[\hat{\rho}] &= \int d\mathbf{y} e^{-\frac{i}{\hbar}\mathbf{p}\cdot\mathbf{y}} \langle \mathbf{q} + \frac{\mathbf{y}}{2} | \hat{\rho} | \mathbf{q} - \frac{\mathbf{y}}{2} \rangle \\
&= \int d\mathbf{y} e^{-\frac{i}{\hbar}\mathbf{p}\cdot\mathbf{y}} \langle \mathbf{q} + \frac{\mathbf{y}}{2} | \psi \rangle \langle \psi | \mathbf{q} - \frac{\mathbf{y}}{2} \rangle \\
&= \int d\mathbf{y} e^{-\frac{i}{\hbar}\mathbf{p}\cdot\mathbf{y}} \psi \left( \mathbf{q} + \frac{\mathbf{y}}{2} \right) \overline{\psi \left( \mathbf{q} - \frac{\mathbf{y}}{2} \right)}
\end{aligned} \tag{3.3}$$

To make  $O_{\mathcal{W}}[\hat{\rho}]$  a probability density of correct dimensions, it can be multiplied by a prefactor

$$W_{\psi}(\mathbf{q}, \mathbf{p}) = \left( \frac{1}{2\pi\hbar} \right)^n O_{\mathcal{W}}[\hat{\rho}] \tag{3.4}$$

The righthand-side of Eq. 3.4 is called the *Wigner Transform* of the pure state  $\psi$  and  $W_{\psi}$  its *Wigner function*.

### 3.2.2 Wigner Transforms

The Wigner Transform can be formulated in terms of a pure or mixed quantum state. First consider the case of a pure state density which is the outer product of square integrable wavefunctions  $\psi \in L_2(\mathbb{R}^n)$ . The Wigner function associated with that state  $W_{\psi}$  is defined in terms of the *Wigner Transform*  $\mathcal{W}$ ,

$$W_{\psi}(\mathbf{q}, \mathbf{p}) = \mathcal{W}[\psi] = \left( \frac{1}{2\pi\hbar} \right)^n \int d\mathbf{y} e^{-\frac{i}{\hbar}\mathbf{p}\cdot\mathbf{y}} \psi \left( \mathbf{q} + \frac{\mathbf{y}}{2} \right) \overline{\psi \left( \mathbf{q} - \frac{\mathbf{y}}{2} \right)}. \tag{3.5}$$

The Wigner transform can be generalized to two states  $|\psi\rangle$  and  $|\phi\rangle$ . For two such functions  $\psi, \phi \in L_2(\mathbb{R}^n)$ , a *Cross Wigner function* is defined in terms of the *Cross Wigner Transform*

$$W_{\psi, \phi}(\mathbf{q}, \mathbf{p}) = \mathcal{W}[\psi, \phi] = \left( \frac{1}{2\pi\hbar} \right)^n \int d\mathbf{y} e^{-\frac{i}{\hbar}\mathbf{p}\cdot\mathbf{y}} \psi \left( \mathbf{q} + \frac{\mathbf{y}}{2} \right) \overline{\phi \left( \mathbf{q} - \frac{\mathbf{y}}{2} \right)}. \tag{3.6}$$

From the definition in Eq. 3.6, its obvious the Wigner Transform is a particular case of the Cross Wigner Transform when  $\phi = \psi$ , namely

$$\mathcal{W}[\psi, \psi] = \mathcal{W}[\psi] \quad \text{and} \quad W_{\psi\psi} = W_{\psi}$$

It also follows that exchanging the arguments of the Cross Wigner Transform yields Cross Wigner functions which are complex conjugates of each other

$$W_{\psi\phi} = \overline{W_{\phi\psi}} \tag{3.7}$$

and that while Cross Wigner functions are generally complex, Wigner functions must be real-valued.<sup>1</sup>

### 3.2.3 Algebraic Properties of the Cross Wigner Transform

The Cross Wigner Transform is a sesquilinear mapping [14]:

$$\mathcal{W}[\psi, \phi_1 + \phi_2] = \mathcal{W}[\psi, \phi_1] + \mathcal{W}[\psi, \phi_2] \tag{3.8}$$

$$\mathcal{W}[\psi_1 + \psi_2, \phi] = \mathcal{W}[\psi_1, \phi] + \mathcal{W}[\psi_2, \phi] \tag{3.9}$$

$$\mathcal{W}[\lambda\psi, \phi] = \lambda\mathcal{W}[\psi, \phi] \tag{3.10}$$

$$\mathcal{W}[\psi, \lambda\phi] = \bar{\lambda}\mathcal{W}[\psi, \phi] \tag{3.11}$$

where  $\lambda \in \mathbb{C}$ . The transform is seqsuilinear in the sense it is linear in its right argument and anti-linear in its left argument. But the plain (uncrossed) Wigner transform is not linear it

---

<sup>1</sup>Wigner Transforms and functions are used in many fields outside of quantum mechanics, particularly signal processing. A Wigner function is sometimes called the Self Wigner function or Auto Wigner function and the Cross Wigner function is sometimes called a Mixed Wigner function [110].

its argument. Namely,

$$\mathcal{W}[\psi_1 + \psi_2] \neq \mathcal{W}[\psi_1] + \mathcal{W}[\psi_2] \quad (3.12)$$

Instead for a sum of functions  $\psi_1 + \psi_2$ , the Wigner transform will contain cross terms,

$$\begin{aligned} \mathcal{W}[\psi_1 + \psi_2] &= \mathcal{W}[\psi_1] + \mathcal{W}[\psi_2] + \mathcal{W}[\psi_1, \psi_2] + \mathcal{W}[\psi_2, \psi_1] \\ &= \mathcal{W}[\psi_1] + \mathcal{W}[\psi_2] + 2\text{Re}(\mathcal{W}[\psi_1, \psi_2]) \end{aligned} \quad (3.13)$$

The cross terms are the Cross Wigner functions of each function in sum. In general, the Wigner function of a linear combination of wavefunctions, a superposition, is not a simple linear combination of each wavefunction's Wigner function. Nonetheless the cross terms can be related to the individual Wigner functions through the polarization identities,

$$\begin{aligned} \text{Re}(\mathcal{W}[\psi, \phi]) &= \frac{1}{4}(\mathcal{W}[\psi + \phi] - \mathcal{W}[\phi + \psi]) \\ &= \frac{1}{2}(\mathcal{W}[\psi + \phi] - \mathcal{W}[\psi] - \mathcal{W}[\phi]) \\ &= \frac{1}{2}(\mathcal{W}[\psi] + \mathcal{W}[\phi] - \mathcal{W}[\psi + \phi]) \end{aligned} \quad (3.14)$$

In general for a  $N$  component superposition  $\Psi = \sum_{m=1}^N c_m \psi_m$  where  $\psi_m \in L_2(\mathbb{R}^n)$ , its Wigner function is given by the Wigner transform

$$\mathcal{W}[\Psi] = \sum_{m=1}^N |c_m|^2 \mathcal{W}[\psi_m] + 2\text{Re} \left( \sum_{\substack{m=1 \\ n>m}}^N \sum_{n=1}^N c_m \bar{c}_n \mathcal{W}[\psi_m, \psi_n] \right) \quad (3.15)$$

The Wigner function for an  $N$  component superposition is a sum  $N$  Wigner functions and the real portion of  $\binom{N}{2}$  Cross Wigner functions. The cross Wigner functions are interference terms responsible for the quantum coherence between the  $N$  components of the quantum state. To make this more explicit,  $\Psi$  written as a density matrix  $\hat{\rho} = |\Psi\rangle\langle\Psi|$  will have

elements

$$\hat{\rho} = c_m \bar{c}_n \begin{pmatrix} \psi_1 \bar{\psi}_1 & \cdots & \psi_1 \bar{\psi}_N \\ \vdots & \ddots & \vdots \\ \psi_m \bar{\psi}_1 & \cdots & \psi_m \bar{\psi}_N \end{pmatrix} \quad (3.16)$$

The Wigner function of the density matrix is defined in terms of the Cross Wigner functions of its elements,

$$W_\rho = \mathcal{W}[\hat{\rho}] = \begin{pmatrix} w_1 & \cdots & w_{1N} \\ \vdots & \ddots & \vdots \\ w_{N1} & \cdots & w_N \end{pmatrix} \quad (3.17)$$

with elements given by the Cross Wigner functions

$$w_{mn}(\mathbf{q}, \mathbf{p}) = c_m \bar{c}_n \left( \frac{1}{2\pi\hbar} \right)^n \int d\mathbf{y} e^{-\frac{i}{\hbar} \mathbf{p} \cdot \mathbf{y}} \psi_m \left( \mathbf{q} + \frac{\mathbf{y}}{2} \right) \overline{\psi_n \left( \mathbf{q} - \frac{\mathbf{y}}{2} \right)} \quad (3.18)$$

where  $w_{mm} = w_m$ . Thus the diagonal elements are Wigner functions called *population Wigner functions* and the off-diagonal elements are Cross Wigner functions called *coherence Wigner functions*.

## 3.3 Wigner Functions

### 3.3.1 Statistics of Pure State Wigner Functions

The Wigner function is the Weyl Symbol of the density operator and is interpreted as a (quasi)-probability distribution on phase space [118]. For a  $N$  degrees of freedom system it is a  $N$ -fold bivariate distribution joint in each degree of freedom's canonical conjugate variables. Integrating over  $\mathbf{p}$  marginalizes the distribution in momentum yielding the position

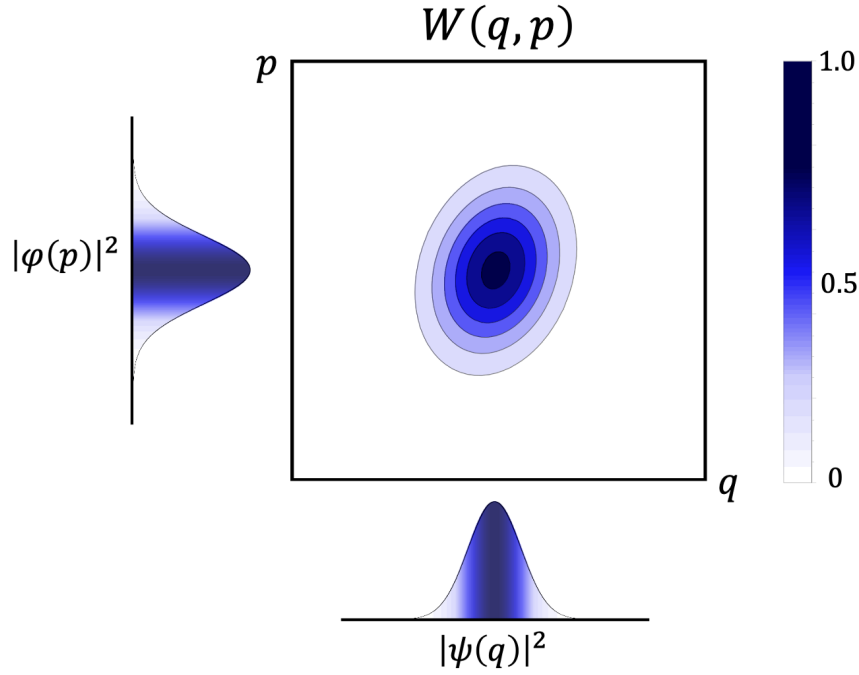


Figure 3.1: A Wigner function contains the marginals  $|\psi(q)|^2$  and  $|\phi(p)|^2$  as projections in phase space along the  $q$  and  $p$  axes.

distribution of the quantum state (Fig. 3.1),

$$|\psi(\mathbf{q})|^2 = \int d\mathbf{p} W_\psi(\mathbf{q}, \mathbf{p}) \quad (3.19)$$

Likewise one can marginalize over  $\mathbf{q}$  to obtain the momentum distribution

$$|\phi(\mathbf{p})|^2 = \int d\mathbf{q} W_\psi(\mathbf{q}, \mathbf{p}) \quad (3.20)$$

where  $\psi(\mathbf{q})$  and  $\phi(\mathbf{p})$  are the position and momentum representations of the quantum state related by the  $\hbar$ -dependent Fourier Transforms,

$$\phi(\mathbf{p}) = \left( \frac{1}{2\pi\hbar} \right)^{N/2} \int d\mathbf{q} e^{-\frac{i}{\hbar}\mathbf{p}\cdot\mathbf{q}} \psi(\mathbf{q}) \quad (3.21)$$

and

$$\psi(\mathbf{q}) = \left(\frac{1}{2\pi\hbar}\right)^{N/2} \int d\mathbf{p} e^{+\frac{i}{\hbar}\mathbf{q}\cdot\mathbf{p}} \phi(\mathbf{p}). \quad (3.22)$$

Although the Wigner function is generally not positive-definite, it like the density operator  $\hat{\rho}$  is normalizable. A normalized density  $\text{Tr}(\hat{\rho}) = 1$  yields a normalized Wigner distribution

$$1 = \int \int d\mathbf{p} d\mathbf{q} W_\psi(\mathbf{q}, \mathbf{p}) = \text{Tr}(W_\psi) \quad (3.23)$$

Expectations  $\langle A \rangle = \text{Tr}(\hat{\rho}\hat{A})$  are calculated analogous to classical statistical ensemble averages as a phase space traces,

$$\langle A \rangle = \int \int d\mathbf{p} d\mathbf{q} A(\mathbf{q}, \mathbf{p}) W_\psi(\mathbf{q}, \mathbf{p}) = \text{Tr}(AW_\psi) \quad (3.24)$$

Taking  $\hat{A}$  to be the density  $\hat{\rho}$ , we can recover the idempotency criterion of a pure state density  $\text{Tr}(\hat{\rho}) = \text{Tr}(\hat{\rho}^2)$

$$\begin{aligned} \langle W_\psi \rangle &= \int \int d\mathbf{p} d\mathbf{q} W_\psi(\mathbf{q}, \mathbf{p}) W_\psi(\mathbf{q}, \mathbf{p}) = \text{Tr}(W_\psi W_\psi) \\ &= \left(\frac{1}{2\pi\hbar}\right)^N \text{Tr}(W_\psi) = \left(\frac{1}{2\pi\hbar}\right)^N \end{aligned} \quad (3.25)$$

Similarly, for two different densities  $\hat{\rho}_1$  and  $\hat{\rho}_2$  corresponding to two quantum states  $\psi_1$  and  $\psi_2$ , their overlap is calculated by the trace  $\text{Tr}(\hat{\rho}_1\hat{\rho}_2) = |\langle\psi_1|\psi_2\rangle|^2$ . In phase space, the overlap of two states is

$$\int \int d\mathbf{p} d\mathbf{q} W_1(\mathbf{q}, \mathbf{p}) W_2(\mathbf{q}, \mathbf{p}) = \text{Tr}(W_1 W_2) = \left(\frac{1}{2\pi\hbar}\right)^N |\langle\psi_1|\psi_2\rangle|^2 \quad (3.26)$$

If states  $\psi_1$  and  $\psi_2$  are orthogonal so are their Wigner functions

$$\int \int d\mathbf{p} d\mathbf{q} W_1(\mathbf{q}, \mathbf{p}) W_2(\mathbf{q}, \mathbf{p}) = \text{Tr}(W_1 W_2) = 0 \quad (3.27)$$

As a consequence of Eq. 3.27, Wigner functions can't generally be positive-definite and must possess some regions of negative probability (Fig. 3.2).

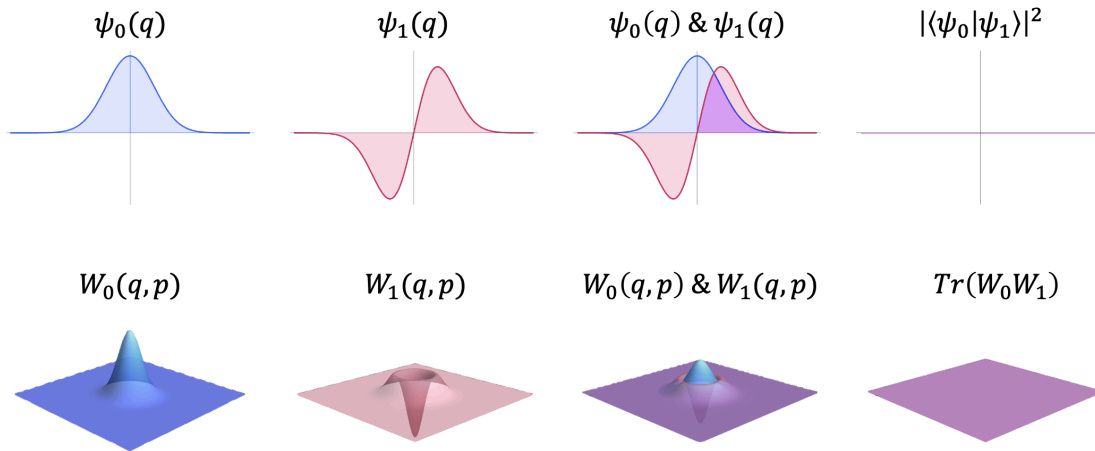


Figure 3.2: Example of two orthogonal Wigner functions for the harmonic oscillator. Ground state (blue). First excited state (red). Wavefunctions (top). Wigner functions (bottom). The ground state Wigner function is positive-definite. The first excited state is not positive definite.

### 3.3.2 Inversion: Recovering the Wavefunction from the Wigner Function

Not only does the Wigner function contain the correct marginal distributions of canonical coordinates, for a pure state Wigner function the wavefunction up to an overall phase can be recovered by Fourier Transforming over the Wigner function [119]. This procedure is often employed experimentally in quantum tomography, where from the observed Wigner function the pure state wavefunction is reconstructed [120]. It can also be used in simulation to isolate the wavefunction from a trajectory ensemble representation of the pure state Wigner function.

To recover the position representation of the wavefunction, Fourier Transforming Eq. 3.4

gives

$$\int d\mathbf{p} e^{+i\mathbf{p}\cdot\mathbf{q}_0/\hbar} W_\psi(\mathbf{q}, \mathbf{p}) = \overline{\psi(\mathbf{q} - \frac{\mathbf{q}_0}{2})} \psi(\mathbf{q} + \frac{\mathbf{q}_0}{2}). \quad (3.28)$$

The transformed distribution factorizes in  $\psi$ . Recentering the Wigner function and the wavefunctions, by letting  $\mathbf{q} = \frac{\mathbf{q}}{2}$  and  $\mathbf{q}_0 = \mathbf{q}$ , Eq. 3.28 can be rearranged with

$$\psi(\mathbf{q}) = \frac{1}{N_\psi} \int d\mathbf{p} e^{+i\mathbf{p}\cdot\mathbf{q}/\hbar} W_\psi\left(\frac{\mathbf{q}}{2}, \mathbf{p}\right) \quad (3.29)$$

where the constant  $N_\psi$  is determined by normalization of Eq. 3.29.

### 3.3.3 Symmetries of Pure State Wigner Functions

The Wigner function contains numerous symmetries which can be expressed in terms of transformations of the wavefunction used to construct it [112]. For real wavefunctions  $\psi(\mathbf{q}) = \overline{\psi(\mathbf{q})}$  and  $\phi(\mathbf{q}) = \overline{\phi(\mathbf{q})}$ , the Wigner function has the symmetries

$$\mathcal{W}[\overline{\psi(\mathbf{q})}] = W_\psi(\mathbf{q}, -\mathbf{p}) \quad (3.30)$$

and

$$\mathcal{W}[\overline{\phi(\mathbf{p})}] = W_\phi(-\mathbf{q}, \mathbf{p}). \quad (3.31)$$

For even wavefunctions  $\psi(\mathbf{q}) = \psi(-\mathbf{q})$  and  $\phi(\mathbf{q}) = \phi(-\mathbf{q})$ , the Wigner function has the symmetries

$$\mathcal{W}[\psi(-\mathbf{q})] = W_\psi(-\mathbf{q}, -\mathbf{p}) \quad (3.32)$$

$$\mathcal{W}[\phi(-\mathbf{p})] = W_\phi(-\mathbf{q}, -\mathbf{p}). \quad (3.33)$$

And because the same Wigner function results from construction in the position or momentum representation,  $W_\psi(\mathbf{q}, \mathbf{p}) = W_\phi(\mathbf{q}, \mathbf{p})$ . The Wigner function also possesses invariance to phase space translations (called Galilei invariance) and phase space reflections. These



symmetries can be summarized as

$$\mathcal{W}[\psi(\mathbf{q} - \mathbf{q}_0)] = W_\phi(\mathbf{q} - \mathbf{q}_0, \mathbf{p}) \quad (3.34)$$

$$\mathcal{W}[\phi(\mathbf{p} - \mathbf{p}_0)] = W_\phi(\mathbf{q}, \mathbf{p} - \mathbf{p}_0) \quad (3.35)$$

$$\mathcal{W}[\psi(\mathbf{q} - \mathbf{q}_0) e^{+i\mathbf{p}_0 \cdot \mathbf{q}/\hbar}] = W_\psi(\mathbf{q} - \mathbf{q}_0, \mathbf{p} - \mathbf{p}_0) \quad (3.36)$$

These properties can be generally derived from actions of Heisenberg displacement (translation) operators and Grossman-Royer (reflections) operators acted on the wavefunctions used in the Cross Wigner Transform [14].

### 3.4 The Star Product

Having discussed Weyl symbols and Wigner functions, a quantum mechanical way to multiply them is needed. The star product provides this. There are different star products relating to different operator orderings and their correspondence rules [111]. The star product used in the Wigner-Moyal representation is the Moyal product. Because the discussion is restricted to this representation, star product and Moyal product will be used synonymously. There are many equivalent definitions of the star product which involve differentiation or integration. The particular definition employed in evaluating a star product is a matter of convenience and application.

### 3.4.1 Janus Operator Definition

The star product between two arbitrary  $N$  degrees of freedom Weyl symbols  $f(\mathbf{q}, \mathbf{p})$  and  $g(\mathbf{q}, \mathbf{p})$  can be defined as

$$f(\mathbf{q}, \mathbf{p}) \star b(\mathbf{q}, \mathbf{p}) = f(\mathbf{q}, \mathbf{p}) e^{\frac{i\hbar}{2} \overleftrightarrow{\Lambda}} b(\mathbf{q}, \mathbf{p}) \quad (3.37)$$

where  $\overleftrightarrow{\Lambda} = \overleftarrow{\nabla}_q \overrightarrow{\nabla}_p - \overleftarrow{\nabla}_p \overrightarrow{\nabla}_q$  [121, 122]. This bidirectional operator  $\overleftrightarrow{\Lambda}$  called the *Janus operator* acts its gradients in the directions of its arrows between two Weyl symbols, differentiating them and adding powers of  $\frac{i\hbar}{2}$ . Weyl symbols are “deformed” by differentiation and quantized through powers of  $\frac{i\hbar}{2}$  introduced. Eq. 3.37 is a formal expression. To evaluate the action of  $e^{\frac{i\hbar}{2} \overleftrightarrow{\Lambda}}$  on Weyl symbols, recognize it as a function of an operator which can be evaluated through standard Taylor expansion like the classical Liouvillian

$$\begin{aligned} f(\mathbf{q}, \mathbf{p}) e^{\frac{i\hbar}{2} \overleftrightarrow{\Lambda}} g(\mathbf{q}, \mathbf{p}) &= f(\mathbf{q}, \mathbf{p}) \left( \sum_{n=0}^{\infty} \frac{\left( \frac{i\hbar}{2} \overleftrightarrow{\Lambda} \right)^n}{n!} \right) g(\mathbf{q}, \mathbf{p}) \\ &= f(\mathbf{q}, \mathbf{p}) \left( 1 + \frac{i\overleftrightarrow{\Lambda}\hbar}{2} - \frac{\overleftrightarrow{\Lambda}^2 \hbar^2}{8} + \dots \right) g(\mathbf{q}, \mathbf{p}) \\ &= f(\mathbf{q}, \mathbf{p}) g(\mathbf{q}, \mathbf{p}) + \frac{i\hbar}{2} f(\mathbf{q}, \mathbf{p}) \overleftrightarrow{\Lambda} g(\mathbf{q}, \mathbf{p}) - \frac{\hbar^2}{8} f(\mathbf{q}, \mathbf{p}) \overleftrightarrow{\Lambda}^2 g(\mathbf{q}, \mathbf{p}) + \dots + \mathcal{O}(\hbar^n) \end{aligned} \quad (3.38)$$

Depending on the  $\mathbf{q}, \mathbf{p}$ -dependences in  $f$  and  $g$ , the differential series in Eq. 3.38 may never terminate. For polynomial Weyl symbols  $f(\mathbf{q}, \mathbf{p}) = \mathbf{q}^m \mathbf{p}^n$  and  $g(\mathbf{q}, \mathbf{p}) = \mathbf{q}^{m'} \mathbf{p}^{n'}$  where  $m, n, m'$ , and  $n'$  are positive integers, the series will terminate by  $\mathcal{O}(\hbar^{k+1})$  through the vanishing of derivatives where  $k$  is the largest integer of  $\{m, n, m'n'\}$ . In many cases, this series representation is truncated to a desired order  $\mathcal{O}(\hbar^k)$ . Truncation to zeroth order  $\mathcal{O}(\hbar^0)$  recovers classical multiplication,

$$f(\mathbf{q}, \mathbf{p}) \star g(\mathbf{q}, \mathbf{p}) = f(\mathbf{q}, \mathbf{p}) g(\mathbf{q}, \mathbf{p}) + \mathcal{O}(\hbar) \quad (3.39)$$

while to first order  $\mathcal{O}(\hbar^1)$  yields the first order semiclassical result

$$\begin{aligned} f(\mathbf{q}, \mathbf{p}) \star g(\mathbf{q}, \mathbf{p}) &= f(\mathbf{q}, \mathbf{p})g(\mathbf{q}, \mathbf{p}) + \frac{i\hbar}{2} f(\mathbf{q}, \mathbf{p}) \overleftrightarrow{\Lambda} g(\mathbf{q}, \mathbf{p}) + \mathcal{O}(\hbar^2) \\ &= f(\mathbf{q}, \mathbf{p})g(\mathbf{q}, \mathbf{p}) + \frac{i\hbar}{2} [f, g] + \mathcal{O}(\hbar^2). \end{aligned} \quad (3.40)$$

Note the Janus operator to the first power is just the classical Poisson bracket. In approximate quantum dynamics theories, such as mixed quantum-classical or semiclassical methods, this form of the star product is used to approximate the exact quantum dynamics with terms of greater than  $\mathcal{O}(\hbar^0)$  interpreted as quantum corrections to the classical dynamics [10, 123].

More interesting behavior emerges when Weyl symbols being multiplied possess a convergent series representation for their resulting product. The series can be resummed to yield a closed form expression without approximation. This is often the case when the Weyl symbols being multiplied are transcendental functions or smooth distributions of canonical variables. For such cases, it is often more convenient to express the star product in terms of an operator which acts in only one direction.

### 3.4.2 Bivector Definition

The Janus operator definition of the star product can be unwieldy because it generates a generally infinite differential series in both directions of its action. A slightly different definition of the star product in terms of a quantity called *Poisson bivector*  $\hat{\Pi} = \sum_{i,j} C_{ij} \nabla_i \wedge \nabla_j$  avoids this [124]. Here  $C_{ij}$  is a constant determined by  $\hat{\Pi}$ 's action on a function and  $\wedge$  denotes the exterior product. The star product can be expressed in terms of the Poisson bivector can be expressed as

$$f(\mathbf{q}, \mathbf{p}) \star g(\mathbf{q}, \mathbf{p}) = \sum_{n=0}^{\infty} \left( \frac{i\hbar}{2} \right)^n \hat{\Pi}^n(f, g) \quad (3.41)$$

where the  $n^{\text{th}}$  Poisson Bivector  $\Pi^n$  is given by

$$\hat{\Pi}^n(f, g) = \sum_{k=0}^n (-1)^k \binom{n}{k} (\nabla_p^k \nabla_q^{(n-k)} f(\mathbf{q}, \mathbf{p})) \wedge (\nabla_p^{(n-k)} \nabla_q^k g(\mathbf{q}, \mathbf{p})). \quad (3.42)$$

One can easily verify order-by-order the Janus operator definition and the bivector definition yield the same result. Oftentimes the  $n^{\text{th}}$  Poisson bivector  $\hat{\Pi}^n$  is denoted  $[\cdot, \cdot]_n$  because  $\hat{\Pi}^1$  is the Poisson bracket. For example for 1 degree of freedom,

$$\hat{\Pi}^0(f, g) \equiv [f, g]_0 = fg \quad (3.43)$$

$$\hat{\Pi}^1(f, g) \equiv [f, g]_1 \equiv [f, g] = \frac{\partial f}{\partial q} \frac{\partial g}{\partial p} - \frac{\partial f}{\partial p} \frac{\partial g}{\partial q} \quad (3.44)$$

$$\hat{\Pi}^2(f, g) \equiv [f, g]_2 = \frac{\partial^2 f}{\partial^2 q} \frac{\partial^2 g}{\partial^2 p} - 2 \frac{\partial^2 f}{\partial p \partial q} \frac{\partial^2 g}{\partial p \partial q} + \frac{\partial^2 f}{\partial^2 p} \frac{\partial^2 g}{\partial^2 q} \quad (3.45)$$

$$\hat{\Pi}^3(f, g) \equiv [f, g]_3 = -\frac{\partial^3 f}{\partial^3 q} \frac{\partial^3 g}{\partial^3 p} + 3 \frac{\partial^3 f}{\partial p \partial^2 q} \frac{\partial^3 g}{\partial^2 p \partial q} - 3 \frac{\partial^3 f}{\partial^2 p \partial q} \frac{\partial^3 g}{\partial^2 q \partial p} + \frac{\partial^3 f}{\partial^3 p} \frac{\partial^3 g}{\partial^3 q} \quad (3.46)$$

Note that even order  $[\cdot, \cdot]_n$  are symmetric and thus not a proper bracket. Explicitly for the star product on two arbitrary 1 degree of freedom Weyl symbols  $f_a = f_a(q, p)$  and  $f_b = f_b(q, p)$ . By Eq. 3.41, their star product is

$$\begin{aligned} f_a(q, p) \star f_b(q, p) &= f_a f_b + \frac{i\hbar}{2} \left( f_a^{(1,0)} f_b^{(0,1)} - f_a^{(0,1)} f_b^{(1,0)} \right) \\ &- \frac{\hbar^2}{8} \left( -2 f_a^{(1,1)} f_b^{(1,1)} + f_a^{(2,0)} f_b^{(0,2)} + f_a^{(0,2)} + f_b^{(2,0)} \right) \\ &+ \frac{i\hbar^3}{48} \left( 3 \left( f_a^{(2,1)} f_b^{(1,2)} - f_a^{(1,2)} f_b^{(2,1)} \right) - f_a^{(3,0)} f_b^{(0,3)} + f_a^{(0,3)} f_b^{(3,0)} \right) \\ &+ \frac{\hbar^4}{384} \left( 6 f_a^{(2,2)} f_b^{(2,2)} - 4 \left( f_a^{(3,1)} f_b^{(1,3)} - f_a^{(1,3)} f_b^{(3,1)} \right) + f_a^{(4,0)} f_b^{(0,4)} + f_a^{(0,4)} f_b^{(4,0)} \right) \\ &+ \frac{i\hbar^5}{3840} \left( 10 \left( f_a^{(3,2)} f_b^{(2,3)} - f_a^{(2,3)} f_b^{(3,2)} \right) - 5 \left( f_a^{(4,1)} f_b^{(1,4)} + f_a^{(1,4)} f_b^{(4,1)} \right) + f_a^{(5,0)} f_b^{(0,5)} - f_a^{(0,5)} f_b^{(5,0)} \right) \\ &- \frac{\hbar^6}{46080} \left( -20 f_a^{(3,3)} f_b^{(3,3)} + 15 \left( f_a^{(4,2)} f_b^{(2,4)} + f_a^{(2,4)} f_b^{(4,2)} \right) \right. \\ &\quad \left. - 6 \left( f_a^{(5,1)} f_b^{(1,5)} - f_a^{(1,5)} f_b^{(5,1)} \right) + f_a^{(6,0)} f_b^{(0,6)} + f_a^{(0,6)} f_b^{(6,0)} \right) + \mathcal{O}(\hbar^7). \end{aligned} \quad (3.47)$$

where  $f^{(n,m)}(q,p) = \left(\frac{d^n}{dq^n}\right) \left(\frac{d^m}{dp^m}\right) f(q,p)$ .

To illustrate a convergent example of the star product, the product of two Gaussian Weyl symbols of different widths is worked out below.

---

**Example:** Analytic resummation of the star product of two Gaussian Weyl symbols  
Substituting two Gaussian Weyl symbols into Eq. 3.47 for  $f_a$  and  $f_b$ ,

$$f_a = e^{-a(q^2+p^2)}, \quad f_b = e^{-b(q^2+p^2)}$$

and one obtains

$$\begin{aligned} f_a(q,p) \star f_b(q,p) &= e^{-((a+b)(p^2+q^2))} + 0 \hbar \\ &+ \hbar^2 abe^{-((a+b)(p^2+q^2))} ((a+b)(p^2+q^2) - 1) + 0 \hbar^3 \\ &+ \frac{\hbar^4}{2} a^2 b^2 e^{-((a+b)(p^2+q^2))} ((a+b)(p^2+q^2) ((a+b)(p^2+q^2) - 4) + 2) + 0 \hbar^5 \end{aligned}$$

with odd powers in  $\hbar$  cancelling. The classical product  $f_a f_b$  can be factored out from higher order moments in the series with the latter identified as Laguerre polynomials,

$$L_n(x) = \sum_{k=0}^n \binom{n}{k} \frac{(-1)^k}{k!} x^k, \quad (3.48)$$

where  $x = (a+b)(p^2+q^2)$ . These can be resummed according to the generating function identity,

$$\sum_{n=0}^{\infty} t^n L_n(x) = \frac{1}{1-t} e^{-tx/(1-t)} \quad (3.49)$$

where  $t = -ab\hbar^2$  to yield

$$\begin{aligned}
f_a(q, p) \star f_b(q, p) &= \exp\left(-((a+b)(p^2+q^2))\right) \left(\sum_{n=0}^{\infty} (-ab\hbar^2)^n L_n((a+b)(p^2+q^2))\right) \\
&= \underbrace{\exp\left(-((a+b)(p^2+q^2))\right)}_{g_C(q,p)} \underbrace{\frac{\exp\left(\frac{ab(a+b)}{1+ab\hbar^2}(p^2+q^2)\hbar^2\right)}{1+ab\hbar^2}}_{g_Q(q,p)}.
\end{aligned} \tag{3.50}$$

This leads to an interesting result. The full quantum product of  $f_a(q, p) \star f_b(q, p)$  factorizes into a classical product of the zeroth order product  $g_C(q, p)$  and a quantum function  $g_Q(q, p)$  containing all powers of quantization. Multiplying  $g_C$  with  $g_Q$  yields a closed form expression for star product of  $f_a$  with  $f_b$ ,

$$f_a(q, p) \star f_b(q, p) = g_C(q, p)g_Q(q, p) = \frac{1}{1+ab\hbar^2} \exp\left(-\frac{(a+b)}{1+ab\hbar^2}(p^2+q^2)\right) \tag{3.51}$$


---

Eq. 3.51 has been coined as the “hyperbolic tangent composition law” of Gaussian Weyl symbols [13], because the coefficients on the quadratic variables  $(p^2+q^2)$  in the product  $f_a(q, p) \star f_b(q, p)$  composing akin to hyperbolic tangent functions under addition,

$$\tanh(a+b) = \frac{\tanh(a) + \tanh(b)}{1 + \tanh(a)\tanh(b)}.$$

The calculation of star product of Gaussian Weyl symbols is essential to quantum dynamical calculations in phase space because oftentimes the Wigner functions of the quantum density are Gaussian Weyl symbols. Similarly phase space delta function represented as localized Gaussian multiply in this way. This result is generalized for Gaussian form Weyl symbols with distinct means, variances, and correlations in Appendix B. The key point is that for products with convergent series, they can be resummed to obtain a closed for expression for

the star product of the two Weyl symbols without approximation.

### 3.4.3 Bopp Shifts

The star product possesses a translational property called *Bopp Shifts* [125],

$$\begin{aligned} f(\mathbf{q}, \mathbf{p}) \star g(\mathbf{q}, \mathbf{p}) &= f\left(\mathbf{q} + \frac{i\hbar}{2}\nabla_p, \mathbf{p} - \frac{i\hbar}{2}\nabla_q\right)g(\mathbf{q}, \mathbf{p}) \\ &= g\left(\mathbf{q} - \frac{i\hbar}{2}\nabla_p, \mathbf{p} + \frac{i\hbar}{2}\nabla_q\right)f(\mathbf{q}, \mathbf{p}). \end{aligned} \quad (3.52)$$

Bopp shifts still require one to create Taylor series representation of the translated function to evaluate its derivatives, however Bopp shifts are useful when the Weyl symbols being multiplied depend on a single canonical conjugate variable  $\mathbf{q}$  or  $\mathbf{p}$ . For example, for two 1 degree of freedom Weyl symbols  $f = f(q)$  and  $g(q, p)$ , the star product evaluated through a Bopp shift is

$$f(q) \star g(q, p) = f\left(q + \frac{i\hbar}{2}\partial_p\right)g(q, p) = \sum_{k=0}^{\infty} \frac{i\hbar^k}{2} \frac{d^k f}{dq^k} \partial_p^k g(q, p) \quad (3.53)$$

This is particularly useful when  $f$  and  $g$  are polynomials of canonical variables or distributions with well-known moment expansions.

### 3.4.4 Integral Definitions

Evaluating the star product through differentiation can be quite cumbersome. In spite of this, the Janus operator definition seems to be the primary method for calculation in chemical physics literature, owing perhaps to its semiclassical interpretation. Ironically simpler integral definitions of the star product were provided by Weyl [126] and von Neumann [127] preceding the work of Wigner, Moyal, Bopp, and Groenewold. The most basic integral

definition of the star product is in terms of the Weyl Transform

$$O_{\mathcal{W}} \left[ \hat{A}\hat{B} \right] = A(\mathbf{q}, \mathbf{p}) \star B(\mathbf{q}, \mathbf{p}). \quad (3.54)$$

In contrast, von Neumann's integral form of the star product relies on the fact Weyl symbols are generally Schwartz class functions  $\mathcal{S}$  on phase space and "Fourier transformable" [128]. All integral definitions of the star product derive from the fact it can be expressed through a symplectic Fourier Transform or convolution.

For two 1 degree of freedom Weyl symbols  $f$  and  $g$ , their star product is the integral [13]:

$$\begin{aligned} f(q, p) \star g(q, p) \\ = \left( \frac{1}{\pi\hbar} \right)^2 \int dp' \int dp'' \int dq' \int dq'' f(q + q', p + p') g(q + q'', p + p'') e^{\frac{2i}{\hbar}(q'p'' - q''p')} \end{aligned} \quad (3.55)$$

where  $q'$ ,  $q''$ ,  $p'$ , and  $p''$  are dummy variables to be integrated over. Using a Fourier shift, the integral in Eq. 3.55 can be rewritten as

$$\begin{aligned} f(q, p) \star g(q, p) \\ = \left( \frac{1}{\pi\hbar} \right)^2 \int dp' \int dp'' \int dq' \int dq'' f(q', p') g(q'', p'') e^{-\frac{2i}{\hbar}p(q' - q'') + p'(q'' - q) + p''(q - q')} \end{aligned} \quad (3.56)$$

Letting  $\mathbf{u} = (q', p')$  and  $\mathbf{v} = (q'', p'')$ , the argument of the exponential of Eq. 3.55 can be seen to define a phase space area  $A = \text{Det}((\mathbf{u}, \mathbf{v}))$  as shown in Fig. 3.3.

The underlying symplectic structure of the integrand can be made more transparent by vectorizing Eq. 3.55 and Eq. 3.56. Letting  $\mathbf{z} = (q, p)^T$  Eqs. 3.55-3.56 become

$$f(\mathbf{z}) \star g(\mathbf{z}) = \left( \frac{1}{\pi\hbar} \right)^2 \int d\mathbf{u} \int d\mathbf{v} f(\mathbf{z} + \mathbf{u}) g(\mathbf{z} + \mathbf{v}) e^{\frac{2i}{\hbar} \mathbf{u}^T \mathbf{J} \mathbf{v}} \quad (3.57)$$



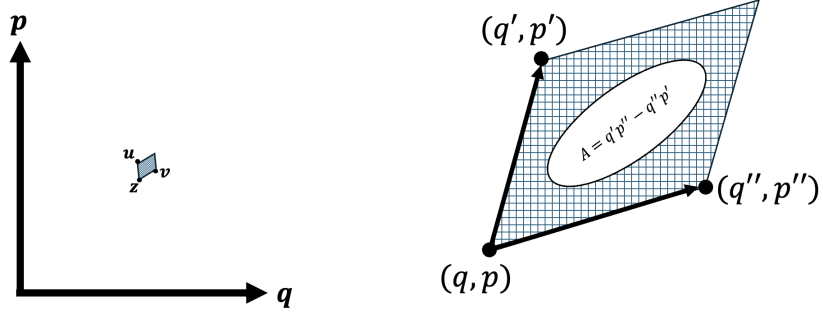


Figure 3.3: The symplectic phase space volume element of the integral representation of the star product.

and

$$f(\mathbf{z}) \star g(\mathbf{z}) = \left(\frac{1}{\pi\hbar}\right)^2 \int d\mathbf{u} \int d\mathbf{v} f(\mathbf{z})g(\mathbf{z})e^{-\frac{2i}{\hbar}(\mathbf{z}-\mathbf{u})^T\mathbf{J}(\mathbf{z}-\mathbf{v})} \quad (3.58)$$

where

$$\mathbf{J} = \begin{pmatrix} 0 & 1 \\ -1 & 0 \end{pmatrix} \quad (3.59)$$

is the symplectic structure matrix for a 1 degree of freedom phase space. The integral form of the star product for Weyl symbols of  $N$  degree of freedom with  $\mathbf{z} = (\mathbf{q}, \mathbf{p})^T$  are

$$f(\mathbf{z}) \star g(\mathbf{z}) = \left(\frac{1}{\pi\hbar}\right)^{2N} \int d\mathbf{u} \int d\mathbf{v} f(\mathbf{z} + \mathbf{u})g(\mathbf{z} + \mathbf{v})e^{\frac{2i}{\hbar}\mathbf{u}^T\mathbf{J}\mathbf{v}} \quad (3.60)$$

and

$$f(\mathbf{z}) \star g(\mathbf{z}) = \left(\frac{1}{\pi\hbar}\right)^{2N} \int d\mathbf{u} \int d\mathbf{v} f(\mathbf{z})g(\mathbf{z})e^{-\frac{2i}{\hbar}(\mathbf{z}-\mathbf{u})^T\mathbf{J}(\mathbf{z}-\mathbf{v})} \quad (3.61)$$

where

$$\mathbf{J} = \begin{pmatrix} \mathbf{0}_N & \mathbf{1}_N \\ -\mathbf{1}_N & \mathbf{0}_N \end{pmatrix}$$

and

$$\mathbf{u} = (q'_1, \dots, q'_N, p'_1, \dots, p'_N)^T = \mathbf{z}'$$

and

$$\mathbf{v} = (q_1'', \dots, q_N'', p_1'', \dots, p_N'')^T = \mathbf{z}''.$$

The star product can be viewed as a specific kind of Fourier transform or convolution. To see this, one needs to define a few related quantities. Letting

$$\hat{\mathcal{F}}[f(\mathbf{x})] = \left(\frac{1}{2\pi\hbar}\right)^{M/2} \int d\mathbf{x}' e^{-\frac{i}{\hbar}\mathbf{x}\cdot\mathbf{x}'} f(\mathbf{x}') \quad (3.62)$$

denote the  $\hbar$ -dependent Fourier transform over  $\mathbf{x} \in \mathbb{R}^M$  and its inverse

$$\hat{\mathcal{F}}^{-1}[f(\mathbf{x}')] = \left(\frac{1}{2\pi\hbar}\right)^{M/2} \int d\mathbf{x} e^{+\frac{i}{\hbar}\mathbf{x}'\cdot\mathbf{x}} f(\mathbf{x}) \quad (3.63)$$

and letting  $M = 2N$ , the symplectic Fourier Transform is [14]:

$$\hat{\mathcal{F}}_J[f(\mathbf{z})] = \left(\frac{1}{2\pi\hbar}\right)^N \int d\mathbf{z}' e^{-\frac{i}{\hbar}\mathbf{z}'^T \mathbf{J} \mathbf{z}} f(\mathbf{z}') \quad (3.64)$$

with its inverse

$$\hat{\mathcal{F}}_J[f(\mathbf{z}')] = \left(\frac{1}{2\pi\hbar}\right)^N \int d\mathbf{z} e^{+\frac{i}{\hbar}\mathbf{z}^T \mathbf{J} \mathbf{z}'} f(\mathbf{z}) \quad (3.65)$$

Note the  $\hbar$ -dependent Fourier Transform and symplectic Fourier transform are related by

$$\hat{\mathcal{F}}_J[f(\mathbf{z})] = \hat{\mathcal{F}}[f(\mathbf{J}\mathbf{z})] \quad (3.66)$$

Like the standard convolution,

$$f * g = \int d\mathbf{z}' f(\mathbf{z} - \mathbf{z}') g(\mathbf{z}') \quad (3.67)$$

one can define a symplectic convolution of Weyl symbols

$$f *_J g = \left(\frac{1}{2\pi\hbar}\right)^N \int d\mathbf{z}' e^{\frac{i}{2\hbar}\mathbf{z}^T \mathbf{J} \mathbf{z}'} f(\mathbf{z} - \mathbf{z}') g(\mathbf{z}') \quad (3.68)$$

The symplectic convolution in Eq. 3.68 is sometimes called the *twisted convolution* of symbols  $f$  and  $g$  [129]. Using these forms, star product can be expressed as [130–132] :

$$\begin{aligned} f \star g &= \hat{\mathcal{F}}_J [f] *_J g = f *_J \hat{\mathcal{F}}_J^{-1} [g] \\ &= \hat{\mathcal{F}}^{-1} \left[ \hat{\mathcal{F}} [f] *_J \hat{\mathcal{F}} [g] \right] = \hat{\mathcal{F}} \left[ \hat{\mathcal{F}}^{-1} [f] *_J \hat{\mathcal{F}}^{-1} [g] \right] \end{aligned} \quad (3.69)$$

where the lower equality follows Eq. 3.66 and the fact that  $\mathbf{J}^{-1} = \mathbf{J}^T = -\mathbf{J}$ .

Eq. 3.69 indicates the star product can be calculated as the twisted convolution of one symplectic Fourier transformed Weyl symbol and one untransformed Weyl symbol. The lower equality indicates the star product can be calculated solely in terms of ( $\hbar$ -dependent) Fourier transforms and the twisted convolution.

The star product can be interpreted as a kind of convolution theorem where the star multiplied Weyl symbols are calculated in terms of the inverse Fourier transform of their twisted convolution. Working with this definition is often easier than direct integration by Eqs. 3.60-3.61.

To see this consider again the two Weyl Gaussian symbols  $f_a = e^{-a(q^2+p^2)}$  and  $f_b = e^{-b(q^2+p^2)}$ . Their convolution can be calculated by brute force integration using Eq. 3.67 [133]:

$$f_a * f_b = \int dq' \int dp' f(q - q', p - p') g(q', p') \quad (3.70)$$

or more simply by the the convolution theorem

$$\begin{aligned} f_a * f_b &= \hat{\mathcal{F}}^{-1} \left[ \hat{\mathcal{F}} [f_a] \hat{\mathcal{F}} [f_b] \right] \\ &= \hat{\mathcal{F}}^{-1} \left[ \frac{e^{-\frac{1}{4a}(q'^2+p'^2)}}{\sqrt{2a}} \frac{e^{-\frac{1}{4b}(q'^2+p'^2)}}{\sqrt{2b}} \right] \\ &= \frac{e^{-\frac{ab}{(a+b)}(q^2+p^2)}}{2\sqrt{ab}} \end{aligned} \quad (3.71)$$

Compare this with the star product of  $f_a$  and  $f_b$  calculated by Eq. 3.69 as opposed to direct integration. One has

$$\begin{aligned}
f_a(q, p) \star f_b(q, p) &= \hat{\mathcal{F}}^{-1} \left[ \hat{\mathcal{F}} [f_a] *_J \hat{\mathcal{F}} [f_b] \right] \\
&= \hat{\mathcal{F}}^{-1} \left[ \left( \frac{1}{2\sqrt{a^2}} \left( \exp \left( -\frac{(q'^2 + p'^2)}{4\sqrt{a^2}} \right) \right) \right) \left( \frac{1}{2\sqrt{b^2}} \left( \exp \left( -\frac{(q''^2 + p''^2)}{4\sqrt{b^2}} \right) \right) \right) e^{+\frac{i\hbar}{2} \mathbf{z}''^T \mathbf{J} \mathbf{z}'} \right] \\
&= \frac{1}{1 + ab\hbar^2} \exp \left( -\frac{(a + b)}{1 + ab\hbar^2} (p^2 + q^2) \right)
\end{aligned}$$

To summarize this section, the star product imposes quantization and non-commutativity on phase space functions (Weyl symbols). Historically the star product has been given differential definitions whose utility lies in developing semiclassical approximations through truncation. The disadvantage of the differential definitions of the star product is that they are cumbersome and typically require resumming to obtain analytic results. Because the expansion is asymptotic, convergence is not always guaranteed or obvious [107, 113]. The integral definition of the star product can circumvent these issues altogether. To simplify integration, the star product can be computed in terms of (symplectic) Fourier Transforms and twisted convolutions. This is particularly useful when the star product involves Weyl symbols whose Fourier transforms and convolutions are trivial like Gaussian, exponential, and polynomial Weyl symbols.

### 3.5 The Moyal Bracket

In addition to the definitions of the star product we examined above, the star product can be defined in terms of two brackets, one resembling a commutator of two operators and another resembling their anti-commutator. These brackets have useful algebraic properties which can facilitate calculation and understanding the symmetries of motion in phase space. The most important instance of which, the Moyal bracket, will emerge in the equation of motion

for the Wigner function.

First we define the phase space analog of the commutator. Consider the commutator

$$[\hat{f}, \hat{g}] = (\hat{f}\hat{g} - \hat{g}\hat{f}), \quad (3.72)$$

where  $\hat{f}$  and  $\hat{g}$  are operators in Hilbert space. Weyl Transforming both sides yields

$$[f, g]_{\star} = \frac{1}{i\hbar} (f \star g - g \star f) \quad (3.73)$$

Eq. 3.73 is called the *Moyal bracket*. Likewise the anti-commutator

$$\{\hat{f}, \hat{g}\} = (\hat{f}\hat{g} + \hat{g}\hat{f}) \quad (3.74)$$

becomes in phase space

$$\{f, g\}_{\star} = \frac{1}{i\hbar} (f \star g + g \star f) \quad (3.75)$$

Eq. 3.75 is called the *Baker bracket* [134].

Now the star product can be seen to be related to the Moyal and Baker brackets, by employing Euler's formula and the Janus operator definition of the star product to split the exponential into even and odd terms,

$$f \star g = f e^{i\overleftrightarrow{\Lambda}\hbar/2} g = f \left[ \cos \left( \frac{\overleftrightarrow{\Lambda}\hbar}{2} \right) + i \sin \left( \frac{\overleftrightarrow{\Lambda}\hbar}{2} \right) \right] g \quad (3.76)$$

Consider first the sine term

$$\begin{aligned}
f \left[ \sin \left( \frac{\overleftrightarrow{\Lambda} \hbar}{2} \right) \right] g &= \frac{i}{2} \left( f e^{-i \overleftrightarrow{\Lambda} \hbar / 2} g - f e^{i \overleftrightarrow{\Lambda} \hbar / 2} g \right) \\
&= \frac{i}{2} \left( g e^{i \overleftrightarrow{\Lambda} \hbar / 2} f - f e^{i \overleftrightarrow{\Lambda} \hbar / 2} g \right) \\
&= -\frac{i}{2} \left( f e^{i \overleftrightarrow{\Lambda} \hbar / 2} g - g e^{i \overleftrightarrow{\Lambda} \hbar / 2} f \right) \\
&= -\frac{i}{2} (f \star g - g \star f) \\
&= -\frac{i}{2} [f, g]_{\star} i \hbar = \frac{\hbar}{2} [f, g]_{\star}
\end{aligned} \tag{3.77}$$

then the cosine term,

$$\begin{aligned}
f \left[ \cos \left( \frac{\overleftrightarrow{\Lambda} \hbar}{2} \right) \right] g &= \frac{1}{2} \left( f e^{-i \overleftrightarrow{\Lambda} \hbar / 2} g - f e^{i \overleftrightarrow{\Lambda} \hbar / 2} g \right) \\
&= \frac{1}{2} \left( g e^{i \overleftrightarrow{\Lambda} \hbar / 2} f + f e^{i \overleftrightarrow{\Lambda} \hbar / 2} g \right) \\
&= \frac{1}{2} \left( f e^{i \overleftrightarrow{\Lambda} \hbar / 2} g + g e^{i \overleftrightarrow{\Lambda} \hbar / 2} f \right) \\
&= \frac{1}{2} (f \star g + g \star f) \\
&= \frac{1}{2} \{f, g\}_{\star} i \hbar = \frac{i \hbar}{2} \{f, g\}_{\star}
\end{aligned} \tag{3.78}$$

and the star product is recovered as

$$\begin{aligned}
f \star g &= \frac{i \hbar}{2} \{f, g\}_{\star} + \frac{i \hbar}{2} [f, g]_{\star} \\
&= \frac{i \hbar}{2} \left( \frac{1}{i \hbar} (f \star g + g \star f) + \frac{1}{i \hbar} (f \star g - g \star f) \right) \\
&= \frac{i \hbar}{2} \frac{1}{i \hbar} (2f \star g) = f \star g.
\end{aligned} \tag{3.79}$$

This is just the phase space form of the operator identity

$$\hat{f} \hat{g} = \frac{1}{2} \left( [\hat{f}, \hat{g}] + \{\hat{f}, \hat{g}\} \right). \tag{3.80}$$

### 3.5.1 The Moyal Bracket as a Lie Bracket

The Moyal bracket has the same significance as a commutator in quantum equations of motion or the Poisson bracket classical dynamics. The Moyal bracket is a Lie bracket and satisfies the axioms of a Lie bracket [135]:

$$[f, g]_{\star} = -[g, f]_{\star} \quad (\text{Antisymmetry}) \quad (3.81)$$

$$[af + bg, h]_{\star} = a[f, g]_{\star} + b[g, h]_{\star} \quad (\text{Left Linearity}) \quad (3.82)$$

$$[h, af + gb]_{\star} = a[h, f]_{\star} + b[h, g]_{\star} \quad (\text{Right Linearity}) \quad (3.83)$$

$$[f, [g, h]_{\star}]_{\star} + [g, [h, f]_{\star}]_{\star} + [h, [f, g]_{\star}]_{\star} = 0 \quad (\text{Jacobi Identity}) \quad (3.84)$$

Like the classical Poisson bracket, the Moyal bracket obeys a product rule, but with star (as opposed to classical) multiplication

$$[f \star g, h]_{\star} = [f, h]_{\star} \star g + f \star [g, h]_{\star} \quad (3.85)$$

with constants  $a, b \in \mathbb{R}$  and where  $f, g$  are arbitrary Weyl symbol on phase space. The Baker bracket is not antisymmetric and thus not a Lie bracket. Although it lacks the same physical significance of the Moyal bracket, the two can be combined to obtain the superalgebra Jacobi identities [136],

$$[\{f, g\}_{\star}, h]_{\star} + \{[h, f]_{\star}, g\}_{\star} + \{[h, g]_{\star}, f\}_{\star} = 0 \quad (3.86)$$

and

$$[\{f, g\}_{\star}, h]_{\star} + \{[h, f]_{\star}, g\}_{\star} + \{[g, h]_{\star}, f\}_{\star} = 0 \quad (3.87)$$

### 3.5.2 The Wigner Moyal Equation

Recall a pure state density  $\hat{\rho}$  in Hilbert space evolves according the quantum Liouville equation

$$\frac{\partial \hat{\rho}}{\partial t} = \frac{1}{i\hbar} [\hat{H}, \hat{\rho}] = \frac{1}{i\hbar} (\hat{H}\hat{\rho} - \hat{\rho}\hat{H}) \quad (3.88)$$

Weyl transforming both sides yields

$$\frac{\partial W_\rho}{\partial t} = \frac{1}{i\hbar} (\hat{H} \star W_\rho - W_\rho \star H) = [H, W_\rho]_\star \quad (3.89)$$

Eq. 3.91 is called the *Wigner-Moyal equation* and is the exact equation of motion for the quantum state represented by the Wigner function  $W_\rho$  in phase space. The Wigner-Moyal equation resembles the classical Liouville equation and in the classical limit reduces to it

$$\lim_{\hbar \rightarrow 0} \frac{\partial W_\rho}{\partial t} = [H, \rho]. \quad (3.90)$$

Similarly the Wigner-Moyal equation can be expressed formally in terms of a superoperator Liouvillian

$$\frac{\partial W_\rho}{\partial t} = \hat{\mathcal{L}}_\star W_\rho \quad (3.91)$$

with  $\hat{\mathcal{L}}_\star = [H, \cdot]_\star$ .

It is often said that the Wigner-Moyal equation is identical to classical Liouville equation for specific case of linear dynamics (viz. quadratic Hamiltonian Weyl symbols) [13]. Indeed, if one considers a 1 degree of freedom quantum system with the  $H = \frac{p^2}{2m} + U(q)$  for a pure state  $\psi$ , the Wigner-Moyal equation becomes

$$\frac{\partial W_\psi}{\partial t} = -\frac{p}{m} \frac{\partial W_\psi}{\partial q} + \sum_{k=0} \frac{(-\hbar^2)^k}{(2k+1)!} \left(\frac{1}{2}\right)^{2k} \frac{\partial^{2k+1} U(q)}{\partial^{2k+1}} \left(\frac{\partial}{\partial p}\right)^{2k+1} W_\psi(q, p) \quad (3.92)$$

If  $U(q)$  is quadratic  $U(q) = c_2 q^2 + c_1 q + c_0$  with  $c_n \in \mathbb{R}$ , the derivatives greater than second



order vanish and the Eq. 3.92 reduces to classical Liouville equation

$$\frac{\partial W_\psi}{\partial t} = -\frac{p}{m} \frac{\partial W_\psi(q, p)}{\partial q} + \frac{\partial U}{\partial q} \frac{\partial W_\psi(q, p)}{\partial p} \quad (3.93)$$

The important subtlety is: this is true only for single component pure state. If the state is prepared in a superposition  $\Psi = \psi_1 + \psi_2$ , the equations of motion of the coherence Wigner function do not obey the classical Liouville equation. One of the primary contributions of this thesis and a topic discussed in the following chapter is how the exact quantum motion of superposition in phase space deviates from the classical picture.

A second important point regarding Eq. 3.92 is that for nonlinear dynamic (non quadratic potentials), the dynamic vector field prescribed by Wigner-Moyal equation is nonconservative. This means the quantum probability density in phase space (the Wigner function) does not flow incompressibly like its classical analog. As a consequence, a given region in phase space does not preserve the number of trajectories emanating from an arbitrary point and the flow of trajectories are no longer deterministic [13]. Thus the Wigner-Moyal equation resembles the classical Liouville equation in only the limited case of a single component pure state undergoing linear dynamics under a quadratic potential.

## 3.6 Star Algebra and Identities

Having introduced Weyl symbols, the star product, and the Moyal bracket, the question is how this formalism can be applied to practical quantum mechanical calculations. It's thus necessary to understand the algebraic properties of Weyl symbols under star multiplication and Moyal bracket. Fortunately, nearly all algebraic properties of the non-commutative Moyal algebra can be understood as being inherited from the non-commutative matrix algebra of operators in Hilbert space. In this section, the essential ones are highlighted.

### 3.6.1 Moyal Algebra

The star product algebra (Moyal algebra) is defined by the following axioms [135]:

$$f \star g \neq g \star f \quad (\text{Non-commutativity}) \quad (3.94)$$

$$f \star (g \star h) = (f \star g) \star h = f \star g \star h \quad (\text{Associativity}) \quad (3.95)$$

$$f \star \mathbb{1} = \mathbb{1} \star f = f \quad (\text{Identity}) \quad (3.96)$$

$$\overline{f \star g \star h} = \bar{h} \star \bar{g} \star \bar{f} \quad (\text{Adjoint}) \quad (3.97)$$

$$f \star g = fg + \mathcal{O}(\hbar) = gf + \mathcal{O}(\hbar) \quad (\text{Classical Product}) \quad (3.98)$$

That is the star product is generally non-commutative. This, of course, does not mean that  $f \star g$  can never equal  $g \star f$ , but the star product only commutes when the Hilbert space operators which form its Weyl symbols do  $[\hat{f}, \hat{g}] = 0$ . Like matrix multiplication, star multiplication is associative. Formally a quantum algebra, like the Moyal algebra, requires an identity element. In this case, the identity Weyl symbol  $\mathbb{1}$  is the identity operator in the undeformed algebra. Like operators in Hilbert space which possess the adjoint rule  $(\hat{f}\hat{g}\hat{h})^\dagger = \hat{h}^\dagger\hat{g}^\dagger\hat{f}^\dagger$ , so does the Moyal algebra. And the Moyal algebra must contain the classical commuting algebra to zeroth order in the deformation parameter  $\hbar$ . These axioms together define the basic algebra of star products.

### 3.6.2 Trace Properties

Because in experiment and simulation, one is often interested in expectations and correlation functions of observables, it's necessary to know the properties of the star product within a trace. Just as the trace of Hilbert space operators is invariant to cyclic permutation, so to

is the trace for star products of Weyl symbols

$$\mathrm{Tr}(f_1 \star f_2 \star \cdots \star f_k \star f_{k+1} \star \cdots \star f_n) = \mathrm{Tr}(f_{k+1} \star \cdots \star f_n \star f_1 \star f_2 \star \cdots \star f_k) \quad (3.99)$$

and like the commutator, it immediately follows the trace of a Moyal Bracket is zero

$$\mathrm{Tr}([f, g]_\star) = 0 \quad (3.100)$$

A property unique to traces over star product is an important reduction rule [13]. One can show through integration-by-parts, a single star product within a trace vanishes. And thus for arbitrary Weyl symbols  $f, g$  one has

$$\mathrm{Tr}(f \star g) = \mathrm{Tr}(fg) \quad (3.101)$$

This is why, for example, in Eqs. 3.24-3.27 the star product was omitted. The trace reduction identity also applies to a trace over a  $n$ -fold star product of Weyl symbols. For a product of three Weyl symbols  $f, g$ , and  $h$  using Eq. 3.102 and cyclic invariance of the trace (Eq. 3.99) one has

$$\mathrm{Tr}(f \star g \star h) = \mathrm{Tr}(f(g \star h)) = \mathrm{Tr}((f \star g)h) = \mathrm{Tr}((h \star f)g). \quad (3.102)$$

Lastly, the cyclic invariance of the trace can be combined with star Leibniz rule can be used to derive the following relations,

$$\mathrm{Tr}([f, g]_\star \star h) = \mathrm{Tr}(f \star [g, h]_\star) \quad (3.103)$$

$$\mathrm{Tr}(\{f, g\}_\star \star h) = \mathrm{Tr}(f \star \{g, h\}_\star) \quad (3.104)$$

The properties of the trace and those of the Moyal algebra can be used to derive a host of identities. Additional ones are provided in Appendix A.

### 3.7 Gaussian Weyl Symbols and Hudson States

What bars a Wigner from being a “proper” probability distribution is that the Wigner function is generally not positive-definite, containing some regions of negative probability in phase space. The Wigner function of the first excited state of a harmonic oscillator is a typical example of this (Fig. 3.2). The negative regions can be seen to be a consequence of the position (or momentum) wavefunction having a node (a region where the wavefunction cross through zero and its probability density touches zero). Because nodal structure increases with energy, Wigner functions formed from excited state wavefunctions have negative probabilities. Negative probabilities also arise, in Wigner functions of superpositions, resulting from the coherence between the states. For the purposes of developing trajectory-based quantum dynamics methods, it is necessary to know when or in what cases the Wigner function is non-negative (positive-definite) and can be used as a proper probability distribution to sample trajectories from. An important theorem developed by Hudson provides this criterion [137].

Hudson’s Theorem stipulates a pure state Wigner function is positive-definite if and only if the wavefunction used to construct it through the Wigner Transform is a generalized Gaussian. Generalized Gaussians will be defined below, but note the operative words in the theorem are “pure state” and “Wigner Transform.” A positive-definite Wigner function is not necessarily a Hudson state. For example, consider the Wigner function of a thermal oscillator [79],

$$W(q, p) = \kappa(T) \exp \left( -\kappa(T) \left( \frac{m\omega}{\hbar} q^2 + \frac{1}{m\omega\hbar} p^2 \right) \right) \quad (3.105)$$

where

$$\kappa(T) = 2 \tanh \left( \frac{\hbar\omega}{2kT} \right) \quad (3.106)$$

where  $k$  is Boltzmann’s constant.  $W(q, p)$  in Eq. 3.105 is positive-definite, but it is a mixed state and can’t be obtained from the Wigner Transform of a wavefunction. Moreover, Hud-

son's Theorem does not address explicitly Cross Wigner functions and their transforms. In fact, the Cross Wigner Transform between two distinct generalized Gaussians is generally complex.

Hudson's Theorem only argues that a sufficient and necessary condition for a positive definite pure state Wigner function is that its wavefunction is a generalized Gaussian. Thus if a pure state Wigner function is positive-definite the wavefunction used to construct it or obtained by inverting that Wigner function is a generalized Gaussian and if a wavefunction is a generalized Gaussian, its Wigner function necessarily is positive-definite.

In this section, Hudson's Theorem and generalized Gaussians are defined. The important work of de Gosson [14] is revisited which shows that the Wigner Transform of a generalized Gaussian is itself a generalized Gaussian in phase space. This is true not only for the Wigner Transform of a single generalized Gaussian, but also the Cross Wigner transform of two generalized Gaussians. Despite this, the Cross Wigner function of two generalized Gaussian wavefunctions is generally not positive-definite. Another way to define Hudson states is in terms of their property of minimum uncertainty. Hudson states are normal distributions in canonical variables which saturate the Schrödinger-Robertson inequality. Viewed in this light, Hudson states are nothing more than the Wigner function of squeezed coherent states. For the purposes of trajectory ensemble quantum dynamics methods, Hudson's Theorem is important because it identifies quantum distributions that classical trajectory ensembles can be fit to.

### 3.7.1 Hudson's Theorem

A *generalized Gaussian*  $G(\mathbf{x})$  of  $n$  variables  $\mathbf{x} = (x_1, \dots, x_n)^T$  is the function

$$G_{\mathbf{M}}(\mathbf{x}) = A(\mathbf{X})e^{-\mathbf{x}^T \mathbf{M} \mathbf{x}} \quad (3.107)$$

with

$$\mathbf{M} = \mathbf{X} + i\mathbf{Y} \quad (3.108)$$

where  $A(\mathbf{X})$  is a normalization factor and the matrices  $\mathbf{X} \in \mathbb{R}^{n \times n}$  and  $\mathbf{Y} \in \mathbb{R}^{n \times n}$  are symmetric:  $\mathbf{X} = \mathbf{X}^T$  and  $\mathbf{Y} = \mathbf{Y}^T$ , and  $\mathbf{X}$  is positive-definite  $\mathbf{X} > 0$ . Note:  $\mathbf{M} \in \mathbb{C}^{n \times n}$  is symmetric  $\mathbf{M}^T = \mathbf{M}$  because  $\mathbf{X}$  and  $\mathbf{Y}$  are.

A normalized generalized Gaussian wavefunction is

$$\psi_{\mathbf{M}}(\mathbf{q}) = \left( \frac{\det(\mathbf{X})}{(\pi\hbar)^n} \right)^{1/4} \exp\left(-\frac{1}{2\hbar} \mathbf{q}^T \mathbf{M} \mathbf{q}\right) \quad (3.109)$$

*Hudson's Theorem* states that the Wigner Transform of Eq. 3.109 is necessarily a positive-definite Wigner function. The Wigner function associated with  $\psi_{\mathbf{M}}$  was worked out by de Gosson [14] and shown to be

$$W_{\mathbf{S}}(\mathbf{q}, \mathbf{p}) = \mathcal{W}[\psi_{\mathbf{M}}] = \left( \frac{1}{\pi\hbar} \right)^n \exp\left(-\frac{1}{\hbar} \mathbf{z}^T \mathbf{S} \mathbf{z}\right) \quad (3.110)$$

with where  $\mathbf{z} = (\mathbf{q}, \mathbf{p})^T$  and

$$\mathbf{S} = \begin{pmatrix} \mathbf{X} + \mathbf{Y}\mathbf{X}^{-1}\mathbf{Y} & \mathbf{Y}\mathbf{X}^{-1} \\ \mathbf{X}^{-1}\mathbf{Y} & \mathbf{X}^{-1} \end{pmatrix} \quad (3.111)$$

The matrix  $\mathbf{S} \in \mathbb{R}^{2N \times 2N}$  is symmetric  $\mathbf{S} = \mathbf{S}^T$  and symplectic  $\mathbf{S}^T \mathbf{J} \mathbf{S} = \mathbf{J}$ . Wigner functions of the form of satisfying Eqs. 3.110-3.111 are called *Hudsons states*.

Again following de Gosson, the Cross Wigner function of two generalized Gaussians

$$\psi_{\mathbf{M}_j}(\mathbf{q}) = \left( \frac{\det(\mathbf{X}_j)}{(\pi\hbar)^n} \right)^{1/4} \exp\left(-\frac{1}{2\hbar} \mathbf{q}^T \mathbf{M}_j \mathbf{q}\right) \quad (3.112)$$

with  $\mathbf{M}_j = \mathbf{X}_j + i\mathbf{Y}$  with  $j = 1, 2$  is given by

$$W_{\mathbf{S}_{12}}(\mathbf{q}, \mathbf{p}) = \mathcal{W}[\psi_{\mathbf{M}_1}, \psi_{\mathbf{M}_2}] = \left(\frac{1}{\pi\hbar}\right)^n \exp\left(-\frac{1}{\hbar}\mathbf{z}^T \mathbf{S}_{12} \mathbf{z}\right) \quad (3.113)$$

with where  $\mathbf{z} = (\mathbf{q}, \mathbf{p})^T$  and

$$\mathbf{S}_{12} = \begin{pmatrix} 2\bar{\mathbf{M}}_2 (\mathbf{M}_1 + \bar{\mathbf{M}}_2)^{-1} \mathbf{M}_1 & -i (\mathbf{M}_1 - \bar{\mathbf{M}}_2) (\mathbf{M}_1 + \bar{\mathbf{M}}_2)^{-1} \\ -i (\mathbf{M}_1 + \bar{\mathbf{M}}_2)^{-1} (\mathbf{M}_1 - \bar{\mathbf{M}}_2) & 2 (\mathbf{M}_1 + \bar{\mathbf{M}}_2)^{-1} \end{pmatrix}. \quad (3.114)$$

Note unlike a Hudson state Wigner function, the Cross Wigner function of two generalized Gaussian yields a matrix which is still symmetric  $\mathbf{S}_{12} = \mathbf{S}_{12}^T$ , but no longer real  $\mathbf{S}_{12} \in \mathbb{C}^{2N \times 2N}$ . Thus Cross Wigner function of two generalized Gaussians is not generally positive-definite.

### 3.7.2 Hudson States

Returning to the Hudson state Wigner function  $W_{\mathbf{S}}$ , note it is invariant to phase space displacements. Displacing  $W_{\mathbf{S}}$  by  $\hat{T}(\mathbf{Z})$  and normalizing, the Hudson state Wigner function can be written

$$W_{\mathbf{S}}(\mathbf{q}, \mathbf{p}) = \frac{1}{\sqrt{(\pi\hbar)^n \det(\mathbf{S}^{-1})}} \exp\left(-\frac{1}{\hbar} [\mathbf{z} - \mathbf{Z}]^T \mathbf{S} [\mathbf{z} - \mathbf{Z}]\right) \quad (3.115)$$

Hudson states can be viewed as a special class of even dimensional ( $d = 2n$ ) multinormal distributions [138],

$$g(\mathbf{z}) = \frac{1}{\sqrt{(2\pi)^{2n} \det(\boldsymbol{\Sigma})}} \exp\left(-\frac{1}{2} [\mathbf{z} - \mathbf{Z}]^T \boldsymbol{\Sigma}^{-1} [\mathbf{z} - \mathbf{Z}]\right) \quad (3.116)$$

with  $\mathbf{z} = (z_1, \dots, z_{2n}) \in \mathbb{R}^{2n}$ .  $\mathbf{z}$  is a random vector distributed according to  $g(\mathbf{z})$ , viz.

$\mathbf{z} \sim g(\mathbf{z})$ .  $g(\mathbf{z})$  is thus parametrized by the mean vector  $\mathbf{Z} = (Z_1, \dots, Z_{2n}) \in \mathbb{R}^{2n}$  and the covariance matrix  $\Sigma$ ,

$$\Sigma = \Sigma_{i,j} = r_{i,j} \sigma_i \sigma_j = \begin{pmatrix} \sigma_1^2 & \cdots & r_{1,k} \sigma_1 \sigma_k & \cdots & r_{1,2n} \sigma_1 \sigma_{2n} \\ \vdots & \cdots & \vdots & \cdots & \vdots \\ r_{2n,1} \sigma_{2n} \sigma_1 & \cdots & r_{2n,k} \sigma_{2n} \sigma_k & \cdots & \sigma_{2n}^2 \end{pmatrix}. \quad (3.117)$$

Not any Gaussian of the form of Eq. 3.116 is a Hudson state, but rather those whose covariance matrix elements satisfy a minimum uncertainty constraint between canonical conjugate variables

$$r_{i,i+n} \sigma_i^2 \sigma_{i+n}^2 (1 - r_{i,i+n}^2) = \frac{\hbar^2}{4}. \quad (3.118)$$

To make this more explicit consider a Hudson state for 1 degree of freedom. Eq. 3.116 reduces to a normalized bivariate Gaussian given by [139],

$$g(q, p) = \frac{1}{2\pi\sigma_q\sigma_p\sqrt{1-r^2}} \exp\left(-\frac{1}{2(1-r^2)} \left(\frac{(p-P)^2}{\sigma_p^2} + \frac{(q-Q)^2}{\sigma_q^2} - \frac{2r(p-P)(q-Q)}{\sigma_q\sigma_p}\right)\right) \quad (3.119)$$

where position-momentum correlation  $r$  constrained by

$$0 \leq r^2 < 1 \quad (3.120)$$

and where  $(\sigma_q^2, \sigma_p^2, Q, P) \in \mathbb{R}$  are the expectations and variances of position and momentum respectively. In accordance with the Uncertainty Principle,

$$\sigma_A^2 \sigma_B^2 (1 - r^2) \geq \frac{1}{4} |\langle [\hat{A}, \hat{B}] \rangle|^2 \quad (3.121)$$

for  $\hat{A} = \hat{q}$  and  $\hat{B} = \hat{p}$ , only  $g(q, p)$ 's with their variances and correlation constrained by



Schrödinger-Robertson inequality

$$\sigma_p^2 \sigma_q^2 (1 - r^2) \geq \frac{\hbar^2}{4}, \quad (3.122)$$

will correspond to a physical quantum state. When the Schrödinger-Robertson inequality is an equality for all degrees of freedom, the multinormal Wigner function is a Hudson state.

Because Hudson state form an important class of Weyl symbols used in subsequent analysis, they are given their own symbol  $\eta$  with the set of their statistical parameters labelled as  $\chi = \{Q, P, \sigma_q, \sigma_p, r\}$ . In this notation, Eq. 3.119 is written

$$\begin{aligned} \eta(q, p; \chi) &= \frac{1}{2\pi\sigma_q\sigma_p\sqrt{1-r^2}} \exp\left(-\frac{1}{2(1-r^2)} \left(\frac{(p-P)^2}{\sigma_p^2} + \frac{(q-Q)^2}{\sigma_q^2} - \frac{2r(p-P)(q-Q)}{\sigma_q\sigma_p}\right)\right). \end{aligned} \quad (3.123)$$

The parametrization associated with Eq. 3.123 is illustrated in Fig. 3.4a.

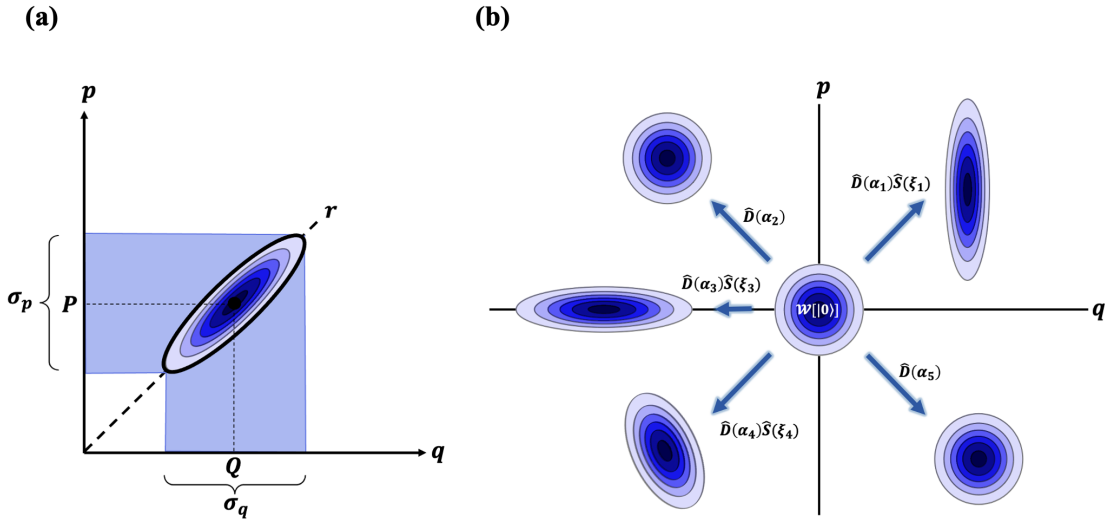


Figure 3.4: (a) Statistical parametrization of a Hudson state Wigner function. (b) Examples of Hudson states generated by squeeze  $\hat{S}$  and displacement  $\hat{D}$  of the harmonic oscillator ground state.

### 3.7.3 Connection with Squeezed Coherent States

A Hudson state is a positive-definite pure state Wigner function. Although not explicitly in Hudson's original theorem, as a consequence of positive-definiteness, a Hudson state is minimum uncertainty in all its canonically conjugate variables. In the language of quantum optics, Hudson states are known as *squeezed coherent states*. It has been known since Schrödinger that coherent states are quantum states most closely resembling classical trajectories and radiation fields [140]. This is even more clearly illustrated in phase space.

Coherent states have a number of ways of being defined [141]. The simplest definition of a coherent state  $|\alpha\rangle$  is defined as an eigenstate of the annihilation operator  $\hat{a}$  of the quantum harmonic oscillator

$$\hat{a}|\alpha\rangle = \alpha|\alpha\rangle. \quad (3.124)$$

A coherent state, in turn, is generated by displacements  $\hat{D}(\alpha)$  to the ground state of the harmonic oscillator (vacuum state),

$$|\alpha\rangle = \hat{D}(\alpha)|0\rangle \quad (3.125)$$

where  $\alpha \in \mathbb{C}$  is a complex number typically represented as a real amplitude  $A$  and phase  $\phi$ ,  $\alpha = |A|e^{i\phi}$ . Importantly, a coherent state is a symmetric minimum uncertainty state ( $r = 0$  and  $\sigma_p = \sigma_q$ ) such that the Schrödinger-Robertston equality reduces to the Heisenberg equality

$$\sigma_p^2 \sigma_q^2 = \frac{\hbar^2}{4}. \quad (3.126)$$

In phase space this means, a coherent state is the Wigner function with a circular distribution of equal variances in its canonical conjugate variables centered about any mean in phase space determined by the displacement (Fig. 3.4b). By introducing a squeeze operator  $\hat{S}(\xi)$ , a coherent state can be compressed or sheared such that the variances in canonical conjugate

variables are no longer equal ( $\sigma_p \neq \sigma_q$ ) and position-momentum correlation can exist  $r > 0$ . A squeezed coherent state is defined by

$$|\alpha, \xi\rangle = \hat{D}(\alpha)\hat{S}(\xi)|0\rangle \quad (3.127)$$

where  $\xi$  is the squeeze parameter. In phase space, this amounts to deforming the circular coherent state Wigner function into an ellipsoidal or “cigar shaped” distribution, where its major and minor axis are the variances of canonical conjugate variables. The ellipsoidal distribution’s center is still the mean of the distribution like the coherent state, but its axes are no longer equal. Moreover, the major axes of a squeezed state Wigner function need not be along the position and momentum axes of phase space, but any angle subtended. This in effect produces position-momentum correlation.

It’s important to note not all squeezing operations preserve the minimum uncertainty constraint of the Schrödinger-Roberston equality. In other words, not all squeezed states are coherent states. Squeezed coherent states are squeezed states which retain the condition of minimum uncertainty. This condition can be explained in terms of metaplectic transformations of the harmonic oscillator ground state wavefunction [142] or the Lie groups of linear canonical transforms [143]. The criterion of minimum uncertainty allows squeezed coherent states (like coherent states) to form a (over)complete basis with a resolution of identity. Consequently, Hudson states can be used as a basis to represent any pure state density in phase space.

## Chapter 4

# Wigner-Moyal Solution to Displaced Oscillator Model

In this chapter, a model for the dynamics of quantum coherences for a two state system undergoing linear motion in the Wigner-Moyal representation is derived. Using a Thawed Gaussian ansatz for the coherence Wigner function, exact quantum equations of motion are obtained and used to simulate the vibrational coherence between two electronic states generated from a vertical (Franck-Condon) excitation in displaced oscillator systems. This model is a simple molecular realization of a “Schrödinger’s cat” state for a coherent superpositions. The evolution of the coherence Wigner function is modulated by contributions of both the ground and excited state potentials. Because both are harmonic and their dynamics are linear, an intuitive picture of the time-dependence of the coherence emerges with its coherence Wigner function evolving on arithmetic averages of each states potential. For these systems, phase space portraits, time correlation functions, and linear absorption spectra of the coherence are calculated and analyzed.

Using the same framework, approximate solutions to the Wigner-Moyal equation for the

coherence are derived. The semiclassical solution is obtained by truncating the Wigner-Moyal equation to  $\mathcal{O}(\hbar)$ . It is found that semiclassical solution to the coherence is unstable, and experiences secular growth of oscillatory terms resulting in a spurious decay of the coherence. However, through a second approximation: —linearizing of the difference potential, the secular terms vanish and the spurious decoherence of the semiclassical result is amended. Exact quantum and approximate solutions are studied for displaced oscillator systems in 1 and 2 dimensions, with the latter providing a crude model of vibrational coherences generated by nuclear wavepacket passage through a conical intersection. Although, results are limited to linear systems (quadratic potentials) with zero off-diagonal coupling, their significance is three-fold

Foremost, contrary to common assumption: the motion of a Wigner function does not generally reduce to classical equations of motion for linear systems for a coherence Wigner function. Even to first order  $\mathcal{O}(\hbar)$ , the semiclassical solution to the equations of motion for a coherence Wigner function are qualitatively incorrect. Mixed-quantum classical and semiclassical methods which implicitly assume the average potential for the coherence equations of motion inherit this error. Second, the quantum solution for the coherence, suggests a more general approach for simulating the dynamics of coherence in terms of evolution of statistical parameters of each state's population. This insight is independent of the system's potential or coupling and is derived in Chapter 5. Third, although the displaced oscillator with zero diabatic coupling is a crude model: the methods for adding anharmonic effects or coupling are well-understood and can be improved upon standard techniques of perturbation theory.

The structure of this chapter is as follows. The first section, provides some brief background on the displaced oscillator model and Thawed Gaussian wavepackets. The next section details the derivation of the exact equation of the motion for the coherence in the Wigner-Moyal representation, solutions using a Thawed Gaussian ansatz, and approximate solutions through truncation or linearization. This framework is called Thawed Moyal Dynamics.

The Thawed Moyal equations of motion are simulated for displaced oscillator models in the results section. The chapter concludes with a discussion of the solutions and their kinematic interpretation.

## 4.1 Background

### 4.1.1 Displaced Oscillator Model

Displaced oscillator models are often used to model linear absorption spectra in simple molecules. By taking the molecular diabatic potentials to be harmonic, Frank-Condon factors associated with excitations of vibrational wavefunctions between the ground and excited electronic manifolds can be calculated analytically. Likewise in the time-domain, the dynamics of the system is linear, analytically soluble, and the absorption spectrum can be calculated by means of time correlation functions.

A 1-D displaced oscillator model is defined by harmonic potentials

$$U_j(q) = \frac{1}{2}m\Omega_j^2 (q - Q_j^e)^2 + E_j \quad (4.1)$$

where  $q$ ,  $m$ ,  $\Omega_j$ ,  $Q_j$ , and  $E_j$  are the vibrational coordinate, mass, frequency, equilibrium position, and energy datum of state  $j$  respectively. For a molecular model,  $q$  is a nuclear vibrational degree of freedom while states  $j$  label different electronic state manifolds, each of which contain a progression of vibrational eigenstates described by a quantum harmonic oscillator. The oscillators  $U_j(q)$  are “displaced” from one another by their different equilibrium positions  $Q_j^e$  and energy data  $E_j$  (Fig. 4.1a).

For a Franck-Condon transition generated by an ultrafast laser pulse, the initial wavefunction is copied from the ground state to the excited state. The excited state wavefunction will

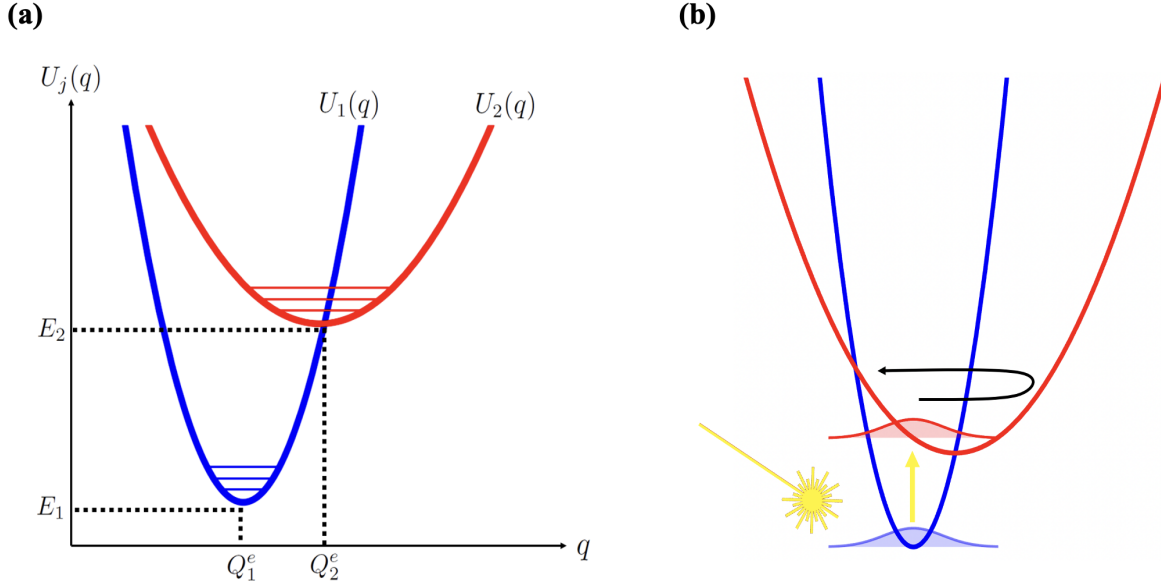


Figure 4.1: (a) Displaced oscillator model for electronic states  $j = 1, 2$  and a nuclear coordinate  $q$ . (b) Franck-Condon excitation of the displaced oscillator by an ultrafast laser pulse.

then undergo motion according to the excited potential and generate a vibrational coherence with the ground state (Fig. 4.1b). The vibrational coherence can be measured by the linear absorption spectrum. In the energy-domain, this is

$$\sigma(\Omega) = \sum_{m,n} |\langle g_m | e_n \rangle|^2 \delta(\Omega - \Omega_{e_n g_m}) \quad (4.2)$$

where  $g_n$  and  $e_m$  are vibrational energy eigenstates of the ground and excited electronic state manifold.  $\Omega_{e_n g_m}$  is the frequency of transition from  $|g_m\rangle \rightarrow |e_n\rangle$  whose intensity is given by the Frank-Condon factors  $|\langle g_m | e_n \rangle|^2$ . The same spectrum can be calculated directly in the time-domain as

$$\sigma(\Omega) = \frac{1}{2\pi} \int dt e^{i\Omega t} \langle \Psi(0) | \Psi(t) \rangle \quad (4.3)$$

where  $\Psi(0)$  is the initial wavepacket and  $\Psi(t)$  is the time evolved copy.

### 4.1.2 Thawed Gaussian Wavepackets

Localized wavefunctions (wavepackets) of a Gaussian form have a long history in the study of coherent states and as a numerical tool for solving the time-dependent Schrödinger equation. Thawed Gaussian wavepackets are a special subset of Gaussian wavepackets which have “thawed” or time-varying widths. In one dimension and in the position representation, a *Thawed Gaussian wavepacket* is a wavefunction of the form

$$\psi(q, t) = \exp\left(-\frac{\beta(t)}{\hbar} (q - Q(t))^2 + \frac{iP(t)}{\hbar} (q - Q(t)) + \frac{i}{\hbar}\gamma(t)\right) \quad (4.4)$$

where  $\beta, \gamma \in \mathbb{C}$  and  $Q, R \in \mathbb{R}$  are time-dependent variables which parametrize the wavefunction. For  $\beta$ , its real part  $\text{Re}(\beta)$  determines the width or variances of the wavepacket while its imaginary part  $\text{Im}(\beta)$  controls position-momentum correlation. The term *thawed* denotes that the width of the wavepacket changes as a function of time  $\beta = \beta(t)$  as opposed to being constant or *frozen*  $\frac{\partial\beta}{\partial t} = 0$ .  $\gamma$  is a complex phase and is typically used to normalize the wavepacket by

$$\text{Re}(\gamma(0)) = \frac{\hbar}{4} \ln\left(\frac{\pi\hbar}{2\text{Re}(\beta(0))}\right).$$

$Q$  and  $P$  are the average position and momentum and momentum of the wavepacket derived from the expectations

$$Q = \langle \psi(q, t) | \hat{q} | \psi(q, t) \rangle \quad \text{and} \quad P = \langle \psi(q, t) | \hat{p} | \psi(q, t) \rangle,$$

respectively. The four statistical parameters  $(\beta, \gamma, Q, P)$  together specify the state of a Gaussian wavepacket of the form in Eq. 4.4. As was shown by Heller, if Eq. 4.4 is used as an ansatz for the solution wavefunction for a quadratic Hamiltonian, one can obtain equations of motions for the four statistical parameters by substituting it into the time-dependent



Schrödinger Equation

$$i\hbar \frac{\partial \psi(q, t)}{\partial t} = \hat{H} \psi(q, t) = \left( \frac{-\hbar^2}{2m} \frac{\partial^2}{\partial q^2} + V(q, t) \right) \psi(q, t) \quad (4.5)$$

and equating like-powers in  $(q - Q(t))^n$ . This gives the following set of differential equations

$$\boxed{(q - Q(t))^2} \quad \beta \dot{t} = \frac{2\beta(t)^2}{m} - \frac{V''(Q(t))}{2} \quad (4.6)$$

$$\boxed{(q - Q(t))^1} \quad \dot{Q}(t) = \frac{P(t)}{m} \quad (4.7)$$

$$\dot{P}(t) = -V'(Q(t)) \quad (4.8)$$

$$\boxed{(q - Q(t))^0} \quad \begin{aligned} \dot{\gamma}(t) &= -V(Q(t)) - \frac{\beta(t)\hbar}{m} + P(t)\dot{Q}(t) - \frac{P(t)^2}{2m} + V(Q(t)) \\ &= -\frac{\beta(t)\hbar}{m} + L(t). \end{aligned} \quad (4.9)$$

Note Eqs. 4.7-4.8 are Hamilton's equation for the expectations  $(Q, P)$ . Together they define a Ehrenfest trajectory. The phase equation of motion (Eq. 4.9) contains a Lagrangian for this trajectory with energy  $E(t) = \frac{P(t)^2}{2m} + V(Q(t))$ ,

$$L(t) = P(t)\dot{Q}(t) - E(t). \quad (4.10)$$

Applied to anharmonic potentials, the Thawed Gaussian equation of motion are 2<sup>nd</sup> order truncation to the actual dynamics. However, the expansion point  $(q - Q(t))$  can be taken as a function of time and continuously evolved for smooth potentials. And anharmonic potential

can be approximated by a succession of harmonic potentials of change widths,

$$V(q, t) \approx V(Q(t)) + V'(Q(t))(q - Q(t)) + \frac{1}{2}V''(Q(t))(q - Q(t))^2 + \dots$$

allowing some anharmonicity to be accounted for. Applied to anharmonic potentials Eqs. 4.7-4.8 are called the *Thawed Gaussian Approximation*.

## 4.2 Thawed Moyal Dynamics: Derivation and Approximations

That Thawed Gaussian wavepackets can be used to solve multi-state quantum dynamics in phase space isn't a large conceptual leap. For multi-state systems, so long as their potentials are harmonic with zero diabatic coupling, the Thawed Gaussian wavepacket equations of motion are exact. The simplest instance of such a system is the displaced oscillator model. As for evolution in phase space, one can see that a Thawed Gaussian wavepacket (Eq. 4.4) is a generalized Gaussian (Eq. 3.109) and its Wigner transform and Cross Wigner Transform are easily calculated. Together, this implies the dynamics of the displaced oscillator system can be solved a number of ways using Thawed Gaussians and their (Cross) Wigner Transforms. In this chapter, two such approaches are considered.

One route is to substitute a Thawed Gaussian ansatz for the coherence Wigner function to into the Wigner-Moyal equation. This approach is called *Thawed Moyal Dynamics*. A second approach is to directly use Thawed Gaussian wavepackets to construct the coherence by their Cross Wigner Transform and solve the Wigner-Moyal equation in terms of the wavepacket's parameters. The two approaches are equivalent with the wavepacket providing a check of the Thawed Moyal Dynamics solutions. The advantage of the Thawed Moyal approach is that equations of motion are obtained in terms of statistical parameters of the coherence

distribution directly. These solutions are easily interpreted in phase space and provide a framework for further approximations to the dynamics.

### 4.2.1 The Coherence Wigner Function Equation of Motion

Returning to the displaced oscillator model for two electronic states with a single nuclear vibrational degree of freedom in the diabatic representation. The quantum Liouville equation is

$$\frac{d\hat{\rho}}{dt} = \frac{1}{i\hbar} \left[ \begin{pmatrix} \hat{H}_{11} & \hat{H}_{12} \\ \hat{H}_{21} & \hat{H}_{22} \end{pmatrix}, \begin{pmatrix} \hat{\rho}_{11} & \hat{\rho}_{12} \\ \hat{\rho}_{21} & \hat{\rho}_{22} \end{pmatrix} \right] \quad (4.11)$$

where the diagonal elements of the Hamiltonian are displaced oscillators

$$\hat{H}_{jj} = \frac{\hat{p}^2}{2m} + \hat{U}_j(\hat{q}) = \frac{\hat{p}^2}{2m} + \frac{1}{2}m\Omega_j^2 (\hat{q} - Q_j^e)^2 + E_j \quad (4.12)$$

and off-diagonal coupling elements are zero ( $\hat{H}_{12} = \hat{H}_{21} = 0$ ). Focusing on the coherence ( $\hat{\rho}_{12} = \hat{\rho}_{21}^\dagger$ ), its evolution is

$$i\hbar \frac{\partial \hat{\rho}_{12}}{\partial t} = \hat{H}_{11} \hat{\rho}_{12} - \hat{\rho}_{12} \hat{H}_{22} \quad (4.13)$$

Weyl Transforming both sides of Eq. 4.13, yields the Wigner-Moyal equation for the coherence Wigner function

$$\frac{\partial \rho_{12}}{\partial t} = \frac{1}{i\hbar} (H_{11} \star \rho_{12} - \rho_{12} \star H_{22}) \quad (4.14)$$

with Weyl symbols  $H_{jj} = T + U_j(q)$  for  $j = 1, 2$  and  $T = \frac{p^2}{2m}$  is kinetic energy. The kinetic energy terms for each state  $j$  can be collected from the potentials as

$$\frac{\partial \rho_{12}}{\partial t} = [T, \rho_{12}]_\star - \frac{i}{\hbar} (U_1 \star \rho_{12} - \rho_{12} \star U_2). \quad (4.15)$$

Because  $T$  is quadratic in  $p$ , its Moyal Bracket to reduce to the classical Poisson Bracket,  $[T, \rho_{12}]_\star \rightarrow [T, \rho_{12}]$ . The star products in Eq. 4.15 can be evaluated using Bopp shifts

(Eq. 3.52) to give

$$\frac{\partial \rho_{12}}{\partial t} = [T, \rho_{12}] - \frac{i}{\hbar} \left( U_1 \left( q + \frac{i\hbar}{2} \partial_p \right) - U_2 \left( q - \frac{i\hbar}{2} \partial_p \right) \right) \quad (4.16)$$

For smooth potentials  $U_j(q)$  that permit the Taylor series representation, one has

$$U_j \left( q \pm \frac{i\hbar}{2} \partial_p \right) = \sum_{k=0}^{\infty} \left( \frac{\pm i\hbar}{2} \right)^k \frac{d^k U_j(q)}{dq^k} \partial_p^k \quad (4.17)$$

and Eq. 4.16 can be written

$$\begin{aligned} \frac{\partial \rho_{12}}{\partial t} &= [T, \rho_{12}] - \frac{i}{\hbar} \left[ \sum_{k=0}^{\infty} \frac{1}{k!} \left( \frac{i\hbar}{2} \right)^k \frac{d^k}{dq^k} \left( U_1(q) - (-1)^k U_2(q) \right) \right] \partial_p^k \rho_{12} \\ &= [T, \rho_{12}] - \frac{i}{\hbar} (U_1 - U_2) \rho_{12} + \frac{1}{2} (U_1' + U_2') \partial_p \rho_{12} + \frac{i\hbar}{8} (U_1'' - U_2'') \partial_p^2 \rho_{12} + \dots \end{aligned} \quad (4.18)$$

For general potentials, this series is infinite and approximate solutions are obtained by truncating to a given  $\mathcal{O}(\hbar^n)$ . For quadratic Hamiltonians, however, the series terminates at second order

$$\frac{\partial \rho_{12}}{\partial t} = [H_0, \rho_{12}] - i\omega \rho_{12} + \frac{i\hbar\omega''}{8} \frac{\partial^2 \rho_{12}}{\partial p^2} \quad (4.19)$$

where  $H_0 = (H_1 + H_2)/2$  is an average Hamiltonian and  $\omega = (U_1 - U_2)/\hbar$  is the difference potential. Eq. 4.19 is the exact equation of motion for the coherence for linear dynamics. If, instead, one truncates to first order  $\mathcal{O}(\hbar)$  the original semiclassical result of Martens and Fang [123],

$$\frac{\partial \rho_{12}}{\partial t} = [H_0, \rho_{12}] - i\omega \rho_{12} \quad (4.20)$$

is recovered.

## 4.2.2 Thawed Gaussian Wigner Function Approach

With an equation of motion for the coherence Wigner function in hand, the form of its solution  $\rho_{12}(q, p, t)$  needs to be determined. Supposing a Thawed Gaussian ansatz for the coherence Wigner function,

$$\begin{aligned} \rho_{12}(q, p, t) = & \exp \left( -a(t) (q - Q(t))^2 - b(t) (p - P(t))^2 \right. \\ & \left. + c(t) (q - Q(t)) (p - P(t)) + u(t) (q - Q(t)) + v(t) (p - P(t)) + w(t) \right) \end{aligned} \quad (4.21)$$

One can derive equations of motion for parameters  $(a, b, c, Q, P, u, v, w)$  by substituting the ansatz into Wigner-Moyal equation and equating like powers in  $(q - Q(t))^n (p - P(t))^m$  (akin to the original Heller's original Thawed Gaussian wavepacket derivation). Substituting Eq. 4.21 into Eq. 4.19 and equating like powers gives

$$\boxed{(q - Q(t))^2} \quad \dot{a} = -cU_0'' + \frac{i}{2}\omega'' - \frac{i\hbar^2}{8}\omega''c^2 \quad (4.22)$$

$$\boxed{(p - P(t))^2} \quad \dot{b} = \frac{c}{m} - \frac{i\hbar^2}{8}\omega''b^2 \quad (4.23)$$

$$\boxed{(q - Q(t)) (p - P(t))} \quad \dot{c} = -2bU_0'' + \frac{2a}{m} - \frac{i\hbar}{2}\omega''bc \quad (4.24)$$

$$\boxed{(q - Q(t))} \quad 2a\dot{Q} - c\dot{P} + \dot{u} = cU_0'(Q) + v\dot{U}_0'' + \frac{2}{m}aP - i\omega'(Q) + \frac{i\hbar^2}{4}\omega''vc \quad (4.25)$$

$$\boxed{(p - P(t))} \quad 2b\dot{P} - c\dot{Q} + \dot{v} = -2bU_0'(Q) - \frac{1}{m}cP - \frac{1}{m}u - \frac{i\hbar^2}{2}\omega''vb \quad (4.26)$$

$$\boxed{1} \quad \dot{w} - u\dot{Q} - v\dot{P} = vU_0'(Q) - \frac{1}{m}uP - i\omega(Q) + \frac{i\hbar^2}{8}\omega''(v^2 - 2b) \quad (4.27)$$

Note because the potentials are quadratic, the second derivatives of  $\omega$  and  $U_0$  are constant and these eight equations can be rearranged into three separate sets. One for  $(a, b, c)$

$$\dot{a} = -cU_0'' + \frac{i}{2}\omega'' - \frac{i\hbar^2}{8}\omega''c^2 \quad (4.28)$$

$$\dot{b} = \frac{c}{m} - \frac{i\hbar^2}{8}\omega''b^2 \quad (4.29)$$

$$\dot{c} = -2bU_0'' + \frac{2a}{m} - \frac{i\hbar^2}{2}\omega''bc \quad (4.30)$$

one for  $(Q, P, u, v)$ ,

$$\dot{Q} = \frac{P}{m} \quad (4.31)$$

$$\dot{P} = -U_0'(Q) - \frac{i\hbar^2}{4}\omega''v \quad (4.32)$$

$$\dot{u} = -i\omega'(Q) + U_0''v \quad (4.33)$$

$$\dot{v} = -\frac{1}{m}u \quad (4.34)$$

and a single equation of motion for the phase,

$$\dot{w} = -i\omega(Q) - \frac{i\hbar^2}{8}\omega''v^2 - \frac{i\hbar^2}{4}\omega''b \quad (4.35)$$

Note  $(a, b, c, w) \in \mathbb{C}$ ,  $(Q, P) \in \mathbb{R}$ , and  $(u, v)$  are purely imaginary. It can be shown that  $(a, b, c)$  are not mutually independent, but instead related through a constant of motion

$$4ab - c^2 = \frac{4}{\hbar^2} \quad (4.36)$$

The set of differential equations  $(a, b, c)$  and phase  $w$  can be solved analytically or numerically. The set  $(Q, P, u, v)$  are a closed set of linear inhomogeneous differential equations. For

harmonic systems their analytic solutions are

$$Q(t) = \frac{1}{2} (Q_1(t) + Q_2(t)) \quad (4.37)$$

$$P(t) = \frac{1}{2} (P_1(t) + P_2(t)) \quad (4.38)$$

$$u(t) = \frac{i(P_1(t) - P_2(t))}{\hbar} \quad (4.39)$$

$$v(t) = \frac{-i(Q_1(t) - Q_2(t))}{\hbar} \quad (4.40)$$

with

$$Q_j(t) = Q_j^e + (Q_j(0) - Q_j^e) \cos(\Omega_j t) + \frac{P_j(0)}{m\Omega_j} \sin(\Omega_j t) \quad (4.41)$$

$$P_j(t) = P_j(0) \cos(\Omega_j t) - m\Omega_j (Q_j(0) - Q_j^e) \sin(\Omega_j t) \quad (4.42)$$

for states  $j = 1, 2$ . The average position  $Q$  and momentum  $P$  of the coherence Wigner function is thus an arithmetic average of each state's expectation for its canonical variables  $(Q_j, P_j)$ .

### 4.2.3 Thawed Gaussian Wavepacket Approach

Alternatively, the Wigner-Moyal equation can be solved in terms of the wavepacket's statistical parameters through the cross Wigner Transform

$$\rho_{12}(q, p, t) = \frac{1}{2\pi\hbar} \int dy \psi_1^* \left( q + \frac{y}{2}, t \right) \psi_2 \left( q - \frac{y}{2}, t \right) e^{-ipy/\hbar} \quad (4.43)$$

Integration yields the the same form for the coherence Wigner function as the Gaussian ansatz (Eq. 4.21) but in terms of wavepacket parameters,

$$a(t) = \frac{4\beta_1(t)\beta_2^*(t)}{\hbar(\beta_1(t) + \beta_2^*(t))} \quad (4.44)$$

$$b(t) = \frac{1}{\hbar(\beta_1(t) + \beta_2^*(t))} \quad (4.45)$$

$$c(t) = \frac{2i(\beta_1(t) - \beta_2^*(t))}{\hbar(\beta_1(t) + \beta_2^*(t))} \quad (4.46)$$

$$Q(t) = \frac{1}{2}(Q_1(t) + Q_2(t)) \quad (4.47)$$

$$P(t) = \frac{1}{2}(P_1(t) + P_2(t)) \quad (4.48)$$

$$u(t) = \frac{i(P_1(t) - P_2(t))}{\hbar} \quad (4.49)$$

$$v(t) = \frac{-i(Q_1(t) - Q_2(t))}{\hbar} \quad (4.50)$$

$$w(t) = \frac{i(\gamma_1 - \gamma_2^*)}{\hbar} - \frac{i}{\hbar} \left( \frac{P_1 + P_2}{2} \right) (Q_1 - Q_2) - \ln \left( \frac{\beta_1 + \beta_2^*}{\beta_1(0) + \beta_2(0)} \right) \quad (4.51)$$

The equations of motion for these eight parameters are in turn solved by solving the Thawed Gaussian wavepacket equations (Eqs. 4.6-4.9) for states  $j = 1, 2$ . For harmonic potentials  $(Q_j, P_j)$  are the same for those obtained by Thawed Moyal approach (Eqs. 4.41-4.42). For the widths, one obtains

$$\beta_j(t) = \frac{m\Omega_j}{2} \left( \frac{\beta_j(0)\cos(\Omega_j t) + \frac{im\Omega_j}{2}\sin(\Omega_j t)}{\frac{m\Omega_j}{2}\cos(\Omega_j t) + i\beta_j(0)\sin(\Omega_j t)} \right) \quad (4.52)$$

and for the phases

$$\begin{aligned} \gamma_j(t) = & P_j(0) (Q_j^e - Q_j(0)) \sin^2(\Omega_j t) + E_j t + \frac{\hbar}{2} \tan^{-1} \left( \frac{m\Omega_j \cot(\Omega_j t)}{2\beta_j(0)} \right) \\ & + \frac{i\hbar}{4} (\ln(2) + 2\ln(\Omega_j m) - \ln(4\beta_j^2(0) + m^2\Omega_j^2 + (m^2\Omega_j^2 - 4\beta_j^2(0)) \cos(2\Omega_j t))) \\ & - \frac{\pi\hbar}{4} \text{sign}(\beta_j(0)) + \frac{(P_j(0) + m(Q_j(0) - Q_j^e)\Omega_j)(P_j(0) + m(Q_j^e - Q_j(0))\Omega_j) \sin(2\Omega_j t)}{4m\Omega_j} \end{aligned} \quad (4.53)$$



## 4.2.4 Approximations to Thawed Moyal Dynamics

Within exact Thawed Moyal solutions, there are two obvious approximations to simplify dynamics: (1) truncation and (2) linearization. Truncating to  $\mathcal{O}(\hbar)$  reduces the exact Wigner Moyal equation (Eq. 4.19) to the semiclassical form (Eq. 4.20), removing  $\hbar^2$  terms from the equations of motion for  $(a, b, c, Q, P, u, v, w)$  in  $\rho_{12}$ .

Alternatively, the difference potential  $\omega$  can be linearized by expanding about its local minima  $Q_{min}$ ,

$$\omega(Q) \approx \omega(Q_{min}) + \omega'(Q_{min})(Q - Q_{min}). \quad (4.54)$$

This cancels  $\omega''$  terms from the Thawed Moyal equations of motion for the parameters. Together these two approximations suggest four levels of dynamics: exact quantum treatment or Moyal (no truncation nor linearization), Linearized Moyal (linearization, but no truncation), Semiclassical (truncation, but no linearization), and Linearized Semiclassical (truncation and linearization).

### Truncation: Semiclassical Dynamics

Substituting the thawed Gaussian Wigner function Eq. 4.21 into the truncated Wigner-Moyal equation Eq. 4.20 and equating like-powers gives

$$\dot{a} = -cU_0'' + \frac{i}{2}\omega'' \quad (4.55)$$

$$\dot{b} = \frac{c}{m} \quad (4.56)$$

$$\dot{c} = -2bU_0'' + \frac{2a}{m} \quad (4.57)$$

$$\dot{Q} = \frac{P}{m} \quad (4.58)$$

$$\dot{P} = -U'_0(Q) \quad (4.59)$$

$$\dot{u} = -i\omega'(Q) + U''_0 v \quad (4.60)$$

$$\dot{v} = -\frac{1}{m}u \quad (4.61)$$

$$\dot{w} = -i\omega(Q) \quad (4.62)$$

Unlike the Moyal case, the equation of motion for  $P$  lacks dependence on  $v$  and  $(Q, P)$  separates from  $(u, v)$ . To solve the former, rewrite the average potential as

$$\begin{aligned} U_0(Q) &= \frac{1}{2}U_1(Q) + U_2(Q) \\ &= \frac{1}{2}m (\Omega_1^2 (Q - Q_1^e)^2 + \Omega_2^2 (Q - Q_2^e)^2) + \frac{1}{2} (E_1 + E_2) \\ &= \frac{1}{2}m\Omega_0^2 (Q - Q_0)^2 + E_0 \end{aligned} \quad (4.63)$$

with and average frequency,

$$\Omega_0 = \sqrt{\frac{\Omega_1^2 + \Omega_2^2}{2}} \quad (4.64)$$

and the average equilibrium and energy datum

$$Q_0 = \frac{\Omega_1^2 Q_1^e + \Omega_2^2 Q_2^e}{\Omega_1^2 + \Omega_2^2} \quad (4.65)$$

$$E_0 = \frac{1}{4}m \left( \frac{\Omega_1^2 \Omega_2^2}{\Omega_1^2 + \Omega_2^2} \right) (Q_1^e - Q_2^e)^2 + \frac{1}{2} (E_1 + E_2) \quad (4.66)$$

Because  $U'_0(Q) = U'_0(Q_0) + U''_0(Q - Q_0) = m\Omega_0^2 (Q - Q_0)$  and defining  $R = Q - Q_0$ , the canonical equations for the expectations become

$$\dot{R} = \frac{P}{m} \quad (4.67)$$

$$\dot{P} = -m\Omega_0^2 R \quad (4.68)$$

which describes motion of  $(R, P)$  with the average frequency  $\Omega_0$ . For the average potential, their solutions in terms of  $(Q, P)$  are

$$Q(t) = Q_0 + (Q(0) - Q_0) \cos(\Omega_0 t) + \frac{P(0)}{m\Omega_0} \sin(\Omega_0 t) \quad (4.69)$$

$$P(t) = P(0) \cos(\Omega_0 t) - m\Omega_0 (Q(0) - Q_0) \sin(\Omega_0 t) \quad (4.70)$$

Inspecting Eqs. 4.58-4.61, note  $(u, v)$  are not independent of  $(Q, P)$ , where the latter is an external perturbation acting on the former. Letting  $\omega'(Q) = \omega'(Q_0) + \omega''(Q(0) - Q_0)$  gives

$$\dot{u} = -i(\omega'(Q_0) + \omega''(Q(t) - Q_0)) + m\Omega_0^2 v \quad (4.71)$$

$$\dot{v} = -\frac{1}{m} u \quad (4.72)$$

then differentiating  $\dot{u}$  again yields

$$\ddot{u} + \Omega_0^2 u = -i\omega''\dot{Q}(t) \quad (4.73)$$

Assuming initial conditions  $R(0) = Q(0) - Q_0$  and  $P(0) = 0$ , Eq. 4.73 becomes

$$\ddot{u} + \Omega_0^2 u = i\omega''\Omega_0 R(0) \sin(\Omega_0 t) \quad (4.74)$$

This is the equation of motion for a resonantly driven harmonic oscillator subject to a sinusoidal forcing with frequency  $\Omega_0$ . For initial conditions  $u(0) = 0$  and  $v(0) = 0$  gives a solution,

$$u(t) = \frac{i\omega''R(0)}{4\Omega_0} (\sin(\Omega_0 t) - 2\Omega_0 t \cos(\Omega_0 t)) \quad (4.75)$$

$$v(t) = \frac{i\omega''R(0)}{4m\Omega_0^2} (3\cos(\Omega_0 t) - 3 + 2\Omega_0 t \sin(\Omega_0 t)) \quad (4.76)$$

Note the presence of terms linear in  $t$ , leads to secular growth of  $(u, v)$ . And finally the

semiclassical phase is given by

$$w(t) = w(0) - i \int_0^t ds \omega(Q(s)) \quad (4.77)$$

which for harmonic systems can be integrated analytically.

## Linearization

In all the Thawed Moyal equations of motion for the statistical parameters, truncated or not,  $\hbar^2$  terms appear with  $\omega''$  in all, but one equation of motion, namely  $a$ . Superficially it would appear the effect of linearization is not very different from truncation or semiclassical. Nonetheless linearization produces very different coherence dynamics for the semiclassical theory by removing the secular terms in  $u$  and  $v$ . Upon linearization the semiclassical equations become

$$\dot{a} = -cU_0''(Q) \quad (4.78)$$

$$\dot{b} = \frac{c}{m} \quad (4.79)$$

$$\dot{c} = -2bU_0''(Q) + \frac{2a}{m} \quad (4.80)$$

and  $(Q, P, u, v)$ ,

$$\dot{Q} = \frac{P}{m} \quad (4.81)$$

$$\dot{P} = -U_0'(Q) \quad (4.82)$$

$$\dot{u} = -i\omega'(Q) + U_0''v \quad (4.83)$$

$$\dot{v} = -\frac{1}{m}u \quad (4.84)$$

and  $w$ ,

$$\dot{w} = -i\omega(Q) \quad (4.85)$$

## 4.3 Results

There are three domains the coherence dynamics of the Thawed Moyal solutions can be viewed in: (1) in phase space as a phase portrait  $\text{Re}[\rho_{12}(q, p, t)]$ , (2) in time as a correlation function of the coherence,

$$\text{Tr}(\rho_{12}) = \int \int dqdp \rho_{12}(q, p, t) = \langle \Psi(0) | \Psi(t) \rangle$$

and (3) in frequency as the linear absorption spectrum

$$\sigma_{12}(\Omega) = \mu^2 \int dt \text{Re}[c_{12}(t)] e^{-i\Omega t}.$$

Phase portraits offer insight into the kinematics of the coherence and while the time correlation function and absorption spectrum are Fourier pairs containing the same information. Both are reported for illustration with  $\mu = 1$ .

### 4.3.1 Thawed Moyal Solution to 1-D Displaced Oscillator

Using the the four levels of theory: Moyal, Linearized Moyal, Semiclassical, and Linearized Semiclassical, the Thawed Moyal Dynamics equations of motion are solved for a 1-D displaced oscillator with system parameters (Telluride I) and initialization (Initialization I) tabulated in Tab. 4.1 and Tab. 4.2.

Telluride I.	
$m$	2000
$\hbar$	1
$\Omega_1$	0.01
$\Omega_2$	0.004
$Q_1^e$	0
$Q_2^e$	1
$E_1$	0
$E_2$	0.1

Table 4.1: System Parameters (Telluride I) for displaced oscillator model in atomic units.

Initialization I.	
$Q_1(0)$	$Q_1^e$
$Q_2(0)$	$Q_1^e$
$P_1(0)$	0
$P_2(0)$	0
$a(0)$	$m\Omega_1/\hbar$
$b(0)$	$1/m\Omega_1\hbar$
$c(0)$	0

Table 4.2: Initialization parameters for displaced oscillator model in atomic units.

## Moyal (Exact Quantum)

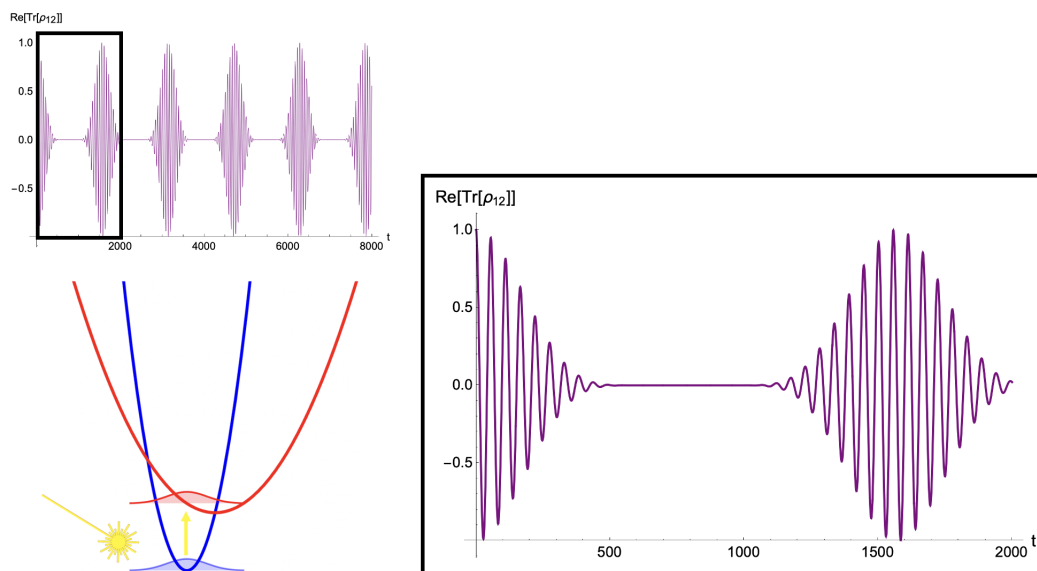


Figure 4.2: Coherence correlation function for Telluride I (Initialization I) calculated by Thawed Moyal Dynamics (Moyal).

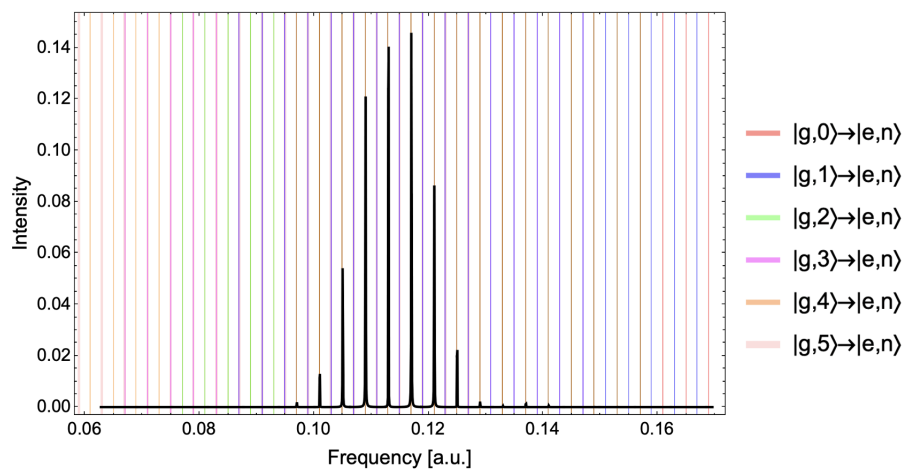


Figure 4.3: Linear absorption spectrum for Telluride I (Initialization I) calculated by Thawed Moyal Dynamics (Moyal).

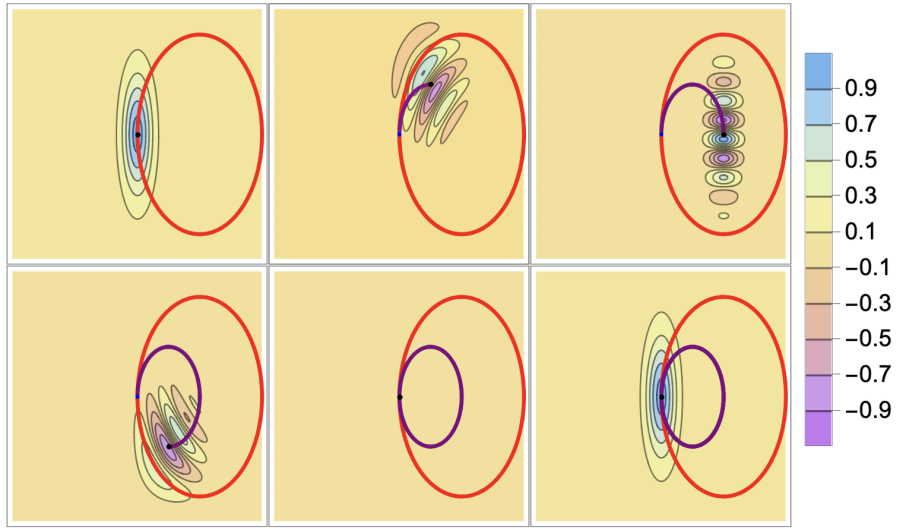


Figure 4.4: Phase space portraits for  $\text{Re}(\rho_{12}(q, p, t))$  for Telluride I (Initialization I) calculated by Thawed Moyal Dynamics (Moyal). Time increasing left-to-right, top-to-bottom ( $t = 0, t = \tau_M/4, t = \tau_M/2, t = 3\tau_M/4, t = \tau_M, t = 4\tau_M$ ) for vibrational period  $\tau_M$ . Ground state orbit:  $(Q_1(t), P_1(t))$  (blue). Excited state orbit:  $(Q_2(t), P_2(t))$  (red). Coherence orbit:  $(Q(t), P(t))$  (purple). Coherence mean (black).



## Linearized Moyal

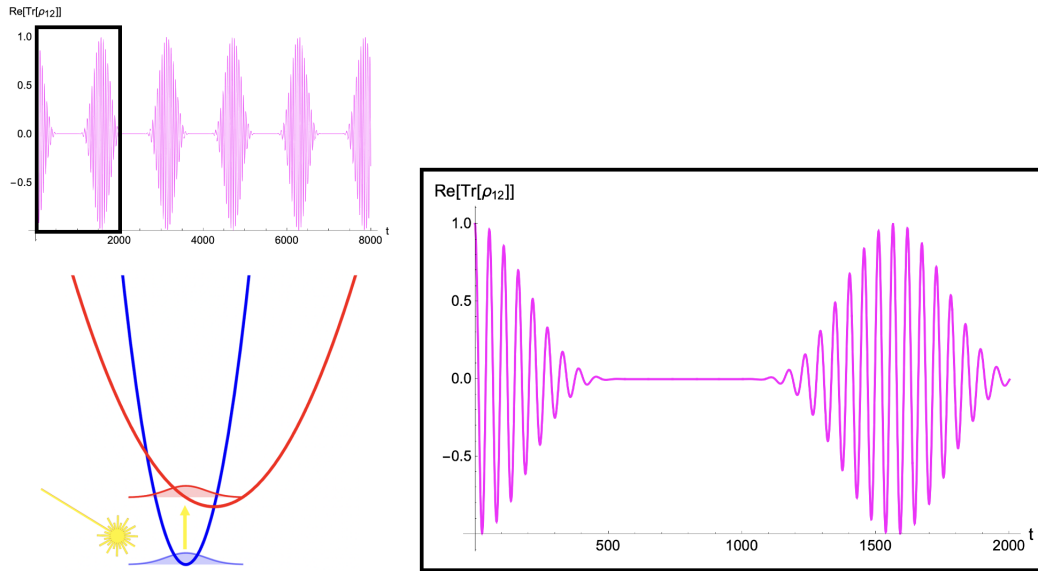


Figure 4.5: Coherence correlation function for Telluride I (Initialization I) calculated by Thawed Moyal Dynamics (Linearized Moyal).

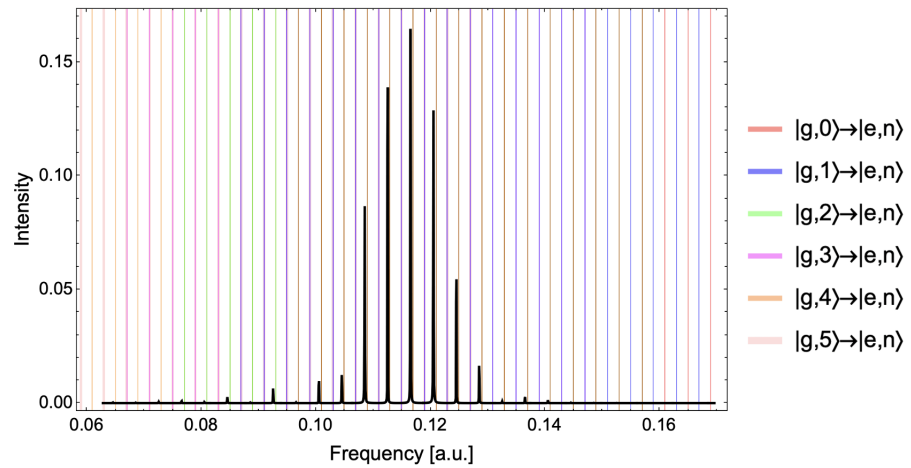


Figure 4.6: Linear absorption spectrum for Telluride I (Initialization I) calculated by Thawed Moyal Dynamics (Linearized Moyal).

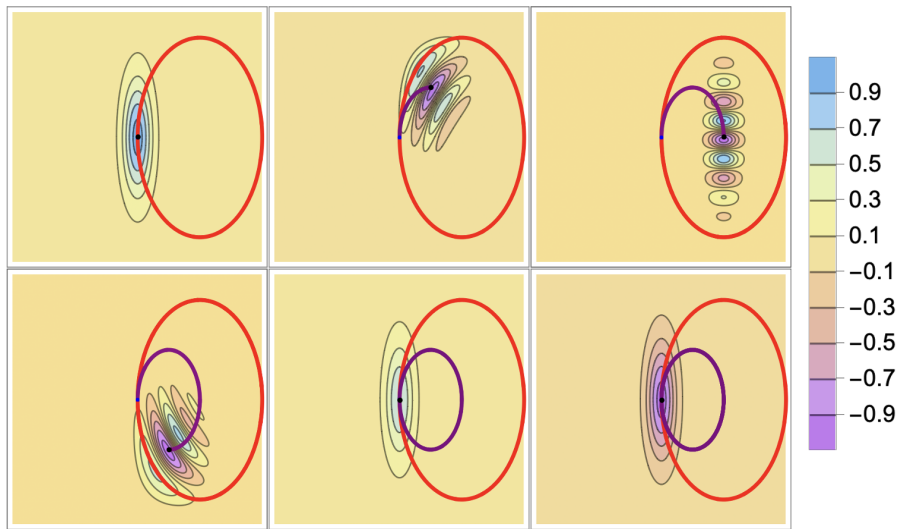


Figure 4.7: Phase space portraits for  $\text{Re}(\rho_{12}(q, p, t))$  for Telluride I (Initialization I) calculated by Thawed Moyal Dynamics (Linearized Moyal). Time increasing left-to-right, top-to-bottom ( $t = 0, t = \tau_M/4, t = \tau_M/2, t = 3\tau_M/4, t = \tau_M, t = 4\tau_M$ ) for vibrational period  $\tau_M$ . Ground state orbit:  $(Q_1(t), P_1(t))$  (blue). Excited state orbit:  $(Q_2(t), P_2(t))$  (red). Coherence orbit:  $(Q(t), P(t))$  (purple). Coherence mean (black).

## Semiclassical

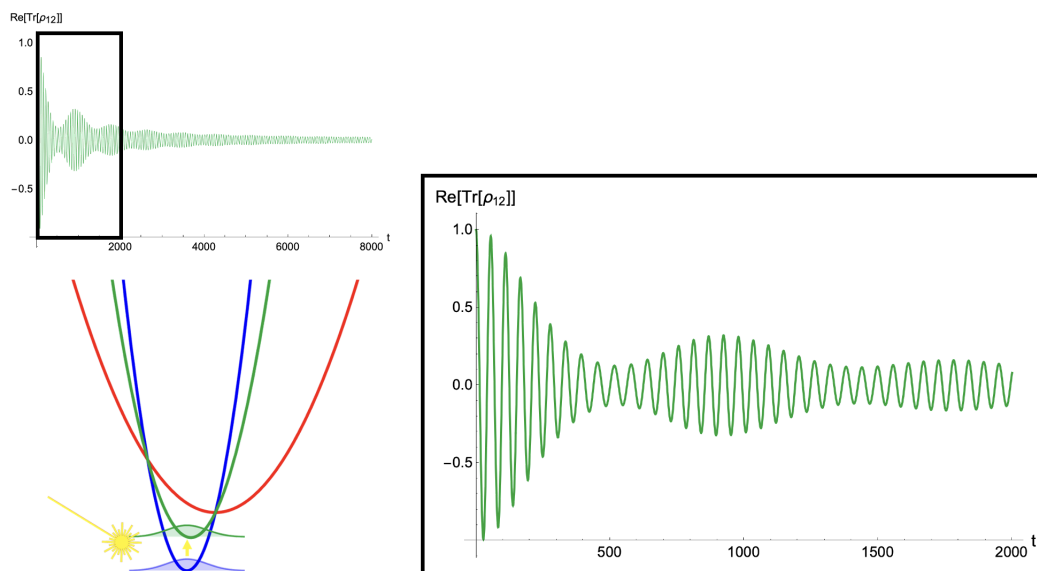


Figure 4.8: Coherence correlation function for Telluride I (Initialization I) calculated by Thawed Moyal Dynamics (Semiclassical).

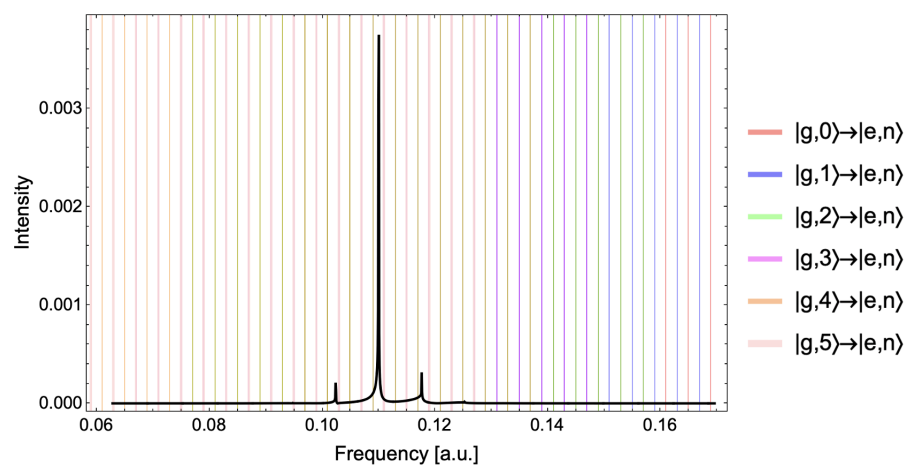


Figure 4.9: Linear absorption spectrum for Telluride I (Initialization I) calculated by Thawed Moyal Dynamics (Semiclassical).

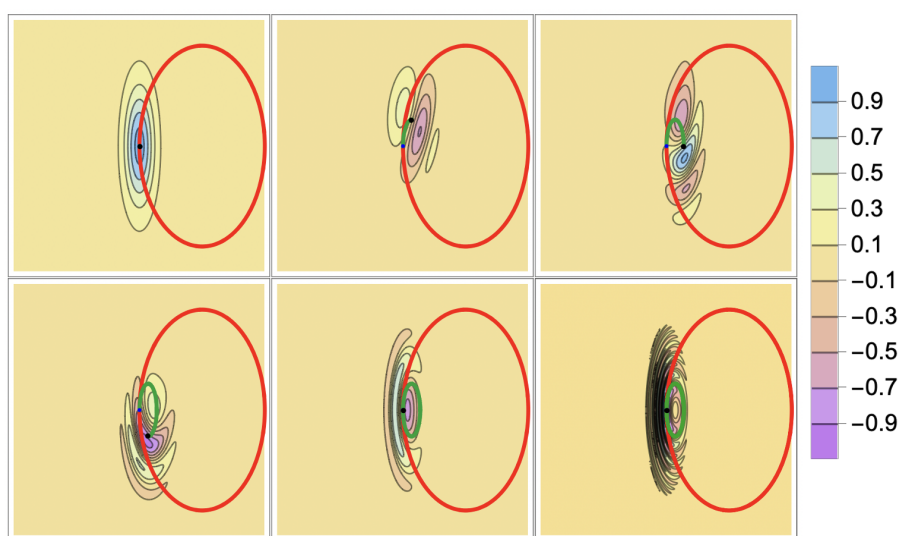


Figure 4.10: Phase space portraits for  $\text{Re}(\rho_{12}(q, p, t))$  for Telluride I (Initialization I) calculated by Thawed Moyal Dynamics (Semiclassical). Time increasing left-to-right, top-to-bottom ( $t = 0, t = \tau_{SC}/4, t = \tau_{SC}/2, t = 3\tau_M/4, t = \tau_{SC}, t = 4\tau_{SC}$ ) for vibrational period  $\tau_{SC}$ . Ground state orbit:  $(Q_1(t), P_1(t))$  (blue). Excited state orbit:  $(Q_2(t), P_2(t))$  (red). Coherence orbit:  $(Q(t), P(t))$  (green). Coherence mean (black).

## Linearized Semiclassical

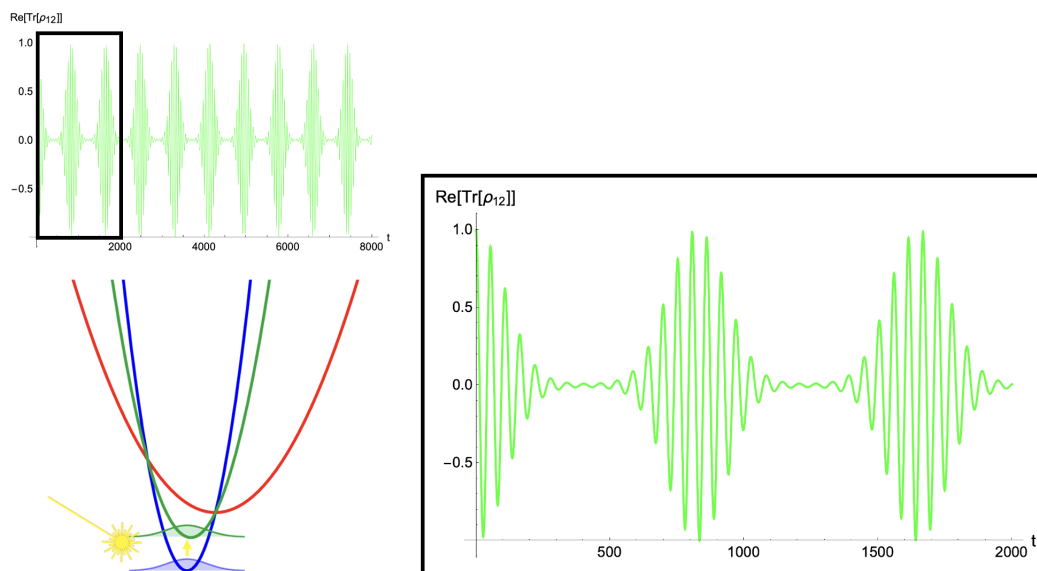


Figure 4.11: Coherence correlation function for Telluride I (Initialization I) calculated by Thawed Moyal Dynamics (Linearized Semiclassical).

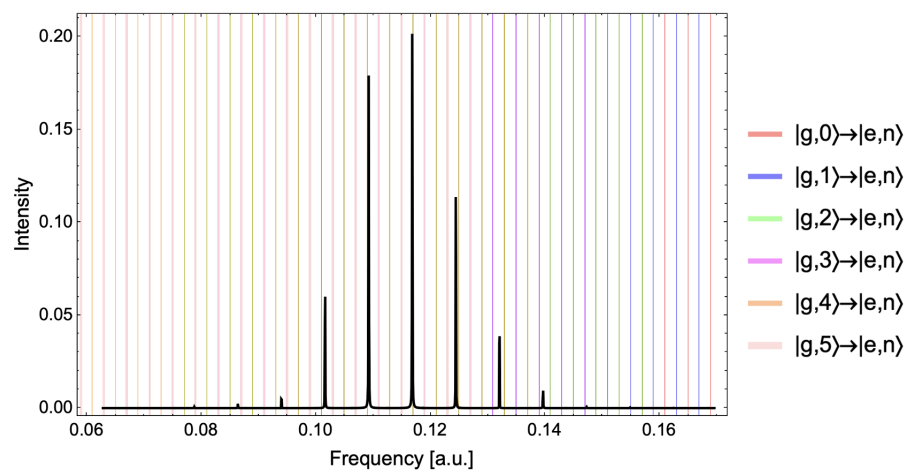


Figure 4.12: Linear absorption spectrum for Telluride I (Initialization I) calculated by Thawed Moyal Dynamics (Linearized Semiclassical).

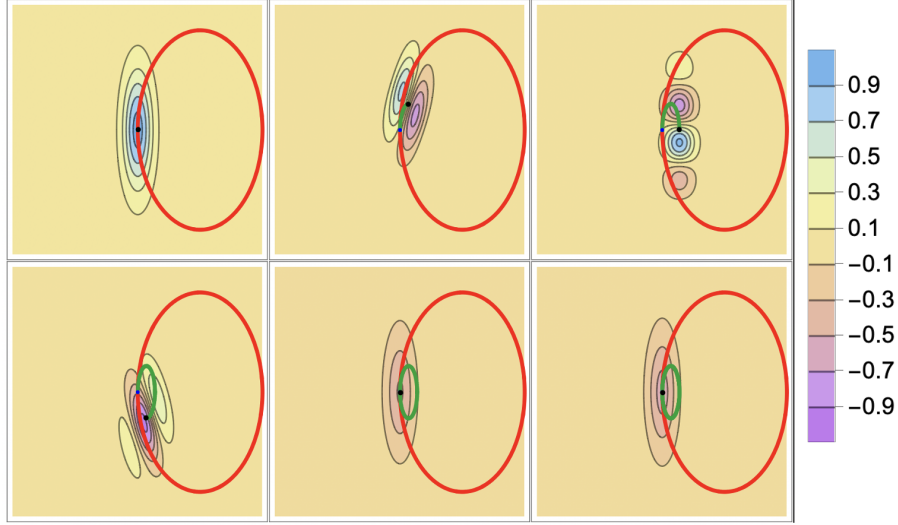


Figure 4.13: Phase space portraits for  $\text{Re}(\rho_{12}(q, p, t))$  for Telluride I (Initialization I) calculated by Thawed Moyal Dynamics (Linearized Semiclassical). Time increasing left-to-right, top-to-bottom ( $t = 0, t = \tau_{SC}/4, t = \tau_{SC}/2, t = 3\tau_M/4, t = \tau_{SC}, t = 4\tau_{SC}$ ) for vibrational period  $\tau_{SC}$ . Ground state orbit:  $(Q_1(t), P_1(t))$  (blue). Excited state orbit:  $(Q_2(t), P_2(t))$  (red). Coherence orbit:  $(Q(t), P(t))$  (green). Coherence mean (black).

### 4.3.2 Comparison with Trajectory Ensemble Solution

The traditional way the semiclassical Liouville equation for the coherence (Eq. 4.20) is solved is by using an ensemble of classical trajectories weighted by some phase factor. This phase factor imparts order  $\mathcal{O}(\hbar)$  interference effects [144, 145]. The solution calculated in this way is

$$\rho_{12}(q, p, t) = \frac{1}{\mathcal{N}} \sum_{n=1}^{\mathcal{N}} e^{-i\phi_n(t)} \delta(q - q_n(t)) \delta(p - p_n(t)) \quad (4.86)$$

where  $\mathcal{N}$  is the number of trajectories in the ensemble. The each  $n$  trajectory is given by integrating Hamilton's equations,

$$\dot{q}_n(t) = \left( \frac{\partial H_0}{\partial p_n} \right) \quad (4.87)$$

$$\dot{p}_n(t) = \left( \frac{-\partial H_0}{\partial q_n} \right) \quad (4.88)$$

under the average Hamiltonian of the two states  $H_0 = (H_1 + H_2)/2$  weighted by a phase factor

$$\phi_n(t) = \int_0^t ds \omega(q_n(s)) \quad (4.89)$$

where  $\omega$  is the difference potential. The Linearized Semiclassical trajectory ensemble solution uses the linearized difference potential

$$\omega(Q) \approx \omega(Q_0) + \omega'(Q_0)(Q - Q_0) \quad (4.90)$$

in Eq. 4.89.

To compare the Thawed Moyal Dynamics solution with trajectory ensemble solution for the Semiclassical and Linearized Semiclassical theories, the trajectory ensembles initial conditions corresponding to Telluride I (Initialization I) were generated from a Gaussian distribution of

$$g(q, p) = \exp \left( \frac{1}{\sqrt{a(0)}} (q - Q_1^e) + \frac{1}{\sqrt{a(0)}} (p - 0) \right) \quad (4.91)$$

The coherence correlation function were calculated by

$$\text{Re}[c_{12}(t)] = \text{Re}[\text{Tr}(\rho_{12}(q, p, t))] = \frac{1}{\mathcal{N}} \sum_{n=1}^{\mathcal{N}} \text{Re}[e^{-i\theta_n(t)}] = \frac{1}{\mathcal{N}} \sum_{n=1}^{\mathcal{N}} \cos(\theta_n), \quad (4.92)$$

this, its resulting linear absorption spectrum, and phase portraits are shown below.

## Semiclassical

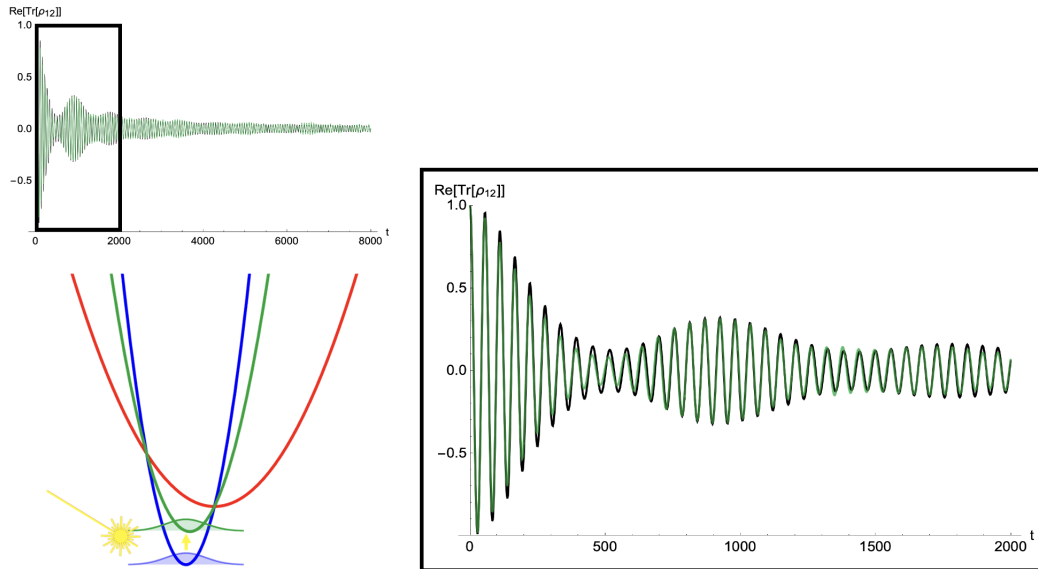


Figure 4.14: Coherence correlation function for Telluride I (Initialization I) calculated by Semiclassical Thawed Moyal Dynamics (black) compared with Semiclassical trajectory ensemble (green) for  $\mathcal{N} = 1000$ .

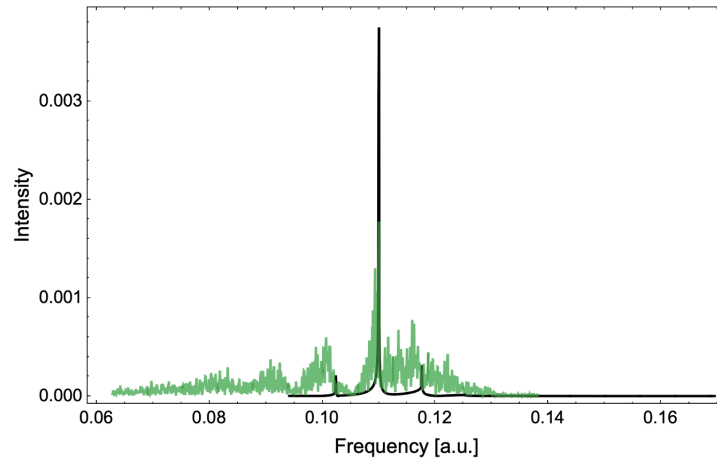


Figure 4.15: Linear absorption spectrum for Telluride I (Initialization I) calculated by Semiclassical Thawed Moyal Dynamics (black) compared with Semiclassical trajectory ensemble (green) for  $\mathcal{N} = 1000$ .



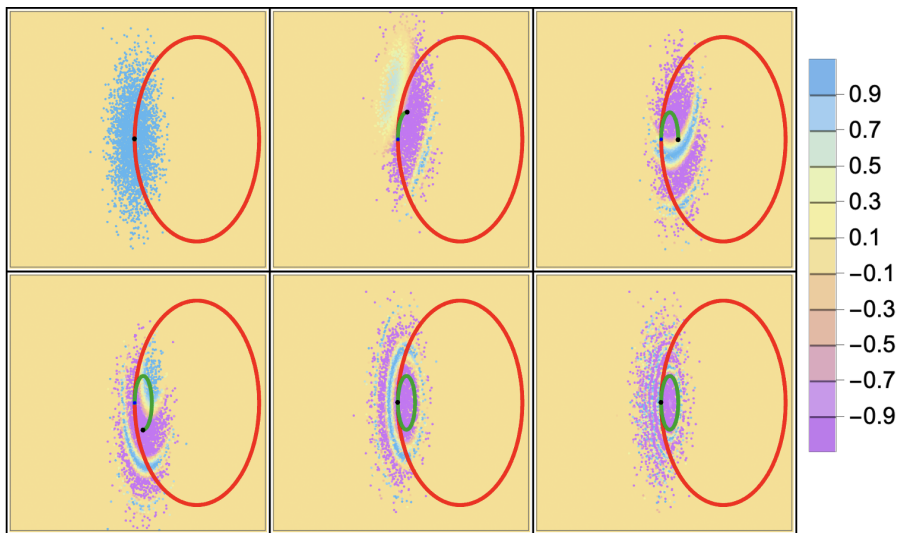


Figure 4.16: Phase space portraits for  $\text{Re}(\rho_{12}(q, p, t))$  for Telluride I (Initialization I) calculated by Semiclassical Thawed Moyal Dynamics (black) compared with Semiclassical trajectory ensemble (green) for  $\mathcal{N} = 2500$ . Time increasing left-to-right, top-to-bottom ( $t = 0$ ,  $t = \tau_{SC}/4$ ,  $t = \tau_{SC}/2$ ,  $t = 3\tau_M/4$ ,  $t = \tau_{SC}$ ,  $t = 4\tau_{SC}$ ) for vibrational period  $\tau_{SC}$ . Ground state orbit:  $(Q_1(t), P_1(t))$  (blue). Excited state orbit:  $(Q_2(t), P_2(t))$  (red). Coherence orbit:  $(Q(t), P(t))$  (green). Coherence mean (black).

## Linearized Semiclassical

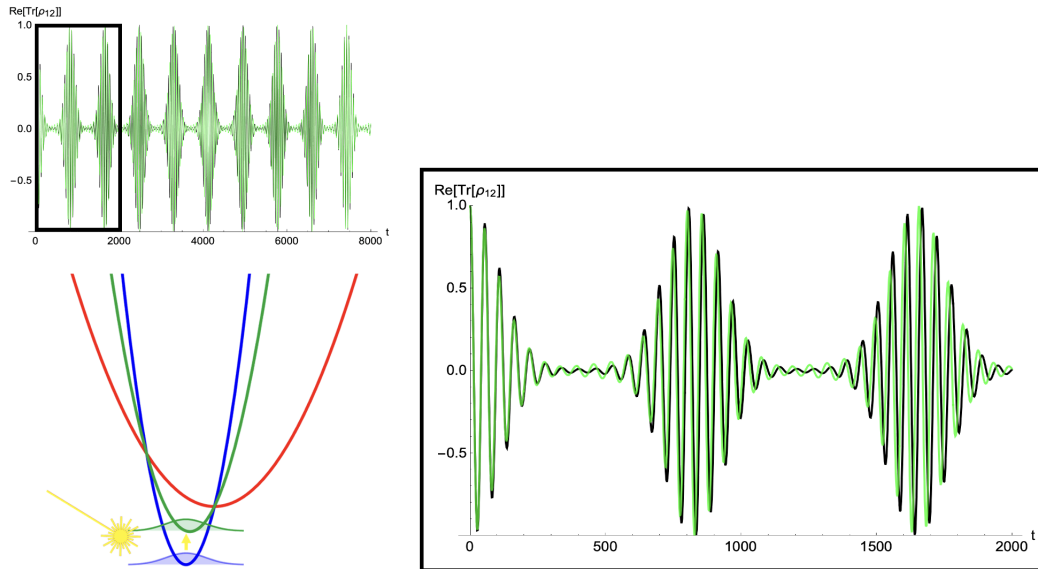


Figure 4.17: Coherence correlation function for Telluride I (Initialization I) calculated by Linearized Semiclassical Thawed Moyal Dynamics (black) compared with Linearized Semiclassical trajectory ensemble (light green) for  $\mathcal{N} = 1000$ .

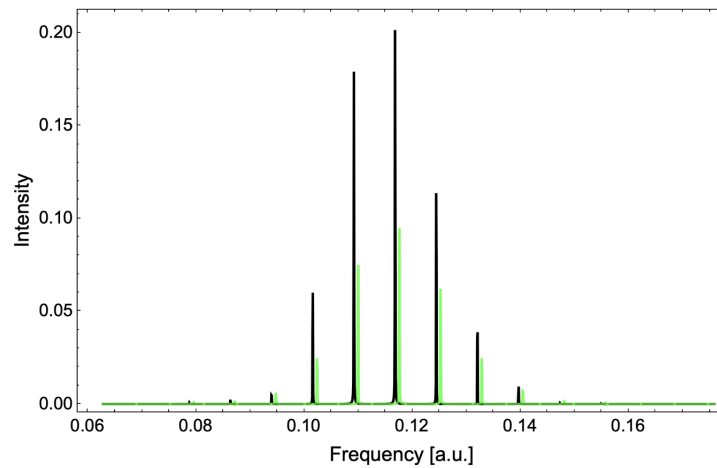


Figure 4.18: Linear absorption spectrum for Telluride I (Initialization I) calculated by Linearized Semiclassical Thawed Moyal Dynamics (black) compared with Linearized Semiclassical trajectory ensemble (light green) for  $\mathcal{N} = 1000$ .

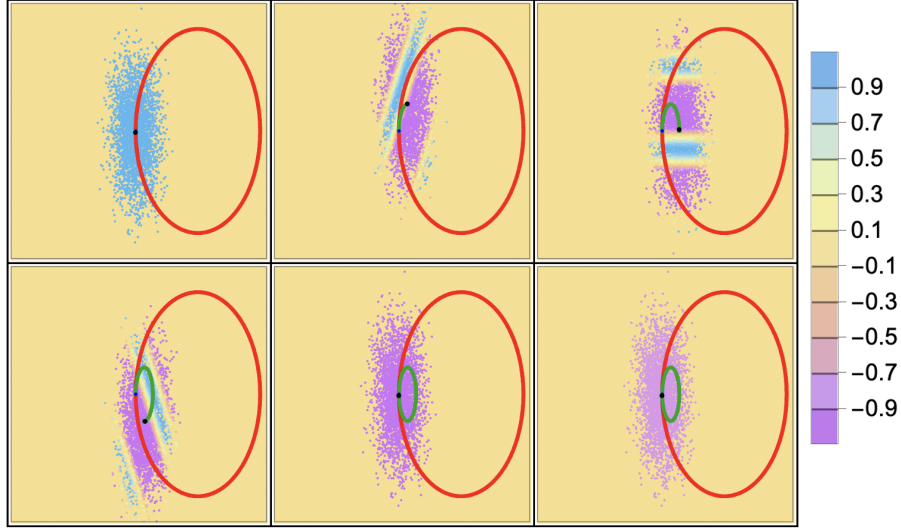


Figure 4.19: Phase space portraits for  $\text{Re}(\rho_{12}(q, p, t))$  for Telluride I (Initialization I) calculated by Linearized Semiclassical Thawed Moyal Dynamics (black) compared with Linearized Semiclassical trajectory ensemble (green) for  $\mathcal{N} = 2500$ . Time increasing left-to-right, top-to-bottom ( $t = 0, t = \tau_{SC}/4, t = \tau_{SC}/2, t = 3\tau_M/4, t = \tau_{SC}, t = 4\tau_{SC}$ ) for vibrational period  $\tau_{SC}$ . Ground state orbit:  $(Q_1(t), P_1(t))$  (blue). Excited state orbit:  $(Q_2(t), P_2(t))$  (red). Coherence orbit:  $(Q(t), P(t))$  (light green). Coherence mean (black).

### 4.3.3 Equal Frequency Case and Hot Bands

#### Symmetric Frequency 1-D

Analytic solutions to the displaced oscillator model typically assume the case of equal frequencies  $\Omega_1 = \Omega_2$ . This case happens to be the only case where the semiclassical solution matches the exact quantum solution. The solutions for Thawed Moyal and Linearized Semiclassical theories are illustrated below for this case with their system and initialization parameters given in Tab. 4.3 and Tab. 4.2.

Telluride I-S.	
$m$	2000
$\hbar$	1
$\Omega_1$	0.01
$\Omega_2$	0.01
$Q_1^e$	0
$Q_2^e$	1
$E_1$	0
$E_2$	0.1

Table 4.3: System Parameters (Telluride I-S) for displaced oscillator model in atomic units.

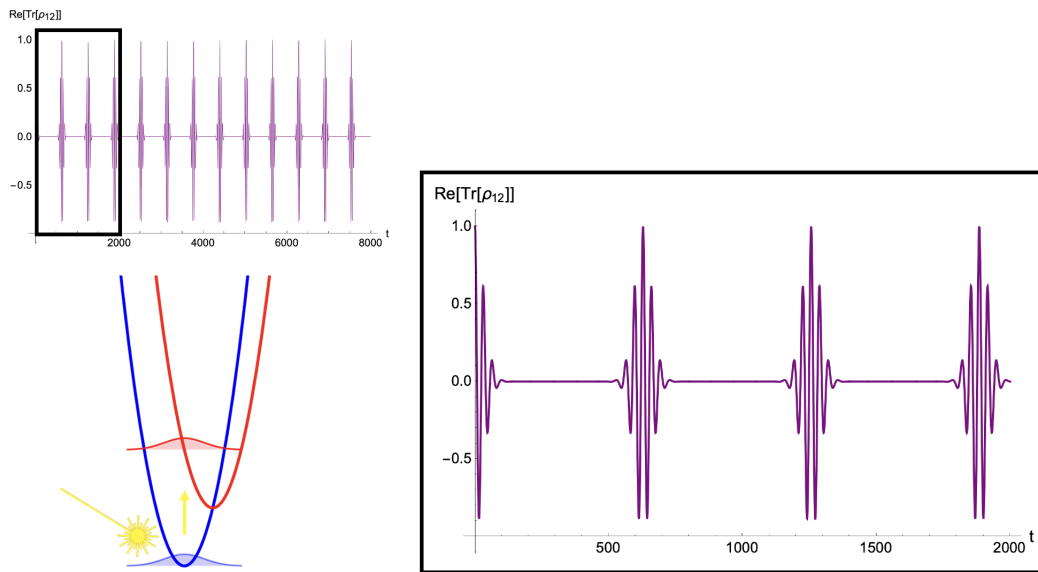


Figure 4.20: Coherence correlation function for Telluride I-S (Initialization I) calculated by Thawed Moyal Dynamics (Moyal).

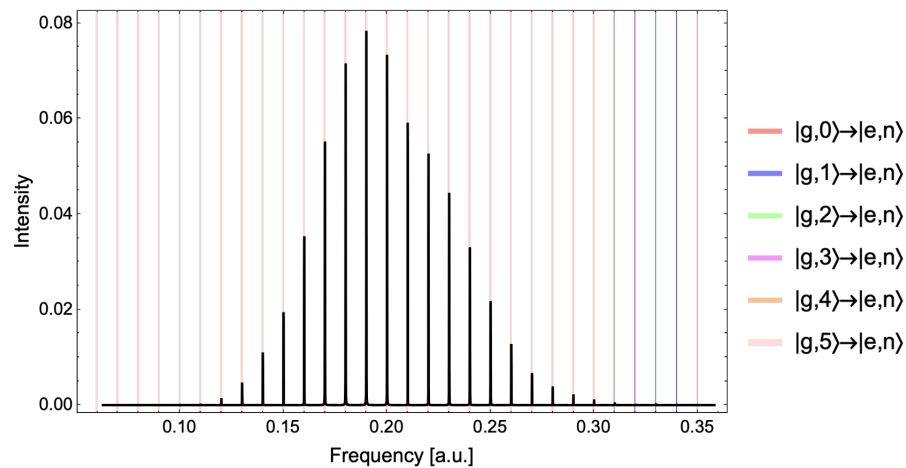


Figure 4.21: Linear absorption spectrum for Telluride I-S (Initialization I) calculated by Thawed Moyal Dynamics (Moyal).

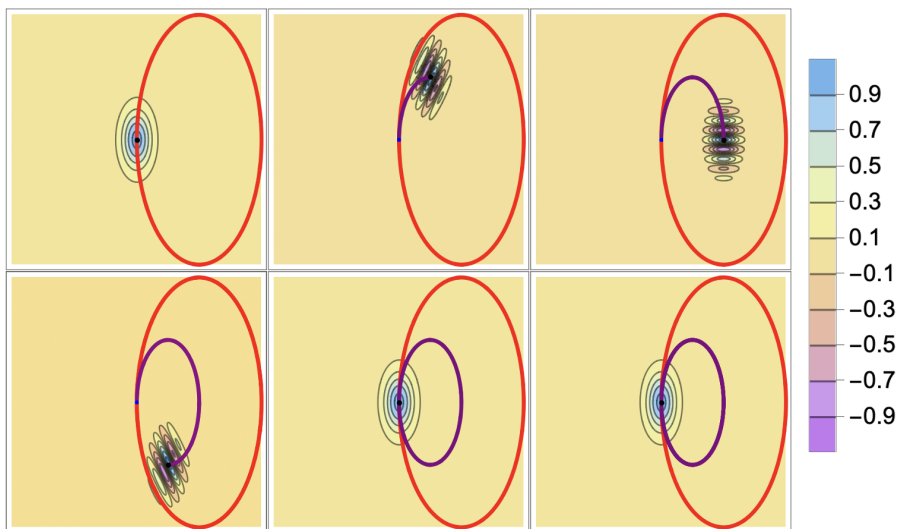


Figure 4.22: Phase space portraits for  $\text{Re}(\rho_{12}(q, p, t))$  for Telluride I-S (Initialization I) calculated by Thawed Moyal Dynamics (Moyal). Time increasing left-to-right, top-to-bottom ( $t = 0, t = \tau_M/4, t = \tau_M/2, t = 3\tau_M/4, t = \tau_M, t = 4\tau_M$ ) for vibrational period  $\tau_M$ . Ground state orbit:  $(Q_1(t), P_1(t))$  (blue). Excited state orbit:  $(Q_2(t), P_2(t))$  (red). Coherence orbit:  $(Q(t), P(t))$  (purple). Coherence mean (black).

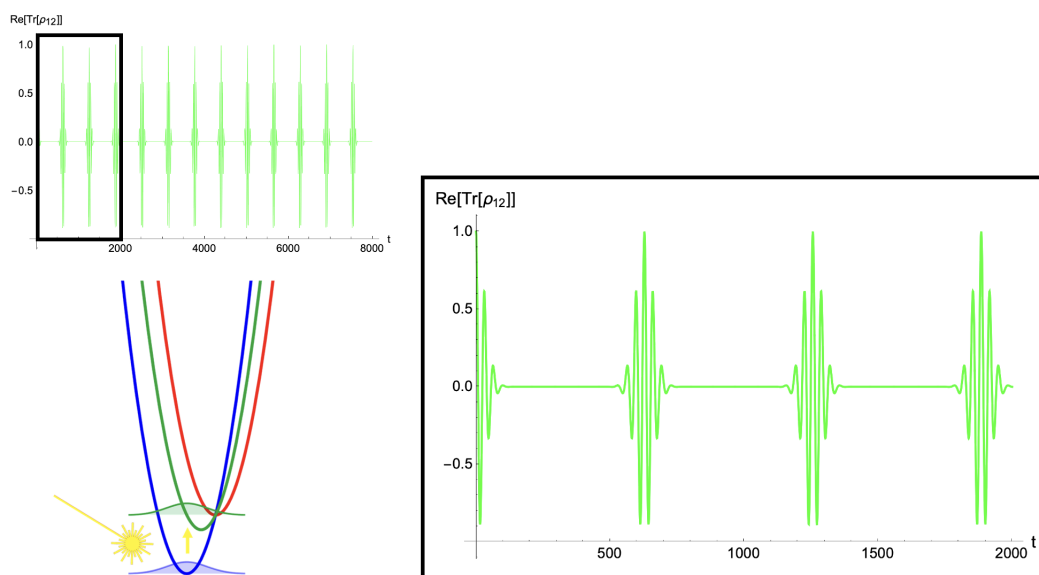


Figure 4.23: Coherence correlation function for Telluride I-S (Initialization I) calculated by Thawed Moyal Dynamics (Linearized Semiclassical).

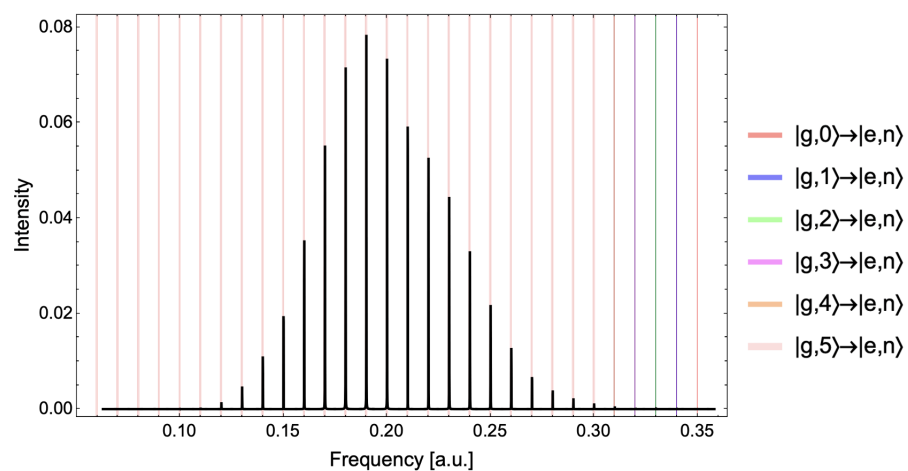


Figure 4.24: Linear absorption spectrum for Telluride I-S (Initialization I) calculated by Thawed Moyal Dynamics (Linearized Semiclassical).

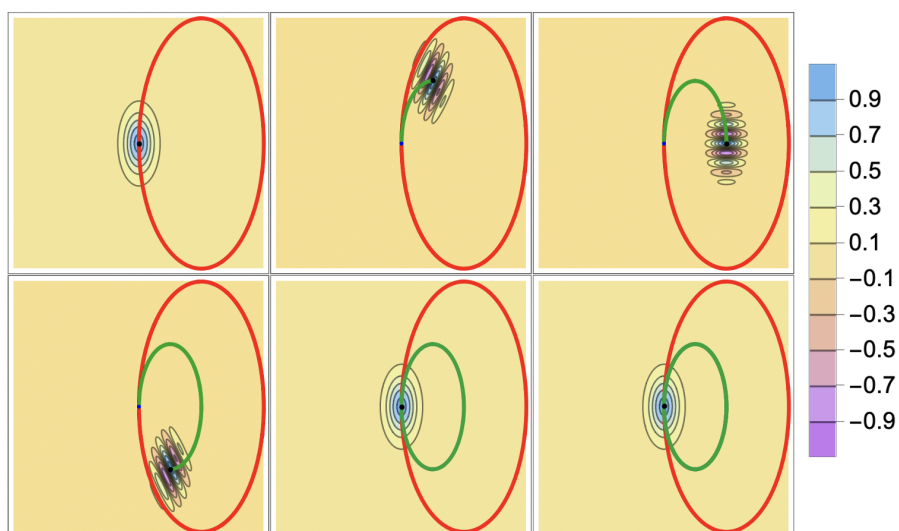


Figure 4.25: Phase space portraits for  $\text{Re}(\rho_{12}(q, p, t))$  for Telluride I-S (Initialization I) calculated by Thawed Moyal Dynamics (Linearized Semiclassical). Time increasing left-to-right, top-to-bottom ( $t = 0, t = \tau_{SC}/4, t = \tau_{SC}/2, t = 3\tau_M/4, t = \tau_{SC}, t = 4\tau_{SC}$ ) for vibrational period  $\tau_{SC}$ . Ground state orbit:  $(Q_1(t), P_1(t))$  (blue). Excited state orbit:  $(Q_2(t), P_2(t))$  (red). Coherence orbit:  $(Q(t), P(t))$  (green). Coherence mean (black).

## Hot Bands

Hot bands are spectral lines that arise due to transitions involving populated excited vibrational states due to finite thermal energy  $kT$ . Although the Thawed Moyal equations do not include temperature and simulates coherence dynamics for a pure quantum density, the model captures “hot bands” lines resulting from initialization out of mechanical equilibrium position of the ground state potential  $Q_0 \neq Q_1^e$ . Initialized outside the ground state minimum  $Q_1^e$ , the ground state wavepacket will contain higher vibrational states and the spectrum will become more rich with these transitions. To illustrate this, the Telluride I system was initialized in the minimum of the average potential  $Q_0$  with parameters tabulated in Tab. 4.4.

Initialization 2.	
$Q_1(0)$	$Q_0$
$Q_2(0)$	$Q_0$
$P_1(0)$	0
$P_2(0)$	0
$a(0)$	$m\Omega_1/\hbar$
$b(0)$	$1/m\Omega_1\hbar$
$c(0)$	0

Table 4.4: Initialization parameters for “hot band” displaced oscillator model in atomic units.



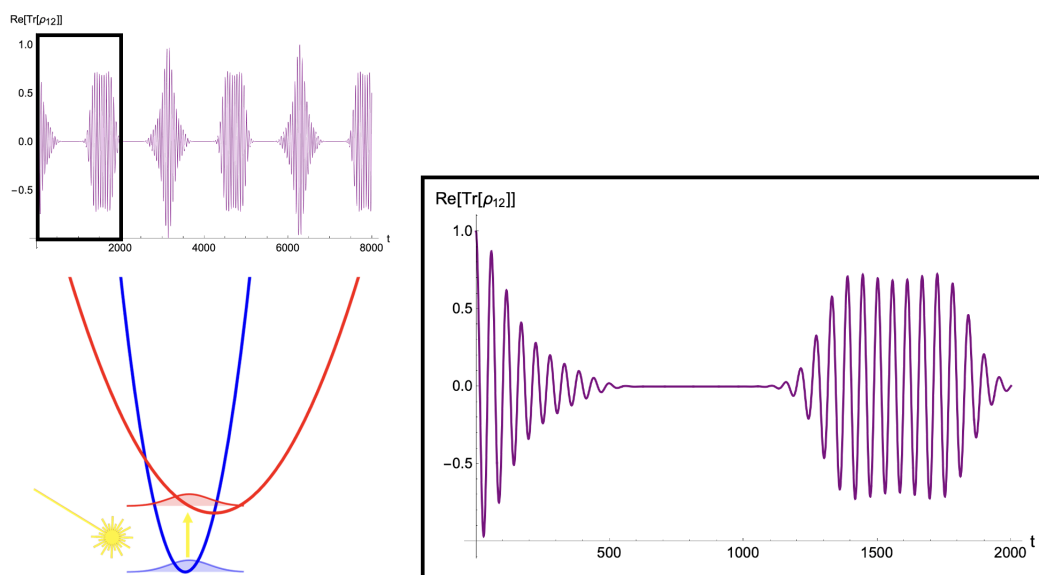


Figure 4.26: Coherence correlation function for Telluride I (Initialization II) calculated by Thawed Moyal Dynamics (Moyal).

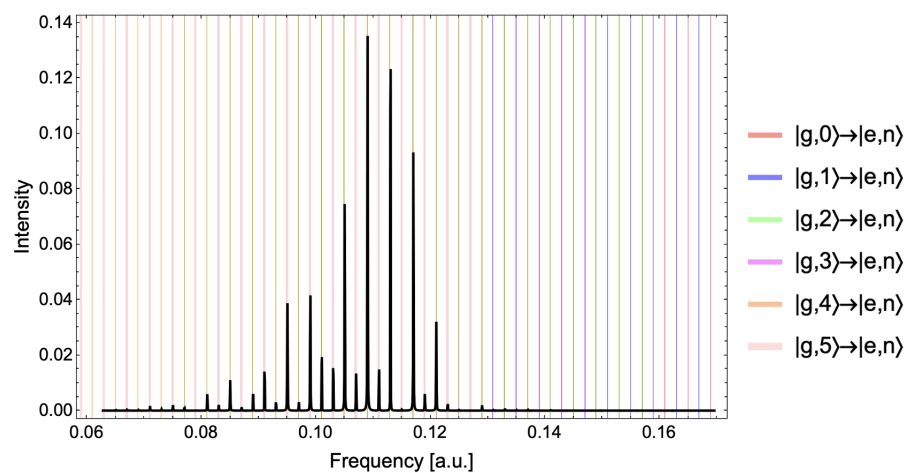


Figure 4.27: Linear absorption spectrum for Telluride I (Initialization II) calculated by Thawed Moyal Dynamics (Moyal).

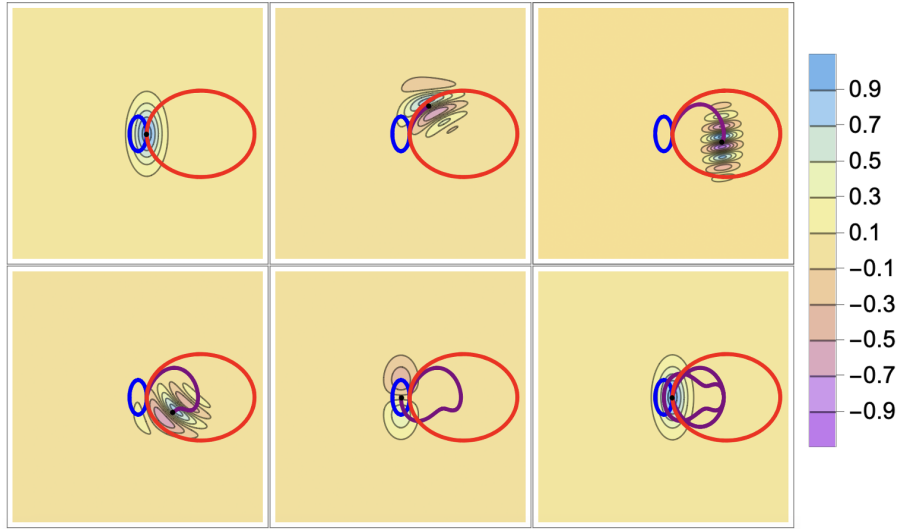


Figure 4.28: Phase space portraits for  $\text{Re}(\rho_{12}(q, p, t))$  for Telluride I (Initialization II) calculated by Thawed Moyal Dynamics (Moyal). Time increasing left-to-right, top-to-bottom ( $t = 0, t = \tau_M/4, t = \tau_M/2, t = 3\tau_M/4, t = \tau_M, t = 4\tau_M$ ) for vibrational period  $\tau_M$ . Ground state orbit:  $(Q_1(t), P_1(t))$  (blue). Excited state orbit:  $(Q_2(t), P_2(t))$  (red). Coherence orbit:  $(Q(t), P(t))$  (purple). Coherence mean (black).

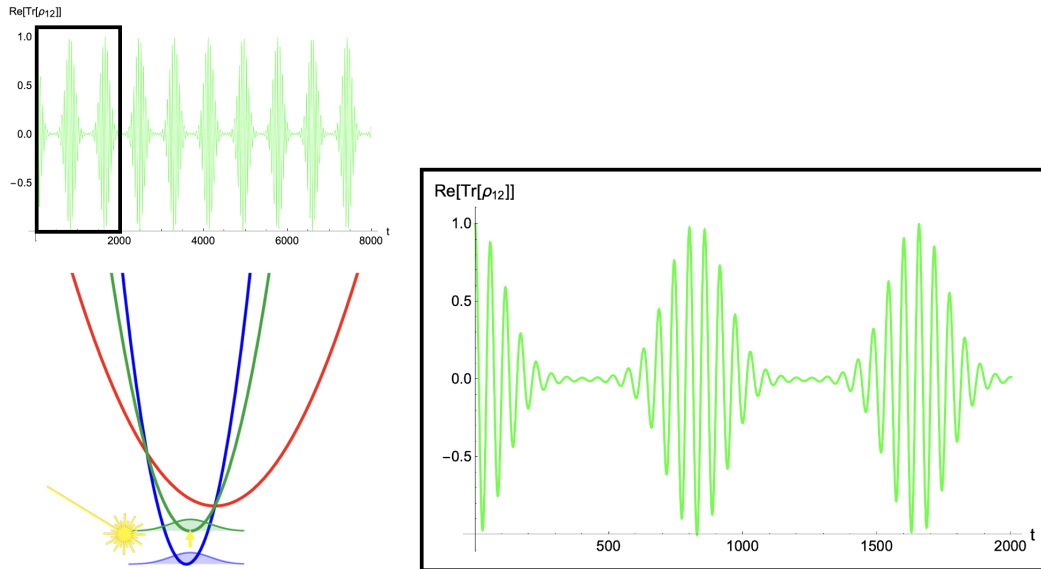


Figure 4.29: Coherence correlation function for Telluride I (Initialization II) calculated by Thawed Moyal Dynamics (Linearized Semiclassical).

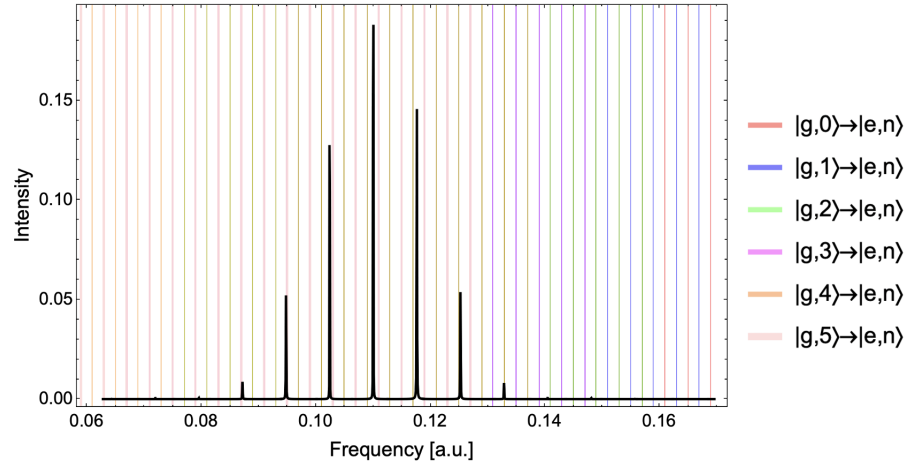


Figure 4.30: Linear absorption spectrum for Telluride I (Initialization II) calculated by Thawed Moyal Dynamics (Linearized Semiclassical).

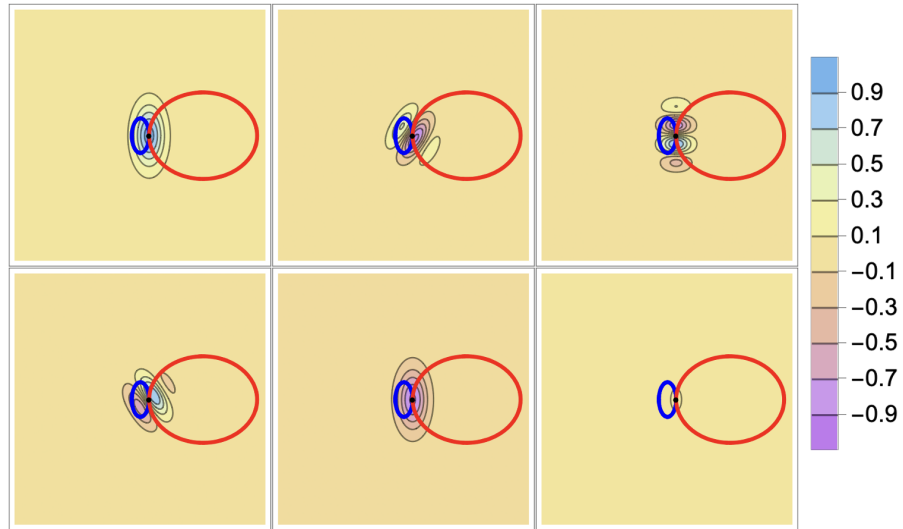


Figure 4.31: Phase space portraits for  $\text{Re}(\rho_{12}(q, p, t))$  for Telluride I (Initialization II) calculated by Thawed Moyal Dynamics (Linearized Semiclassical). Time increasing left-to-right, top-to-bottom ( $t = 0$ ,  $t = \tau_{SC}/4$ ,  $t = \tau_{SC}/2$ ,  $t = 3\tau_M/4$ ,  $t = \tau_{SC}$ ,  $t = 4\tau_{SC}$ ) for vibrational period  $\tau_{SC}$ . Ground state orbit:  $(Q_1(t), P_1(t))$  (blue). Excited state orbit:  $(Q_2(t), P_2(t))$  (red). Coherence orbit:  $(Q(t), P(t))$  (green). Coherence mean (black).

### 4.3.4 Thawed Moyal Solution to 2-D Displaced Oscillator

The Thawed Moyal solutions for the uncoupled case easily generalize arbitrary dimensions.

Consider the Hamiltonian Weyl symbol for the 2-D displaced oscillator

$$H_{jj} = \frac{p_x^2}{2m} + \frac{p_y^2}{2m} + \frac{1}{2}m (\Omega_j^x)^2 (q_x - Q_j^x)^2 + \frac{1}{2}m (\Omega_j^y)^2 (q_y - Q_j^y)^2 + E_j \quad (4.93)$$

for states  $j = 1, 2$  with  $H_{12} = H_{21} = 0$ . The coherence factorizes as

$$\rho_{12}(\mathbf{q}, \mathbf{p}, t) = \rho_{12}^x(q_x, p_x, t) \rho_{12}^y(q_y, p_y, t) \quad (4.94)$$

and the solutions to each direction are given by the Thawed Moyal equations above. This 2-D oscillator was solved for using the system parameters and initializations in Tab. 4.5 and Tab. 4.6 for three distinct resonances on the excited surface. A 1:1 resonance with  $\Omega_2^x = 0.01$  and  $\Omega_2^y = 0.01$ , a 2:1 resonance with  $\Omega_2^x = 0.01$  and  $\Omega_2^y = 0.005$ , and the irrationally related case of a  $1 : \sqrt{2}$  resonance with  $\Omega_2^x = 0.01$  and  $\Omega_2^y = 0.0141421$ . This was done for the exact Moyal and Linearized Semiclassical Thawed Moyal solutions with the correlation functions, spectra, and phase portraits illustrated below.

Telluride II.	
$m$	2000
$\hbar$	1
$\Omega_1^x = \Omega_1^y$	0.01
$\Omega_2^x$	0.01
$Q_1^x = Q_1^y$	0
$Q_2^x = Q_2^y$	1
$E_1$	0
$E_2$	0.1

Table 4.5: System Parameters (Telluride II) for 2-D displaced oscillator model in atomic units.

Initialization III.	
$Q_1^x(0) = Q_1^y(0)$	$Q_1^e$
$Q_2^x(0) = Q_2^y(0)$	$Q_1^e$
$P_1^x(0) = P_1^y(0)$	0
$P_2^x(0) = P_2^y(0)$	0
$a_x(0)$	$m\Omega_1^x/\hbar$
$b_x(0)$	$1/m\Omega_1^x\hbar$
$a_y(0)$	$m\Omega_1^y/\hbar$
$b_y(0)$	$1/m\Omega_1^y\hbar$
$c_x(0) = c_y(0)$	0

Table 4.6: Initialization parameters for 2-D displaced oscillator model in atomic units.

## 1 : 1 Resonance

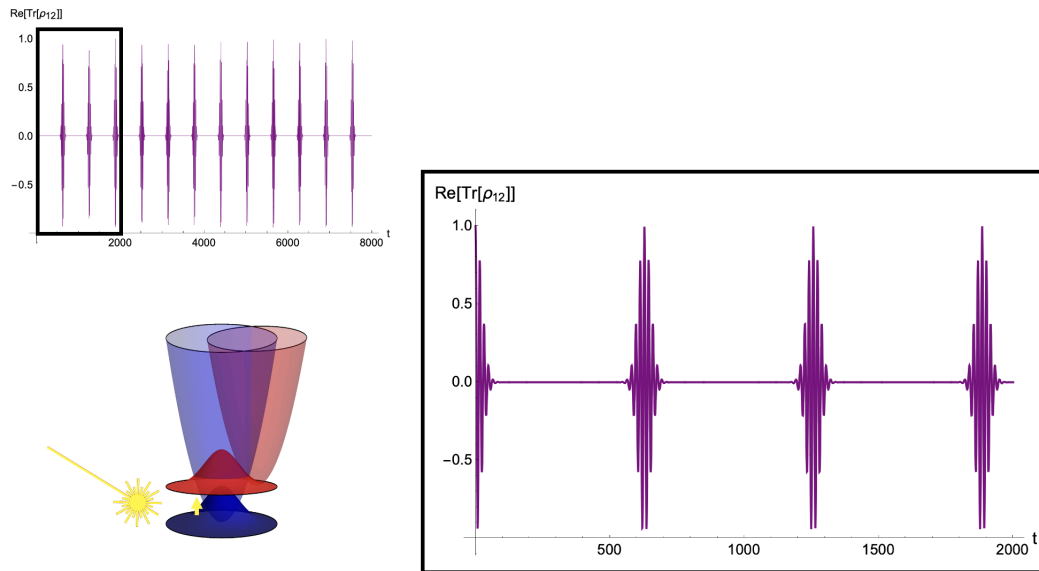


Figure 4.32: Coherence correlation function for Telluride II (Initialization III) with 1 : 1 resonance calculated by Thawed Moyal Dynamics (Moyal).

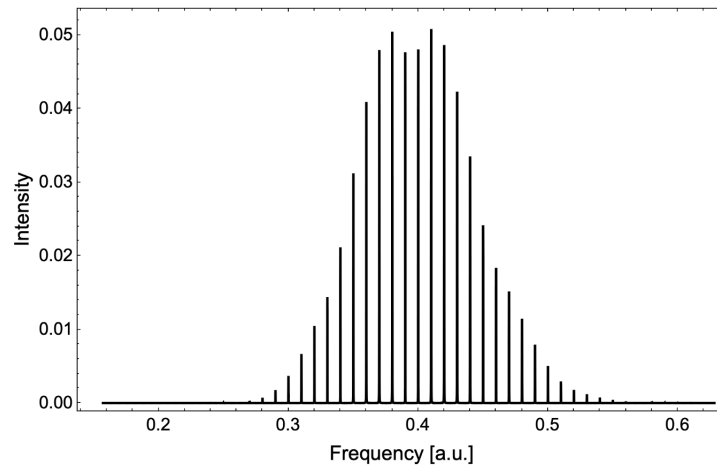


Figure 4.33: Linear absorption spectrum for Telluride II (Initialization III) with 1 : 1 resonance calculated by Thawed Moyal Dynamics (Moyal).

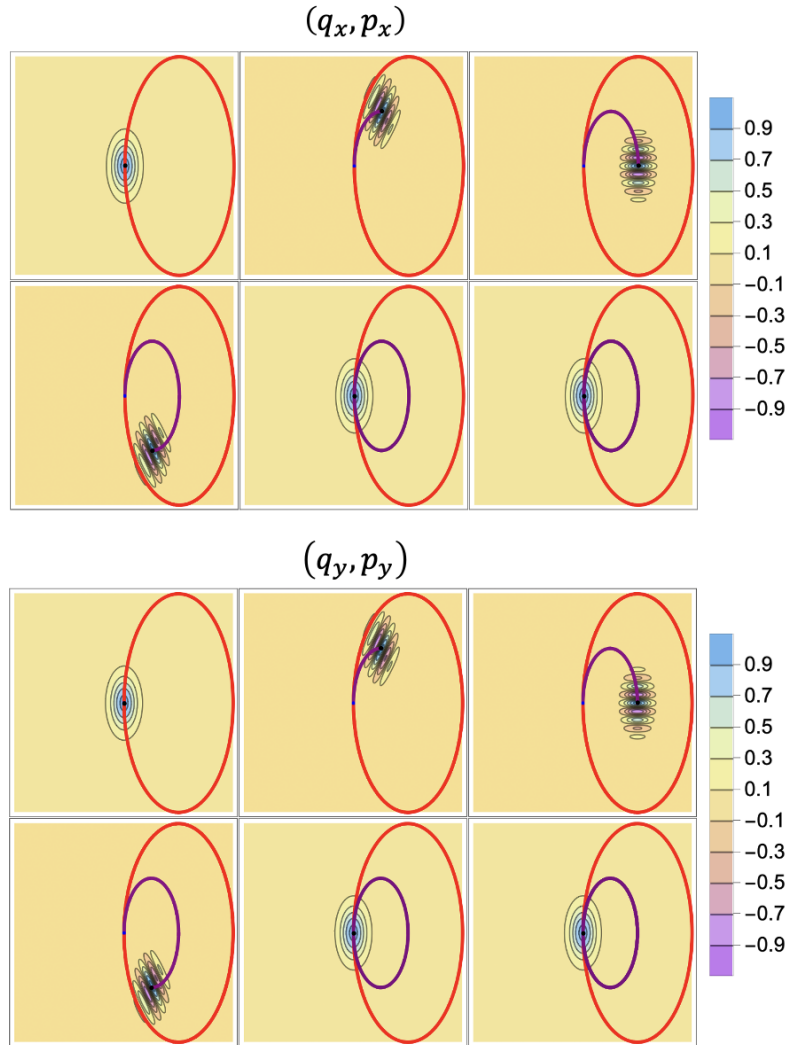


Figure 4.34: Phase space portraits for  $\text{Re}(\rho_{12}(q, p, t))$  for Telluride II (Initialization III) with 1 : 1 resonance calculated by Thawed Moyal Dynamics (Moyal). Time increasing left-to-right, top-to-bottom ( $t = 0, t = \tau_M/4, t = \tau_M/2, t = 3\tau_M/4, t = \tau_M, t = 4\tau_M$ ) for vibrational period  $\tau_M$ . Ground state orbit:  $(Q_1(t), P_1(t))$  (blue). Excited state orbit:  $(Q_2(t), P_2(t))$  (red). Coherence orbit:  $(Q(t), P(t))$  (purple). Coherence mean (black).

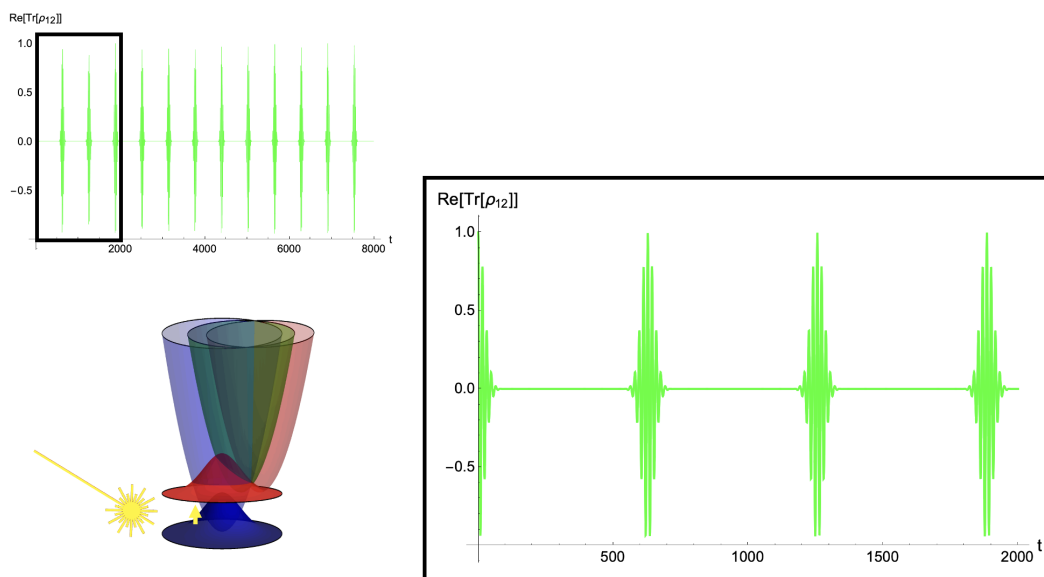


Figure 4.35: Coherence correlation function for Telluride II (Initialization III) with 1 : 1 resonance calculated by Thawed Moyal Dynamics (Linearized Semiclassical).

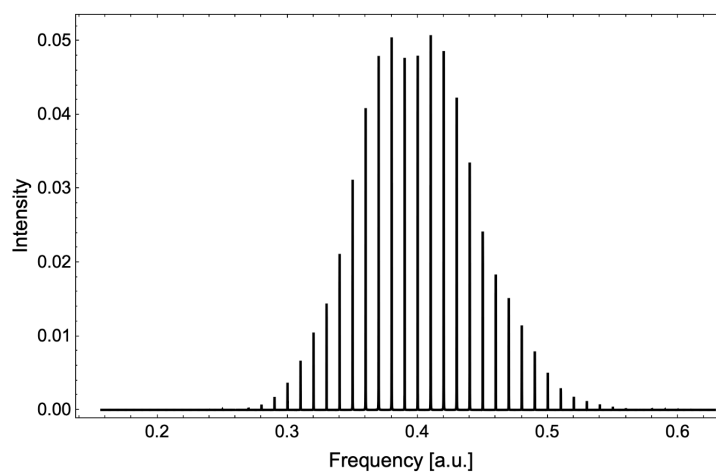


Figure 4.36: Linear absorption spectrum for Telluride II (Initialization III) with 1 : 1 resonance calculated by Thawed Moyal Dynamics (Linearized Semiclassical).



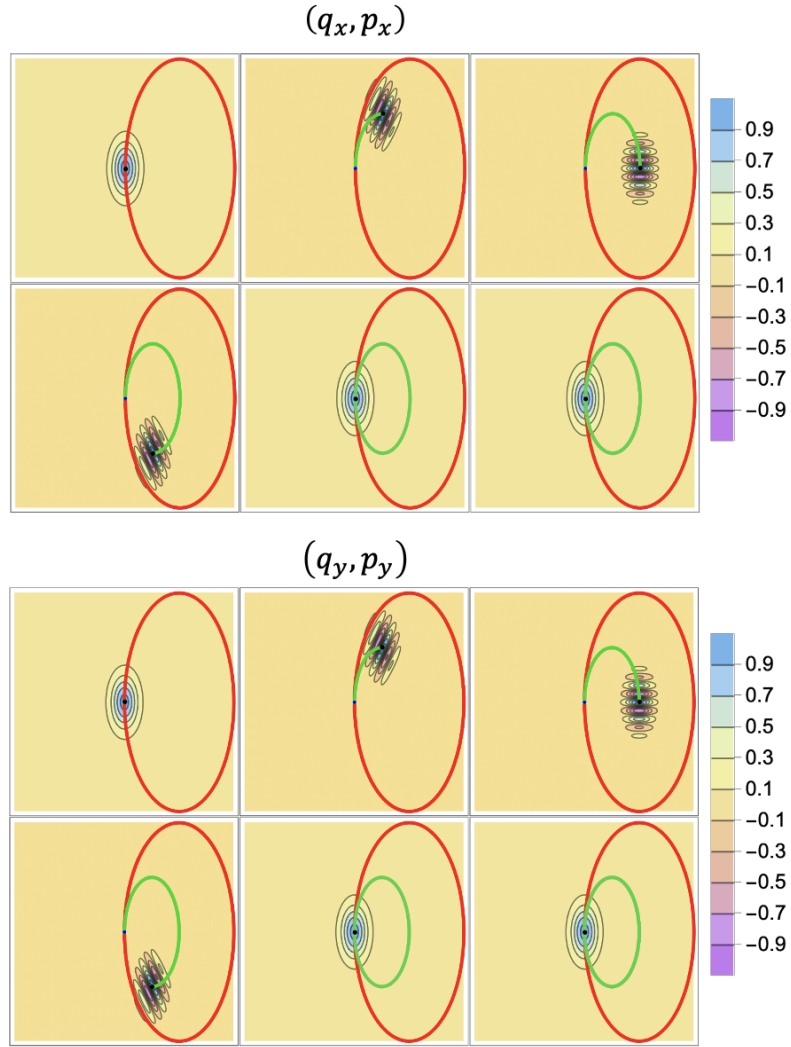


Figure 4.37: Phase space portraits for  $\text{Re}(\rho_{12}(q, p, t))$  for Telluride II (Initialization III) with 1 : 1 resonance calculated by Thawed Moyal Dynamics (Linearized Semiclassical). Time increasing left-to-right, top-to-bottom ( $t = 0, t = \tau_{SC}/4, t = \tau_{SC}/2, t = 3\tau_M/4, t = \tau_{SC}, t = 4\tau_{SC}$ ) for vibrational period  $\tau_{SC}$ . Ground state orbit:  $(Q_1(t), P_1(t))$  (blue). Excited state orbit:  $(Q_2(t), P_2(t))$  (red). Coherence orbit:  $(Q(t), P(t))$  (green). Coherence mean (black).

## 2 : 1 Resonance

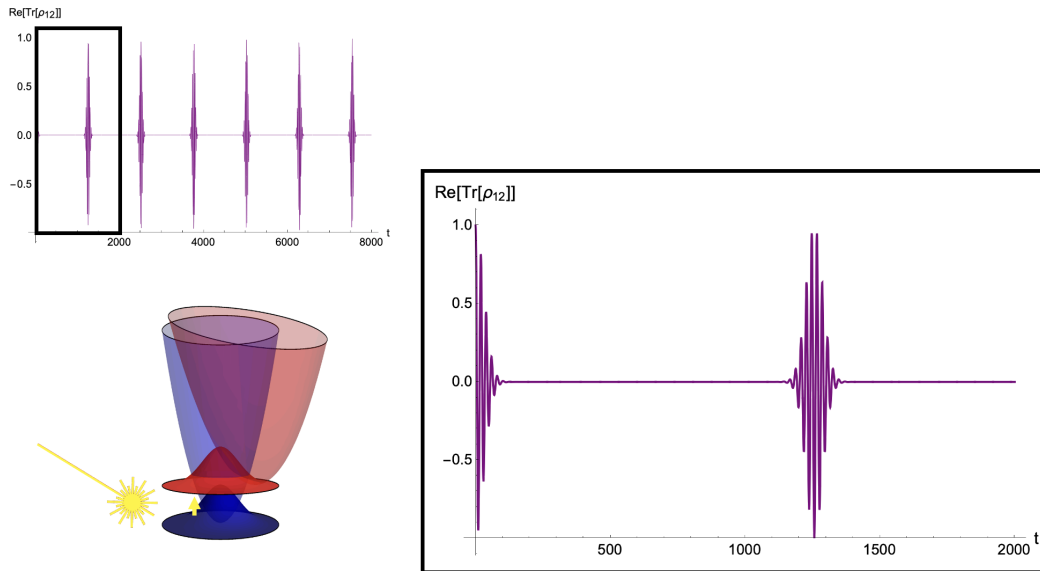


Figure 4.38: Coherence correlation function for Telluride II (Initialization III) with 2 : 1 resonance calculated by Thawed Moyal Dynamics (Moyal).

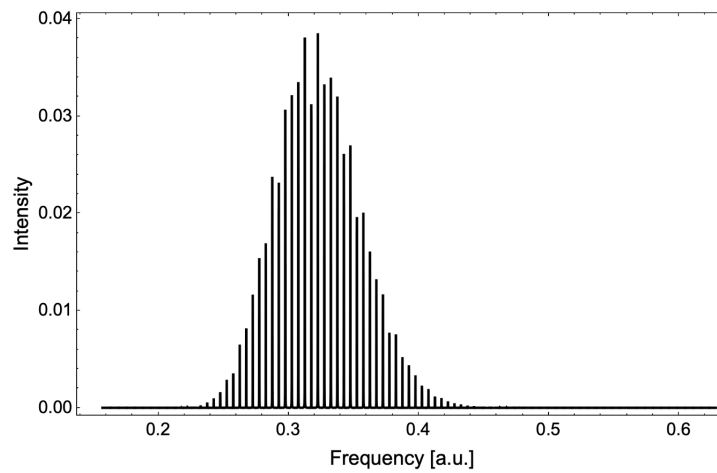


Figure 4.39: Linear absorption spectrum for Telluride II (Initialization III) with 2 : 1 resonance calculated by Thawed Moyal Dynamics (Moyal).

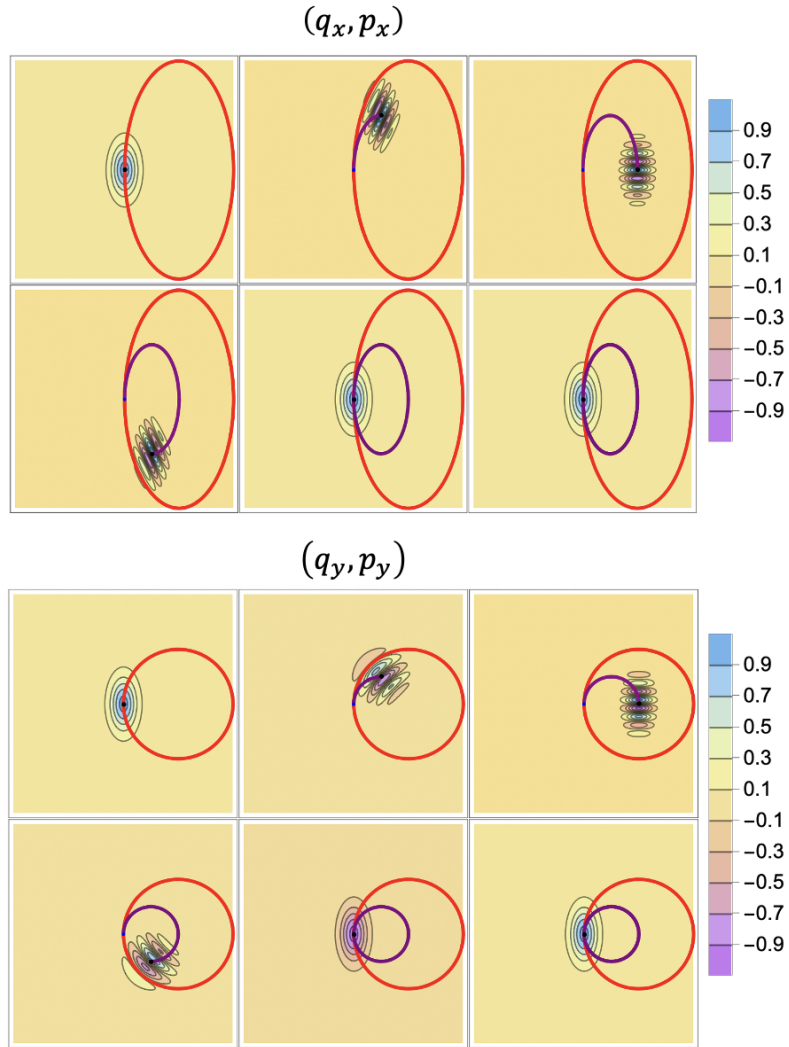


Figure 4.40: Phase space portraits for  $\text{Re}(\rho_{12}(q, p, t))$  for Telluride II (Initialization III) with 2 : 1 resonance calculated by Thawed Moyal Dynamics (Moyal). Time increasing left-to-right, top-to-bottom ( $t = 0, t = \tau_M/4, t = \tau_M/2, t = 3\tau_M/4, t = \tau_M, t = 4\tau_M$ ) for vibrational period  $\tau_M$ . Ground state orbit:  $(Q_1(t), P_1(t))$  (blue). Excited state orbit:  $(Q_2(t), P_2(t))$  (red). Coherence orbit:  $(Q(t), P(t))$  (purple). Coherence mean (black).

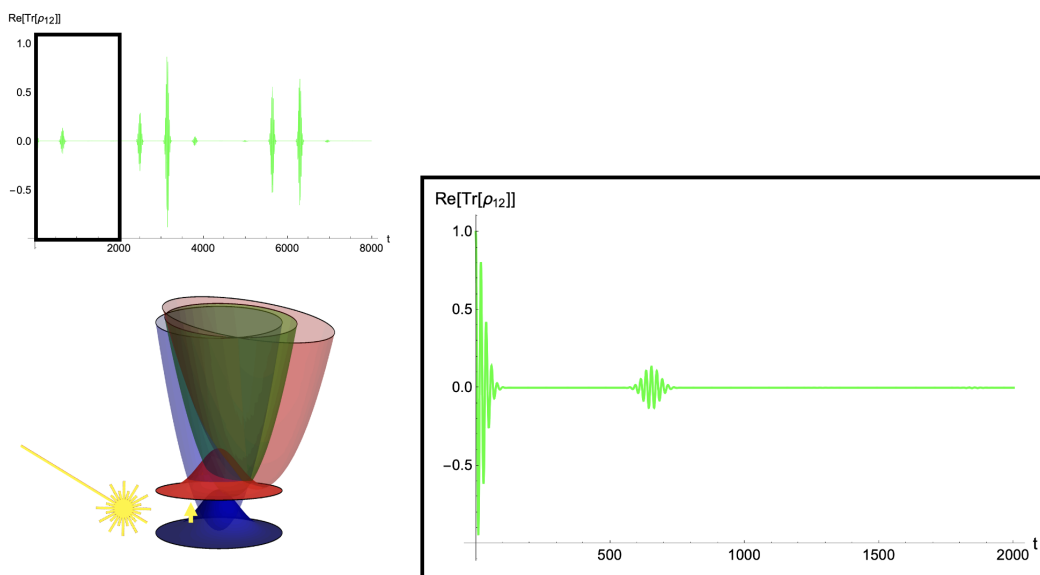


Figure 4.41: Coherence correlation function for Telluride II (Initialization III) with 2 : 1 resonance calculated by Thawed Moyal Dynamics (Linearized Semiclassical).

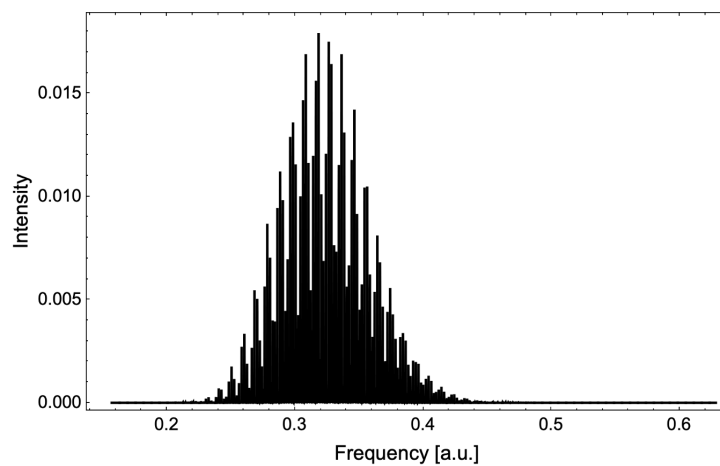


Figure 4.42: Linear absorption spectrum for Telluride II (Initialization III) with 2 : 1 resonance calculated by Thawed Moyal Dynamics (Linearized Semiclassical).

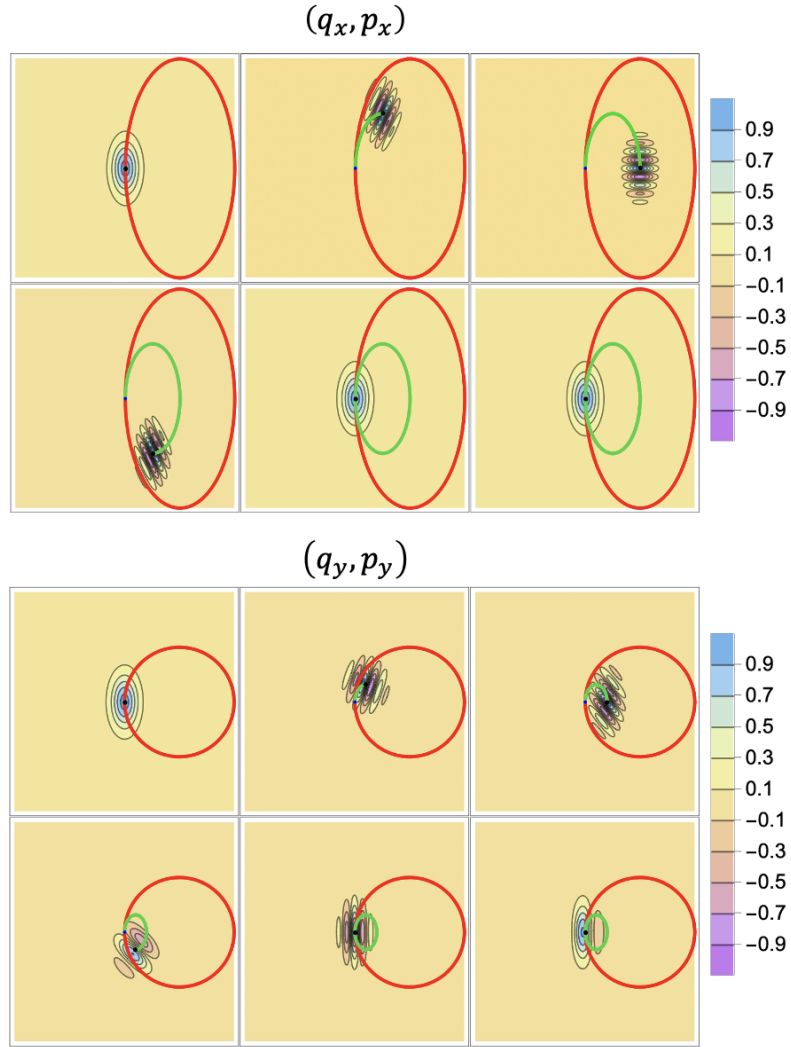


Figure 4.43: Phase space portraits for  $\text{Re}(\rho_{12}(q, p, t))$  for Telluride II (Initialization III) with 2 : 1 resonance calculated by Thawed Moyal Dynamics (Linearized Semiclassical). Time increasing left-to-right, top-to-bottom ( $t = 0, t = \tau_{SC}/4, t = \tau_{SC}/2, t = 3\tau_M/4, t = \tau_{SC}, t = 4\tau_{SC}$ ) for vibrational period  $\tau_{SC}$ . Ground state orbit:  $(Q_1(t), P_1(t))$  (blue). Excited state orbit:  $(Q_2(t), P_2(t))$  (red). Coherence orbit:  $(Q(t), P(t))$  (green). Coherence mean (black).

## 1 : $\sqrt{2}$ Resonance

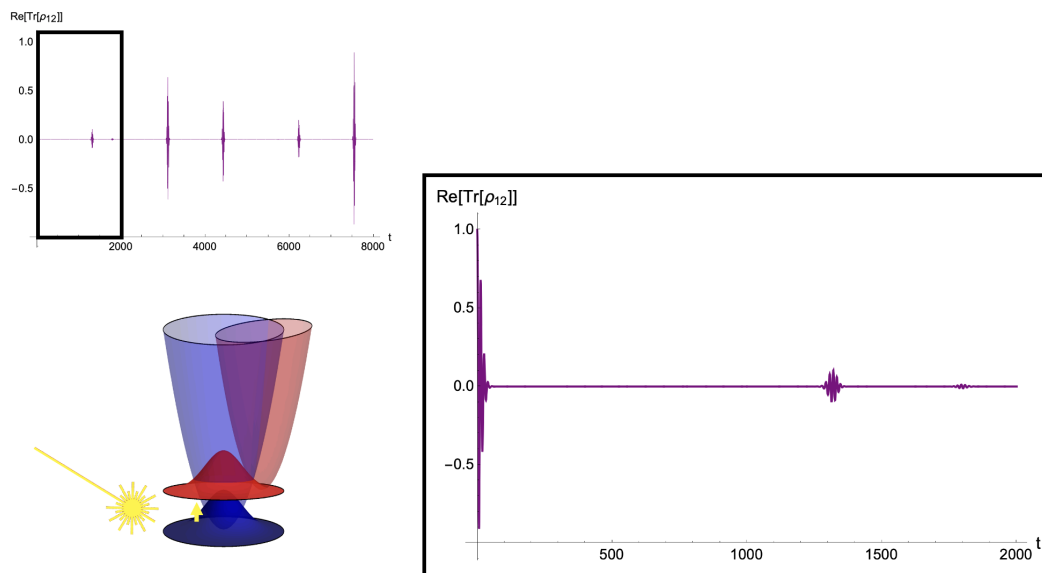


Figure 4.44: Coherence correlation function for Telluride II (Initialization III) with  $1 : \sqrt{2}$  resonance calculated by Thawed Moyal Dynamics (Moyal).

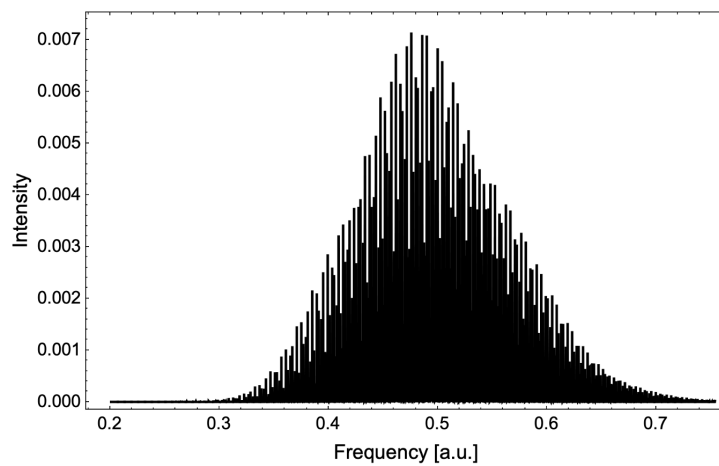


Figure 4.45: Linear absorption spectrum for Telluride II (Initialization III) with  $1 : \sqrt{2}$  calculated by Thawed Moyal Dynamics (Moyal).

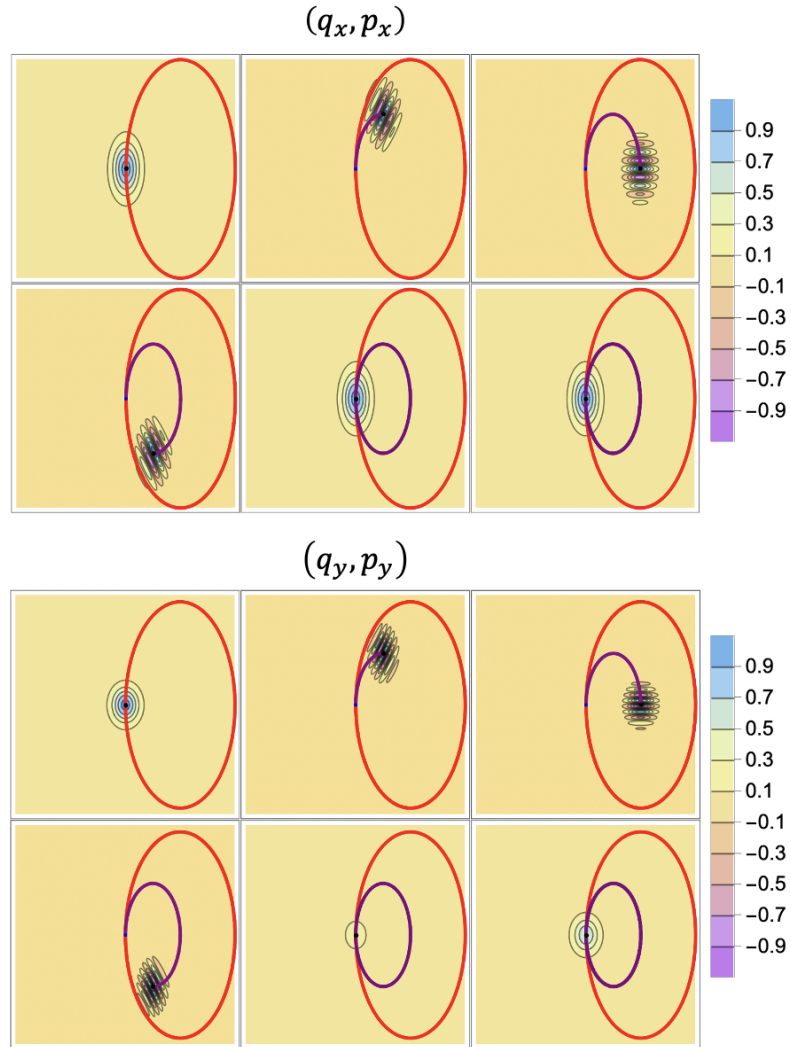


Figure 4.46: Phase space portraits for  $\text{Re}(\rho_{12}(q, p, t))$  for Telluride II (Initialization III) with  $1 : \sqrt{2}$  resonance calculated by Thawed Moyal Dynamics (Moyal). Time increasing left-to-right, top-to-bottom ( $t = 0, t = \tau_M/4, t = \tau_M/2, t = 3\tau_M/4, t = \tau_M, t = 4\tau_M$ ) for vibrational period  $\tau_M$ . Ground state orbit:  $(Q_1(t), P_1(t))$  (blue). Excited state orbit:  $(Q_2(t), P_2(t))$  (red). Coherence orbit:  $(Q(t), P(t))$  (purple). Coherence mean (black).

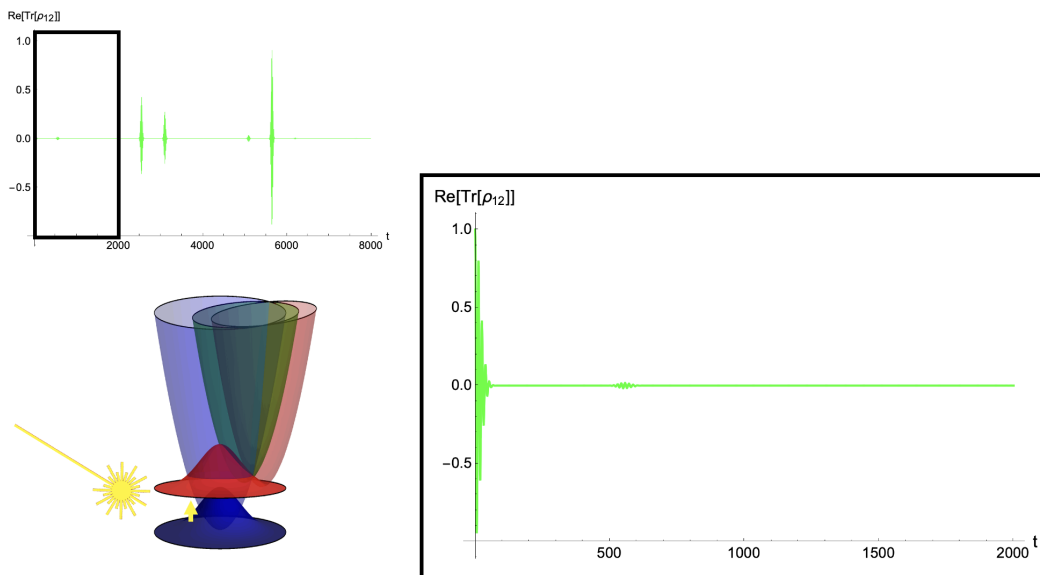


Figure 4.47: Coherence correlation function for Telluride II (Initialization III) with  $1 : \sqrt{2}$  resonance calculated by Thawed Moyal Dynamics (Linearized Semiclassical).

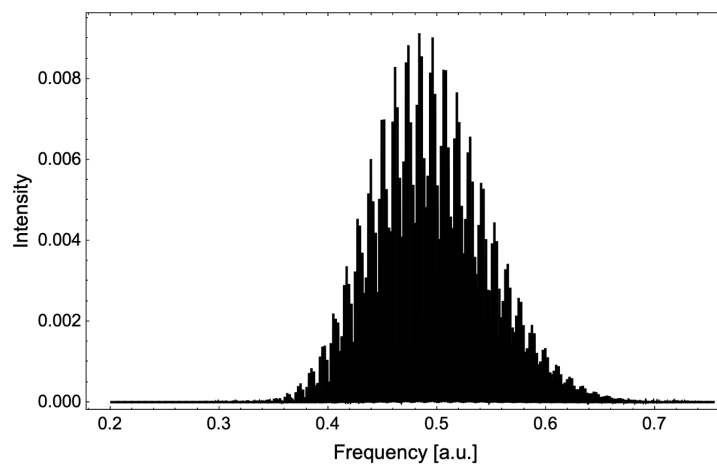


Figure 4.48: Linear absorption spectrum for Telluride II (Initialization III) with  $1 : \sqrt{2}$  resonance calculated by Thawed Moyal Dynamics (Linearized Semiclassical).



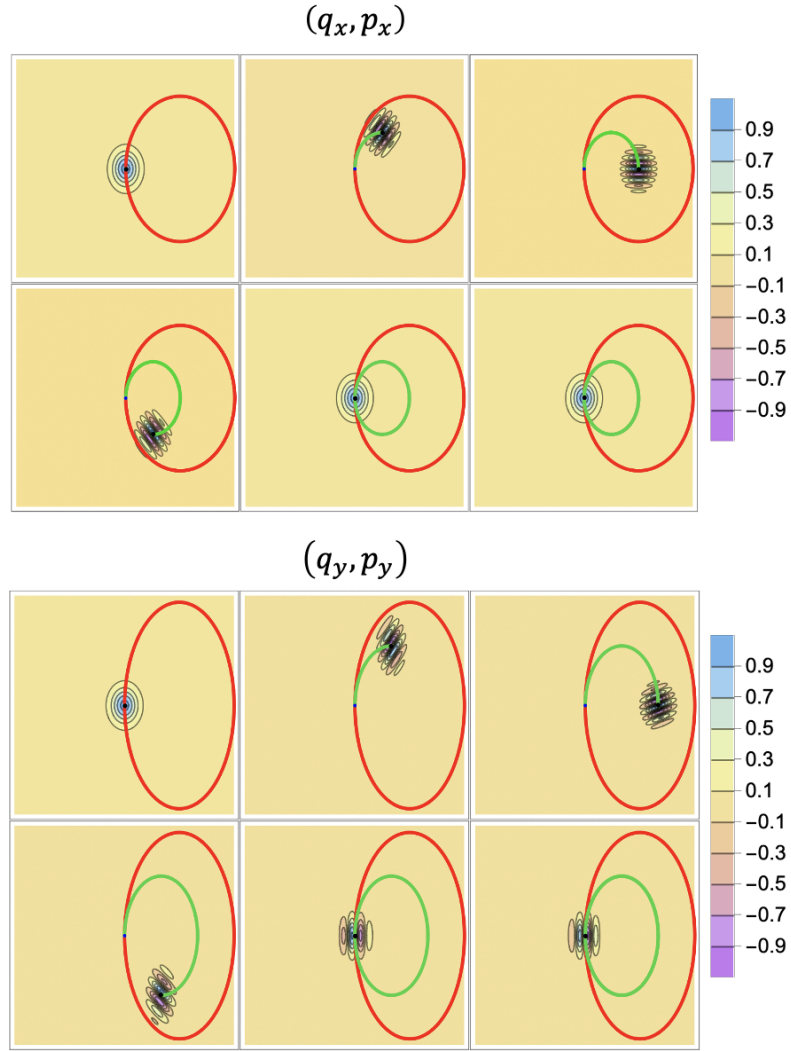


Figure 4.49: Phase space portraits for  $\text{Re}(\rho_{12}(q, p, t))$  for Telluride II (Initialization III) with  $1 : \sqrt{2}$  resonance calculated by Thawed Moyal Dynamics (Linearized Semiclassical). Time increasing left-to-right, top-to-bottom ( $t = 0, t = \tau_{SC}/4, t = \tau_{SC}/2, t = 3\tau_M/4, t = \tau_{SC}, t = 4\tau_{SC}$ ) for vibrational period  $\tau_{SC}$ . Ground state orbit:  $(Q_1(t), P_1(t))$  (blue). Excited state orbit:  $(Q_2(t), P_2(t))$  (red). Coherence orbit:  $(Q(t), P(t))$  (green). Coherence mean (black).

## 4.4 Discussion

### 4.4.1 Kinematics of the Quantum and Semiclassical Coherence

All the results of the Thawed Moyal solutions are subsumed into an intuitive phase space picture for the coherence dynamics of the displaced oscillator system. Recall the general Thawed Moyal solution for the coherence Wigner function is the Gaussian form

$$\begin{aligned} \rho_{12}(q, p, t) = & \exp \left( -a(t) (q - Q(t))^2 - b(t) (p - P(t))^2 \right. \\ & \left. + c(t) (q - Q(t)) (p - P(t)) + u(t) (q - Q(t)) + v(t) (p - P(t)) + w(t) \right) \end{aligned}$$

where  $(Q, P) \in \mathbb{R}$  and the remaining parameters are complex or purely imaginary.  $Q$  and  $P$  are the expectations of position and momentum of the coherence Wigner function. For the quantum solutions (Moyal and Linearized Moyal), these are given by arithmetic averages of the expectations

$$Q(t) = \frac{Q_1(t) + Q_2(t)}{2}, \quad \text{and} \quad P(t) = \frac{P_1(t) + P_2(t)}{2}$$

with each  $(Q_j, P_j)$  is modulated by the frequency of its potential  $\Omega_1$  or  $\Omega_2$ . In contrast, the semiclassical solutions (Semiclassical and Linearized Semiclassical) have their average position and momentum modulated by a single frequency which is the geometric average of each potential's frequency

$$\Omega_0 = \sqrt{\frac{\Omega_1^2 + \Omega_2^2}{2}}$$

The average trajectory of the coherence at the quantum level has character of both states simultaneously, ground (dead) and excited (alive) and has been called a “cat-jectory” [146]. In contrast, at the semiclassical level, the average trajectory of the coherence has character of neither states, but rather something in between and has been called a “zombie cat.” The

“cat-jjectory” versus “zombie cat” has been illustrated below in Fig. 4.50.

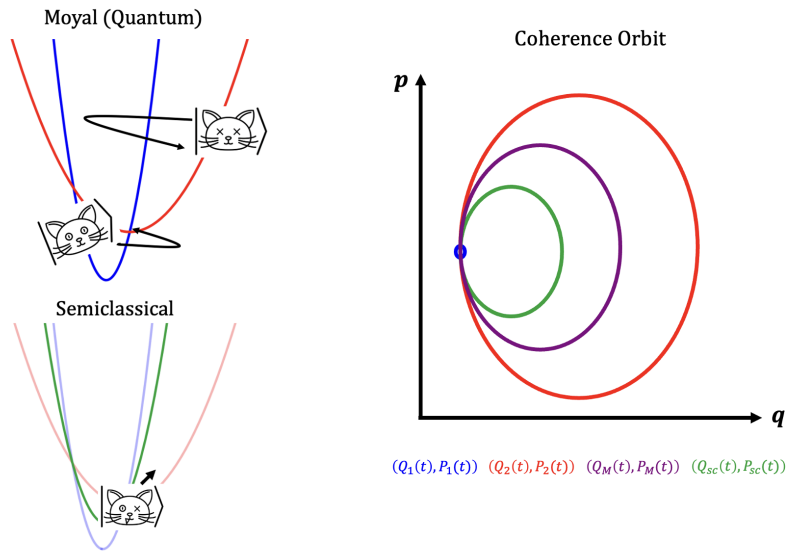


Figure 4.50: Cat-jjectory and zombie cat. The average orbits of the quantum coherence follow a cat-jjectory modulated by each state’s frequency whereas semiclassically approximated coherence follows an average frequency orbit or zombie cat.

In Telluride I (Initialization I) because the system is initialized in the equilibrium of the ground potential  $Q_1(0) = Q_2(0) = Q_1^e$ , the lower surface’s wavepacket is stationary and in phase space its orbit contracts to a point which is the initial position and momentum (Fig. 4.4, Fig. 4.7, Fig. 4.10, Fig. 4.13). The cat-jjectory orbit is an average of this point and the excited state’s orbit  $(Q_2(t), P_2(t))$  with the coherence Wigner function evolving on elliptic orbit at the frequency of the excited state  $\tau_M = 2\pi/\Omega_2$ . In contract, the coherence Wigner function at the semiclassical level evolves on an orbit defined by the incorrect average frequency of both states  $\Omega_0$ .

The Initialization II of Telluride I, makes the kinematic difference between the quantum and semiclassical solutions more evident. Initialized instead at the equilibrium of the average potential  $Q_1(0) = Q_2(0) = Q_0$ , neither state’s wavepackets are stationary and in phase space the cat-jjectory orbit undergoes spirographic motion resulting from the distinct frequencies of each state’s orbit. In plane geometrical terms, the cat-jjectory is generally a *trochoid* [147] and

only undergoes simple elliptic orbit when initialized in the one of the minima equilibrium the state's potentials. More exotic initializations and frequency resonances can generate a diverse family of phase space trochoids for the displaced oscillator model resembling the Lissajous curves of parametric systems (Fig. 4.51) [81]. In contrast, the semiclassical coherence Wigner function when initialized at  $Q_0$  remains stationary and rotates about its equilibrium point in phase space.

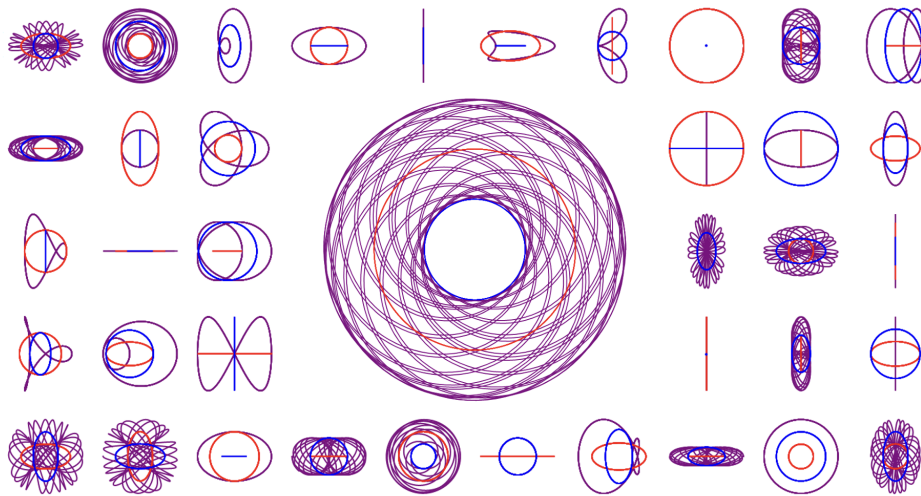


Figure 4.51: Examples of cat-jjectory trochoid orbits of the quantum coherence.

For the equal frequency case of Telluride I-S (Initialization I), the quantum and semiclassical dynamics of the coherence are identical (Fig. 4.20 - Fig. 4.25). This is, in part, because this is the only case for which the cat-jjectory and zombie orbits coincide

$$Q(t) = \frac{Q_1(t; \Omega_1) + Q_2(t; \Omega_2)}{2} = Q(t; \Omega_0)$$

$$P(t) = \frac{P_1(t; \Omega_1) + P_2(t; \Omega_2)}{2} = P(t; \Omega_0)$$

And this subtlety is missed by traditional ladder operator solutions to the displaced oscillator model which assume equal frequencies [20, 148, 149].

## Covariance and Interference

The Thawed Moyal ansatz for the coherence Wigner function can be rewritten in a slightly more suggestive form as

$$\rho_{12}(q, p, t) = \exp\left(-\frac{1}{2}(\mathbf{z} - \mathbf{Z}(t))^T \mathbf{S}(t) (\mathbf{z} - \mathbf{Z}(t)) + \mathbf{y}^T(t)\mathbf{z} + w(t)\right) \quad (4.95)$$

where

$$(\mathbf{z} - \mathbf{Z}(t))^T = (q - Q(t), p - P(t)), \quad (4.96)$$

$$\mathbf{S}(t) = \begin{pmatrix} 2a(t) & -c(t) \\ -c(t) & 2b(t) \end{pmatrix}, \quad (4.97)$$

and

$$\mathbf{y}^T = (u(t), v(t)). \quad (4.98)$$

Complex parameters  $a$ ,  $b$ , and  $c$  are inversely related to the position covariance, momentum covariance, and position-momentum correlation. The determinant of  $S$  is a constant of motion alluded to in Eq. 4.36,

$$\det(\mathbf{S}(t)) = 4a(t)b(t) - c(t)^2 = \frac{4}{\hbar^2}. \quad (4.99)$$

Eq. 4.99 can be interpreted as the generalization of the Schrödinger-Robertson equality for the coherence formed by two minimum uncertainty states (Hudson states). But unlike  $\sigma_q$ ,  $\sigma_p$ , and  $r$  in the Schrödinger-Robertson equality,  $a$ ,  $b$ , and  $c$  are generally complex. Geometrically, the minimum uncertainty phase space volume of  $\hbar^2/4$  is shared at all times during evolution by a real and imaginary space (Fig. 4.52). This is true of both quantum (Moyal and Linearized Moyal) and Linearized Semiclassical solutions. The  $\det(\mathbf{S}(t))$  for unlinearized Semiclassical, by contrast is not constant because of the resonantly driven secular terms in

$u$  coupled to the covariance parameters through  $(Q, P)$ .

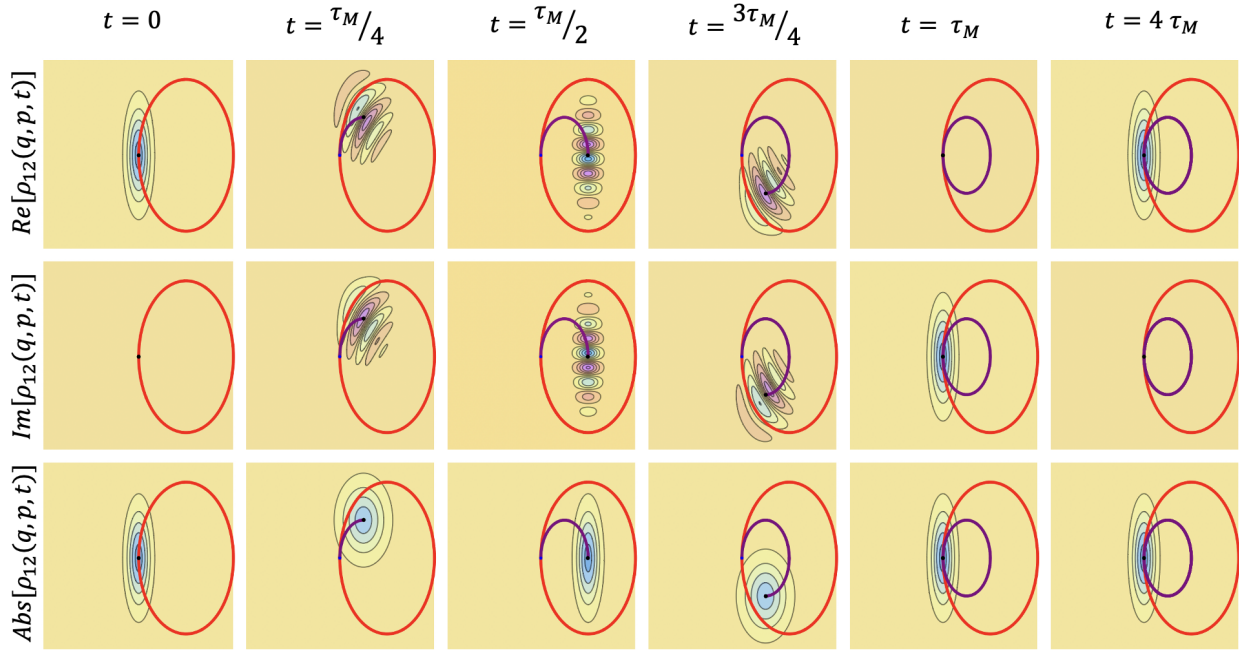


Figure 4.52: Example of preservation of the minimum uncertainty volume in real and imaginary phase spaces for Telluride I (Initialization I) calculated by the Thawed Moyal Dynamics quantum solution.

For all Thawed Moyal solutions the parameters the linear terms  $u$  and  $v$  impart interference fringes over the phase space ellipse of the coherence Wigner function. While these linear terms can be removed by completing the square in the exponential of  $\rho_{12}$  in Eq. 4.95, this comes at the expense of making the expectation orbits  $(Q, P)$  complex.

#### 4.4.2 Correlation Functions and Spectra

The coherence correlation functions and spectra for all levels of the Thawed Moyal solutions on the different displaced oscillator models can be rationalized in terms of the kinematic picture discussed above. For Telluride I (Initialization I), the recurrence times of the correlation functions occur at the frequency of the expectation orbit with the fast oscillations modulated by the electronic energy gap  $E_2 - E_1 = 0.1$ . For the quantum results (Moyal and Linearized

Moyal) the recurrence time is  $\tau_M$  fixed by the excited state's frequency (Fig. 4.2 and Fig. 4.5). For the semiclassical results (Semiclassical and Linearized Semiclassical) the recurrence time is fixed by the frequency of the average potential's expectation orbit,  $\tau_{SC} = 2\pi/\Omega_0$  (Fig. 4.8 and Fig. 4.11). But unlike Linearized Semiclassical, the Semiclassical's correlation function's recurrences are obscured by the secular growth at resonant terms in  $u$  which cause artificial decoherence and dampening of the signal. Linearization of the difference potential removes these secular terms and restores the recurrences for the semiclassical level of theory. For the quantum level, linearization doesn't appear to qualitatively change the signal. This picture obscured in the equal frequency of Telluride I-S (Initialization I) case (Fig. 4.20 and Fig. 4.23) because only in this case will the quantum and semiclassical kinematics agree. For the "hot band" case Telluride I (Initialization II) (Fig. 4.26 and Fig. 4.29), the correlation functions become more rich as a result of more vibrational eigenstates in the ground level being excited.

The linear absorption spectra are just Fourier transforms of the coherence correlation function and contain the same information. In all models the lineshapes are centered around the electronic energy gap  $E_2 - E_1 = 0.1$ . In Telluride I (Initialization I), the spectra were calculated at all levels of the Thawed Moyal theory. For the quantum results (Moyal and Linearized Moyal) the spectral features are spaced according to the excited state's frequency (Fig. 4.3 and Fig. 4.6). For the semiclassical results (Semiclassical and Linearized Semiclassical) spectral features are spaced by the incorrect average potential's frequency (Fig. 4.8 and Fig. 4.11). The exact transitions are superimposed behind the spectra to help illustrate this distinction. The frequency error implicit in the semiclassical treatment is also evident in the "hot band" case with more lower frequency transitions from the vibrational eigenstates of the ground state potential (Fig. 4.27 and Fig. 4.30).

### 4.4.3 Trajectory Ensemble Solutions and 2-D Oscillators

The Semiclassical and Linearized Semiclassical correlation functions (Fig. 4.14 and Fig. 4.17), spectra (Fig. 4.15 and Fig. 4.18), and phase portraits (Fig. 4.16 and Fig. 4.19) were calculated for Telluride I (Initialization I) and to compare with their Thawed Moyal analogs. Both levels of semiclassical trajectory ensemble theories show strong quantitative agreement with their Thawed Moyal Dynamics result, capturing the key features and failures of the semiclassical approach. The trajectory ensemble Semiclassical solution undergoes spurious decoherence and linearization of the difference potential removes this. The spectra are resolved at the incorrect average frequency of  $\Omega_0$ . The kinematics of the phase portraits match the Thawed Moyal picture. What is illustrated is the utility of linearization approximation for trajectory ensembles solutions to semiclassical Liouville dynamics.

The 2-D displaced oscillator models with their dynamics illustrated in Fig. 4.32 through Fig. 4.49 demonstrates the Thawed Moyal Dynamics and their approximation implementations can be applied to systems with several degrees of freedom without much difficulty. The theory captures how the spectrum is modulated by resonances between excited state frequencies  $\Omega_2^x$  and  $\Omega_2^y$ . The 1 : 1 spectra (Fig. 4.33 and Fig. 4.36) spectral features are split into mirror images, a vibrational doublet around  $\omega \approx 0.04$ . Because the excited state frequencies are also equal to the ground state frequencies the difference between the exact quantum (Moyal) and semiclassical (Linearized Semiclassical) theories is obscured. Breaking the symmetry of the excited state, for the 2 : 1 resonance the distinction between the true quantum (Fig. 4.39) and semiclassical result (Fig. 4.42) becomes apparent. The latter's spectrum is spaced more densely according to the incorrect zombie frequencies, while the quantum result is spaced by the frequencies of the cat-jectorys in each direction. Making the resonance irrationally related 1 :  $\sqrt{2}$  (Fig. 4.45 and Fig. 4.48), the same picture is reiterated but with the lineshape being broadened as expected.



## 4.5 Applications and Future Work

In this chapter an exact phase space solution to the dynamics of a quantum coherence generated by Frank-Condon transitions in a displaced oscillator model was derived and illustrated on various systems. The quantum Thawed Moyal Dynamics theory is an exact solution for displaced oscillator systems with no off-diagonal coupling in the diabatic representation. Approximations to the quantum solution were considered: semiclassical truncation and linearization of the difference potential. It was shown the traditional semiclassical Liouville equation solution is accurate only in the limit of equal frequency potentials. The semiclassical solution undergoes artificial decoherence and resolves spectral lineshapes at the incorrect average frequency. In contrast, the quantum Thawed Moyal solution is exact and correctly resolves the linear absorption spectrum at the excited state frequency. The Thawed Moyal Dynamics theory has an intuitive interpretation in terms of the orbital kinematics of the coherence Wigner function in phase space. Quantum solutions evolve on trochoidal orbits defined by the arithmetic average of each state's expectation orbit, possessing character of both states simultaneous, and is termed a "cat-jjectory." In contrast, semiclassical solutions evolve on an orbit defined by the average frequency of the potentials and is termed a "zombie-cat."

The insights of linearization were applied to the traditional trajectory ensemble route of solving the semiclassical Liouville equation and were demonstrated to match their Thawed Moyal solutions. Linearization of the difference potentials removes the secular pathologies of the semiclassical solution and removes artificial decoherence. This approximation can dramatically improve semiclassical simulations in multi-state systems with distinct frequencies. To illustrate the Thawed Moyal solutions on systems with more degrees of freedom, 2-D displaced oscillators with different frequencies resonances in the excited state were studied. These spectra qualitatively match what one would expect for different resonant conditions.

A clearer picture of the dynamics of quantum coherences for linear systems (quadratic potentials) has been obtained, but the Thawed Moyal solutions are limited by the fact they are exact only in systems with harmonic potentials without off-diagonal coupling. While the Thawed Moyal solution can be extended using standard methods of Thawed/Frozen Gaussian Approximations and perturbation theory, to accommodate anharmonicity and coupling a more general phase space formalism can be derived. The Thawed Moyal Dynamics solution to the coherence Wigner function revealed how the time-dependent statistics of the coherence are related to the properties of the states compromising the coherence. This was most obvious in the wavepacket solution, but is implicit in the generalization of the Schrödinger-Robertson equality (Eq. 4.99). In the following chapter, this idea is pursued by deriving a representation of the coherence in terms of its populations. The advantage of this approach is that the quantum coherences can be calculated directly in terms of low cost trajectory ensembles of trajectories which sample the population Wigner functions and this framework is general.

# Chapter 5

## The Star Coherence Representation

In the previous chapter, a Thawed Gaussian ansatz was used to solve the quantum dynamics of a coherence generated by a Frank-Condon transition in a displaced oscillator model. The theory exactly simulates the dynamics of quantum coherences under quadratic potentials in 2 level systems without off-diagonal coupling. The solution was shown to be obtainable by solving equations of motion for wavepacket parameters and or parameters for the coherence Wigner function directly (Thawed Moyal Dynamics). The “cat-trajectory” picture illustrated how the evolution of the coherence Wigner function’s statistical parameters are in turn a function of the instantaneous statistical parameters associated with each state composing the coherence. This suggests that the time-dependent statistical properties of coherence Wigner functions should relate to the time-dependent statistical properties of each state’s the population Wigner function. The advantage of solving the dynamics of the coherence in terms of populations as opposed to wavefunctions, is that the former are real distributions and can be estimated in terms of linearly scaling trajectory ensembles. The question is: “How to solve coherence dynamics in terms of populations?”

The answer provided in this chapter is to exploit a phase space relation called the Star

Coherence Identity. This chapter begins by introducing the identity. By itself the Star Coherence Identity isn't immediately useful because it resolves a quantum coherence into a product of populations up to an undetermined time-dependent phase. In order to determine the phase, the identity must be substituted into the set of equations of motion used to evolve the density. The second section details this approach for the Wigner-Moyal equation. New equations of motion for a pure state density of an N level quantum system expressed solely in terms of population Wigner functions and quantum phases are obtained. These equations are equivalent to the Wigner-Moyal equation, but with explicit dependence on off-diagonal elements removed. These equations of motion are called the Star Coherence Representation. The derivation of the Star Coherence Representation of the Wigner-Moyal equation is simple, but a bit cumbersome. It is included because it one of the primary original contributions of this thesis. The third section examines limiting case and approximations of the Star Coherence equations of motion. The chapter concludes with a discussion of the new equations of motion and points toward the following chapter which illustrates how they are solved using trajectory ensembles.

## 5.1 Star Coherence Identity

Throughout this thesis there have been a handful of hints that coherences can be regarded as some function of their populations. The Cross Wigner Transform of a coherent superposition factorizes into a sum population Wigner functions plus real portions of the coherence Wigner function (Eq. 3.12). This is nothing more than the phase space representation of double-slit experiment with the coherence Wigner function containing the quantum interference. Similarly, the Schwartz equality for a pure state densities relates the product of any two populations to a coherence element and its Hermitian conjugate  $\hat{\rho}_{11}\hat{\rho}_{22} = \hat{\rho}_{mn}\hat{\rho}_{nm}$ . In this section, a new phase space identity which relates a coherence Wigner function to the star

product of its populations Wigner function and a quantum phase is derived.

Let  $\{|\psi_n\rangle\}$  denote some an arbitrary basis, the elemental operators of the pure state density  $\hat{\rho}$  are

$$\hat{\rho}_{mm} = |\psi_m\rangle\langle\psi_m|, \quad \hat{\rho}_{mn} = |\psi_m\rangle\langle\psi_n|, \quad \hat{\rho}_{nm} = |\psi_n\rangle\langle\psi_m|, \quad \hat{\rho}_{nn} = |\psi_n\rangle\langle\psi_n|. \quad (5.1a - d)$$

the product of the two population elements  $\hat{\rho}_{mm}$  and  $\hat{\rho}_{nn}$  yield the relations

$$\hat{\rho}_{mm}\hat{\rho}_{nn} = |\psi_m\rangle\langle\psi_m|\psi_n\rangle\langle\psi_n| = \text{Tr}(\hat{\rho}_{nm})\hat{\rho}_{mn}, \quad (5.2)$$

and

$$\hat{\rho}_{nn}\hat{\rho}_{mm} = |\psi_n\rangle\langle\psi_n|\psi_m\rangle\langle\psi_m| = \text{Tr}(\hat{\rho}_{mn})\hat{\rho}_{nm}. \quad (5.3)$$

These products can be rearranged to show the coherence matrix elements are in turn proportional to their populations,

$$\hat{\rho}_{mn} = \frac{\hat{\rho}_{mm}\hat{\rho}_{nn}}{\text{Tr}(\hat{\rho}_{nm})} \quad \text{and} \quad \hat{\rho}_{nm} = \frac{\hat{\rho}_{nn}\hat{\rho}_{mm}}{\text{Tr}(\hat{\rho}_{mn})}. \quad (5.4a - b)$$

The traces over the coherence elements can be expressed as the inner products  $\text{Tr}(\hat{\rho}_{mn}) = \langle\psi_n|\psi_m\rangle$  and  $\text{Tr}(\hat{\rho}_{nm}) = \langle\psi_m|\psi_n\rangle$  with  $\text{Tr}(\hat{\rho}_{mn}) = \text{Tr}(\hat{\rho}_{nm})^*$ . Tracing over Eq. 5.4 gives

$$|\text{Tr}(\rho_{mn})|^2 = \text{Tr}(\hat{\rho}_{mm}\hat{\rho}_{nn}). \quad (5.5)$$

The trace of the coherence yields a complex number which can be expressed in polar form as a real magnitude and phase

$$\text{Tr}(\rho_{mn}) = |\text{Tr}(\rho_{mn})|e^{+i\phi} = \sqrt{\text{Tr}(\hat{\rho}_{11}\hat{\rho}_{22})}e^{+i\phi}. \quad (5.6)$$

One then arrive at the exact relationship between populations and coherence for two nonorthog-

onal pure states:

$$\hat{\rho}_{12} = \frac{\hat{\rho}_{11}\hat{\rho}_{22}e^{+i\phi}}{\sqrt{\text{Tr}(\hat{\rho}_{11}\hat{\rho}_{22})}}. \quad (5.7)$$

Weyl transforming both sides of Eq. 5.7 gives

$$\rho_{12}(\mathbf{q}, \mathbf{p}, t) = \frac{\rho_{11}(\mathbf{q}, \mathbf{p}, t) \star \rho_{22}(\mathbf{q}, \mathbf{p}, t)e^{+i\phi}}{\sqrt{\text{Tr}(\rho_{11}(\mathbf{q}, \mathbf{p}, t)\rho_{22}(\mathbf{q}, \mathbf{p}, t))}}. \quad (5.8)$$

Eq. 5.67 is called the *Star Coherence Identity*. This identity can be seen as a direct consequence of the Weyl symbol definition of the star product. Recall the Weyl Transform of the product of two Hilbert space operators can be expressed as the  $O_{\mathcal{W}}[\hat{A}\hat{B}] = A \star B$ . Taking

$$\hat{A} = \hat{\rho}_{mm} = |\psi_m\rangle\langle\psi_m| \quad \hat{B} = \hat{\rho}_{nn} = |\psi_n\rangle\langle\psi_n|,$$

gives

$$\begin{aligned} O_{\mathcal{W}}[\hat{\rho}_{mm}\hat{\rho}_{nn}] &= O_{\mathcal{W}}[|\psi_m\rangle\langle\psi_m|\psi_n\rangle\langle\psi_n|] = \rho_{mm} \star \rho_{nn} \\ &= \langle\psi_m|\psi_n\rangle O_{\mathcal{W}}[|\psi_m\rangle\langle\psi_n|] = \text{Tr}(\hat{\rho}_{nm}) O_{\mathcal{W}}[\hat{\rho}_{mn}] = \rho_{mm} \star \rho_{nn} \end{aligned} \quad (5.9)$$

which immediately yields

$$\rho_{mn} = \frac{\rho_{mm} \star \rho_{nn}}{\text{Tr}(\rho_{nm})} \quad (5.10)$$

where the trace in the denominator can be decomposed into a magnitude and phase according to Eq. 5.6.

## 5.2 Derivation of Star Coherence Equations of Motion

The fundamental issue with exploiting the Star Coherence Identity to solve the dynamics of quantum coherences in terms of populations is that the phase  $\phi$  is undetermined. Fortunately, an equation of motion for the phase can be obtained by substituting the identity into

the equation of motion for any exact or approximate representation of the Wigner-Moyal equation. In this section, this is done for an  $N$  level quantum system. The derivation has two main steps: first, the Star Coherence Identity is substituted into the populations equations of motion to eliminate the coherence. Second, an equation of motion for the phase is obtained by substituting the population equations of motion into the trace of the coherence.

### 5.2.1 Population Equation of Motion

Consider a  $N$  level quantum system undergoing unitary evolution. The equation of motion for an arbitrary matrix element is given by the quantum Liouville equation

$$i\hbar \frac{\partial \hat{\rho}_{mn}}{\partial t} = \sum_{l \in [1, N]} \hat{H}_{ml} \hat{\rho}_{ln} - \hat{\rho}_{ml} \hat{H}_{nl}. \quad (5.11)$$

For populations ( $m = n$ ), we have

$$i\hbar \frac{\partial \hat{\rho}_{nn}}{\partial t} = \sum_{l \in [1, N]} \hat{H}_{nl} \hat{\rho}_{ln} - \hat{\rho}_{nl} \hat{H}_{ln}. \quad (5.12)$$

Translating into the Wigner-Moyal Representation, yields the phase space equation

$$\frac{\partial \rho_{nm}}{\partial t} = \frac{1}{i\hbar} \sum_{l \in [1, N]} H_{nl} \star \rho_{ln} - \rho_{nl} \star H_{ln}. \quad (5.13)$$

There are two distinct case in the sum: (1)  $l \neq n$  and (2)  $l = n$ , factoring out the latter gives

$$\begin{aligned} \frac{\partial \rho_{nn}}{\partial t} &= \frac{1}{i\hbar} (H_{nn} \star \rho_{nn} - \rho_{nn} \star H_{nn}) + \frac{1}{i\hbar} \sum_{\substack{l \in [1, N] \\ l \neq n}} H_{nl} \star \rho_{ln} - \rho_{nl} \star H_{ln} \\ &= [H_{nn}, \rho_{nn}]_{\star} + \frac{1}{i\hbar} \sum_{\substack{l \in [1, N] \\ l \neq n}} H_{nl} \star \rho_{ln} - \rho_{nl} \star H_{ln} \end{aligned} \quad (5.14)$$

Now because  $\rho$  and  $H$  are Hermitian

$$\rho_{mn} = \overline{\rho_{nm}} \quad \text{and} \quad H_{mn} = \overline{H_{nm}}.$$

using the conjugation  $\overline{f \star g} = \bar{g} \star \bar{f}$  and the identity

$$\text{Im}(z) = \frac{1}{2i} (z - \bar{z}) \quad (5.15)$$

Eq. 5.14 becomes

$$\frac{\partial \rho_{nn}}{\partial t} = [H_{nn}, \rho_{nn}]_{\star} + \frac{2}{\hbar} \sum_{\substack{l \in [1, N] \\ l \neq n}} \text{Im}(H_{nl} \star \rho_{ln}). \quad (5.16)$$

Now recall the Star Coherence Identity,

$$\rho_{ln} = \frac{\rho_{ll} \star \rho_{nn} e^{+i\phi_{ln}}}{\sqrt{\text{Tr}(\rho_{ll} \star \rho_{nn})}}. \quad (5.17)$$

Hermiticity of  $\rho$  implies  $\rho_{ln} = \overline{\rho_{nl}}$ ,  $\phi_{ln} = -\phi_{nl} \in \mathbb{R}$ , and  $\sqrt{\text{Tr}(\rho_{ll} \star \rho_{nn})} \in \mathbb{R}$ . Substituting Eq. 5.17 into Eq. 5.16 gives an exact formal representation of the population elements in terms of only other populations and phases,

$$\frac{\partial \rho_{nn}}{\partial t} = [H_{nn}, \rho_{nn}]_{\star} + \frac{2}{\hbar} \sum_{\substack{l \in [1, N] \\ l \neq n}} \frac{\text{Im}(H_{nl} \star \rho_{ll} \star \rho_{nn} e^{+i\phi_{ln}})}{\sqrt{\text{Tr}(\rho_{ll} \star \rho_{nn})}}. \quad (5.18)$$

Now need an equations of motion for the phases  $\phi$  are needed.



## 5.2.2 Phase Equation of Motion

To obtain an equations of motion for  $\phi$  in terms of the populations, two equations of motion for the trace of the coherence element are derived and equated. This then allows one them to isolate equations of motion for the phases  $\phi$ . Let

$$X_{mn} = \text{Tr}(\rho_{mn}) \quad (5.19)$$

and let  $\dot{X}_{mn}$  denote its time-derivative. (1) The first equation of motion for  $X_{mn}$  is obtained by tracing over the Star Coherence Identity (Eq. 5.17) to give

$$X_{mn} = \sqrt{\text{Tr}(\rho_{mm} \star \rho_{nn})} e^{+i\phi_{mn}} \quad (5.20)$$

then differentiating  $\dot{X}_{mn} = \frac{d}{dt} X_{mn}$ . (2) The second equation of motion is obtained by tracing over the equation of motion for off-diagonal ( $m \neq n$ ) elements in the Wigner-Moyal equation

$$\dot{X}_{mn} = \frac{dX_{mn}}{dt} = \frac{\partial \text{Tr}(\rho_{mn})}{\partial t} = \frac{1}{i\hbar} \sum_{\substack{l \in [1, N] \\ m \neq n}} \text{Tr}(H_{ml} \star \rho_{ln} - \rho_{ml} \star H_{ln}). \quad (5.21)$$

Equating expressions obtained for  $\dot{X}_{mn}$  by (1) and (2) allows one to isolate equations of motion for  $\phi_{mn}$  exclusively in terms of the instantaneous values of populations and other phases. Although the algebra is straightforward, the derivation is lengthy so (1) and (2) are split into separate sub-subsections for clarity.

## $\dot{X}_{mn}$ by Star Coherence Identity

Differentiating with respect to time and applying the product rule to Eq. 5.20 gives

$$\begin{aligned}\dot{X}_{mn} &= \frac{e^{+i\phi_{mn}} \left( \frac{d}{dt} \text{Tr}(\rho_{mm} \star \rho_{nn}) \right)}{2\sqrt{\text{Tr}(\rho_{mm} \star \rho_{nn})}} + ie^{+i\phi_{mn}} \sqrt{\text{Tr}(\rho_{mm} \star \rho_{nn})} \dot{\phi}_{mn} \\ &= \frac{e^{+i\phi_{mn}} (\text{Tr}(\dot{\rho}_{mm} \star \rho_{nn} + \rho_{mm} \star \dot{\rho}_{nn}))}{2\sqrt{\text{Tr}(\rho_{mm} \star \rho_{nn})}} + ie^{+i\phi_{mn}} \sqrt{\text{Tr}(\rho_{mm} \star \rho_{nn})} \dot{\phi}_{mn}.\end{aligned}\quad (5.22)$$

The next step is to substitute in the population equations of motion into the argument of the trace in Eq. 5.22. By Eq. 5.18, the population equations are

$$\dot{\rho}_{mm} = \frac{\partial \rho_{mm}}{\partial t} = [H_{mm}, \rho_{mm}]_{\star} + \frac{2}{\hbar} \sum_{\substack{l \in [1, N] \\ l \neq m}} \frac{\text{Im} (H_{ml} \star \rho_{ll} \star \rho_{mm} e^{+i\phi_{lm}})}{\sqrt{\text{Tr}(\rho_{ll} \star \rho_{mm})}} \quad (5.23)$$

and

$$\dot{\rho}_{nn} = \frac{\partial \rho_{nn}}{\partial t} = [H_{nn}, \rho_{nn}]_{\star} + \frac{2}{\hbar} \sum_{\substack{l \in [1, N] \\ l \neq n}} \frac{\text{Im} (H_{nl} \star \rho_{ll} \star \rho_{nn} e^{+i\phi_{ln}})}{\sqrt{\text{Tr}(\rho_{ll} \star \rho_{nn})}}, \quad (5.24)$$

Splitting the trace,  $\text{Tr}(X + Y) = \text{Tr}(X) + \text{Tr}(Y)$ , consider the first trace in the numerator of Eq. 5.22. Upon substituting  $\dot{\rho}_{mm}$ :

$$\text{Tr}(\dot{\rho}_{mm} \star \rho_{nn}) = \text{Tr}([H_{mm}, \rho_{mm}]_{\star} \star \rho_{nn}) + \frac{2}{\hbar} \sum_{\substack{l \in [1, N] \\ l \neq m}} \frac{\text{Im} (\text{Tr}(H_{ml} \star \rho_{ll} \star \rho_{mm} \star \rho_{nn} e^{+i\phi_{lm}}))}{\sqrt{\text{Tr}(\rho_{ll} \star \rho_{mm})}} \quad (5.25)$$

because  $\text{Tr}(\text{Im}(Z)) = \text{Im}(\text{Tr}(Z))$ . Pulling from the sum the term for which  $l = n$  gives,

$$\begin{aligned}\text{Tr}(\dot{\rho}_{mm} \star \rho_{nn}) &= \text{Tr}([H_{mm}, \rho_{mm}]_{\star} \star \rho_{nn}) + \frac{2}{\hbar} \frac{\text{Im} (\text{Tr}(H_{mn} \star \rho_{nn} \star \rho_{mm} \star \rho_{nn} e^{+i\phi_{nm}}))}{\sqrt{\text{Tr}(\rho_{nn} \star \rho_{mm})}} \\ &\quad + \frac{2}{\hbar} \sum_{\substack{l \in [1, N] \\ l \neq m \neq n}} \frac{\text{Im} (\text{Tr}(H_{ml} \star \rho_{ll} \star \rho_{mm} \star \rho_{nn} e^{+i\phi_{lm}}))}{\sqrt{\text{Tr}(\rho_{ll} \star \rho_{mm})}}\end{aligned}\quad (5.26)$$

To simplify the second term, recognize that

$$\begin{aligned}\rho_{nn} \star \rho_{mm} \star \rho_{nn} &= \hat{\rho}_{nm} \hat{\rho}_{mm} \hat{\rho}_{nn} = |n\rangle \langle n|m\rangle \langle m|n\rangle \langle n| \\ &= \langle n|m\rangle \langle m|n\rangle |n\rangle \langle n| = X_{mn} X_{nm} \rho_{nn} = |X_{mn}|^2 \rho_{nn}\end{aligned}\quad (5.27)$$

where

$$\langle n|m\rangle = \text{Tr}(\rho_{mn}) = X_{mn} = \sqrt{\text{Tr}(\rho_{mm} \star \rho_{nn})} e^{+i\phi_{mn}}. \quad (5.28)$$

Hermiticity implies  $X_{mn} = \bar{X}_{nm}$ . Thus Eq. 5.31 becomes

$$\rho_{nn} \star \rho_{mm} \star \rho_{nn} = \text{Tr}(\rho_{mm} \star \rho_{nn}) \rho_{nn} \quad (5.29)$$

and

$$\begin{aligned}& \frac{2 \text{Im} \left( \text{Tr} \left( H_{mn} \star \rho_{nn} \star \rho_{mm} \star \rho_{nn} e^{+i\phi_{nm}} \right) \right)}{\hbar \sqrt{\text{Tr}(\rho_{nn} \star \rho_{mm})}} \\ &= \frac{2}{\hbar} \sqrt{\text{Tr}(\rho_{mm} \star \rho_{nn})} \text{Im} \left( \text{Tr} \left( H_{mn} \star \rho_{nn} e^{+i\phi_{nm}} \right) \right)\end{aligned}\quad (5.30)$$

by using cyclic permutation of the trace,  $\text{Tr}(Y \star Z) = \text{Tr}(Z \star Y)$ .

By a similar analysis the third term in Eq. 5.26 can be simplified. Noting

$$\begin{aligned}\rho_{ll} \star \rho_{mm} \star \rho_{nn} &= \hat{\rho}_{ll} \hat{\rho}_{mm} \hat{\rho}_{nn} = |l\rangle \langle l|m\rangle \langle m|n\rangle \langle n| \\ &= \langle m|l\rangle \langle n|m\rangle |l\rangle \langle n| = X_{ml} X_{nm} \rho_{ln} \\ &= \sqrt{\text{Tr}(\rho_{mm} \star \rho_{ll})} e^{+i\phi_{ml}} \sqrt{\text{Tr}(\rho_{nn} \star \rho_{mm})} e^{+i\phi_{nm}} \frac{\rho_{ll} \star \rho_{nn} e^{+i\phi_{ln}}}{\sqrt{\text{Tr}(\rho_{ll} \star \rho_{nn})}} \\ &= \frac{\sqrt{\text{Tr}(\rho_{mm} \star \rho_{ll})} \sqrt{\text{Tr}(\rho_{nn} \star \rho_{mm})} e^{+i(\phi_{ln} + \phi_{ml} + \phi_{nm})}}{\sqrt{\text{Tr}(\rho_{ll} \star \rho_{nn})}} \rho_{ll} \star \rho_{nn}\end{aligned}\quad (5.31)$$

then

$$\begin{aligned}
& \frac{2}{\hbar} \sum_{\substack{l \in [1, N] \\ l \neq m \neq n}} \frac{\text{Im} \left( \text{Tr} \left( H_{ml} \star \rho_{ll} \star \rho_{mm} \star \rho_{nn} e^{+i\phi_{lm}} \right) \right)}{\sqrt{\text{Tr} \left( \rho_{ll} \star \rho_{mm} \right)}} \\
&= \frac{2}{\hbar} \sum_{\substack{l \in [1, N] \\ l \neq m \neq n}} \frac{\sqrt{\text{Tr} \left( \rho_{nm} \star \rho_{mm} \right)}}{\sqrt{\text{Tr} \left( \rho_{ll} \star \rho_{nn} \right)}} \text{Im} \left( \text{Tr} \left( H_{ml} \star \rho_{ll} \star \rho_{nn} \right) e^{+i(\phi_{ln} + \phi_{nm})} \right)
\end{aligned} \tag{5.32}$$

where the fact  $\phi_{ml} = -\phi_{lm}$  has been applied. Combining results from Eq. 5.30 and Eq. 5.32, Eq. 5.26 becomes

$$\begin{aligned}
\text{Tr} \left( \dot{\rho}_{mm} \star \rho_{nn} \right) &= \text{Tr} \left( [H_{mm}, \rho_{mm}]_{\star} \star \rho_{nn} \right) + \frac{2}{\hbar} \sqrt{\text{Tr} \left( \rho_{mm} \star \rho_{nn} \right)} \text{Im} \left( \text{Tr} \left( H_{mn} \star \rho_{nn} \right) e^{+i\phi_{nm}} \right) \\
&+ \frac{2}{\hbar} \sum_{\substack{l \in [1, N] \\ l \neq m \neq n}} \frac{\sqrt{\text{Tr} \left( \rho_{nn} \star \rho_{mm} \right)}}{\sqrt{\text{Tr} \left( \rho_{ll} \star \rho_{nn} \right)}} \text{Im} \left( \text{Tr} \left( H_{ml} \star \rho_{ll} \star \rho_{nn} \right) e^{+i(\phi_{ln} + \phi_{nm})} \right)
\end{aligned} \tag{5.33}$$

And because  $\text{Tr} \left( \rho_{mm} \star \dot{\rho}_{nn} \right) = \text{Tr} \left( \dot{\rho}_{nn} \star \rho_{mm} \right)$ , swapping indices  $m$  with  $n$  in Eq. 5.33 gives

$$\begin{aligned}
\text{Tr} \left( \dot{\rho}_{nn} \star \rho_{mm} \right) &= \text{Tr} \left( [H_{nn}, \rho_{nn}]_{\star} \star \rho_{mm} \right) + \frac{2}{\hbar} \sqrt{\text{Tr} \left( \rho_{nn} \star \rho_{mm} \right)} \text{Im} \left( \text{Tr} \left( H_{nm} \star \rho_{mm} \right) e^{+i\phi_{mn}} \right) \\
&+ \frac{2}{\hbar} \sum_{\substack{l \in [1, N] \\ l \neq m \neq n}} \frac{\sqrt{\text{Tr} \left( \rho_{mm} \star \rho_{nn} \right)}}{\sqrt{\text{Tr} \left( \rho_{ll} \star \rho_{mm} \right)}} \text{Im} \left( \text{Tr} \left( H_{nl} \star \rho_{ll} \star \rho_{mm} \right) e^{+i(\phi_{lm} + \phi_{mn})} \right)
\end{aligned} \tag{5.34}$$

Combining Eq. 5.33 and Eq. 5.34 yields

$$\begin{aligned}
& \text{Tr}(\dot{\rho}_{mm} \star \rho_{nn} + \rho_{mm} \star \dot{\rho}_{nn}) \\
&= \underbrace{\text{Tr}([H_{mm}, \rho_{mm}]_{\star} \star \rho_{nn}) + \text{Tr}([H_{nn}, \rho_{nn}]_{\star} \star \rho_{mm})}_{(A)} \\
&+ \underbrace{\frac{2}{\hbar} \sqrt{\text{Tr}(\rho_{mm} \star \rho_{nn})} (\text{Im}(\text{Tr}(H_{mn} \star \rho_{nn}) e^{+i\phi_{nm}}) + \text{Im}(\text{Tr}(H_{nm} \star \rho_{mm}) e^{+i\phi_{mn}}))}_{(B)} \\
&+ \underbrace{\frac{2}{\hbar} \sum_{\substack{l \in [1, N] \\ l \neq m \neq n}} \frac{\sqrt{\text{Tr}(\rho_{nn} \star \rho_{mm})}}{\sqrt{\text{Tr}(\rho_{ll} \star \rho_{nn})}} \text{Im}(\text{Tr}(H_{ml} \star \rho_{ll} \star \rho_{nn}) e^{+i(\phi_{ln} + \phi_{nm})})}_{(C_1)} \\
&+ \underbrace{\frac{2}{\hbar} \sum_{\substack{l \in [1, N] \\ l \neq m \neq n}} \frac{\sqrt{\text{Tr}(\rho_{mm} \star \rho_{nn})}}{\sqrt{\text{Tr}(\rho_{ll} \star \rho_{mm})}} \text{Im}(\text{Tr}(H_{nl} \star \rho_{ll} \star \rho_{mm}) e^{+i(\phi_{lm} + \phi_{mn})})}_{(C_2)}.
\end{aligned} \tag{5.35}$$

Now to simplify term (A), expand the commutators and collect like terms:

$$\begin{aligned}
(A) &= \text{Tr}([H_{mm}, \rho_{mm}]_{\star} \star \rho_{nn}) + \text{Tr}([H_{nn}, \rho_{nn}]_{\star} \star \rho_{mm}) \\
&= \frac{1}{i\hbar} (\text{Tr}((H_{mm} - H_{nn}) \star \rho_{mm} \star \rho_{nn}) - \text{Tr}((H_{mm} - H_{nn}) \star \rho_{nn} \star \rho_{mm})) \\
&= \frac{1}{i} (\text{Tr}(\omega_{mn} \star \rho_{mm} \star \rho_{nn}) - \text{Tr}(\omega_{mn} \star \rho_{nn} \star \rho_{mm}))
\end{aligned} \tag{5.36}$$

where the difference potential Weyl symbol

$$\omega_{mn} = \frac{H_{mm} - H_{nn}}{\hbar}. \tag{5.37}$$

has been introduced. Cyclicly permuting the rightmost trace in the last equality of Eq. 5.36

yields

$$\begin{aligned}
\textcircled{A} &= \frac{1}{i} (\text{Tr} (\omega_{mn} \star \rho_{mm} \star \rho_{nn}) - \text{Tr} (\rho_{nn} \star \rho_{mm} \star \omega_{mn})) \\
&= \frac{1}{i} \left( \text{Tr} (\omega_{mn} \star \rho_{mm} \star \rho_{nn}) - \overline{\text{Tr} (\omega_{mn} \star \rho_{mm} \star \rho_{nn})} \right).
\end{aligned} \tag{5.38}$$

This follows from the fact  $\omega_{mn} \in \mathbb{R}$ ,  $\rho_{mm} \in \mathbb{R}$ , and  $\rho_{nn} \in \mathbb{R}$  and

$$\overline{\omega_{mn} \star \rho_{mm} \star \rho_{nn}} = \overline{\rho_{nn}} \star \overline{\rho_{mm}} \star \overline{\omega_{mn}} = \rho_{nn} \star \rho_{mm} \star \omega_{mn}. \tag{5.39}$$

Thus,

$$\textcircled{A} = 2 \text{Im} (\text{Tr} (\omega_{mn} \star \rho_{mm} \star \rho_{nn})). \tag{5.40}$$

Now to simplify  $\textcircled{B}$ . Recall,

$$\textcircled{B} = \frac{2}{\hbar} \sqrt{\text{Tr} (\rho_{mm} \star \rho_{nn})} (\text{Im} (\text{Tr} (H_{mn} \star \rho_{nn}) e^{+i\phi_{nm}}) + \text{Im} (\text{Tr} (H_{nm} \star \rho_{mm}) e^{+i\phi_{mn}})) \tag{5.41}$$

Expanding the sum of two imaginary terms gives and because  $H_{mn} = \overline{H_{nm}}$  and  $\phi_{mn} = -\phi_{nm}$ , Eq. 5.41 becomes

$$\begin{aligned}
&\text{Im} (\text{Tr} (H_{mn} \star \rho_{nn}) e^{+i\phi_{nm}}) + \text{Im} (\text{Tr} (H_{nm} \star \rho_{mm}) e^{+i\phi_{mn}}) \\
&= \frac{1}{2i} (-\text{Tr} (H_{mn} \star \delta_{mn}) e^{-i\phi_{mn}} + \text{Tr} (\delta_{mn} \star \overline{H_{mn}}) e^{+i\phi_{mn}}) \\
&= -\frac{1}{2i} (\text{Tr} (H_{mn} \star \delta_{mn}) e^{-i\phi_{mn}} - \text{Tr} (\delta_{mn} \star \overline{H_{mn}}) e^{+i\phi_{mn}}) \\
&= -\text{Im} (\text{Tr} (H_{mn} \star \delta_{mn}) e^{-i\phi_{mn}})
\end{aligned} \tag{5.42}$$

where the population difference Weyl symbol

$$\delta_{mn} = \rho_{mm} - \rho_{nn} \tag{5.43}$$

has been introduced. And thus Eq. 5.41 reduces to

$$\textcircled{B} = -\frac{2}{\hbar} \sqrt{\text{Tr}(\rho_{mm} \star \rho_{nn})} \text{Im}(\text{Tr}(H_{mn} \star \delta_{mn}) e^{-i\phi_{mn}}). \quad (5.44)$$

The trace in the numerator of Eq. 5.22 reduces to:

$$\begin{aligned} \text{Tr}(\dot{\rho}_{mm} \star \rho_{nn} + \rho_{mm} \star \dot{\rho}_{nn}) &= \textcircled{A} + \textcircled{B} + \textcircled{C_1} + \textcircled{C_2} \\ &= 2 \text{Im}(\text{Tr}(\omega_{mn} \star \rho_{mm} \star \rho_{nn})) - \frac{2}{\hbar} \sqrt{\text{Tr}(\rho_{mm} \star \rho_{nn})} \text{Im}(\text{Tr}(H_{mn} \star \delta_{mn}) e^{-i\phi_{mn}}) \\ &+ \frac{2}{\hbar} \sum_{\substack{l \in [1, N] \\ l \neq m \neq n}} \frac{\sqrt{\text{Tr}(\rho_{nn} \star \rho_{mm})}}{\sqrt{\text{Tr}(\rho_{ll} \star \rho_{nn})}} \text{Im}(\text{Tr}(H_{ml} \star \rho_{ll} \star \rho_{nn}) e^{+i(\phi_{ln} + \phi_{nm})}) \\ &+ \frac{2}{\hbar} \sum_{\substack{l \in [1, N] \\ l \neq m \neq n}} \frac{\sqrt{\text{Tr}(\rho_{mm} \star \rho_{nn})}}{\sqrt{\text{Tr}(\rho_{ll} \star \rho_{mm})}} \text{Im}(\text{Tr}(H_{nl} \star \rho_{ll} \star \rho_{mm}) e^{+i(\phi_{lm} + \phi_{mn})}) \end{aligned} \quad (5.45)$$

Substituting Eq. 5.45 into Eq. 5.22, the first equation of motion for  $X_{mn}$  is recovered

$$\begin{aligned} \dot{X}_{mn} &= i e^{+i\phi_{mn}} \sqrt{\text{Tr}(\rho_{mm} \star \rho_{nn})} \dot{\phi}_{mn} + \frac{\text{Im}(\text{Tr}(\omega_{mn} \star \rho_{mm} \star \rho_{nn})) e^{+i\phi_{mn}}}{\sqrt{\text{Tr}(\rho_{mm} \star \rho_{nn})}} \\ &- \frac{1}{\hbar} \text{Im}(\text{Tr}(H_{mn} \star \delta_{mn}) e^{-i\phi_{mn}}) e^{+i\phi_{mn}} \\ &+ \frac{1}{\hbar} \sum_{\substack{l \in [1, N] \\ l \neq m \neq n}} \frac{e^{+i\phi_{mn}}}{\sqrt{\text{Tr}(\rho_{ll} \star \rho_{nn})}} \text{Im}(\text{Tr}(H_{ml} \star \rho_{ll} \star \rho_{nn}) e^{+i(\phi_{ln} + \phi_{nm})}) \\ &+ \frac{1}{\hbar} \sum_{\substack{l \in [1, N] \\ l \neq m \neq n}} \frac{e^{+i\phi_{mn}}}{\sqrt{\text{Tr}(\rho_{ll} \star \rho_{mm})}} \text{Im}(\text{Tr}(H_{nl} \star \rho_{ll} \star \rho_{mm}) e^{+i(\phi_{lm} + \phi_{mn})}). \end{aligned} \quad (5.46)$$

### $\dot{X}_{mn}$ by Wigner-Moyal Equation

Returning to Eq. 5.21 splitting the trace over the difference  $\text{Tr}(Y - Z) = \text{Tr}(Y) - \text{Tr}(Z)$  gives

$$\dot{X}_{mn} = \frac{1}{i\hbar} \sum_{\substack{l \in [1, N] \\ m \neq n}} \text{Tr}(H_{ml} \star \rho_{ln}) - \text{Tr}(\rho_{ml} \star H_{ln}) \quad (5.47)$$

With an eye towards expressing  $\dot{X}_{mn}$  such that the difference potential  $\omega_{mn}$  and population difference  $\delta_{mn}$  are segregated from non-adjacent couplings, recognize three distinct cases in the sum of Eq. 5.47. There is (i)  $l = m, m \neq n$ , (ii)  $l = n, m \neq n$ , and (iii)  $l \neq m \neq n$ . Pulling  $l = m$  and  $l = n$  from the sum gives:

$$\begin{aligned} \dot{X}_{mn} &= \frac{1}{i\hbar} \text{Tr}(H_{mm} \star \rho_{mn}) - \text{Tr}(\rho_{mm} \star H_{mn}) + \frac{1}{i\hbar} \text{Tr}(H_{mn} \star \rho_{nn}) - \text{Tr}(\rho_{mn} \star H_{nn}) \\ &\quad + \frac{1}{i\hbar} \sum_{\substack{l \in [1, N] \\ l \neq m \neq n}} \text{Tr}(H_{ml} \star \rho_{ln}) - \text{Tr}(\rho_{ml} \star H_{ln}) \\ &= \frac{1}{i\hbar} (\text{Tr}(H_{mm} \star \rho_{mn}) - \text{Tr}(H_{nn} \star \rho_{mn}) - \text{Tr}(H_{mn} \star \rho_{mm}) + \text{Tr}(H_{mn} \star \rho_{nn})) \\ &\quad + \frac{1}{i\hbar} \sum_{\substack{l \in [1, N] \\ l \neq m \neq n}} \text{Tr}(H_{ml} \star \rho_{ln}) - \text{Tr}(\rho_{ml} \star H_{ln}) \\ &= \frac{1}{i\hbar} (\text{Tr}((H_{mm} - H_{nn}) \star \rho_{mn}) - \text{Tr}(H_{mn} \star (\rho_{mm} - \rho_{nn}))) \\ &\quad + \frac{1}{i\hbar} \sum_{\substack{l \in [1, N] \\ l \neq m \neq n}} \text{Tr}(H_{ml} \star \rho_{ln}) - \text{Tr}(\rho_{ml} \star H_{ln}) \\ &= \underbrace{\frac{1}{i} \text{Tr}(\omega_{mn} \star \rho_{mn})}_{(A')} - \underbrace{\frac{1}{i\hbar} \text{Tr}(H_{mn} \star \delta_{mn})}_{(B')} + \underbrace{\frac{1}{i\hbar} \sum_{\substack{l \in [1, N] \\ l \neq m \neq n}} \text{Tr}(H_{ml} \star \rho_{ln})}_{(C'_1)} - \underbrace{\frac{1}{i\hbar} \sum_{\substack{l \in [1, N] \\ l \neq m \neq n}} \text{Tr}(\rho_{ml} \star H_{ln})}_{(C'_2)} \end{aligned} \quad (5.48)$$



Now substituting the Star Coherence Identities:

$$\rho_{mn} = \frac{\rho_{mm} \star \rho_{nn} e^{+i\phi_{mn}}}{\sqrt{\text{Tr}(\rho_{mm} \star \rho_{nn})}} \quad (5.49)$$

$$\rho_{ln} = \frac{\rho_{ll} \star \rho_{nn} e^{+i\phi_{ln}}}{\sqrt{\text{Tr}(\rho_{ll} \star \rho_{nn})}} \quad (5.50)$$

$$\rho_{ml} = \frac{\rho_{mm} \star \rho_{ll} e^{+i\phi_{ml}}}{\sqrt{\text{Tr}(\rho_{mm} \star \rho_{ll})}} \quad (5.51)$$

into  $\textcircled{A'}$ ,  $\textcircled{C'_1}$ , and  $\textcircled{C'_2}$  gives the following equations:

$$\begin{aligned} \textcircled{A'} &= \frac{1}{i} \text{Tr}(\omega_{mn} \star \rho_{mn}) = \frac{1}{i} \text{Tr} \left( \omega_{mn} \star \frac{\rho_{mm} \star \rho_{nn} e^{+i\phi_{mn}}}{\sqrt{\text{Tr}(\rho_{mm} \star \rho_{nn})}} \right) \\ &= \frac{1}{i} \frac{\text{Tr}(\omega_{mn} \star \rho_{mm} \star \rho_{nn}) e^{+i\phi_{mn}}}{\sqrt{\text{Tr}(\rho_{mm} \star \rho_{nn})}}, \end{aligned} \quad (5.52)$$

$$\begin{aligned} \textcircled{C'_1} &= \frac{1}{i\hbar} \sum_{\substack{l \in [1, N] \\ l \neq m \neq n}} \text{Tr}(H_{ml} \star \rho_{ln}) = \frac{1}{i\hbar} \sum_{\substack{l \in [1, N] \\ l \neq m \neq n}} \text{Tr} \left( H_{ml} \star \frac{\rho_{ll} \star \rho_{nn} e^{+i\phi_{ln}}}{\sqrt{\text{Tr}(\rho_{ll} \star \rho_{nn})}} \right) \\ &= \frac{1}{i\hbar} \sum_{\substack{l \in [1, N] \\ l \neq m \neq n}} \frac{\text{Tr}(H_{ml} \star \rho_{ll} \star \rho_{nn}) e^{+i\phi_{ln}}}{\sqrt{\text{Tr}(\rho_{ll} \star \rho_{nn})}}, \end{aligned} \quad (5.53)$$

$$\begin{aligned}
\textcircled{C}'_2 &= -\frac{1}{i\hbar} \sum_{\substack{l \in [1, N] \\ l \neq m \neq n}} \text{Tr} (H_{ln} \star \rho_{ml}) = -\frac{1}{i\hbar} \sum_{\substack{l \in [1, N] \\ l \neq m \neq n}} \text{Tr} \left( H_{ln} \star \frac{\rho_{mm} \star \rho_{ll} e^{+i\phi_{ml}}}{\sqrt{\text{Tr} (\rho_{mm} \star \rho_{ll})}} \right) \\
&= -\frac{1}{i\hbar} \sum_{\substack{l \in [1, N] \\ l \neq m \neq n}} \frac{\text{Tr} (H_{ln} \star \rho_{mm} \star \rho_{ll}) e^{+i\phi_{ml}}}{\sqrt{\text{Tr} (\rho_{mm} \star \rho_{ll})}}.
\end{aligned} \tag{5.54}$$

Thus,

$$\begin{aligned}
\dot{X}_{mn} &= \textcircled{A}' + \textcircled{B}' + \textcircled{C}'_1 + \textcircled{C}'_2 \\
&= \frac{1}{i} \frac{\text{Tr} (\omega_{mn} \star \rho_{mm} \star \rho_{nn}) e^{+i\phi_{mn}}}{\sqrt{\text{Tr} (\rho_{mm} \star \rho_{nn})}} - \frac{1}{i\hbar} \text{Tr} (H_{mn} \star \delta_{mn}) \\
&\quad + \frac{1}{i\hbar} \sum_{\substack{l \in [1, N] \\ l \neq m \neq n}} \frac{\text{Tr} (H_{ml} \star \rho_{ll} \star \rho_{nn}) e^{+i\phi_{ln}}}{\sqrt{\text{Tr} (\rho_{ll} \star \rho_{nn})}} - \frac{1}{i\hbar} \sum_{\substack{l \in [1, N] \\ l \neq m \neq n}} \frac{\text{Tr} (H_{ln} \star \rho_{mm} \star \rho_{ll}) e^{+i\phi_{ml}}}{\sqrt{\text{Tr} (\rho_{mm} \star \rho_{ll})}}.
\end{aligned} \tag{5.55}$$

## Equating $X_{mn}$ Equations of Motion

Now equating the first equation of motion (Eq. 5.46) with the second (Eq. 5.55) gives

$$\begin{aligned}
& \frac{1}{i} \frac{\text{Tr}(\omega_{mn} \star \rho_{mm} \star \rho_{nn}) e^{+i\phi_{mn}}}{\sqrt{\text{Tr}(\rho_{mm} \star \rho_{nn})}} - \frac{1}{i\hbar} \text{Tr}(H_{mn} \star \delta_{mn}) \\
& + \frac{1}{i\hbar} \sum_{\substack{l \in [1, N] \\ l \neq m \neq n}} \frac{\text{Tr}(H_{ml} \star \rho_{ll} \star \rho_{nn}) e^{+i\phi_{ln}}}{\sqrt{\text{Tr}(\rho_{ll} \star \rho_{nn})}} - \frac{1}{i\hbar} \sum_{\substack{l \in [1, N] \\ l \neq m \neq n}} \frac{\text{Tr}(H_{ln} \star \rho_{mm} \star \rho_{ll}) e^{+i\phi_{ml}}}{\sqrt{\text{Tr}(\rho_{mm} \star \rho_{ll})}} \\
& = i e^{+i\phi_{mn}} \sqrt{\text{Tr}(\rho_{mm} \star \rho_{nn})} \dot{\phi}_{mn} + \frac{\text{Im}(\text{Tr}(\omega_{mn} \star \rho_{mm} \star \rho_{nn})) e^{+i\phi_{mn}}}{\sqrt{\text{Tr}(\rho_{mm} \star \rho_{nn})}} \\
& - \frac{1}{\hbar} \text{Im}(\text{Tr}(H_{mn} \star \delta_{mn}) e^{-i\phi_{mn}}) e^{+i\phi_{mn}} \\
& + \frac{1}{\hbar} \sum_{\substack{l \in [1, N] \\ l \neq m \neq n}} \frac{e^{+i\phi_{mn}}}{\sqrt{\text{Tr}(\rho_{ll} \star \rho_{nn})}} \text{Im}(\text{Tr}(H_{ml} \star \rho_{ll} \star \rho_{nn}) e^{+i(\phi_{ln} + \phi_{nm})}) \\
& + \frac{1}{\hbar} \sum_{\substack{l \in [1, N] \\ l \neq m \neq n}} \frac{e^{+i\phi_{mn}}}{\sqrt{\text{Tr}(\rho_{ll} \star \rho_{mm})}} \text{Im}(\text{Tr}(H_{nl} \star \rho_{ll} \star \rho_{mm}) e^{+i(\phi_{lm} + \phi_{mn})}).
\end{aligned} \tag{5.56}$$

To begin to isolate  $\dot{\phi}$ , divide both sides by  $ie^{+i\phi_{mn}} \sqrt{\text{Tr}(\rho_{mm} \star \rho_{nn})}$  and Eq. 5.56 becomes

$$\begin{aligned}
& - \frac{\text{Tr}(\omega_{mn} \star \rho_{mm} \star \rho_{nn})}{\text{Tr}(\rho_{mm} \star \rho_{nn})} + \frac{1}{\hbar} \frac{\text{Tr}(H_{mn} \star \delta_{mn}) e^{+i\phi_{mn}}}{\sqrt{\text{Tr}(\rho_{mm} \star \rho_{nn})}} \\
& - \frac{1}{\hbar} \sum_{\substack{l \in [1, N] \\ l \neq m \neq n}} \frac{\text{Tr}(H_{ml} \star \rho_{ll} \star \rho_{nn}) e^{+i(\phi_{ln} - \phi_{mn})}}{\sqrt{\text{Tr}(\rho_{mm} \star \rho_{nn})} \sqrt{\text{Tr}(\rho_{ll} \star \rho_{nn})}} + \frac{1}{\hbar} \sum_{\substack{l \in [1, N] \\ l \neq m \neq n}} \frac{\text{Tr}(H_{ln} \star \rho_{mm} \star \rho_{ll}) e^{+i(\phi_{ml} - \phi_{mn})}}{\sqrt{\text{Tr}(\rho_{mm} \star \rho_{nn})} \sqrt{\text{Tr}(\rho_{mm} \star \rho_{ll})}} \\
& = \dot{\phi}_{mn} + \frac{1}{i} \frac{\text{Im}(\text{Tr}(\omega_{mn} \star \rho_{mm} \star \rho_{nn}))}{\text{Tr}(\rho_{mm} \star \rho_{nn})} - \frac{1}{i\hbar} \frac{\text{Im}(\text{Tr}(H_{mn} \star \delta_{mn}) e^{-i\phi_{mn}})}{\sqrt{\text{Tr}(\rho_{mm} \star \rho_{nn})}} \\
& + \frac{1}{i\hbar} \sum_{\substack{l \in [1, N] \\ l \neq m \neq n}} \frac{\text{Im}(\text{Tr}(H_{ml} \star \rho_{ll} \star \rho_{nn}) e^{+i(\phi_{ln} + \phi_{nm})})}{\sqrt{\text{Tr}(\rho_{mm} \star \rho_{nn})} \sqrt{\text{Tr}(\rho_{ll} \star \rho_{nn})}} \\
& + \frac{1}{i\hbar} \sum_{\substack{l \in [1, N] \\ l \neq m \neq n}} \frac{\text{Im}(\text{Tr}(H_{nl} \star \rho_{ll} \star \rho_{mm}) e^{+i(\phi_{lm} + \phi_{mn})})}{\sqrt{\text{Tr}(\rho_{mm} \star \rho_{nn})} \sqrt{\text{Tr}(\rho_{ll} \star \rho_{mm})}}.
\end{aligned} \tag{5.57}$$

Pulling  $\dot{\phi}_{mn}$  to the lefthand side yields

$$\begin{aligned}
\dot{\phi}_{mn} = & \underbrace{-\frac{\text{Tr}(\omega_{mn} \star \rho_{mm} \star \rho_{nn})}{\text{Tr}(\rho_{mm} \star \rho_{nn})} + \frac{i\text{Im}(\text{Tr}(\omega_{mn} \star \rho_{mm} \star \rho_{nn}))}{\text{Tr}(\rho_{mm} \star \rho_{nn})}}_{\textcircled{A''}} \\
& + \underbrace{\frac{\text{Tr}(H_{mn} \star \delta_{mn}) e^{+i\phi_{mn}}}{\hbar\sqrt{\text{Tr}(\rho_{mm} \star \rho_{nn})}} - \frac{i\text{Im}(\text{Tr}(H_{mn} \star \delta_{mn}) e^{+i\phi_{mn}})}{\hbar\sqrt{\text{Tr}(\rho_{mm} \star \rho_{nn})}}}_{\textcircled{B''}} \\
& - \underbrace{\frac{1}{\hbar} \sum_{\substack{l \in [1, N] \\ l \neq m \neq n}} \left( \frac{\text{Tr}(H_{ml} \star \rho_{ll} \star \rho_{nn}) e^{+i(\phi_{ln} - \phi_{mn})}}{\sqrt{\text{Tr}(\rho_{mm} \star \rho_{nn})} \sqrt{\text{Tr}(\rho_{ll} \star \rho_{nn})}} - \frac{i\text{Im}(\text{Tr}(H_{ml} \star \rho_{ll} \star \rho_{nn}) e^{+i(\phi_{ln} - \phi_{mn})})}{\sqrt{\text{Tr}(\rho_{mm} \star \rho_{nn})} \sqrt{\text{Tr}(\rho_{ll} \star \rho_{nn})}} \right)}_{\textcircled{C''_1}} \\
& + \underbrace{\frac{1}{\hbar} \sum_{\substack{l \in [1, N] \\ l \neq m \neq n}} \left( \frac{\text{Tr}(H_{ln} \star \rho_{mm} \star \rho_{ll}) e^{+i(\phi_{ml} - \phi_{mn})}}{\sqrt{\text{Tr}(\rho_{mm} \star \rho_{nn})} \sqrt{\text{Tr}(\rho_{ll} \star \rho_{mm})}} + \frac{i\text{Im}(\text{Tr}(H_{ln} \star \rho_{ll} \star \rho_{mm}) e^{+i(\phi_{lm} + \phi_{mn})})}{\sqrt{\text{Tr}(\rho_{mm} \star \rho_{nn})} \sqrt{\text{Tr}(\rho_{ll} \star \rho_{mm})}} \right)}_{\textcircled{C''_2}}.
\end{aligned} \tag{5.58}$$

Now to simplify  $\textcircled{A''}$ ,  $\textcircled{B''}$ ,  $\textcircled{C''_1}$ , and  $\textcircled{C''_2}$ . In  $\textcircled{A''}$ , let  $z_A = \text{Tr}(\omega_{mn} \star \rho_{mm} \star \rho_{nn})$ . Then

$$\begin{aligned}
\textcircled{A''} &= \frac{-(\text{Re}(z_A) + i\text{Im}(z_A)) + i\text{Im}(z_A)}{\text{Tr}(\rho_{mm} \star \rho_{nn})} = -\frac{\text{Re}(z_A)}{\text{Tr}(\rho_{mm} \star \rho_{nn})} \\
&= -\frac{\text{Re}(\text{Tr}(\omega_{mn} \star \rho_{mm} \star \rho_{nn}))}{\text{Tr}(\rho_{mm} \star \rho_{nn})}.
\end{aligned} \tag{5.59}$$

In  $\textcircled{B''}$ , let  $z_B = \text{Tr}(H_{mn} \star \delta_{mn}) e^{-i\phi_{mn}}$ . Then one has

$$\begin{aligned}
\textcircled{B''} &= \frac{\text{Re}(z_B) + i\text{Im}(z_B) - i\text{Im}(z_B)}{\hbar\sqrt{\text{Tr}(\rho_{mm} \star \rho_{nn})}} = \frac{\text{Re}(z_B)}{\hbar\sqrt{\text{Tr}(\rho_{mm} \star \rho_{nn})}} \\
&= \frac{\text{Re}(\text{Tr}(H_{mn} \star \delta_{mn}) e^{-i\phi_{mn}})}{\hbar\sqrt{\text{Tr}(\rho_{mm} \star \rho_{nn})}},
\end{aligned} \tag{5.60}$$

and similarly for  $\widehat{\textcircled{C}}_1''$ ,

$$\begin{aligned}
\widehat{\textcircled{C}}_1'' &= -\frac{1}{\hbar} \sum_{\substack{l \in [1, N] \\ l \neq m \neq n}} \left( \frac{\text{Tr} (H_{ml} \star \rho_{ll} \star \rho_{nn}) e^{+i(\phi_{ln} - \phi_{mn})}}{\sqrt{\text{Tr} (\rho_{mm} \star \rho_{nn})} \sqrt{\text{Tr} (\rho_{ll} \star \rho_{nn})}} - \frac{i \text{Im} (\text{Tr} (H_{ml} \star \rho_{ll} \star \rho_{nn}) e^{+i(\phi_{ln} - \phi_{mn})})}{\sqrt{\text{Tr} (\rho_{mm} \star \rho_{nn})} \sqrt{\text{Tr} (\rho_{ll} \star \rho_{nn})}} \right) \\
&= -\frac{1}{\hbar} \sum_{\substack{l \in [1, N] \\ l \neq m \neq n}} \frac{\text{Re} (\text{Tr} (H_{ml} \star \rho_{ll} \star \rho_{nn}) e^{+i(\phi_{ln} - \phi_{mn})})}{\sqrt{\text{Tr} (\rho_{mm} \star \rho_{nn})} \sqrt{\text{Tr} (\rho_{ll} \star \rho_{nn})}}.
\end{aligned} \tag{5.61}$$

For  $\widehat{\textcircled{C}}_2''$ , because  $\phi_{lm} = -\phi_{ml}$ ,  $H_{nl} = \overline{H_{ln}}$ , and using cyclic permutation of the trace then

$$\begin{aligned}
\widehat{\textcircled{C}}_2'' &= \frac{1}{\hbar} \sum_{\substack{l \in [1, N] \\ l \neq m \neq n}} \left( \frac{\text{Tr} (H_{ln} \star \rho_{mm} \star \rho_{ll}) e^{+i(\phi_{ml} - \phi_{mn})}}{\sqrt{\text{Tr} (\rho_{mm} \star \rho_{nn})} \sqrt{\text{Tr} (\rho_{ll} \star \rho_{mm})}} + \frac{i \text{Im} (\text{Tr} (\rho_{ll} \star \rho_{mm} \star \overline{H_{ln}}) e^{-i(\phi_{ml} - \phi_{mn})})}{\sqrt{\text{Tr} (\rho_{mm} \star \rho_{nn})} \sqrt{\text{Tr} (\rho_{ll} \star \rho_{mm})}} \right)
\end{aligned} \tag{5.62}$$

Let  $z_{C_2} = \text{Tr} (H_{ln} \star \rho_{mm} \star \rho_{ll}) e^{+i(\phi_{ml} - \phi_{mn})}$  then

$$\begin{aligned}
\widehat{\textcircled{C}}_2'' &= \frac{1}{\hbar} \sum_{\substack{l \in [1, N] \\ l \neq m \neq n}} \left( \frac{z_{C_2}}{\sqrt{\text{Tr} (\rho_{mm} \star \rho_{nn})} \sqrt{\text{Tr} (\rho_{ll} \star \rho_{mm})}} + \frac{i \text{Im} (\overline{z_{C_2}})}{\sqrt{\text{Tr} (\rho_{mm} \star \rho_{nn})} \sqrt{\text{Tr} (\rho_{ll} \star \rho_{mm})}} \right) \\
&= \frac{1}{\hbar} \sum_{\substack{l \in [1, N] \\ l \neq m \neq n}} \left( \frac{z_{C_2}}{\sqrt{\text{Tr} (\rho_{mm} \star \rho_{nn})} \sqrt{\text{Tr} (\rho_{ll} \star \rho_{mm})}} - \frac{i \text{Im} (z_{C_2})}{\sqrt{\text{Tr} (\rho_{mm} \star \rho_{nn})} \sqrt{\text{Tr} (\rho_{ll} \star \rho_{mm})}} \right) \\
&= \frac{1}{\hbar} \sum_{\substack{l \in [1, N] \\ l \neq m \neq n}} \left( \frac{\text{Re} (z_{C_2})}{\sqrt{\text{Tr} (\rho_{mm} \star \rho_{nn})} \sqrt{\text{Tr} (\rho_{ll} \star \rho_{mm})}} \right) \\
&= \frac{1}{\hbar} \sum_{\substack{l \in [1, N] \\ l \neq m \neq n}} \frac{\text{Re} (\text{Tr} (H_{ln} \star \rho_{mm} \star \rho_{ll}) e^{+i(\phi_{ml} - \phi_{mn})})}{\sqrt{\text{Tr} (\rho_{mm} \star \rho_{nn})} \sqrt{\text{Tr} (\rho_{ll} \star \rho_{mm})}}
\end{aligned} \tag{5.63}$$

because  $\text{Im} (\overline{z}) = -\text{Im} (z)$ .

Combining Eqs. 5.59-5.63 with Eq. 5.58 finally yields the phase equation of motion

$$\begin{aligned}
\dot{\phi}_{mn} &= \textcircled{A''} + \textcircled{B''} + \textcircled{C''_1} + \textcircled{C''_2} \\
&= -\frac{\text{Re}(\text{Tr}(\omega_{mn} \star \rho_{mm} \star \rho_{nn}))}{\text{Tr}(\rho_{mm} \star \rho_{nn})} + \frac{\text{Re}(\text{Tr}(H_{mn} \star \delta_{mn}) e^{-i\phi_{mn}})}{\hbar \sqrt{\text{Tr}(\rho_{mm} \star \rho_{nn})}} \\
&+ \frac{1}{\hbar} \sum_{\substack{l \in [1, N] \\ l \neq m \neq n}} \left( \frac{\text{Re}(\text{Tr}(H_{ln} \star \rho_{mm} \star \rho_{ll}) e^{+i(\phi_{ml} - \phi_{mn})})}{\sqrt{\text{Tr}(\rho_{mm} \star \rho_{nn})} \sqrt{\text{Tr}(\rho_{ll} \star \rho_{mm})}} - \frac{\text{Re}(\text{Tr}(H_{ml} \star \rho_{ll} \star \rho_{nn}) e^{+i(\phi_{ln} - \phi_{mn})})}{\sqrt{\text{Tr}(\rho_{mm} \star \rho_{nn})} \sqrt{\text{Tr}(\rho_{ll} \star \rho_{nn})}} \right).
\end{aligned} \tag{5.64}$$

Eq. 5.64 is the desired result. It expresses the evolution of the phases  $\phi$  in terms of only diagonal elements (populations) and their phases. The explicit dependence on the off-diagonal elements (coherences) has been removed. To recap, the goal was to obtain a representation of the Wigner-Moyal equation for an  $N$  level system where explicit dependence on the off-diagonal elements, the coherences, has been eliminated in favor of real-valued populations and phases. This was done by substituting the Star Coherence Identity into the Wigner-Moyal equation for an  $N$  level system. The unitary evolution of the density in phase space is thus given by  $N$  population equations of motion

$$\frac{\partial \rho_{nn}}{\partial t} = [H_{nn}, \rho_{nn}]_{\star} + \frac{2}{\hbar} \sum_{\substack{l \in [1, N] \\ l \neq n}} \frac{\text{Im}(H_{nl} \star \rho_{ll} \star \rho_{nn} e^{+i\phi_{ln}})}{\sqrt{\text{Tr}(\rho_{ll} \star \rho_{nn})}} \tag{5.65}$$

and  $N(N-1)/2$  phase equations of motion

$$\begin{aligned}
\dot{\phi}_{mn} &= -\frac{\text{Re}(\text{Tr}(\omega_{mn} \star \rho_{mm} \star \rho_{nn}))}{\text{Tr}(\rho_{mm} \star \rho_{nn})} + \frac{\text{Re}(\text{Tr}(H_{mn} \star \delta_{mn}) e^{-i\phi_{mn}})}{\hbar \sqrt{\text{Tr}(\rho_{mm} \star \rho_{nn})}} \\
&+ \frac{1}{\hbar} \sum_{\substack{l \in [1, N] \\ l \neq m \neq n}} \left( \frac{\text{Re}(\text{Tr}(H_{ln} \star \rho_{mm} \star \rho_{ll}) e^{+i(\phi_{ml} - \phi_{mn})})}{\sqrt{\text{Tr}(\rho_{mm} \star \rho_{nn})} \sqrt{\text{Tr}(\rho_{ll} \star \rho_{mm})}} - \frac{\text{Re}(\text{Tr}(H_{ml} \star \rho_{ll} \star \rho_{nn}) e^{+i(\phi_{ln} - \phi_{mn})})}{\sqrt{\text{Tr}(\rho_{mm} \star \rho_{nn})} \sqrt{\text{Tr}(\rho_{ll} \star \rho_{nn})}} \right).
\end{aligned} \tag{5.66}$$

because  $\phi_{mn} = -\phi_{nm}$  following from Hermiticity of  $\rho$ . Together this set of  $N(N + 1)/2$  differential equations solve the time-evolution of the  $N$  level density with the off-diagonal elements synthesized as needed by the  $N(N - 1)/2$  auxiliary equations:

$$\rho_{mn} = \frac{\rho_{mm} \star \rho_{nn} e^{+i\phi_{mn}}}{\sqrt{\text{Tr}(\rho_{mm} \star \rho_{nn})}}. \quad (5.67)$$

Note the lower triangular elements  $\rho_{nm}$  are obtained by conjugating the  $N(N - 1)/2$  upper triangular elements  $\rho_{mn}$ . Eqs. 5.65-5.67 are the *Star Coherence Representation* of the Wigner-Moyal equation and are an exact phase space representation of the  $N$  level quantum Liouville equation for a pure state density.

Before discussing this general result and some specific case, one can apply one further simplification to the Star Coherence equations of motion. Applying the trace reduction identities (Eqs. 3.101-3.102) to the Star Coherence equations of motion yields the final formal for  $N$ -Level system undergoing unitary evolution in the Wigner-Moyal representation:

$$\frac{\partial \rho_{nn}}{\partial t} = [H_{nn}, \rho_{nn}]_{\star} + \frac{2}{\hbar} \sum_{\substack{l \in [1, N] \\ l \neq n}} \frac{\text{Im} (H_{nl} \star \rho_{ll} \star \rho_{nn} e^{+i\phi_{ln}})}{\sqrt{\text{Tr} (\rho_{ll} \rho_{nn})}} \quad (5.68)$$

$$\begin{aligned} \dot{\phi}_{mn} = & -\frac{\text{Re} (\text{Tr} (\omega_{mn} (\rho_{mm} \star \rho_{nn})))}{\text{Tr} (\rho_{mm} \rho_{nn})} + \frac{\text{Re} (\text{Tr} (H_{mn} \delta_{mn}) e^{-i\phi_{mn}})}{\hbar \sqrt{\text{Tr} (\rho_{mm} \rho_{nn})}} \\ & + \frac{1}{\hbar} \sum_{\substack{l \in [1, N] \\ l \neq m \neq n}} \left( \frac{\text{Re} (\text{Tr} (H_{ln} (\rho_{mm} \star \rho_{ll})) e^{+i(\phi_{ml} - \phi_{mn})})}{\sqrt{\text{Tr} (\rho_{mm} \rho_{nn})} \sqrt{\text{Tr} (\rho_{ll} \rho_{mm})}} - \frac{\text{Re} (\text{Tr} (H_{ml} (\rho_{ll} \star \rho_{nn})) e^{+i(\phi_{ln} - \phi_{mn})})}{\sqrt{\text{Tr} (\rho_{mm} \rho_{nn})} \sqrt{\text{Tr} (\rho_{ll} \rho_{nn})}} \right) \end{aligned} \quad (5.69)$$

$$\rho_{mn} = \frac{\rho_{mm} \star \rho_{nn} e^{+i\phi_{mn}}}{\sqrt{\text{Tr} (\rho_{mm} \rho_{nn})}} \quad (5.70)$$

## 5.3 Special Cases and Approximations

In practice, the formal Star Coherence equations of motion are too complex to solve analytically. It is, however, worth noting there are unique cases and standard approximations of quantum dynamics which greatly simplify the them. Two are considered: the noncyclic nearest neighbor case and semiclassical truncation. The former, provides some insight into the dynamics of two level systems and the latter is nothing more than the semiclassical Liouville equation with dependence on the coherence elements eliminated.

### 5.3.1 Noncyclic Nearest Neighbor: 2LS - Factorization

When the Hamiltonian Weyl symbol can be block diagonalized into  $2 \times 2$  submatrices, this means all off-diagonal elements vanish excluding the nearest neighbors of diagonal (Fig. 5.1).



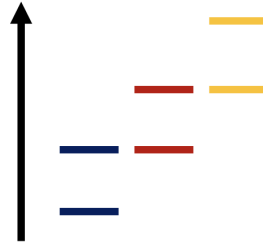
$$\mathbf{H} = \begin{pmatrix} H_{11} & H_{12} & H_{13} & H_{14} \\ H_{21} & H_{22} & H_{23} & H_{24} \\ H_{31} & H_{32} & H_{33} & H_{34} \\ H_{41} & H_{42} & H_{43} & H_{44} \end{pmatrix} = \begin{pmatrix} H_{11} & H_{12} & 0 & 0 \\ H_{21} & H_{22} & H_{23} & 0 \\ 0 & H_{32} & H_{33} & H_{34} \\ 0 & 0 & H_{43} & H_{44} \end{pmatrix}$$


Figure 5.1: Example of a noncyclic nearest neighbor Hamiltonian.

In this case, the  $N$  level system factorizes into  $N - 1$  coupled 2 level systems. In this case, the sum in the population equations of motion collapses to a single term

$$\frac{\partial \rho_{nn}}{\partial t} = [H_{nn}, \rho_{nn}]_{\star} + \frac{2 \operatorname{Im} (H_{nl} \star \rho_{ll} \star \rho_{nn} e^{+i\phi_{ln}})}{\hbar \sqrt{\operatorname{Tr} (\rho_{ll} \rho_{nn})}} \quad (5.71)$$

and vanishing of the the non-nearest neighbor off-diagonal element resulting in the vanishing in the last term in the phase equation of motions to yield

$$\dot{\phi}_{mn} = -\frac{\operatorname{Re} (\operatorname{Tr} (\omega_{mn} (\rho_{mm} \star \rho_{nn})))}{\operatorname{Tr} (\rho_{mm} \rho_{nn})} + \frac{\operatorname{Re} (\operatorname{Tr} (H_{mn} \delta_{mn}) e^{-i\phi_{mn}})}{\hbar \sqrt{\operatorname{Tr} (\rho_{mm} \rho_{nn})}}. \quad (5.72)$$

If the system is a 2 level system, Eqs. 5.71-5.72 are exact. For  $N > 2$  level systems this is an approximation. If, however, non-nearest neighbor off-diagonal elements are small in magnitude to relative to the diagonals and their nearest neighbor, the rightmost term in Eq. 5.69 can be treated perturbatively or approximated by averages over states.

The physical interpretation of Eq. 5.72 is straightforward. The rate of change of the phase between two populations in a coherence is a function of an phase space average of difference potential  $\omega_{mn}$  over the instantaneous values of the populations composing the coherence plus a phase space average of the population difference times its coupling (modulo the instantaneous value of the phase).

### 5.3.2 The 2 Level System and Semiclassical Truncation

Using the semiclassical truncation identities derived for star products and Moyal brackets (Appendix A), the Star Coherence equations of motion can be approximated by successive truncations in  $\mathcal{O}(\hbar)$ . The system's Hamiltonian Weyl symbol is

$$H = \begin{pmatrix} H_{11} & V \\ \bar{V} & H_{22} \end{pmatrix} \quad (5.73)$$

where  $V = H_{12}$ . And the exact quantum Star Coherence equations of motion are:

$$\frac{\partial \rho_{11}}{\partial t} = [H_{11}, \rho_{11}]_{\star} + \frac{2 \operatorname{Im} (V \star \rho_{22} \star \rho_{11} e^{+i\phi})}{\hbar \sqrt{\operatorname{Tr} (\rho_{11} \rho_{22})}}, \quad (5.74)$$

$$\frac{\partial \rho_{22}}{\partial t} = [H_{22}, \rho_{22}]_{\star} + \frac{2 \operatorname{Im} (\bar{V} \star \rho_{11} \star \rho_{22} e^{-i\phi})}{\hbar \sqrt{\operatorname{Tr} (\rho_{11} \rho_{22})}}, \quad (5.75)$$

$$\dot{\phi} = -\frac{\operatorname{Re} (\operatorname{Tr} (\omega (\rho_{11} \star \rho_{22})))}{\operatorname{Tr} (\rho_{11} \rho_{22})} + \frac{\operatorname{Re} (\operatorname{Tr} (V \delta) e^{-i\phi})}{\hbar \sqrt{\operatorname{Tr} (\rho_{11} \rho_{22})}}, \quad (5.76)$$

and

$$\rho_{12} = \frac{\rho_{11} \star \rho_{22} e^{+i\phi}}{\sqrt{\operatorname{Tr} (\rho_{11} \rho_{22})}} \quad (5.77)$$

where subscripts have been dropped:  $\phi = \phi_{12}$ ,  $\omega = \omega_{12}$ , and  $\delta_{12} = \delta$ .

Before proceeding the equation of motion can be shown to preserve probability. For unitary evolution the trace of the density is a constant of motion

$$\frac{\partial}{\partial t} \operatorname{Tr} (\rho) = \operatorname{Tr} \left( \frac{\partial \rho_{11}}{\partial t} + \frac{\partial \rho_{22}}{\partial t} \right) \quad (5.78)$$

Substituting in Eqs. 5.74-5.75, yields

$$\begin{aligned} \frac{\partial}{\partial t} \text{Tr}(\rho) &= \text{Tr}([H_{11}, \rho_{11}]_{\star}) + \text{Tr}([H_{22}, \rho_{22}]_{\star}) \\ &+ \frac{2}{\hbar} \frac{1}{\sqrt{\text{Tr}(\rho_{11} \rho_{22})}} (\text{Im}(\text{Tr}((V \star \rho_{22} \star \rho_{11}) e^{-i\phi})) + \text{Im}(\text{Tr}((\bar{V} \star \rho_{11} \star \rho_{22}) e^{+i\phi}))) \end{aligned}$$

Because the traces over the Moyal brackets vanish and again because  $\text{Im}(z) = -\text{Im}(\bar{z})$ , one has

$$\begin{aligned} \frac{\partial}{\partial t} \text{Tr}(\rho) &= \frac{2}{\hbar} \frac{1}{\sqrt{\text{Tr}(\rho_{11} \rho_{22})}} (\text{Im}(\text{Tr}((V \star \rho_{22} \star \rho_{11}) e^{-i\phi})) - \text{Im}(\text{Tr}((\rho_{22} \star \rho_{11} \star V) e^{-i\phi}))) \\ &= \frac{2}{\hbar} \frac{1}{\sqrt{\text{Tr}(\rho_{11} \rho_{22})}} (\text{Im}(\text{Tr}((V \star \rho_{22} \star \rho_{11}) e^{-i\phi})) - \text{Im}(\text{Tr}((V \star \rho_{22} \star \rho_{11}) e^{-i\phi}))) \\ &= 0 \end{aligned}$$

Having checked that the formal Star Coherences equations of motion preserves the density, they can now be approximated by semiclassical truncation. Truncating  $\mathcal{O}(\hbar^0)$  gives the classical Star Coherence equations of motion:

$$\frac{\partial \rho_{11}}{\partial t} = \frac{2}{\hbar} \frac{\text{Im}(V \rho_{22} \rho_{11} e^{+i\phi})}{\sqrt{\text{Tr}(\rho_{11} \rho_{22})}}, \quad (5.79)$$

$$\frac{\partial \rho_{22}}{\partial t} = \frac{2}{\hbar} \frac{\text{Im}(\bar{V} \rho_{11} \rho_{22} e^{-i\phi})}{\sqrt{\text{Tr}(\rho_{11} \rho_{22})}}, \quad (5.80)$$

$$\dot{\phi} = -\frac{\text{Tr}(\omega \rho_{11} \rho_{22})}{\text{Tr}(\rho_{11} \rho_{22})} + \frac{\text{Re}(\text{Tr}(V \delta) e^{-i\phi})}{\hbar \sqrt{\text{Tr}(\rho_{11} \rho_{22})}}, \quad (5.81)$$

and

$$\rho_{12} = \frac{\rho_{11} \rho_{22} e^{+i\phi}}{\sqrt{\text{Tr}(\rho_{11} \rho_{22})}}. \quad (5.82)$$

Truncating  $\mathcal{O}(\hbar^1)$  gives the first order semiclassical Star Coherence equations of motion

$$\begin{aligned} \frac{\partial \rho_{11}}{\partial t} &= [H_{11}, \rho_{11}] + \frac{2 \operatorname{Im} (V \rho_{22} \rho_{11} e^{+i\phi})}{\hbar \sqrt{\operatorname{Tr}(\rho_{11} \rho_{22})}} \\ &+ \operatorname{Re} ((V [\rho_{22}, \rho_{11}] + \rho_{22} [V, \rho_{11}] + \rho_{11} [V, \rho_{22}]) e^{+i\phi}), \end{aligned} \quad (5.83)$$

$$\begin{aligned} \frac{\partial \rho_{22}}{\partial t} &= [H_{22}, \rho_{22}] + \frac{2 \operatorname{Im} (\bar{V} \rho_{11} \rho_{22} e^{-i\phi})}{\hbar \sqrt{\operatorname{Tr}(\rho_{11} \rho_{22})}} \\ &+ \operatorname{Re} ((\bar{V} [\rho_{11}, \rho_{22}] + \rho_{11} [\bar{V}, \rho_{22}] + \rho_{22} [\bar{V}, \rho_{11}]) e^{-i\phi}), \end{aligned} \quad (5.84)$$

$$\dot{\phi} = -\frac{\operatorname{Tr}(\omega \rho_{11} \rho_{22})}{\operatorname{Tr}(\rho_{11} \rho_{22})} + \frac{\operatorname{Re}(\operatorname{Tr}(V \delta) e^{-i\phi})}{\hbar \sqrt{\operatorname{Tr}(\rho_{11} \rho_{22})}}, \quad (5.85)$$

and

$$\rho_{12} = \frac{(\rho_{11} \rho_{22} + \frac{i\hbar}{2} [\rho_{11}, \rho_{22}]) e^{+i\phi}}{\sqrt{\operatorname{Tr}(\rho_{11} \rho_{22})}}. \quad (5.86)$$

## 5.4 Discussion

To recap, the Star Coherence Identity was introduced and used to derive an exact representation of the Wigner-Moyal equation for an  $N$  level quantum system undergoing unitary evolution in which explicit dependence on the off-diagonal elements were eliminated. Like the Wigner-Moyal equation, the Star Coherence Representation is a formal result where the star products must be evaluated by differentiation or integration or can be approximated by semiclassical truncation. The advantage of the Star Coherence Representation is that by recasting the density's evolution in terms of purely real distributions, the quantum coherence can be estimated by purely classical statistics quantized through the star product. It should be noted, however, the negativity of population Wigner function still generally per-

sists and would, to some extent, be neglected by a purely classical trajectory ensemble. But the negativity associated with coherences is fully captured by the exact relation of the Star Coherence Identity.

Before discussing applications of the Star Coherence Representation, a connection with linear algebra can be drawn. The Star Coherence Representation of the Wigner-Moyal equation is analogous to a polar decomposition of the density matrix. A density matrix undergoing unitary evolution is defined by

$$\hat{\rho}(t) = \hat{U}^\dagger(t)\hat{\rho}(0)\hat{U}(t) \quad (5.87)$$

where  $\hat{U}(t)$  is a unitary operator  $\hat{U}^\dagger\hat{U} = \hat{\mathbf{1}}$ . The density operator has the properties of being Hermitian:  $\hat{\rho} = \hat{\rho}^\dagger$ , positive-semidefinite,  $\hat{\rho} \geq 0$ , and normalized  $\text{Tr}(\hat{\rho}) = 1$ . These properties of the density matrix are preserved under the unitary transform of time evolution in Eq. 5.87. But the unitary similarity transform  $\hat{U}^\dagger(t)\hat{\rho}(0)\hat{U}(t)$  is not the only way to unitarily transform a matrix. Eq. 5.87 could equally be written formally as

$$\hat{\rho}(t) = \hat{\mathcal{U}}(t)\hat{\rho}(0) \quad (5.88)$$

where  $\hat{\mathcal{U}} = e^{-\frac{t}{i\hbar}[\hat{H}, \cdot]}$ .

Compare this with the polar decomposition of a Hermitian matrix. Recall polar decomposition expresses a square matrix  $\mathbf{M}$  as a product of a unitary matrix  $\mathbf{U}$  and a positive-semidefinite matrix  $\mathbf{P}$

$$\mathbf{M} = \mathbf{U}\mathbf{P} \quad (5.89)$$

If the matrix  $\mathbf{M}$  is Hermitian  $\mathbf{M} = \mathbf{M}^\dagger$ ,  $\mathbf{U}$  contains the phase associated with the eigenvalues of  $\mathbf{M}$  and  $\mathbf{P}$  reduces to the absolute value of  $\mathbf{M}$  [150]:

$$\mathbf{P} = |\mathbf{M}| = \sqrt{\mathbf{M}^\dagger\mathbf{M}} = \sqrt{\mathbf{M}^2} \quad (5.90)$$

thus the polar decomposition of Hermitian matrix  $\mathbf{M}$  is given by

$$\mathbf{M} = \mathbf{U}|\mathbf{M}| \quad (5.91)$$

In the Star Coherence Representation, time evolution expressed entirely in the diagonal elements by

$$\rho_{nn}(\mathbf{q}, \mathbf{p}, t) = \hat{\mathcal{U}}_{nn}(t)\rho_{nn}(\mathbf{q}, \mathbf{p}, 0) \quad (5.92)$$

where the operator  $\hat{\mathcal{U}}_{nn}(t) = e^{-\hat{\mathcal{L}}_{nn}t}$  is given in terms of the star-coherence Liouvillian

$$\hat{\mathcal{L}}_{nn} = [H_{nn}, \cdot]_{\star} + \frac{2}{\hbar} \sum_{\substack{l \in [1, N] \\ l \neq n}} \frac{\text{Im} (H_{nl} \star \rho_{ll} \star \cdot e^{+i\phi_{ln}})}{\sqrt{\text{Tr}(\rho_{ll} \cdot)}} \quad (5.93)$$

with the off-diagonal element accounted for in terms the phases  $\phi_{ln}$ .

## 5.5 Applications and Future Work

The Star Coherence Identity can be used to develop a set of equations of motion solely in terms of populations and phases. This was shown in the Wigner-Moyal representation to derive the Star Coherence Representation. These equations of motion are exact and equivalent to the Wigner-Moyal equation which in turn is a phase space representation of the quantum Liouville equation for a pure state density. But this framework is quite flexible and needn't be solved exactly. The Star Coherence Identity can be used for approximate quantum dynamics methods such as mixed quantum classical and semiclassical theories.

It is interesting to note that Star Coherence Identity and its phase equation of motion bears some semblance to the mixed quantum-classical decoherence correction obtained by Rosky and Bittner [151, 152]. In their formalism, the decay rate of the overlap of two coherent

states is given by

$$J(t) = \exp\left(-\frac{t^2}{4m\sigma}(F_1 - F_2)^2\right) \exp(+i(S_1(t) - S_2(t))) \quad (5.94)$$

where  $m$  and  $\sigma$  are the mass and width of a particle's wavepacket and  $F_i$  and  $S_i$  are instantaneous forces acting on and classical action of the trajectories on states  $i = 1, 2$ . The difference potential term in the phase equation of motion captures the same physics with the overlap of the instantaneous populations of each state averaged over the difference potential  $\omega$ . In a similar vein, the Star Coherence formalism can be used to correct the various implementation of Surface Hopping methods as an alternative to cloning and spawning methods which treat symptoms of overcoherence, but not their root cause in Surface Hopping algorithms. The coherence, instead, can be constructed on-the-fly from star product of the Tully density and used to compute hopping probabilities.

For semiclassical methods, the truncations developed above are similar to those of Martens [123], but with an entirely new phase equation of motion derived from first principles of the Wigner-Moyal Representation. A study comparing the numerics of each semiclassical approach would be useful to benchmark the semiclassical first order Star Coherence Representation. For the purpose of nonlinear spectroscopy, the Star Coherence Representation inherits the structure of Liouville Space and is a subspace which excludes coherences. The Star Coherence picture can be applied as a propagation scheme for calculated nonlinear observables. For example, the third-order response function contains three time steps (excluding its initialization), four populations, and nine possible coherences. In Liouville space, it contains eight possible pathways which contribute to the response [20]. Any of these paths can be calculated using the Star Coherence Identity in terms of only the four populations and relative phases Fig. 5.2.

To summarize, in this Chapter the Star Coherence Identity was derived which relates co-

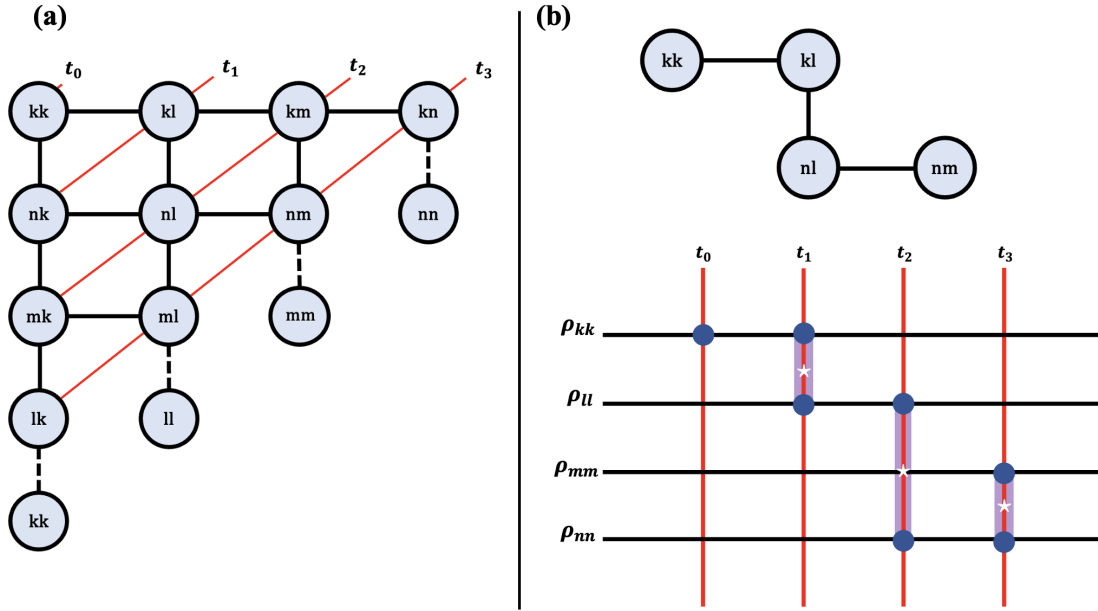


Figure 5.2: (a) Liouville space picture for third order response function. (b) One of eight paths and propagation scheme in the Star Coherence Representation.

herence Wigner functions to the star product of their population Wigner functions and a quantum phase. This identity was substituted into the Wigner-Moyal equation for a  $N$  level system undergoing unitary evolution. The case of a 2 level system was discussed and semiclassical truncations to the exact equations of motion. Because of the generality of the results, they can be applied to a wide array of quantum dynamics problems including nonadiabatic molecular dynamics and nonlinear spectroscopy. Hereto, only the formal properties of these equations have been considered. In the following chapter, algorithms are developed to illustrate how the Star Coherence Representation can be used to solve dynamics in terms of trajectory ensembles.



## Chapter 6

# Moyal Assisted Dynamics and Hudson Density Estimation

In the prior chapter, the Star Coherence Representation was derived for an  $N$  level quantum system. The Star Coherence equations of motion solve the unitary evolution for a pure state density in phase space by evolving the population Wigner functions and quantum phases, with the coherence can be synthesized on-the-fly through the Star Coherence Identity. The prospect of this formal result is to provide a natural framework to estimate quantum coherence dynamics in terms of statistics of classical trajectory ensembles. In this chapter, a protocol for solving the Star Coherence equations of motion is illustrated on 1-D displaced oscillator model analyzed in Chapter 4.

The new method involves two algorithms: *Moyal Assisted Dynamics*, which solves the Star Coherence equations of motion and *Hudson Density Estimation* which is a subroutine in the Moyal Assisted Dynamics which fits the classical trajectory ensembles for each population to Hudson states. A main result is a proof of principle that quantum coherence dynamics can be exactly simulated using nothing more than classical trajectories and an overall quantum

phase for the case of linear coherence dynamics. The algorithm is then generalized to non-quadratic potentials using a cluster density estimation which fits anharmonic trajectory swarms to positive linear combinations of Hudson states.

This chapter begins by introducing the Moyal Assisted Dynamics algorithm and its implementation solving the displaced oscillator model (Telluride I). Because this system has linear dynamics, the population Wigner functions remain Gaussian under time-evolution and only a single Hudson state is required to fit the population ensembles. This approach exactly solves the quantum coherence dynamics of the harmonic displaced oscillator model. In the following section, the breakdown of the single Hudson density estimation is illustrated on a displaced Morse oscillator. To amend this and accommodate general potentials, a clustering density estimation algorithm which fits the population swarm to positive linear combinations of Hudson states is developed. Various clustering algorithms are benchmarked on the displaced Morse oscillator and  $K$ -means density estimation is shown to be useful. The chapter concludes with a discussion of the algorithm, generalizations, and future work.

## 6.1 Single Hudson Density Estimation: Harmonic

As was shown in Chapter 4, the Linearized Semiclassical trajectory provides a dramatic improvement upon the traditional unlinearized Semiclassical approach by removing artificial decoherence. Despite this, the Linearized Semiclassical theory still resolves the linear absorption spectrum at the incorrect average frequency. Nonetheless, one can show using the Star Coherence Representation the exact quantum solution can be obtained for the correct frequency using nothing more than classical trajectories and the star product.

Using the Telluride I (Initialization I), the Star Coherence equations of motion reduce to

$$\frac{\partial \rho_{11}}{\partial t} = [H_{11}, \rho_{11}]_{\star} = [H_{11}, \rho_{11}] \quad (6.1)$$

$$\frac{\partial \rho_{22}}{\partial t} = [H_{22}, \rho_{22}]_{\star} = [H_{22}, \rho_{22}] \quad (6.2)$$

$$\dot{\phi} = -\frac{\text{Re}(\text{Tr}(\omega(\rho_{11} \star \rho_{22})))}{\text{Tr}(\rho_{11} \rho_{22})} \quad (6.3)$$

with the coherence synthesized by

$$\rho_{12} = \frac{\rho_{11} \star \rho_{22} e^{+i\phi}}{\sqrt{\text{Tr}(\rho_{11} \rho_{22})}}. \quad (6.4)$$

An algorithm to solve these equations of motion with classical trajectories called Moyal Assisted Dynamics is outlined below. The name derives from the fact, the Moyal or star product, is being used to assist in recovering quantum interference between the classical population ensembles.

## Moyal Assisted Dynamics - Single Hudson Density Estimation Algorithm

---

**Input:**

$$\{\rho_{ij}, H_{ij}, \mathcal{N}, \Delta\tau, t_0, t_f\}$$

**Initialization:**

$$t \leftarrow t_0, \Gamma_1 = \Gamma_2 \leftarrow \{ \}, \rho_{11} \leftarrow \mathcal{W}[\hat{\rho}_{11}(t_0)], \rho_{22} \leftarrow \mathcal{W}[\hat{\rho}_{22}(t_0)], \phi \leftarrow \phi_0$$

For  $i \in [1, 2]$

For  $n \in [1, \mathcal{N}]$

$$\gamma_i \leftarrow \gamma_i^{(n)} = (q^{(n)}(t_0), p^{(n)}(t_0)) \sim \rho_{ii}(q, p, t_0)$$

$$\Gamma_i \leftarrow \Gamma_i \cup \gamma_i$$

**Propagate:**

For  $t \in [t_0, t_f]$

For  $i \in [1, 2]$

For  $\gamma_i^{(n)} \in \Gamma_i$

$$q_i^{(n)} \leftarrow q_i^{(n)} + \frac{\partial H_{ii}}{\partial p} \Delta t$$

$$p_i^{(n)} \leftarrow p_i^{(n)} - \frac{\partial H_{ii}}{\partial q} \Delta t$$

$$\chi_i = \text{HudsonFit}[\Gamma_i, \eta(q, p, \chi)]$$

$$\phi \leftarrow \phi + \dot{\phi}(\chi_1, \chi_2) \Delta t$$

$$t \leftarrow t + \Delta t$$

**Synthesize:**

At any  $t \in [t_0, t_f]$

$$\rho_{12}(q, p, \chi_1(t), \chi_2(t)) \leftarrow \frac{\eta(q, p, \chi_1(t)) \star \eta(q, p, \chi_2(t)) e^{+i\phi(t)}}{\sqrt{\text{Tr}(\eta(q, p, \chi_1(t)) \eta(q, p, \chi_2(t)))}}$$

The simulation takes as input the initial density  $\hat{\rho}$ , the system Hamiltonian  $H$ , the initial phase  $\phi_0$ , the number of trajectories  $\mathcal{N}$ , the time step  $\Delta t$ , and the initial and final times  $t_0$  and  $t_f$ . The initial density  $\hat{\rho}$  is Wigner transformed to obtained population Wigner functions

for each state,  $\rho_{11}$  and  $\rho_{22}$ .

These population Wigner functions are sampled  $\mathcal{N}$  times to generate the initial conditions for the ensemble of each state's population,  $\Gamma_1$  and  $\Gamma_2$ . These ensembles are propagated by numerical solving Hamilton's equations. At each time step  $\Delta t$ , the trajectory ensembles are fitted to Hudson states by a combination of Method of Moments and Maximum Likelihood Estimation to yield the statistical parameters of each ensemble at that time  $\chi_1 = \{Q_1, P_1, \sigma_1^q, \sigma_1^p, r_1\}$  and  $\chi_2 = \{Q_2, P_2, \sigma_2^q, \sigma_2^p, r_2\}$ . The statistical parameter are then feed into the equation of motion for the phase (Eq. 6.3) which is numerically integrated. At any time in the simulation when the coherence is needed it is analytically synthesized by the Star Coherence Identity (Eq. 6.4) through the instantaneous values of  $\chi_1$  and  $\chi_2$ . (For the analytic star product of two Hudson states see Appendix B).

The approach is illustrated on the Telluride I (Initialization I) model using a symplectic midpoint integrator for the trajectories and an Euler integrator for the phase for  $\mathcal{N} = 1000$  trajectories. The Moyal Assisted Dynamics results shows exact numerical agreement with the exact quantum solution obtained by Thawed Moyal Dynamics. The slight numerical deviation between the two in coherence correlation function (Fig. 6.1) and spectrum (Fig. 6.2) can be removed by increasing the number of trajectories to estimate the population statistics. The phase portraits of the trajectories and single Hudson fits and coherence Wigner function are illustrated in Fig. 6.3.

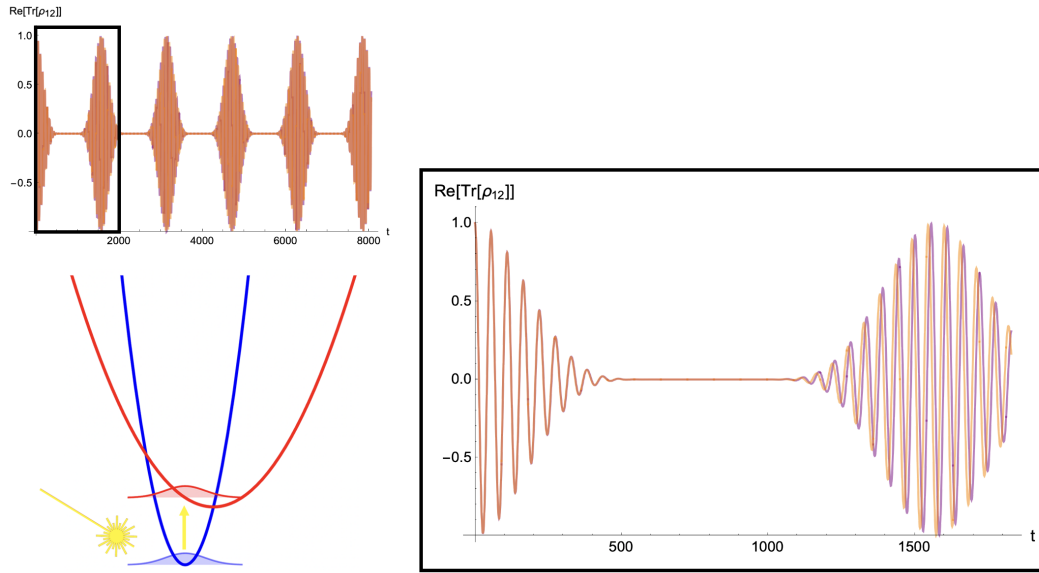


Figure 6.1: Comparison of coherence correlation function for Telluride I (Initialization I) calculated by Moyal Assisted Dynamics - Single Hudson Density Estimation for  $\mathcal{N} = 1000$  (orange) with and exact quantum Thawed Moyal Dynamics (purple).

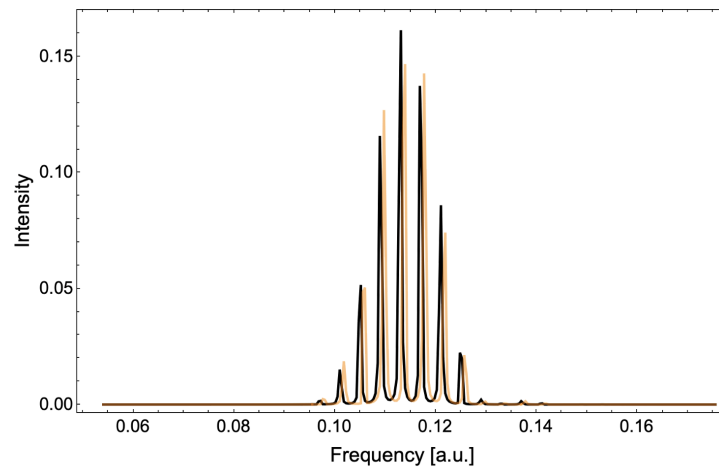


Figure 6.2: Comparison of linear absorption spectrum for Telluride I (Initialization I) calculated by Moyal Assisted Dynamics - Single Hudson Density Estimation for  $\mathcal{N} = 1000$  (orange) with and exact quantum Thawed Moyal Dynamics (black).

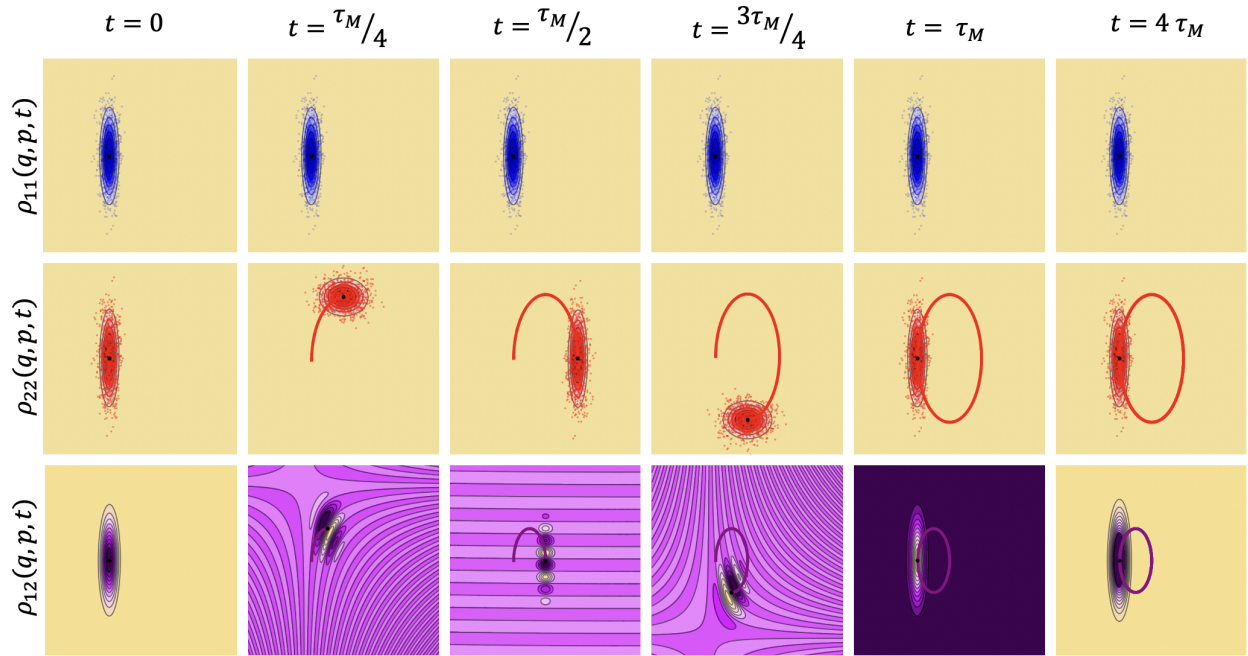


Figure 6.3: Phase space portraits for  $\text{Re}(\rho_{12}(q, p, t))$  for Telluride I (Initialization I) calculated by Moyal Assisted Dynamics - Single Hudson Density Estimation for  $\mathcal{N} = 1000$ . Time increasing left-to-right, top-to-bottom ( $t = 0$ ,  $t = \tau_M/4$ ,  $t = \tau_M/2$ ,  $t = 3\tau_M/4$ ,  $t = \tau_M$ ,  $t = 4\tau_M$ ) for vibrational period  $\tau_M$ . Ground state orbit:  $(Q_1(t), P_1(t))$  (blue). Excited state orbit:  $(Q_2(t), P_2(t))$  (red). Coherence orbit:  $(Q(t), P(t))$  (purple). Coherence mean (black).

## 6.2 Single Hudson Density Estimation: Morse

To illustrate the effect of anharmonicity, the Moyal Assisted Dynamics - Single Hudson Density Estimation algorithm is tested on a displaced oscillator where the excited state  $j = 2$  is a Morse oscillator. This was done for a Morse potential of varying dissociation energies  $D_2$  whose harmonic truncation is the original Telluride I model's upper state surface. This system called Telluride I-M is defined by the potentials:

$$H_{11} = \frac{p^2}{2m} + \frac{1}{2}m\Omega_1^2(q - Q_1^e) + E_1 \quad (6.5)$$

$$H_{22} = \frac{p^2}{2m} + D_2(1 - e^{-a_2(q - Q_2^e)})^2 + E_2 \quad (6.6)$$

with

$$a_2 = \sqrt{\frac{m\Omega_2^2}{2D_2}} \quad (6.7)$$

and the system parameters of Telluride I (Tab. 4.1) and Initialization I (Tab. 4.2).

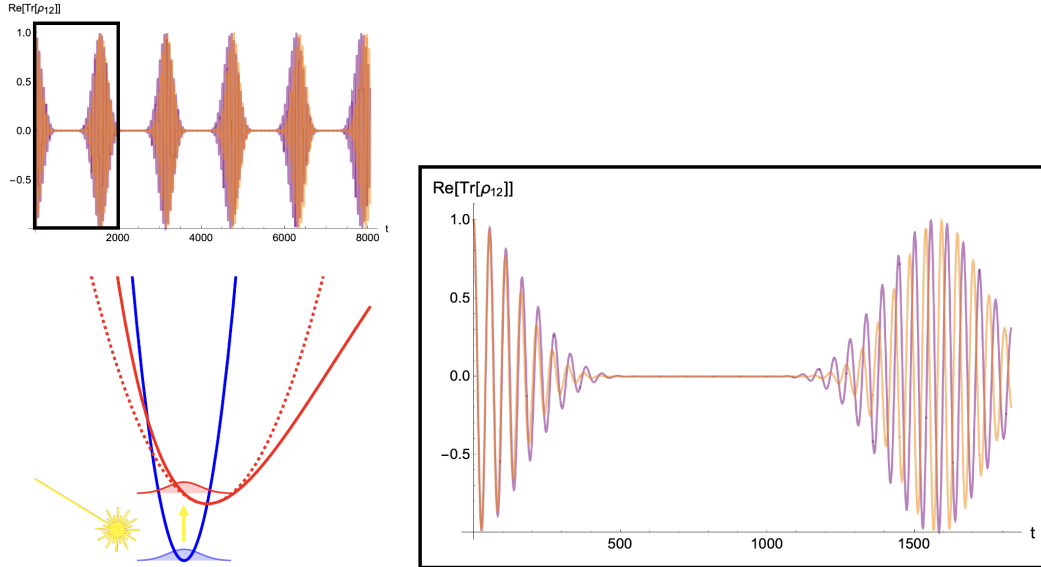


Figure 6.4: Comparison of coherence correlation function for Telluride I-M ( $D_2 = 1$ , Initialization I) calculated by Moyal Assisted Dynamics - Single Hudson Density Estimation (orange) for  $\mathcal{N} = 1000$  with Thawed Moyal Dynamics for the harmonic fit (purple).



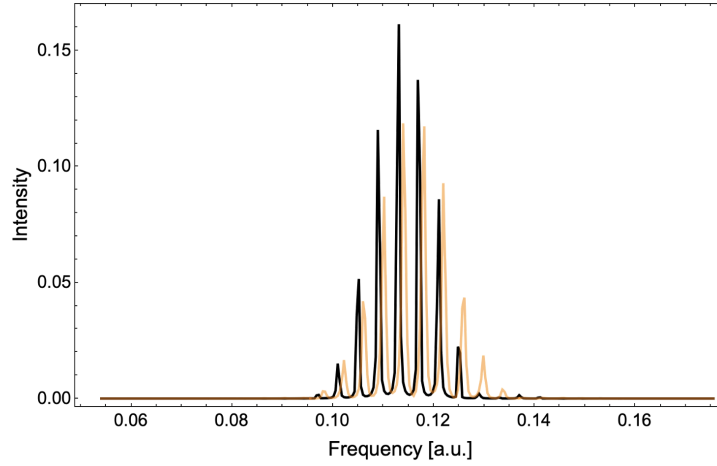


Figure 6.5: Comparison of linear absorption spectrum for Telluride I-M ( $D_2 = 1$ , Initialization I) calculated by Moyal Assisted Dynamics - Single Hudson Density Estimation (orange) for  $\mathcal{N} = 1000$  with Thawed Moyal Dynamics for the harmonic fit (black).

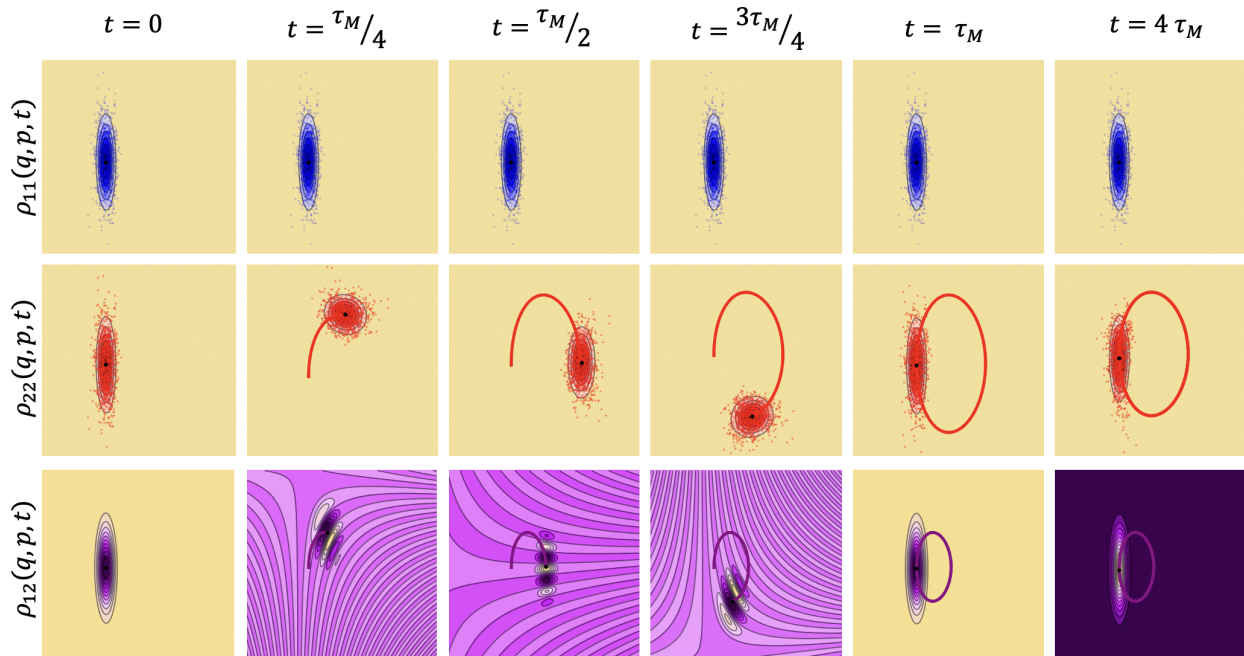


Figure 6.6: Phase space portraits for  $\text{Re}(\rho_{12}(q, p, t))$  for Telluride I-M ( $D_2 = 1$ , Initialization I) calculated by Moyal Assisted Dynamics - Single Hudson Density Estimation for  $\mathcal{N} = 1000$ . Time increasing left-to-right, top-to-bottom ( $t = 0$ ,  $t = \tau_M/4$ ,  $t = \tau_M/2$ ,  $t = 3\tau_M/4$ ,  $t = \tau_M$ ,  $t = 4\tau_M$ ) for vibrational period  $\tau_M$ . Ground state orbit:  $(Q_1(t), P_1(t))$  (blue). Excited state orbit:  $(Q_2(t), P_2(t))$  (red). Coherence orbit:  $(Q(t), P(t))$  (purple). Coherence mean (black).

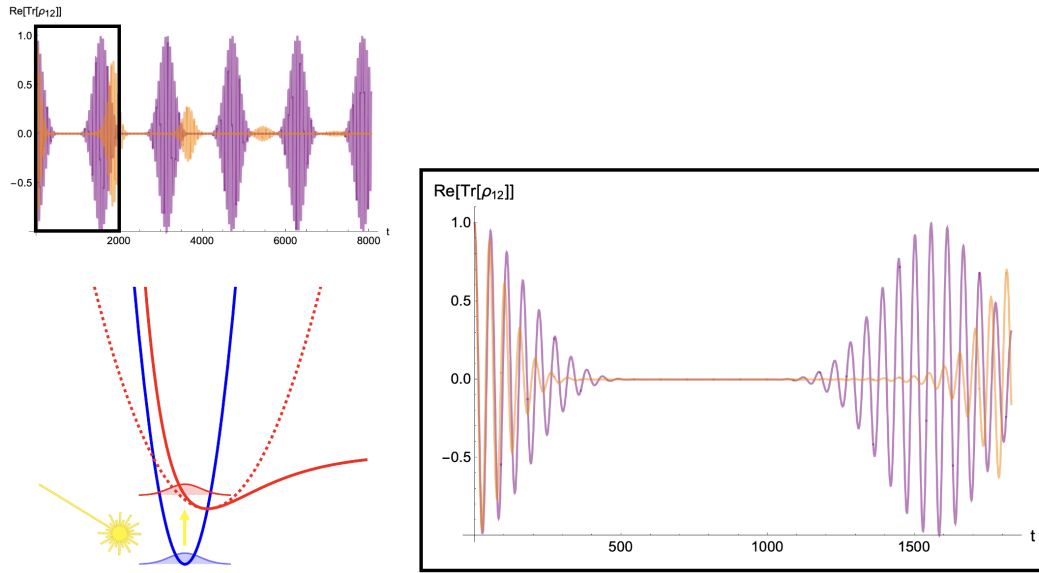


Figure 6.7: Comparison of coherence correlation function for Telluride I-M ( $D_2 = 0.1$ , Initialization I) calculated by Moyal Assisted Dynamics - Single Hudson Density Estimation (orange) for  $\mathcal{N} = 1000$  with Thawed Moyal Dynamics for the harmonic fit (purple).

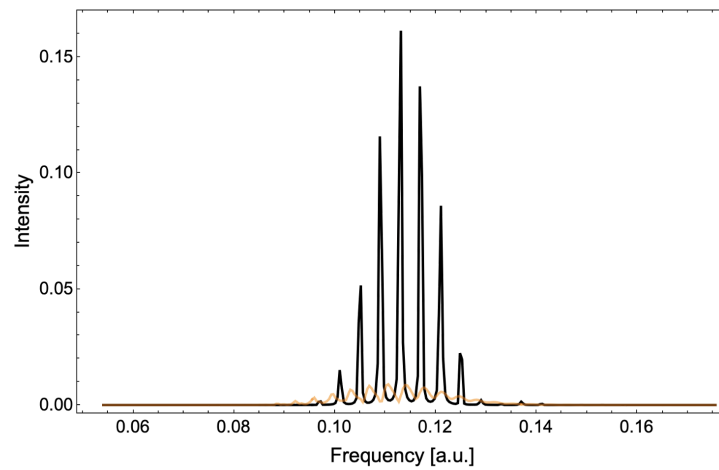


Figure 6.8: Comparison of linear absorption spectrum for Telluride I-M ( $D_2 = 0.1$ , Initialization I) calculated by Moyal Assisted Dynamics - Single Hudson Density Estimation (orange) for  $\mathcal{N} = 1000$  with Thawed Moyal Dynamics for the harmonic fit (black).

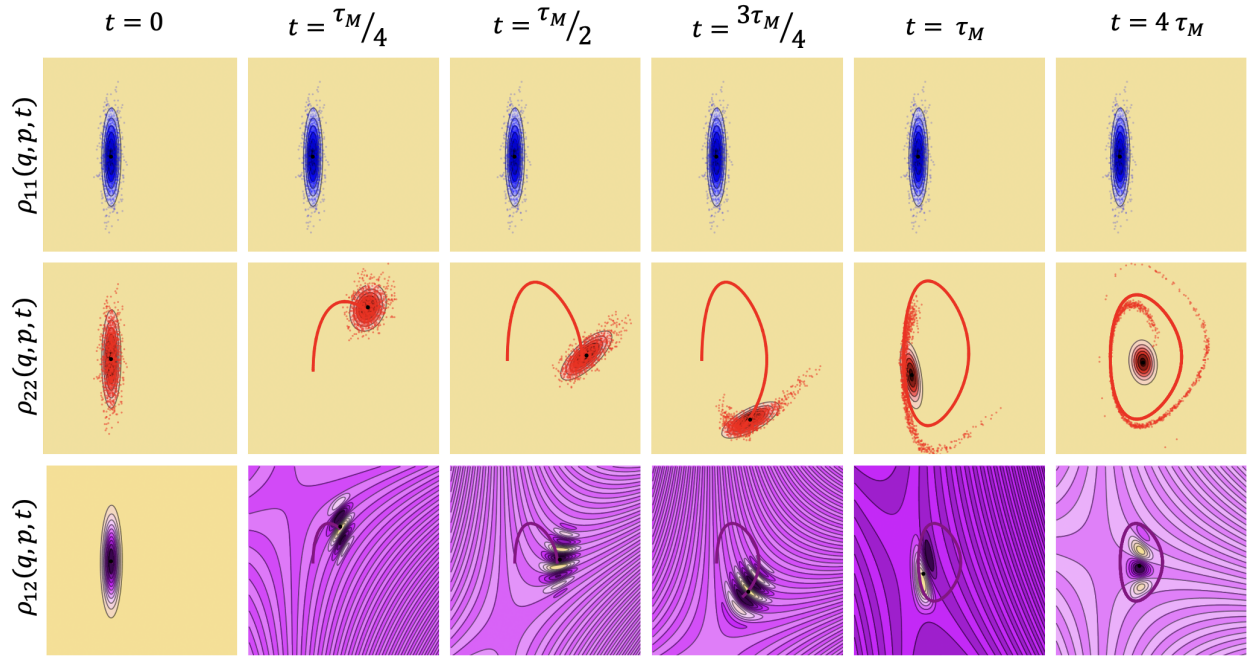


Figure 6.9: Phase space portraits for  $\text{Re}(\rho_{12}(q, p, t))$  for Telluride I-M ( $D_2 = 0.1$ , Initialization I) calculated by Moyal Assisted Dynamics - Single Hudson Density Estimation for  $\mathcal{N} = 1000$ . Time increasing left-to-right, top-to-bottom ( $t = 0$ ,  $t = \tau_M/4$ ,  $t = \tau_M/2$ ,  $t = 3\tau_M/4$ ,  $t = \tau_M$ ,  $t = 4\tau_M$ ) for vibrational period  $\tau_M$ . Ground state orbit:  $(Q_1(t), P_1(t))$  (blue). Excited state orbit:  $(Q_2(t), P_2(t))$  (red). Coherence orbit:  $(Q(t), P(t))$  (purple). Coherence mean (black).

### 6.3 $K$ -Hudson Density Estimation Algorithm

Upon introducing moderate anharmonicity, the excited state population ensemble no longer remains Gaussian and undergoes phase space shearing as time increases (Fig. 6.9), transitioning from a Gaussian, to a “crescent moon”, and finally, to pinched ellipse filling the energy shell of the Morse orbit. While the Single Hudson Fit for the populations is sufficient at low anharmonicity ( $D_2 > 1$ ), the single Hudson Fit is inadequate to qualitatively populations moving under moderately anharmonic potentials ( $D_2 < 1$ ). Error in the quantum coherence estimate introduced by unrepresentative fits of the excited state’s population ensemble.

Taking inspiration from Heller’s Thawed/Frozen Gaussian work [153, 154], the problem of anharmonicity can be addressed by fitting the population ensembles to a positive linear combination of Hudson states. The advantage to working with Hudson states is threefold: (1) Fitting data to linear combinations of normal distributions is a well-studied problem in statistics, signal processing, and machine learning [155, 156], (2) by representing the populations still as Hudson states, the star product can be analytically calculated, and (3) because Hudson states are squeezed coherent states which form a complete (albeit, an overcomplete basis), the density operator can be formally expanded in this basis.

There are many statistical algorithms and machine learning methods to fit data to mixtures of normal distributions, principal component analysis and clustering are two well-known examples. For simplicity consider the latter, any population ensemble  $\Gamma_i$  can be divided into  $K$  subsets

$$\Gamma_i = \{\Gamma_i^{(1)}, \dots, \Gamma_i^{(K)}\} \tag{6.8}$$

by clustering algorithms which partition the ensemble into local groups. Once clustered, each ensemble cluster can be fitted to a single Hudson state with the total population ensemble

represented by a positive linear combination of each cluster's Hudson state

$$\rho_{ii}(q, p, t) \approx \eta_i(q, p, \chi_i) = \sum_{i=1}^K \omega_i^{(k)} \eta_i(q, p, \chi_i^{(k)}) \quad (6.9)$$

with the weights  $w_i^{(k)} \in \mathbb{R}_{>0}$ . A sample pseudocode for this algorithm applied to Moyal Assisted Dynamics is shown below.

## Moyal Assisted Dynamics - K-Hudson Density Estimation Algorithm

---

**Input:**

$$\{\rho_{ij}, H_{ij}, \mathcal{N}, \Delta\tau, t_0, t_f, K\}$$

**Propagate:**

For  $t \in [t_0, t_f]$

For  $i \in [1, 2]$

For  $\gamma_i^{(n)} \in \Gamma_i$

$$q_i^{(n)} \leftarrow q_i^{(n)} + \frac{\partial H_{ii}}{\partial p} \Delta t$$

$$p_i^{(n)} \leftarrow p_i^{(n)} - \frac{\partial H_{ii}}{\partial q} \Delta t$$

$$\chi_i = \text{K - HudsonFit} [K, \Gamma_i, \eta(q, p, \chi^{(k)})]$$

$$\phi \leftarrow \phi + \dot{\phi}(\chi_1, \chi_2) \Delta t$$

$$t \leftarrow t + \Delta t$$

**K-HudsonFit Subroutine:**

$$\Gamma_i^K \leftarrow \text{Cluster} [K, \Gamma_i]$$

$$\chi_i \leftarrow [ ]$$

For  $\gamma_i^{(k)} \in \Gamma_i^K$

$$w_i^{(k)} \leftarrow \text{Length} (\Gamma_i^{(k)}) / \mathcal{N}$$

$$\chi_i^{(k)} \leftarrow \text{K - HudsonFit} [\Gamma_i^{(k)}, \eta(q, p, \chi)]$$

$$\text{Append} [\chi_i, [w_i^{(k)}, \chi_i^{(k)}]]$$

**Synthesize:**

At any  $t \in [t_0, t_f]$

$$\rho_{12}(q, p, \chi_1, \chi_2) \leftarrow \frac{\sum_{k', k} w_1^{(k')} w_2^{(k)} \eta(q, p, \chi_1^{(k')}(t)) \star \eta(q, p, \chi_2^{(k)}(t)) e^{+i\phi(t)}}{\sqrt{\text{Tr} (\eta(q, p, \chi_1^{(k')}(t)) \eta(q, p, \chi_2^{(k)}(t)))}}$$

The question then is: “How what algorithm should be used to cluster the population ensembles?” Different clustering algorithms can yield vastly different clusters based upon the

statistics properties inherent to the dataset or criteria functions used for clustering. Some example algorithms applied to phase portraits of a Morse potential are illustrated below in Fig. 6.10.

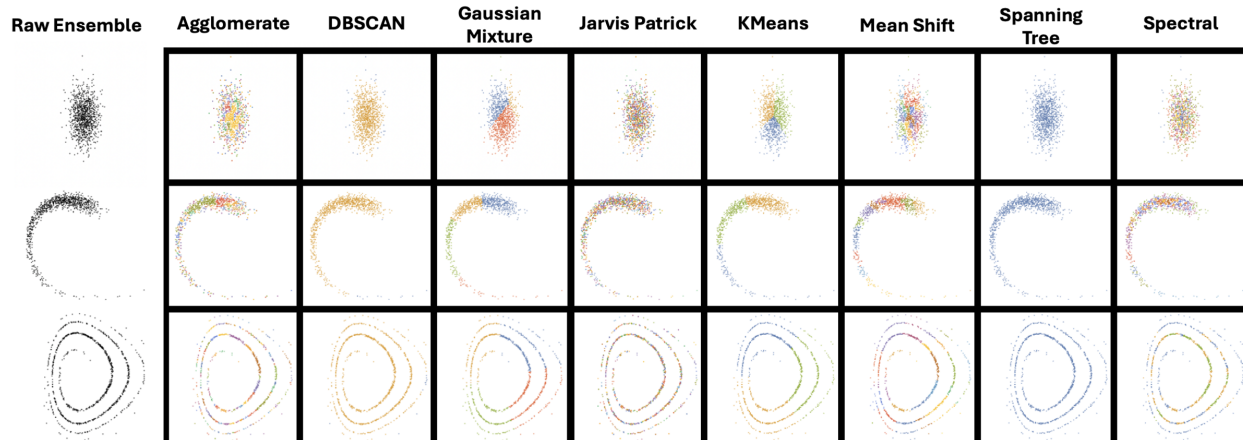


Figure 6.10: Comparison of clustering algorithms for sample trajectory swarms of Morse oscillator.

In examining Fig. 6.10, a few clustering algorithms are suited only in the Gaussian limit of short times/low anharmonicities like Density-based spatial clustering of applications with noise (DBSCAN) and Spanning Tree. While other algorithms like Agglomerate, Jarvis-Patrick, and Spectral appear ill-suited for all times and anharmonicities. What is needed is a clustering method which qualitatively resembles the intended use of providing an accurate estimate of a local subset of the ensemble for all times, but which is not too computationally intensive. To quantify this, qualitatively reasonable cluster algorithms were benchmarked on a data set of 36 different ensemble phase portraits for dissociation energies  $D_2 \in [0.1, 10]$  and several vibrational periods  $t \in [0, 10\tau_M]$ . The average number of clusters used, run-time, and memory used for each fit were recorded with the accuracy of the fit measured by the conditional entropy of the resulting distribution conditioned on the data

$$S_c = \langle -\ln (\eta_i(q, p, \mathbf{x}_i) | \Gamma_i) \rangle \quad (6.10)$$

The results are tabulated in Tab. 6.1.

Method	Run Time [s]	Memory [MB]	$K$	$S_C$
DBSCAN	9.592	9.946	2.000	4.921
Gaussian Mixture	9.806	9.945	3.611	2.840
Neighborhood Contraction	9.329	9.944	3.333	3.113
K-Means = 3	9.124	9.944	3.000	3.048
K-Medoids = 3	9.136	9.944	3.000	3.039
Spectral	9.881	9.944	5.500	3.048

Table 6.1: K-Hudson Cluster Density Estimation benchmark for various cluster algorithms. Run time (seconds), memory (megabytes), number of clusters, and conditional entropy of one fit averaged over training set.

DBSCAN performs the most poorly. It has the least accurate fit evidenced by its high conditional entropy. Moreover, the DBSCAN algorithm tosses out outliers and if used in simulation, the ensemble would hemorrhage trajectories over time through successive fits. In contrast, Gaussian Mixture provides the most accurate fit, but at the cost of a larger run-time. While tenths of a second may appear trivial, the Moyal Assisted Dynamics protocol requires a fit at each time-step to propagate the phase  $\phi$ . And, in practice, to obtain a reasonably resolved spectrum requires  $10^5$  time-steps. Based on accuracy and time performance considerations, K-Means [157] with a variable number of clusters capped at  $K = 4$  was selected as the optimal clustering algorithm and applied to the Telluride I-M system which the phase portraits illustrated in Fig. 6.11.



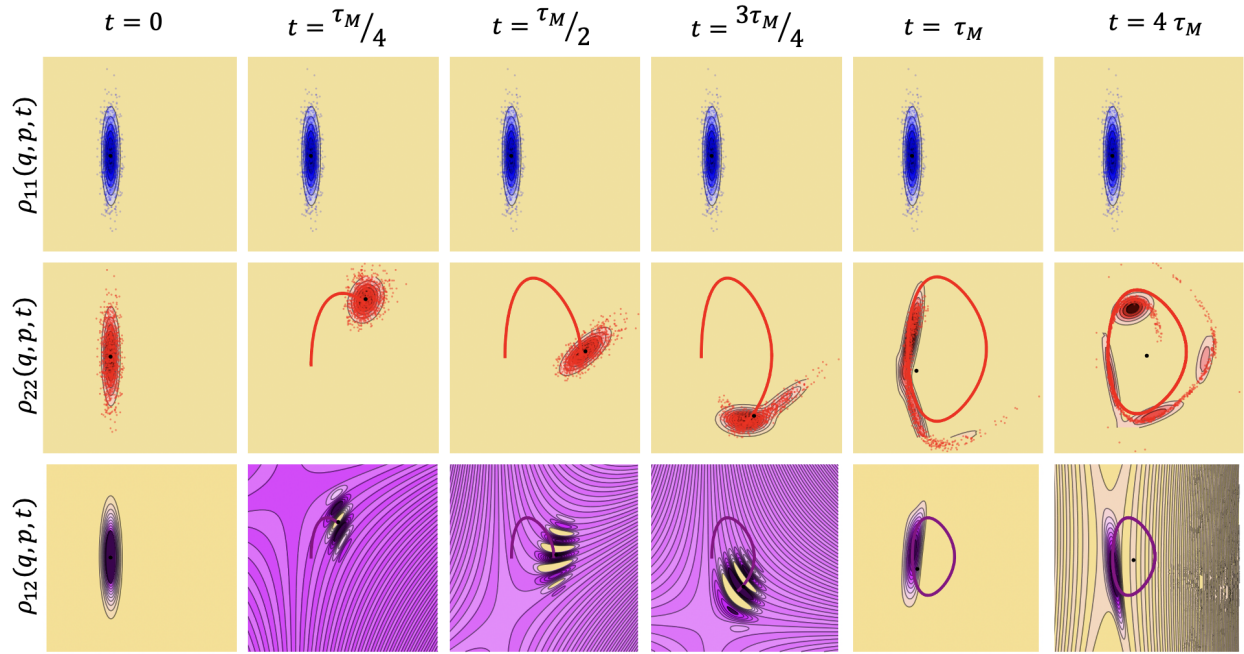


Figure 6.11: Phase space portraits for  $\text{Re}(\rho_{12}(q, p, t))$  for Telluride I-M ( $D_2 = 0.1$ , Initialization I) calculated by Moyal Assisted Dynamics - K-Means Hudson Density Estimation for  $\mathcal{N} = 1000$ . Time increasing left-to-right, top-to-bottom ( $t = 0$ ,  $t = \tau_M/4$ ,  $t = \tau_M/2$ ,  $t = 3\tau_M/4$ ,  $t = \tau_M$ ,  $t = 4\tau_M$ ) for vibrational period  $\tau_M$ . Ground state orbit:  $(Q_1(t), P_1(t))$  (blue). Excited state orbit:  $(Q_2(t), P_2(t))$  (red). Coherence orbit:  $(Q(t), P(t))$  (purple). Coherence mean (black).

## 6.4 Discussion

In this chapter, a protocol for solving the Star Coherence equations of motion was illustrated on a 1-D displaced oscillator models with harmonic and Morse potentials. The Moyal Assisted Dynamics algorithm solves the Star Coherence equations of motion for the populations and phases using statistical estimates obtained from classical trajectories ensembles of the populations. The Hudson Density Estimation procedure provides a way to estimate population densities in terms of Hudson state Wigner functions.

Moyal Assisted Dynamics - Single Hudson Density Estimation exactly solves the vibrational quantum coherence for the harmonic displaced oscillator model. This is evidenced by its agreement with the exact Thawed Moyal solution in the correlation functions (Fig. 6.1), its spectrum (Fig. 6.2), and comparing the phase portraits in Fig. 6.3 with Fig. 4.4 . Although there is some numerical error between the Moyal Assisted Dynamics and Thawed Moyal Dynamics correlation functions and spectra, this can be improved by converging with respect to the number of trajectories (roughly  $\mathcal{N} = 2500$ ) and using a higher order integrator for the phase.

In applying the single Hudson fit to the Morse system, at the high dissociation energies ( $D_2 > 1$ ) the algorithm performs reasonable well (Fig. 6.4, Fig. 6.5, and Fig. 6.6). Although the population Wigner function will not remain a Gaussian after several vibrational periods, a single Hudson state is sufficient to recover the lengthening of the vibrational period as shown by the longer periods of recurrence in the correlation function relative to the harmonic result. In the spectrum this is manifested as the line-shape being shifted and broadened. At the low dissociation energies ( $D_2 = 0.1$ ) the single Hudson fit deviates appreciably from population ensemble (Fig. 6.9) by the first vibrational period  $\tau_m$ . Despite this, because the excited state trajectories are evolving under the correct Morse potential, the lengthening of the vibrational period relative to the harmonic result is still captured in the correlation

function (Fig. 6.7) and spectrum (Fig. 6.8).

To obtain a better statistical estimate of the excited state population in the Morse system, a K-Hudson Density Estimation algorithm was devised which fits the population to a linear combination of Hudson states. It is important to note, this is a *mixed-state* estimation of a pure state density (Eq. 6.9). Despite this, because Hudson states are squeezed coherent states which have completeness and a resolution of identity, a given population Wigner can *exactly* expanded in Hudson states by performing the expansion on a von Neumann Lattice (Fig. 6.12) in phase space and discarding one state [158–160].

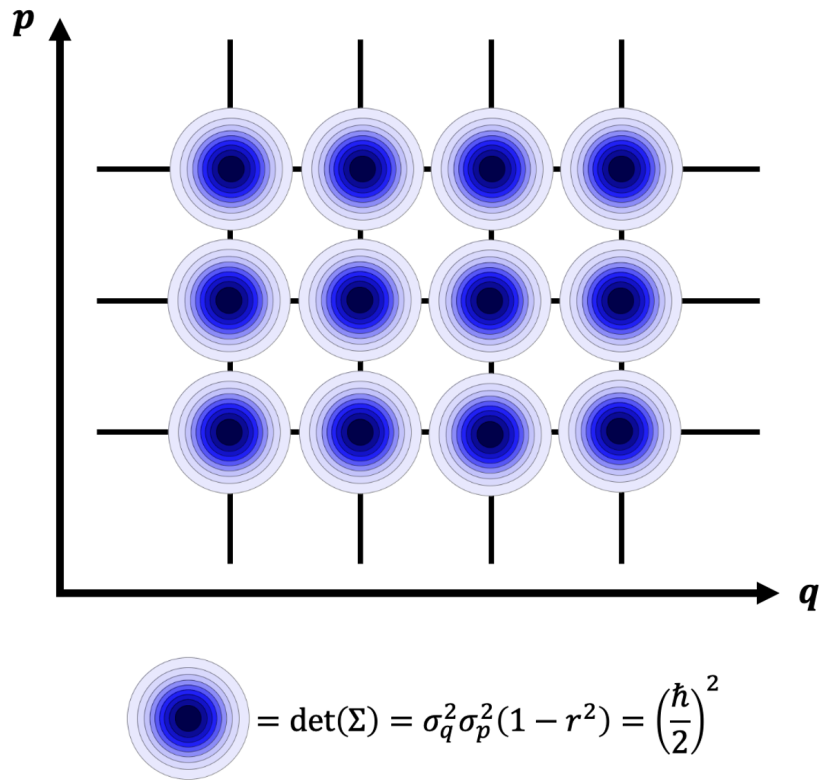


Figure 6.12: von Neumann Lattice of coherent states in phase space.

Thus although the K-Hudson fitting appears superficially like a mixed state, it has an exact pure state limit. For arbitrary  $K$  with not restrictions on the phase space centers  $(Q, P)$  of the Hudson states, the K-Hudson Density Estimation is an approximation. An exact fitting in phase space requires a formal expansion on the von Neumann lattice.

Based upon accuracy and performance, K-Means selected as the clustering algorithm used to determine the K-Hudson fits. This was applied to the low dissociation energy Morse system and the resulting phase portraits calculated (Fig. 6.11). Qualitatively, the K-Hudson Density Estimation performs better than the Single Hudson case (Fig. 6.9). At intermediate times  $t = 4\tau_M$ , the coherence is still constrained to the correct orbit and location in phase space and deformed about the turning points.

What was established was a proof of principle. Despite coherences being very quantum in nature, their dynamics can be simulated using the statistics of classical trajectory ensembles suitably synthesized through the star product. The Moyal Assisted Dynamics framework is quantum general and can be used to improve semiclassical, mixed quantum classical, and Gaussian wavepacket dynamics methods to obtain a better estimate of quantum coherences and be used to calculate nonlinear spectroscopic signals. Moyal Assisted Dynamics is readily generalizable to higher dimensions owing to economy of cluster density estimation. While classical trajectory ensembles are cheap and the star product recaptures much of the quantum inheritance, the quantum complexity has been pushed into fitting at each time-step and propagated the phase.

Nonetheless, the fitting is manageable with modest computing resources and an efficient code. All simulations in this thesis were done on a personal computer (a Macbook Pro II with 12 CPU and 19 GPU cores) using Wolfram Mathematica 14.0. By framing the dynamics of quantum coherences in terms of trajectory ensembles and their statistics, parallelized implementations on better architecture would immediately benefit this approach. Classical dynamics scale linearly, star products of Hudson states are analytic, and simple clustering algorithms like K-Means typically have time and space complexities on  $\mathcal{O}(N^2)$ . The value of Star Coherence representation isn't so much its formalism, but rather the fact it translates quantum coherence dynamics into a problem suited for simulation using the technology of the day.

## 6.5 Applications and Future Work

With additional computing resources, the spectra and correlation functions for the Moyal Assisted Dynamics - K-Hudson Density Estimation simulation of the displaced Morse oscillator can be calculated. These results in turn can be compared with the exact Morse spectrum either through wavepacket simulation or their analytic Frank-Condon factors. The two most important generalizations are to consider systems with more degrees of freedom like the 2-D displaced oscillator models and to add in coupling. The former is trivial because analytic forms for the star products of  $N$  degrees of freedom Hudson states have been worked out [14] and K-Means is an efficient clustering algorithm. Adding in non-diagonal coupling is a more nuanced task, but can be treated using standard perturbative techniques [20]. Once these two generalization are complete, Moyal Assisted Dynamics can be applied to resolve coherence dynamics in realistic conical intersections and simulate their spectroscopic signals. The numerics of mixed state estimate needs to be investigated. In principle, this issue can be addressed by restricted the K-Mean Density Estimation to vertices on the von Neumann lattice.

# Chapter 7

## Conclusion

In this thesis the dynamics of quantum coherences were studied in the Wigner-Moyal representation. Working in phase space has the advantage of generality. Phase space is the natural domain of mechanics, optics, and statistical mechanics and thus provides a unified framework to model the quantum dynamics of particles, radiation, and information. Likewise because the Wigner-Moyal equation has a well-defined classical limit and can be truncated to arbitrary orders in  $\hbar$ , it is tailored to analyzing the emergence of classical physics out of quantum, — and with that (de)coherence. While the phase space formulations of quantum mechanics are not new, the insights which can be drawn its statistical interpretation seem well-posed to tackle many of the new problems in quantum technology. To the degree quantum dynamical simulations in the Wigner-Moyal representation can be recast into classical(like) trajectory ensembles, this representation has the potential to combine with new high-performance computing architectures and machine learning methods to obtain better estimates of statistics from trajectories which in turn can extend an understanding of quantum coherence at scale.

There are three main contributions of this thesis. First is the derivation and solution of the exact dynamics of a quantum coherence in a 2 level displaced oscillator with distinct

frequencies and a model conical intersection without coupling. The Thawed Moyal approach was shown to be equivalent to the historic thawed Gaussian wavepacket approach of Heller, but with several advantages. The Thawed Moyal solution exact solves the dynamics of a the displaced oscillator model and corrects the semiclassical Liouville equation. It was shown the traditional semiclassical solution routinely used in time-domain spectroscopy calculations fails for simple systems with non-identical frequencies, suffering spurious decoherence and predicting an incorrect frequency spacing of the linear absorption spectrum. While the spurious decoherence of the semiclassical solution can be removed by linearization of the difference potential, the resulting spectrum still occurs at the average “zombie” frequency. In contrast, the full Thawed Moyal solution correctly resolves the frequencies at excited state. The kinematic picture that accompanies this is the “cat-jectory.” Namely the dynamics of the coherence is modulated by frequencies of both states potentials simultaneously undergoing trochoidal orbits in phase space. This picture lead to the insight that the dynamics of the coherence should be expressible in terms of the time-dependent statistical properties of the populations. The second contribution is formally demonstrating this hypothesis.

It was shown analytically how coherences can be calculated solely in terms of populations and quantum phases through the Star Coherence Identity. Using this identity an entirely new representation of the Wigner-Moyal equation was derived for the  $N$  level quantum system. This Star Coherence Representation of pure state unitary evolution is exact and equivalent to the quantum Liouville equation. In this framework only the positive diagonal elements of the density and quantum phases are evolved, with the off-diagonal coherences synthesized as needed through the star product. The utility of this representation is that populations behave more classically than coherences. Populations are real and can be estimated more directly than coherences through classical trajectory ensembles.

The third contribution of this thesis was developing algorithms which solve the Star Coherence equations of motion with trajectory ensembles. The Moyal Assisted Dynamics - Hudson

Density Estimation algorithm fits classical trajectory swarms of populations to positive definite Wigner functions (Hudson states) which in turn can be analytically star multiplied to calculate the coherence. This approach was shown to exactly solve the coherence dynamics of displaced oscillator model. To examine the effects of general potentials and anharmonicity, a displaced Morse oscillator was studied. To accommodate the effects of anharmonicity, a cluster density estimation algorithm was developed which fits population ensembles to positive linear combinations of Hudson states. While this creates a mixed state estimate of a pure state, because Hudson states are coherent states there is a pure state limit to this expansion on the von Neumann lattice. A formalism and algorithm embracing this should be explored. Despite this, the prospect of the Star Coherence framework is the low computational overhead and high accuracy estimate of the quantum coherence.

Future work involves simulating applying the methods developed to more complex molecular systems, —systems with more degrees of freedom and diabatic coupling. System which have technological uses for quantum coherence like photoactive molecules with conical intersections or molecular qubits such as optical cycling centers are ideal candidates for these theories. The Star Coherence Identity is quite general and derived from first principles. Although in this thesis it was used to solve simple systems exactly, it can be used to improve standard nonadiabatic quantum dynamics methods. It can be employed to correct the problem of “overcoherence” in mixed quantum-classical methods (viz. Fewest Switches Surface Hopping) without the high degree of parameterization and is derivable from first principles. Similarly, X-ray nonlinear spectroscopic probes which require a high precision estimate of coherence signals could benefit from employing the Star Coherence formalism as a post-processing step if not the default method of simulation. The guiding principle for theories proposed in this thesis was to appreciate what is classical in quantum coherence from what is truly quantum. What was shown is that a surprising amount of quantum coherence, if not classical in origin, can be represented as such.



# Bibliography

- [1] J.C. Hemminger, J. Sarrao, G. Crabtree, G. Flemming, and M. Ratner. Challenges at the Frontiers of Matter and Energy: Transformative Opportunities for Discovery Science. Technical report, U.S. Department of Energy, 2015.
- [2] N. Bohr. *Atomic Physics and Human Knowledge*. John Wiley & Sons, 1958.
- [3] W. Heisenberg. *The Physicist's Conception of Nature*. Hutchinson and Company, 1958.
- [4] W. Yourgrau and S. Mandelstam. *Variational Principles in Dynamics and Quantum Theory*. Dover Publications, 2005.
- [5] M. Born. *Problems of Atomic Dynamics*. MIT Press, 1926.
- [6] E.J. Heller. *The Semiclassical Way to Dynamics and Spectroscopy*. Princeton University Press, 2018.
- [7] M.C. Gutzwiller. *Chaos in Classical and Quantum Mechanics*. Springer, 1990.
- [8] W.H. Miller. Semiclassical Methods in Chemical Physics. *Science*, 233(4760):171–177, 1986.
- [9] J.C. Tully. Mixed Quantum–classical Dynamics. *Faraday Discussions*, 110(0):407–419, 1998.
- [10] R. Kapral. Progress in the Theory of Mixed Quantum-classical Dynamics. *Annual Review of Physical Chemistry*, 57(1):129–157, 2006.
- [11] M.E. Tuckerman. *Statistical Mechanics: Theory and Molecular Simulation*. Oxford University Press, 2010.
- [12] S. Habershon, D.E. Manolopoulos, T.E. Markland, and T.F. Miller III. Ring-Polymer Molecular Dynamics: Quantum Effects in Chemical Dynamics from Classical Trajectories in an Extended Phase Space. *Annual Review of Physical Chemistry*, 64(1):387–413, 2013.
- [13] T.L. Curtright, D.B. Fairlie, and C.K. Zachos. *Quantum Mechanics in Phase Space*. World Scientific, 2014.

- [14] M. de Gosson. *The Wigner Transform*. World Scientific, 2017.
- [15] B. Zweibach. *Mastering Quantum Mechanics: Essentials, Theory, and Applications*. MIT Press, 2022.
- [16] B.L. van der Waerden. *Sources of Quantum Mechanics*. Dover Publications, 1967.
- [17] J.L. McHale. *Molecular Spectroscopy*. CRC Press, 2017.
- [18] D.A. McQuarrie and J.D. Simon. *Physical Chemistry: A Molecular Approach*. University Science Books, 2017.
- [19] D. D’Alessandro. *Introduction to Quantum Control and Dynamics*. CRC Press, 2022.
- [20] S. Mukamel. *Principles of Nonlinear Optical Spectroscopy*. Oxford University Press, 1995.
- [21] E. Hecht. *Optics*. Pearson Education, 2016.
- [22] R.P. Feynman and A.R. Hibbs. *Quantum Mechanics and Path Integrals*. Dover Publications, 1965.
- [23] R.W. Boyd. *Nonlinear Optics*. Academic Press, 2003.
- [24] E.O. Potma. *Foundations of Nonlinear Optical Microscopy*. Wiley, 2024.
- [25] M. Tinkham. *Introduction to Superconductivity*. Dover Publications, 2004.
- [26] N.D. Mermin. *Quantum Computer Science: An Introduction*. Cambridge University Press, 2007.
- [27] T.G. Wong. *Introduction to Classical and Quantum Computing*. Rooted Grove, 2022.
- [28] M.A. Nielsen and I.L. Chuang. *Quantum Computation and Quantum Information*. Cambridge University Press, 2016.
- [29] R.P. Feynman. *Feynman Lectures on Computation*. Perseus Publishing, 1999.
- [30] C. Outeiral, M. Strahm, J. Shi, G.M. Morris, S.C. Benjamin, and C.M. Deane. The Prospects of Quantum Computing in Computational Molecular Biology. *Wiley Interdisciplinary Reviews: Computational Molecular Science*, 11(1), 2021.
- [31] C. Ciliberto, M. Herbster, A.D. Ialongo, M. Pontil, A. Rocchetto, S. Severini, and L. Wossnig. Quantum Machine Learning: A Classical Perspective. *Proceedings of the Royal Society A*, 474(2209):20170551, 2018.
- [32] Y. Alexeev, D. Bacon, K.R. Brown, R. Calderbank, L.D. Carr, F.T. Chong, B. DeMarco, D. Englund, E. Farhi, B. Fefferman, A.V. Gorshkov, A. Houck, J. Kim, S. Kimmel, M. Lange, S. Lloyd, M.D. Lukin, D. Maslov, P. Maunz, C. Monroe, J. Preskill, M. Roetteler, M.J. Savage, and J. Thompson. Quantum Computer Systems for Scientific Discovery. *PRX Quantum*, 2(1), 2021.

- [33] A. Gaita-Ariño, F. Luis, S. Hill, and E. Coronado. Molecular Spins for Quantum Computation. *Nature Chemistry*, 11(4):301–309, 2019.
- [34] M.R. Wasielewski, Malcolm D.E. Forbes, N.L. Frank, K. Kowalski, G.D. Scholes, J. Yuen-Zhou, M.A. Baldo, D.E. Freedman, R.H. Goldsmith, T. Goodson, M.L. Kirk, J.K. McCusker, J.P. Ogilvie, D.A. Shultz, S. Stoll, and K.B. Whaley. Exploiting Chemistry and Molecular Systems for Quantum Information Science. *Nature Reviews Chemistry*, 4(9):490–504, 2020.
- [35] V. Giovannetti, S. Lloyd, and L. Maccone. Advances in Quantum Metrology. *Nature Photonics*, 5(4):222–229, 2011.
- [36] M. Shiddiq, D. Komijani, Y. Duan, A. Gaita-Ariño, E. Coronado, and S. Hill. Enhancing Coherence in Molecular Spin Qubits via Atomic Clock Transitions. *Nature*, 531(7594):348–351, 2016.
- [37] A.H. Zewail. Laser Femtochemistry. *Science*, 242(4886):1645–1653, 1988.
- [38] A.H. Zewail. Femtochemistry. Past, Present, and Future. *Pure and Applied Chemistry*, 72(12):2219–2231, 2000.
- [39] F. Reiter, U. Graf, E.E. Serebryannikov, W. Schweinberger, M. Fiess, M. Schultze, A.M. Azzeer, R. Kienberger, F. Krausz, A.M. Zheltikov, and E. Goulielmakis. Route to Attosecond Nonlinear Spectroscopy. *Physical Review Letters*, 105(24):243902, 2010.
- [40] D. Keefer, S.M. Cavaletto, J.R. Rouxel, M. Garavelli, H. Yong, and S. Mukamel. Ultrafast X-Ray Probes of Elementary Molecular Events. *Annual Review of Physical Chemistry*, 74(1):73–97, 2023.
- [41] M. Kowalewski, K. Bennett, K.E. Dorfman, and S. Mukamel. Catching Conical Intersections in the Act: Monitoring Transient Electronic Coherences by Attosecond Stimulated X-Ray Raman Signals. *Physical Review Letters*, 115(19):193003, 2015.
- [42] D. Keefer, T. Schnappinger, R. de Vivie-Riedle, and S. Mukamel. Visualizing Conical Intersection Passages via Vibronic Coherence Maps Generated by Stimulated Ultrafast X-ray Raman Signals. *Proceedings of the National Academy of Sciences*, 117(39):24069–24075, 2020.
- [43] D. Keefer, V.M. Freixas, H. Song, S. Tretiak, S. Fernandez-Alberti, and S. Mukamel. Monitoring Molecular Vibronic Coherences in a Bichromophoric Molecule by Ultrafast X-ray Spectroscopy. *Chemical Science*, 12(14):5286–5294, 2021.
- [44] S.M. Cavaletto, Y. Nam, J.R. Rouxel, D. Keefer, H. Yong, and S. Mukamel. Attosecond Monitoring of Nonadiabatic Molecular Dynamics by Transient X-ray Transmission Spectroscopy. *Journal of Chemical Theory and Computation*, 19(8):2327–2339, 2023.
- [45] W. Domcke and D.R. Yarkony. Role of Conical Intersections in Molecular Spectroscopy and Photoinduced Chemical Dynamics. *Annual Review of Physical Chemistry*, 63(1):325–352, 2012.

- [46] D.R. Yarkony. Diabolical Conical Intersections. *Reviews of Modern Physics*, 68(4):985–1013, 1996.
- [47] J. Savolainen, R. Fanciulli, N. Dijkhuizen, A.L. Moore, J. Hauer, T. Buckup, M. Motzkus, and J.L. Herek. Controlling the Efficiency of an Artificial Light-harvesting Complex. *Proceedings of the National Academy of Sciences*, 105(22):7641–7646, 2008.
- [48] N. Liu, Y. Zhang, K. Niu, F. Lu, and D. Zhong. Optical Control of Crossing the Conical Intersection in  $\beta$ -Carotene. *The Journal of Physical Chemistry Letters*, 14(41):9215–9221, 2023.
- [49] P.A.M. Dirac. Quantum Mechanics of Many-electron Systems. *Proceedings of the Royal Society of London. Series A, Containing Papers of a Mathematical and Physical Character*, 123(792):714–733, 1929.
- [50] C.L. Janssen and I.D.B. Nielsen. *Parallel Computing in Quantum Chemistry*. CRC Press, 2008.
- [51] E. Merzbacher. *Quantum Mechanics*. John Wiley & Sons, 1970.
- [52] M.H. Stone. Linear Transformations in Hilbert Space. *Proceedings of the National Academy of Sciences*, 16(2):172–175, 1930.
- [53] J.D. Jackson. *Mathematics for Quantum Mechanics: An Introductory Survey of Operators, Eigenvalues, and Linear Vector Spaces*. Dover Publications, 1990.
- [54] G.H. Golub and C.F. van Loan. *Matrix Computations*. Johns Hopkins University Press, 1989.
- [55] M.T. Heath. *Scientific Computing: An Introductory Survey*. McGraw-Hill, 2005.
- [56] W. Schweizer. *Numerical Quantum Dynamics*. Kluwer Academic Publishers, 2001.
- [57] M. Friedman. *There’s No Such Thing as a Free Lunch*. Open Court Publishing Company, 1975.
- [58] J.Z.H. Zhang. *Theory and Application of Quantum Molecular Dynamics*. World Scientific, 1999.
- [59] D.B. Cook. *Handbook of Computational Quantum Chemistry*. Oxford University Press, 1998.
- [60] A. Szabo and N.S. Ostlund. *Modern Quantum Chemistry: Introduction to Advanced Electronic Structure Theory*. McGraw-Hill, 1989.
- [61] M. Born and K. Huang. *Dynamical Theory of Crystal Lattices*. Oxford University Press, 1954.

- [62] V.M. Freixas, W. Malone, X. Li, H. Song, H. Negrin-Yuvero, R. Pérez-Castillo, A. White, T.R. Gibson, D.V. Makhov, D.V. Shalashilin, Y. Zhang, N. Fedik, M. Kulichenko, R. Messerly, L.N. Mohanam, S. Sharifzadeh, A. Bastida, S. Mukamel, S. Fernandez-Alberti, and S. Tretiak. NEXMD v2.0 Software Package for Nonadiabatic Excited State Molecular Dynamics Simulations. *Journal of Chemical Theory and Computation*, 2023.
- [63] S. Kilina, D. Kilin, and S. Tretiak. Light-Driven and Phonon-Assisted Dynamics in Organic and Semiconductor Nanostructures. *Chemical Reviews*, 115(12):5929–5978, 2015.
- [64] J.C. Tully. Molecular Dynamics with Electronic Transitions. *The Journal of Chemical Physics*, 93(2):1061–1071, 1990.
- [65] L. Wang, A. Akimov, and O.V. Prezhdo. Recent Progress in Surface Hopping: 2011–2015. *The Journal of Physical Chemistry Letters*, 7(11):2100–2112, 2016.
- [66] J. Lu and Z. Zhou. Path Integral Molecular Dynamics with Surface Hopping for Thermal Equilibrium Sampling of Nonadiabatic Systems. *The Journal of Chemical Physics*, 146(15):154110, 2017.
- [67] J.R. Mannouch and J.O. Richardson. A Mapping Approach to Surface Hopping. *The Journal of Chemical Physics*, 158(10):104111, 2023.
- [68] J.E. Subotnik, A. Jain, B. Landry, A. Petit, W. Ouyang, and N. Bellonzi. Understanding the Surface Hopping View of Electronic Transitions and Decoherence. *Annual Review of Physical Chemistry*, 67(1):387–417, 2016.
- [69] G. Miao and J. Subotnik. Revisiting the Recoherence Problem in the Fewest Switches Surface Hopping Algorithm. *The Journal of Physical Chemistry A*, 123(26):5428–5435, 2019.
- [70] R. Crespo-Otero and M. Barbatti. Recent Advances and Perspectives on Nonadiabatic Mixed Quantum–classical Dynamics. *Chemical Reviews*, 118(15):7026–7068, 2018.
- [71] H. Song, V.M. Freixas, S. Fernandez-Alberti, A.J. White, Y. Zhang, S. Mukamel, N. Govind, and S. Tretiak. An Ab Initio Multiple Cloning Method for Non-Adiabatic Excited-State Molecular Dynamics in NWChem. *Journal of Chemical Theory and Computation*, 17(6):3629–3643, 2021.
- [72] D.M. Huang, A.T. Green, and C.C. Martens. A First Principles Derivation of Energy-conserving Momentum Jumps in Surface Hopping Simulations. *The Journal of Chemical Physics*, 159(21):214108, 2023.
- [73] M.J.W. Hall. Consistent Classical and Quantum Mixed Dynamics. *Physical Review A*, 78(4):042104, 2008.
- [74] M.S. Child. *Semiclassical Mechanics with Molecular Applications*. Oxford University Press, 2014.

- [75] W.H. Miller. Perspective: Quantum or Classical Coherence? *The Journal of Chemical Physics*, 136(21):210901, 2012.
- [76] M. Thoss and H. Wang. Semiclassical Description of Molecular Dynamics Based on Initial-value Representation Methods. *Annual Review of Physical Chemistry*, 55(1):299–332, 2004.
- [77] M.S. Church and N. Ananth. Semiclassical Dynamics in the Mixed Quantum-classical Limit. *The Journal of Chemical Physics*, 151(13):134109, 2019.
- [78] W.P. Schleich. *Quantum Optics in Phase Space*. Wiley-VCH, 2001.
- [79] D.J. Tannor. *Introduction to Quantum Mechanics: A Time-Dependent Perspective*. University Science Books, 2007.
- [80] V.I. Arnold. *Mathematical Methods of Classical Mechanics*. Springer, 1989.
- [81] H. Goldstein, C. Poole, and J. Safko. *Classical Mechanics*. Pearson Education, 2002.
- [82] A.J. Lichtenberg. *Phase-Space Dynamics of Particles*. John Wiley & Sons, 1969.
- [83] J.V. José and E.J. Saletan. *Classical Dynamics: A Contemporary Approach*. Cambridge University Press, 1998.
- [84] E.C.G. Sudarshan and N. Mukunda. *Classical Dynamics*. World Scientific, 2016.
- [85] R.C. Robinson. *An Introduction to Dynamical Systems: Continuous and Discrete*. Pearson Education, 2004.
- [86] B. Leimkuhler and S. Reich. *Simulating Hamiltonian Dynamics*. Cambridge University Press, 2004.
- [87] T.A. Garrity. *All the Math You Missed (But Need to Know for Graduate School)*. Cambridge University Press, 2021.
- [88] W.E. Boyce and R.C. DiPrima. *Elementary Differential Equations*. John Wiley & Sons, 2005.
- [89] R.L. Burden and J.D. Faires. *Numerical Analysis*. Cengage Learning, 2011.
- [90] R. Zwanzig. *Nonequilibrium Statistical Mechanics*. Oxford University Press, 2001.
- [91] D. Boccaletti and G. Pucacco. *Theory of Orbits 2: Perturbative and Geometric Methods*. Springer, 1999.
- [92] O. Penrose. *Foundations of Statistical Mechanics: A Deductive Treatment*. Dover Publications, 1970.
- [93] R.L. Liboff. *Kinetic Theory: Classical, Quantum, and Relativistic Descriptions*. Springer, 2003.

- [94] I. Prigogine. *Non-Equilibrium Statistical Mechanics*. Wiley, 1962.
- [95] R. Dugas. *A History of Mechanics*. Dover Publications, 1988.
- [96] D.F. Styer, M.S. Balkin, K.M. Becker, M.R. Burns, C.E. Dudley, S.T. Forth, J.S. Gaumer, M.A. Kramer, D.C. Oertel, L.H. Park, M.T. Rinkoski, C.T. Smith, and T.D. Wotherspoon. Nine Formulations of Quantum Mechanics. *American Journal of Physics*, 70(3):288–297, 2002.
- [97] P.A.M. Dirac. *The Principles Of Quantum Mechanics*. Oxford University Press, 1988.
- [98] D. Bohm. *Quantum Theory*. Dover Publications, 1989.
- [99] A.C. Hirshfeld and P. Henselder. Deformation Quantization in the Teaching of Quantum Mechanics. *American Journal of Physics*, 70(5):537–547, 2002.
- [100] F. Bayen, M. Flato, C. Fronsdal, A. Lichnerowicz, and D. Sternheimer. Deformation Theory and Quantization. I. Deformations of Symplectic Structures. *Annals of Physics*, 110(1):247–248, 1978.
- [101] F. Bayen, M. Flato, C. Fronsdal, A. Lichnerowicz, and D. Sternheimer. Deformation Theory and Quantization. II. Physical Applications. *Annals of Physics*, 111(1):111–151, 1978.
- [102] M. Gerstenhaber. On the Deformation of Rings and Algebras. *The Annals of Mathematics*, 79(1):59, 1964.
- [103] G.B. Folland. *Harmonic Analysis in Phase Space*. Princeton University Press, 1989.
- [104] M. Kontsevich. Deformation Quantization of Algebraic Varieties. *Letters in Mathematical Physics*, 56(3):271–294, 2001.
- [105] M. Kontsevich. Deformation Quantization of Poisson Manifolds. *Letters in Mathematical Physics*, 66(3):157–216, 2003.
- [106] M.A. Rieffel.  $C^*$ -Algebras: 1943–1993. *Contemporary Mathematics*, pages 66–97, 1994.
- [107] E.J. Heller. Wigner Phase Space Method: Analysis for Semiclassical Applications. *The Journal of Chemical Physics*, 65(4):1289–1298, 1976.
- [108] D.B. Fairlie. Moyal Brackets, Star Products and the Generalised Wigner Function. *Chaos, Solitons & Fractals*, 10(2-3):365–371, 1999.
- [109] J. Weinbub and D.K. Ferry. Recent Advances in Wigner Function Approaches. *Applied Physics Reviews*, 5(4):041104, 2018.
- [110] A. Torre. *Linear Ray and Wave Optics in Phase Space*. Elsevier, 2005.
- [111] M. Hillery, R.F. O’Connell, M.O. Scully, and E.P. Wigner. Distribution Functions in Physics: Fundamentals. *Physics Reports*, 106(3):121–167, 1984.

- [112] H.-W. Lee. Theory and Application of the Quantum Phase-space Distribution Functions. *Physics Reports*, 259(3):147–211, 1995.
- [113] M.V. Berry. Semiclassical Mechanics in Phase Space: A Study of Wigner’s Function. *Philosophical Transactions of the Royal Society of London. Series A, Mathematical and Physical Sciences*, 287(1343):237–271, 1977.
- [114] T. Takabayasi. The Formulation of Quantum Mechanics in terms of Ensemble in Phase Space. *Progress of Theoretical Physics*, 11(4-5):341–373, 1954.
- [115] A. Donoso and C.C. Martens. Classical Trajectory-based Approaches to Solving the Quantum Liouville Equation. *International Journal of Quantum Chemistry*, 90(4-5):1348–1360, 2002.
- [116] M. Oliva, D. Kakofengitis, and O. Steuernagel. Anharmonic Quantum Mechanical Systems Do Not Feature Phase Space Trajectories. *Physica A: Statistical Mechanics and its Applications*, 502:201–210, 2018.
- [117] M. Oliva and O. Steuernagel. Dynamic Shear Suppression in Quantum Phase Space. *Physical Review Letters*, 122(2):020401, 2019.
- [118] E. Wigner. On the Quantum Correction For Thermodynamic Equilibrium. *Physical Review*, 40(5):749–759, 1932.
- [119] W.B. Case. Wigner Functions and Weyl Transforms for Pedestrians. *American Journal of Physics*, 76(10):937–946, 2008.
- [120] M. Hug, C. Menke, and W.P. Schleich. How to Calculate the Wigner Function from Phase Space. *Journal of Physics A: Mathematical and General*, 31(11):L217, 1999.
- [121] H.J. Groenewold. On the Principles of Elementary Quantum Mechanics. *Physica*, 12(7):405–460, 1946.
- [122] J. E. Moyal. Quantum Mechanics as a Statistical Theory. *Mathematical Proceedings of the Cambridge Philosophical Society*, 45(1):99–124, 1949.
- [123] Craig C Martens and Jian-Yun Fang. Semiclassical-limit Molecular Dynamics on Multiple Electronic Surfaces. *The Journal of Chemical Physics*, 106(12):4918–4930, 1997.
- [124] V. Ovsienko and C. Roger. Deformations of Poisson Brackets and Extensions of Lie Algebras of Contact Vector Fields. *Russian Mathematical Surveys*, 47(6):135–191, 1992.
- [125] F. Bopp. La mécanique Quantique est-elle une Mécanique Statistique Classique Particulière ? *Annales de L’I.H.P.*, 2(15), 1956.
- [126] H. Weyl. *The Theory of Groups and Quantum Mechanics*. Dover Publications, 1950.
- [127] J. v. Neumann. Die Eindeutigkeit der Schrödingerschen Operatoren. *Mathematische Annalen*, 104(1):570–578, 1931.



- [128] R. Strichartz. *A Guide to Distribution Theory and Fourier Transforms*. CRC Press, 1994.
- [129] R. Estrada, J.M. Gracia-Bondía, and J.C. Várilly. On Asymptotic Expansions of Twisted Products. *Journal of Mathematical Physics*, 30(12):2789–2796, 1989.
- [130] J.M. Gracia-Bondía and J.C. Várilly. Algebras of Distributions Suitable for Phase-space Quantum Mechanics. I. *Journal of Mathematical Physics*, 29(4):869–879, 1988.
- [131] J.C. Várilly and J.M. Gracia-Bondía. Algebras of Distributions Suitable for Phase-space Quantum Mechanics. II. Topologies on the Moyal Algebra. *Journal of Mathematical Physics*, 29(4):880–887, 1988.
- [132] J.M. Maillard. On the Twisted Convolution Product and the Weyl Transformation of Tempered Distributions. *Journal of Geometry and Physics*, 3(2):231–261, 1986.
- [133] J.F. James. *A Student's Guide to Fourier Transforms with Applications to Physics and Engineering*. Cambridge University Press, 1995.
- [134] G.A. Baker. Formulation of Quantum Mechanics Based on the Quasi-Probability Distribution Induced on Phase Space. *Physical Review*, 109(6):2198–2206, 1958.
- [135] M. Błaszak and Z. Domański. Phase Space Quantum Mechanics. *Annals of Physics*, 327(2):167–211, 2012.
- [136] D.B. Fairlie and C.A. Manogue. The Formulation of Quantum Mechanics in terms of Phase Space Functions - The Third Equation. *Journal of Physics A: Mathematical and General*, 24(16):3807, 1999.
- [137] R.L. Hudson. When is the Wigner Quasi-probability Density Non-negative? *Reports on Mathematical Physics*, 6(2):249–252, 1974.
- [138] M. Walschaers. Non-Gaussian Quantum States and Where to Find Them. *PRX Quantum*, 2(3):030204, 2021.
- [139] V.I. Tatarskiĭ. The Wigner Representation of Quantum Mechanics. *Soviet Physics Uspekhi*, 26(4):311–327, 1983.
- [140] E. Schrödinger. Der stetige Übergang von der Mikro- zur Makromechanik. *Naturwissenschaften*, 14(28):664–666, 1926.
- [141] L. Mandel and E. Wolf. *Optical Coherence and Quantum Optics*. Cambridge University Press, 1995.
- [142] R.G. Littlejohn. The Semiclassical Evolution of Wave Packets. *Physics Reports*, 138(4-5):193–291, 1986.
- [143] Y.S. Kim and M.E. Noz. *Phase Space Pictures of Quantum Mechanics: Group Theoretical Approach*. World Scientific, 1991.

- [144] J.M. Riga and C.C. Martens. Simulation of Environmental Effects on Coherent Quantum Dynamics in Many-body Systems. *The Journal of Chemical Physics*, 120(15):6863–6873, 2004.
- [145] J.M. Riga and C.C. Martens. Environmental Decoherence of Many-body Quantum Systems: Semiclassical Theory and Simulation. *Chemical Physics*, 322(1-2):108–117, 2006.
- [146] A.T. Green and C.C. Martens. Zombie Cats on the Quantum–classical Frontier: Wigner–Moyal and Semiclassical Limit Dynamics of Quantum Coherence in Molecules. *The Journal of Chemical Physics*, 159(20):204102, 2023.
- [147] J.D. Lawrence. *A Catalog of Special Plane Curves*. Dover Publications, 1972.
- [148] A. Nitzan. *Chemical Dynamics in Condensed Phases: Relaxation, Transfer, and Reactions in Condensed Molecular Systems*. Oxford University Press, 2006.
- [149] G.C. Schatz and M.A. Ratner. *Quantum Mechanics in Chemistry*. Dover Publications, 1993.
- [150] S.R. Garcia and R.A. Horn. *Matrix Mathematics: A Second Course in Linear Algebra*. Cambridge University Press, 2023.
- [151] B.J. Schwartz, E.R. Bittner, O.V. Prezhdo, and P.J. Rossky. Quantum Decoherence and the Isotope Effect in Condensed Phase Nonadiabatic Molecular Dynamics Simulations. *The Journal of Chemical Physics*, 104(15):5942–5955, 1996.
- [152] E.R. Bittner and P.J. Rossky. Quantum Decoherence in Mixed Quantum-classical Systems: Nonadiabatic Processes. *The Journal of Chemical Physics*, 103(18):8130–8143, 1995.
- [153] E.J. Heller. Time-dependent Approach to Semiclassical Dynamics. *The Journal of Chemical Physics*, 62(4):1544–1555, 1975.
- [154] E.J. Heller. Frozen Gaussians: A Very Simple Semiclassical Approximation. *The Journal of Chemical Physics*, 75(6):2923–2931, 1981.
- [155] C.M. Bishop. *Pattern Recognition and Machine Learning*. Springer, 2006.
- [156] C.E. Rasmussen and C.K.I. Williams. *Gaussian Processes for Machine Learning*. MIT Press, 2006.
- [157] J. MacQueen. Some Methods for Classification and Analysis of Multivariate Observations. *Berkeley Symposium on Mathematics, Statistics, and Probability*, 5(1):281–297, 1967.
- [158] Á. Gombkötő, S. Varró, P. Mati, and P. Földi. High-order Harmonic Generation as Induced by a Quantized Field: Phase-space Picture. *Physical Review A*, 101(1):013418, 2020.

- [159] S. Fechner, F. Dimler, T. Brixner, G. Gerber, and D.J. Tannor. The von Neumann Picture: A New Representation for Ultrashort Laser Pulses. *Optics Express*, 15(23):15387, 2007.
- [160] J. Zak. Orthonormal Coherent States on von Neumann Lattices. *Journal of Physics A: Mathematical and General*, 34(5):1063, 2001.

# Appendix A

## Star Product Identities and Truncations

### A.1 Complex Numbers

For a complex number  $z \in \mathbb{C}$  with its conjugate  $\bar{z}$ , its real and imaginary parts, respectively are

$$\operatorname{Re}(z) = \frac{z + \bar{z}}{2} \tag{A.1}$$

$$\operatorname{Im}(z) = \frac{z - \bar{z}}{2i}. \tag{A.2}$$

For the product of two complex numbers  $z \in \mathbb{C}$  and  $w \in \mathbb{C}$ , the real and imaginary parts of their product are respectively,

$$\operatorname{Re}(zw) = \operatorname{Re}(z)\operatorname{Re}(w) - \operatorname{Im}(z)\operatorname{Im}(w) \tag{A.3}$$

$$\operatorname{Im}(zw) = \operatorname{Re}(z)\operatorname{Im}(w) + \operatorname{Im}(z)\operatorname{Re}(w). \tag{A.4}$$

For two Weyl symbols  $f, g \in \mathbb{C}$ , the real and imaginary parts of their star product are

$$\operatorname{Re}(f \star g) = \frac{f \star g + \overline{f \star g}}{2} = \frac{f \star g + \bar{g} \star \bar{f}}{2} \quad (\text{A.5})$$

$$\operatorname{Im}(f \star g) = \frac{f \star g - \overline{f \star g}}{2i} = \frac{f \star g - \bar{g} \star \bar{f}}{2i}. \quad (\text{A.6})$$

As a special case, when  $f, g \in \mathbb{R}$

$$\operatorname{Re}(f \star g) = \frac{f \star g + g \star f}{2} = \left( \frac{i\hbar}{2} \right) \{f, g\}_\star \quad (\text{A.7})$$

$$\operatorname{Im}(f \star g) = \frac{f \star g - g \star f}{2i} = \left( \frac{\hbar}{2} \right) [f, g]_\star. \quad (\text{A.8})$$

Because the trace (integration), differentiation, and real and imaginary parts are linear operations which commute, for  $z \in \mathbb{C}$

$$\operatorname{Re}(\operatorname{Tr}(z)) = \operatorname{Tr}(\operatorname{Re}(z)) \quad \operatorname{Im}(\operatorname{Tr}(z)) = \operatorname{Tr}(\operatorname{Im}(z)) \quad (\text{A.9})$$

$$\operatorname{Re}\left(\frac{dz}{dt}\right) = \frac{d \operatorname{Re}(z)}{dt} \quad \operatorname{Im}\left(\frac{dz}{dt}\right) = \frac{d \operatorname{Im}(z)}{dt} \quad (\text{A.10})$$

with  $t \in \mathbb{R}$ .

## A.2 Truncation Identities

Truncations I. Quick Reference				
$\mathcal{O}(\hbar^n)$	$f \star g$	$f \star g \star h$	$[f, g]_\star$	$\{f, g\}_\star$
$\mathcal{O}(\hbar^0)$	Eq. A.11	Eq. A.14	Eq. A.17	Eq. A.20
$\mathcal{O}(\hbar^1)$	Eq. A.12	Eq. A.15	Eq. A.18	Eq. A.21
$\mathcal{O}(\hbar^2)$	Eq. A.13	Eq. A.16	Eq. A.19	Eq. A.22

Table A.1: Truncation identities for star products.

Truncations II. Quick Reference				
$\mathcal{O}(\hbar^n)$	$\text{Tr}(f \star g)$	$\text{Tr}(f \star g \star h)$	$\text{Tr}([f, g]_\star)$	$\text{Tr}(\{f, g\}_\star)$
$\mathcal{O}(\hbar^0)$	Eq. A.23	Eq. A.26	Eq. A.29	Eq. A.32
$\mathcal{O}(\hbar^1)$	Eq. A.24	Eq. A.27	Eq. A.30	Eq. A.33
$\mathcal{O}(\hbar^2)$	Eq. A.25	Eq. A.28	Eq. A.31	Eq. A.34

Table A.2: Truncation identities for traces of star products.

$$f \star g = fg + \mathcal{O}(\hbar) \quad (\text{A.11})$$

$$f \star g = fg + \frac{i\hbar}{2} [f, g] + \mathcal{O}(\hbar^2) \quad (\text{A.12})$$

$$f \star g = fg + \frac{i\hbar}{2} [f, g] - \frac{\hbar^2}{8} [f, g]_2 + \mathcal{O}(\hbar^3) \quad (\text{A.13})$$

$$f \star g \star h = fgh + \mathcal{O}(\hbar) \quad (\text{A.14})$$

$$f \star g \star h = fgh + \frac{i\hbar}{2} \left( f [g, h] + g [f, h] + h [f, g] \right) + \mathcal{O}(\hbar^2) \quad (\text{A.15})$$

$$\begin{aligned} f \star g \star h = & fgh + \frac{i\hbar}{2} \left( f [g, h] + g [f, h] + h [f, g] \right) \\ & - \frac{\hbar^2}{8} \left( [f, [g, h]] + [[f, g], h] + \frac{1}{2} \left( f [g, h]_2 + [f, g]_2 h + [fg, h]_2 + [f, gh]_2 \right) \right) + \mathcal{O}(\hbar^3) \end{aligned} \quad (\text{A.16})$$

$$[f, g]_\star = 0 + \mathcal{O}(\hbar) \quad (\text{A.17})$$

$$[f, g]_\star = [f, g] + \mathcal{O}(\hbar^2) \quad (\text{A.18})$$

$$[f, g]_\star = [f, g] + \mathcal{O}(\hbar^3) \quad (\text{A.19})$$

$$\{f, g\}_\star = \frac{2}{i\hbar} (fg + \mathcal{O}(\hbar)) \quad (\text{A.20})$$

$$\{f, g\}_\star = \frac{2}{i\hbar} (fg + \mathcal{O}(\hbar^2)) \quad (\text{A.21})$$

$$\{f, g\}_\star = \frac{2}{i\hbar} \left( fg - \frac{\hbar^2}{8} [f, g]_2 + \mathcal{O}(\hbar^3) \right) \quad (\text{A.22})$$

$$\text{Tr}(f \star g) = \text{Tr}(fg) + \mathcal{O}(\hbar) \quad (\text{A.23})$$

$$\text{Tr}(f \star g) = \text{Tr}(fg) + \mathcal{O}(\hbar^2) \quad (\text{A.24})$$

$$\text{Tr}(f \star g) = \text{Tr}(fg) + \mathcal{O}(\hbar^3) \quad (\text{A.25})$$

$$\text{Tr}(f \star g \star h) = \text{Tr}(fgh) + \mathcal{O}(\hbar) \quad (\text{A.26})$$

$$\text{Tr}(f \star g \star h) = \text{Tr}(fgh) + \frac{i\hbar}{2} \text{Tr}\left(f[g, h] + g[f, h] + h[f, g]\right) + \mathcal{O}(\hbar^2) \quad (\text{A.27})$$

$$\begin{aligned} \text{Tr}(f \star g \star h) &= \text{Tr}(fgh) + \frac{i\hbar}{2} \text{Tr}\left(f[g, h] + g[f, h] + h[f, g]\right) \\ &\quad - \frac{\hbar^2}{16} \text{Tr}\left(f[g, h]_2 + [f, g]_2 h + [fg, h]_2 + [f, gh]_2\right) + \mathcal{O}(\hbar^3) \end{aligned} \quad (\text{A.28})$$

$$\text{Tr}([f, g]_\star) = 0 + \mathcal{O}(\hbar) \quad (\text{A.29})$$

$$\text{Tr}([f, g]_\star) = 0 + \mathcal{O}(\hbar^2) \quad (\text{A.30})$$

$$\text{Tr}([f, g]_\star) = 0 + \mathcal{O}(\hbar^3) \quad (\text{A.31})$$

$$\mathrm{Tr}(\{f, g\}_\star) = \frac{2}{i\hbar} \mathrm{Tr}(fg) + \mathcal{O}(\hbar) \quad (\text{A.32})$$

$$\mathrm{Tr}(\{f, g\}_\star) = \frac{2}{i\hbar} \mathrm{Tr}(fg) + \mathcal{O}(\hbar^2) \quad (\text{A.33})$$

$$\mathrm{Tr}(\{f, g\}_\star) = \frac{2}{i\hbar} \mathrm{Tr}(fg) - \frac{\hbar}{4i} \mathrm{Tr}([f, g]_2) + \mathcal{O}(\hbar^3) \quad (\text{A.34})$$



# Appendix B

## Star Product of Two Gaussian Weyl Symbols

Consider two Gaussian form Weyl symbols for 1 degree of freedom

$$g_j(q, p) = A_j e^{-\alpha_j(q-Q_j)^2 - \beta_j(p-P_j)^2 + \gamma_j(q-Q_j)(p-P_j) + \delta_j} = g_j(q, p, \chi_j) \quad (\text{B.1})$$

for  $j = 1, 2$ . Their parameters are denoted by  $\chi_j = (A_j, \alpha_j, \beta_j, \gamma_j, Q_j, P_j)$ . The star product  $g_1(q, p, \chi_1) \star g_2(q, p, \chi_2)$  will yield another Gaussian form Weyl symbol

$$\begin{aligned} g_{12} &= g_1(q, p, \chi_1) \star g_2(q, p, \chi_2) \\ &= A e^{-\alpha(q-Q)^2 - \beta(p-P)^2 + \gamma(q-Q)(p-P) + \delta} = g_{12}(q, p, \chi) \end{aligned} \quad (\text{B.2})$$

where  $\chi$  is the statistical parameters associated with the resulting star product  $\chi = (A, Q, P, \alpha, \beta, \gamma, \delta)$ .

Each parameter in  $\chi$  will generally be a function mixing the parameters  $\chi_1$  and  $\chi_2$  of the two Weyl symbols  $g(q, p, \chi_1)$  and  $g(q, p, \chi_2)$ . The calculation is lengthy and involves computing the star product by Fourier Transform followed by completing the square in the argument of the resulting Gaussian. But when done yields,

$$\begin{aligned}
A &= f_A(\chi_1, \chi_2) = f_A(A_1, \alpha_1, \beta_1, \gamma_1, A_2, \alpha_2, \beta_2, \gamma_2) \\
&= \frac{4 A_1 A_2 \sqrt{4\alpha_1\beta_1 - \gamma_1^2} \sqrt{4\alpha_2\beta_2 - \gamma_2^2}}{\sqrt{\alpha_1}\sqrt{\alpha_2}\sqrt{4\beta_1 - \frac{\gamma_1^2}{\alpha_1}}\sqrt{4\beta_2 - \frac{\gamma_2^2}{\alpha_2}}} \\
&\quad \times \frac{1}{\sqrt{16 + 8\hbar^2(2\alpha_1\beta_2 + 2\alpha_2\beta_1 - \gamma_1\gamma_2) + \hbar^4(4\alpha_1\beta_1 - \gamma_1^2)(4\alpha_2\beta_2 - \gamma_2^2)}}
\end{aligned} \tag{B.3}$$

$$\begin{aligned}
\alpha &= f_\alpha(\chi_1, \chi_2) = -c_{qq} \\
&= \frac{16 \left( (\alpha_1 + \alpha_2) + i\hbar(\alpha_1\gamma_2 - \alpha_2\gamma_1) + \hbar^2 \left( \alpha_1\alpha_2(\beta_1 + \beta_2) - \frac{1}{4}(\alpha_1\gamma_2^2 + \alpha_2\gamma_1^2) \right) \right)}{16 + 8\hbar^2(2\alpha_1\beta_2 + 2\alpha_2\beta_1 - \gamma_1\gamma_2) + \hbar^4(4\alpha_1\beta_1 - \gamma_1^2)(4\alpha_2\beta_2 - \gamma_2^2)} \\
&= f_\alpha(\alpha_1, \alpha_2, \beta_1, \beta_2, \gamma_1, \gamma_2)
\end{aligned} \tag{B.4}$$

$$\begin{aligned}
\beta &= f_\beta(\chi_1, \chi_2) = -c_{pp} \\
&= \frac{16 \left( (\beta_1 + \beta_2) + i\hbar(\beta_1\gamma_2 - \beta_2\gamma_1) + \hbar^2 \left( \beta_1\beta_2(\alpha_1 + \alpha_2) - \frac{1}{4}(\beta_1\gamma_2^2 + \beta_2\gamma_1^2) \right) \right)}{16 + 8\hbar^2(2\alpha_1\beta_2 + 2\alpha_2\beta_1 - \gamma_1\gamma_2) + \hbar^4(4\alpha_1\beta_1 - \gamma_1^2)(4\alpha_2\beta_2 - \gamma_2^2)} \\
&= f_\beta(\alpha_1, \alpha_2, \beta_1, \beta_2, \gamma_1, \gamma_2)
\end{aligned} \tag{B.5}$$

$$\begin{aligned}
\gamma &= f_\gamma(\chi_1, \chi_2) = +c_{qp} \\
&= \frac{16 \left( (\gamma_1 + \gamma_2) + 2i\hbar(\alpha_1\beta_2 - \alpha_2\beta_1) + \hbar^2 \left( \alpha_1\beta_1\gamma_2 + \alpha_2\beta_2\gamma_1 - \frac{1}{4}\gamma_1\gamma_2(\gamma_1 + \gamma_2) \right) \right)}{16 + 8\hbar^2(2\alpha_1\beta_2 + 2\alpha_2\beta_1 - \gamma_1\gamma_2) + \hbar^4(4\alpha_1\beta_1 - \gamma_1^2)(4\alpha_2\beta_2 - \gamma_2^2)} \\
&= f_\gamma(\alpha_1, \alpha_2, \beta_1, \beta_2, \gamma_1, \gamma_2)
\end{aligned} \tag{B.6}$$

$$\begin{aligned}
Q &= f_Q(\chi_1, \chi_2) = h_1 \\
&= \frac{1}{2V} \left( Q_1 (8\alpha_1 (\beta_1 + \beta_2) - 2\gamma_1 (\gamma_1 + \gamma_2) - i (4\alpha_2\beta_2\gamma_1 + 4\alpha_1\beta_1\gamma_2 - \gamma_1\gamma_2 (\gamma_1 + \gamma_2)) \hbar) \right. \\
&\quad + Q_2 (8\alpha_2 (\beta_1 + \beta_2) - 2\gamma_2 (\gamma_1 + \gamma_2) + i (4\alpha_2\beta_2\gamma_1 + 4\alpha_1\beta_1\gamma_2 - \gamma_1\gamma_2 (\gamma_1 + \gamma_2)) \hbar) \quad (\text{B.7}) \\
&\quad \left. + 2 (P_1 + P_2) (-2\beta_2\gamma_1 + i\beta_2 (4 (\alpha_1 + \alpha_2) \beta_1 - \gamma_1^2) \hbar + \beta_1\gamma_2 (2 - i\gamma_2\hbar)) \right) \\
&= f_Q(\alpha_1, \alpha_2, \beta_1, \beta_2, \gamma_1, \gamma_2, Q_1, Q_2, P_1, P_2)
\end{aligned}$$

$$\begin{aligned}
P &= f_P(\chi_1, \chi_2) = h_2 \\
&= \frac{1}{2V} \left( P_1 (8 (\alpha_1 + \alpha_2) \beta_1 - \gamma_1 (\gamma_1 + \gamma_2) + i (4\alpha_2\beta_2\gamma_1 + 4\alpha_1\beta_1\gamma_2 - \gamma_1\gamma_2 (\gamma_1 + \gamma_2)) \hbar) \right. \\
&\quad + 2i (Q_1 - Q_2) (2i\alpha_2\gamma_1 + \alpha_2 (-4\alpha_1 (\beta_1 + \beta_2) + \gamma_1^2) \hbar + \alpha_1\gamma_2 (-2i + \gamma_2\hbar)) \quad (\text{B.8}) \\
&\quad \left. + P_2 ((4\alpha_2\beta_2 - \gamma_2 (\gamma_1 + \gamma_2)) (2 - i\gamma_1\hbar) + \alpha_1 (8\beta_2 - 4i\beta_1\gamma_2\hbar)) \right) \\
&= f_P(\alpha_1, \alpha_2, \beta_1, \beta_2, \gamma_1, \gamma_2, Q_1, Q_2, P_1, P_2)
\end{aligned}$$

$$\begin{aligned}
\delta &= f_\delta(\chi_1, \chi_2) = k \\
&= \frac{1}{V} \left( -4P_1^2 \alpha_1 \beta_1 \beta_2 + 8P_1 P_2 \alpha_1 \beta_1 \beta_2 - 4P_2^2 \alpha_1 \beta_1 \beta_2 - 4P_1^2 \alpha_2 \beta_1 \beta_2 + 8P_1 P_2 \alpha_2 \beta_1 \beta_2 \right. \\
&\quad - 4P_2^2 \alpha_2 \beta_1 \beta_2 + P_1 \beta_2 \gamma_1^2 - 2P_1 P_2 \beta_2 \gamma_1^2 + P_2 \beta_2 \gamma_1^2 + P_1^2 \beta_1 \gamma_2^2 - 2P_1 P_2 \gamma_2^2 + P_2^2 \beta_1 \gamma_2^2 \\
&\quad - (P_1 - P_2) Q_2 (4\alpha_2 \beta_2 \gamma_1 + 4\alpha_1 \beta_1 \gamma_2 - \gamma_1 \gamma_2 (\gamma_1 + \gamma_2)) \\
&\quad + Q_1^2 (\alpha_2 \gamma_1^2 + \alpha_1 (-4\alpha_2 (\beta_1 + \beta_2) + \gamma_2^2)) + Q_2^2 (\alpha_2 \gamma_1^2 + \alpha_1 (-4\alpha_2 (\beta_1 + \beta_2) + \gamma_2^2)) \\
&\quad + Q_1 (Q_2 (8\alpha_1 \alpha_2 (\beta_1 + \beta_2) - 2\alpha_2 \gamma_1^2) + (P_1 - P_2) (4\alpha_2 \beta_2 \gamma_1 + 4\alpha_1 \beta_1 \gamma_2 - \gamma_1 \gamma_2 (\gamma_1 + \gamma_2))) \\
&\quad + 4\alpha_1 \beta_1 \delta_1 + 4\alpha_2 \beta_1 \delta_1 + 4\alpha_1 \beta_2 \delta_1 + 4\alpha_2 \beta_2 \delta_1 - \gamma_1^2 \delta_1 - 2\gamma_1 \gamma_2 \delta_1 - \gamma_2^2 \delta_1 \\
&\quad \left. + 4(\alpha_1 + \alpha_2) (\beta_1 + \beta_2) \delta_2 - (\gamma_1 + \gamma_2)^2 \delta_2 \right) \\
&= f_\delta(\alpha_1, \alpha_2, \beta_1, \beta_2, \gamma_1, \gamma_2, Q_1, Q_2, P_1, P_2)
\end{aligned} \tag{B.9}$$

where,

$$V = \frac{1}{4(\alpha_1 + \alpha_2)(\beta_1 + \beta_2) - (\gamma_1 + \gamma_2)^2}. \tag{B.10}$$

This has the important implication that Gaussian form Weyl symbols are closed under star multiplication. Generally  $\chi \in \mathbb{C}$  and the result is not a Gaussian in the traditional sense because  $Q$  and  $P$  can be complex. Nonetheless two Weyl symbols which are a function of a symmetric complex quadratic form exponentiated, when star multiplied yield another Weyl symbol of the same form.

To compute the star product of two 1 degree of freedom Hudson states, one need only identify

$$A_j = \frac{1}{2\pi \sigma_{q_j} \sigma_{p_j} \sqrt{1 - r_j^2}} \tag{B.11}$$

$$\alpha_j = \frac{1}{2\sigma_{q_j}^2 (1 - r_j^2)} \quad (\text{B.12})$$

$$\beta_j = \frac{1}{2\sigma_{p_j}^2 (1 - r_j^2)} \quad (\text{B.13})$$

$$\gamma_j = \frac{r_j}{\sigma_{q_j} \sigma_{p_j} (1 - r_j^2)} \quad (\text{B.14})$$

$$Q_j = Q_j \quad (\text{B.15})$$

$$P_j = P_j \quad (\text{B.16})$$

$$\delta_j = 0 \quad (\text{B.17})$$

and substitute them into Eqs. B.3-B.10.